National Technical University of Athens
School of Electrical & Computer Engineering
Department of Power Engineering

Methods of Maximizing Power System Voltage Stability Margin using Active Distribution Networks

Ph.D. Thesis

Giorgos D. Prionistis

Supervised By:
Professor Emeritus Costas D. Vournas

Athens
January, 2024

National Technical University of Athens
School of Electrical & Computer Engineering
Department of Power Engineering

Methods of Maximizing Power System Voltage Stability Margin using Active Distribution Networks

Ph.D. Thesis

Giorgos D. Prionistis

Supervising Committee: Costas Vournas (Supervisor)
George N. Korres
Stavros Papathanassiou

Costas Vournas Professor Emeritus NTUA	Georgions N. Korres Professor NTUA	Stavros Papathanassiou Professor NTUA
Vasilis Nikolaidis Assistant Professor NTUA	Anthony Papavasiliou Assistant Professor NTUA	Pavlos Georgilakis Professor NTUA

Maria Vrakopoulou
Assistant Professor
University of Melbourne

. . . . . .

Giorgos D. Prionistis

Doctor of Philosophy in Electrical and Computer Engineering NTUA

Πρόλογος

Αντί προλόγου, κλείνοντας το σημαντικότερο ίσως κεφάλαιο της επαγγελματικής και ακαδημαϊκής μου πορείας, θα ήθελα να ευχαριστήσω όλους αυτούς που με στήριξαν και βοήθησαν, άμεσα ή έμμεσα στην ολοκλήρωση της διδακτορικής μου διατριβής.

Θα ήταν αδύνατο να μην ξεκινήσω τις ευχαριστίες από τον Ομότιμο Καθηγητή του ΕΜΠ και επιβλέποντα της διατριβής, κ. Κώστα Βουρνά, που με καθοδήγησε από την αρχή έως το τέλος, με αμέριστη συμπαράσταση και υπομονή. Τον ευχαριστώ ιδιαιτέρως για όλες τις συζητήσεις που κάναμε - ακαδημαϊκού ενδιαφέροντος και μη - για το χρόνο που αφιέρωσε, διαβάζοντας και διορθώνοντας το κείμενο μου κυριολεκτικά λέξη προς λέξη, αλλά και για την εμπιστοσύνη και την κατανόηση που μου έδειξε καθ΄ όλη τη διάρκεια αυτής της διαδρομής.

Επίσης, θα ήθελα να ευχαριστήσω την επίκουρο καθηγήτρια στο Πανεπιστήμιο της Μελβούρνης, Μαρία Βρακοπούλου για την άριστη συνεργασία μας και τις πολύτιμες για μένα συζητήσεις που κάναμε.

Τους Δρ. Θοδωρή Σουξέ, Παναγιώτη Μανδουλίδη και Ευθύμη Καράγγελο καθώς και τον υποψήφιο διδάκτορα και φίλο Αρτέμη Σεμένογλου, για την υποστήριξη και τις συζητήσεις, ερευνητικές και μη.

Τον κ. Καμπούρη για την ευκαιρία που μου έδωσε να εργαστώ στον ΑΔΜΗΕ για τα τελευταία τέσσερα χρόνια και όλους τους συναδέλφους για το εξαιρετικό κλίμα συνεργασίας. Ιδιαίτερα, θα ήθελα να ευχαριστήσω το συνάδελφο και φίλο Δρ. Νίκο Κουτσούκη για την εξαιρετική συνεργασία μας αλλά και τις συμβουλές που μου έδινε πάντα.

Τα αδέρφια μου, Έλενα και Χρήστο, που με ανιδιοτέλεια με στήριξαν στις πιο σκοτεινές περιόδους της ζωής μου και τα ανηψάκια μου Δημήτρη, Οδυσσέα και Άννα.

Τη σύντροφο μου Ευτυχία, που υπέμενε εμένα και τη γκρίνια μου, δείχνοντας πάντα κατανόηση και στήριξη, αγνοώντας ίσως το πόσο με έχει βοηθήσει σε αυτό το ταξίδι.

Τους γονείς μου, που έφυγαν νωρίς, ωστόσο πρόλαβαν να μου δώσουν τα απαραίτητα εφόδια.

Abstract

The proliferation of distributed energy resources and renewable energy sources that are connected to the grid through power converters, is changing significantly the way that distribution networks operate and consequently also transmission systems. Generation is gradually moving towards the lower voltages, and as a result, ancillary services provided traditionally by thermal power plants, are also vanishing from the transmission system. Despite the challenges, opportunities also appear in terms of service provision from the distribution grids to support the transmission system, thus turning previously passive distribution networks to Active Distribution Networks. Thus, Active Distribution Networks are expected to support the transmission system in dealing with problems such as frequency stability and voltage stability by providing support in both normal and emergency operating conditions.

This thesis examines the support that Active Distribution Networks can offer to the transmission system in terms of Voltage Stability and how can this be achieved most efficiently (optimally). Current practices for voltage stability support, usually from big generating units and/or system connected Wind Farms, include maximum reactive power support, but in some cases this may prove inefficient or even worsen the situation if not coordinated properly, especially when reactive power is coming from the distribution grid where load is also connected. For that reason, it is important to build frameworks for support in case of voltage stability problems, so that the support from the distribution grid is efficient and does not violate operational limitations of the distribution network.

In the current thesis, the voltage stability problem is expressed as an optimization problem, or voltage security margin maximization problem, taking into consideration also possible contingencies in the transmission system. In this way, it can be ensured that support will opt to maximize the stability margins and move the transmission as far away as possible from imminent voltage instabilities, taking also into account possible contingencies, such as the loss of transmission lines or generating units. Following that, different approaches or frameworks are proposed for support from the distribution network, assuming some information exchange between the transmission system operator and the ADN operator. This is very critical in the approaches, as usually, limited communication is established between transmission and distribution in real power systems. In the recent years, a lot of effort is being made between Transmission System Operators and Distribution System Operators to improve communication and data exchange in all time frames, including real time operation.

First, the effect of system connected RES, usually including Wind Farms or big Photovoltaics, on the maximization of the voltage stability margin is examined. In that direction, requirements already imposed by the European legislation, for fast current injections by renewable energy resources are implemented to deal with imminent voltage

instabilities. Good parameterization is deemed critical in order to not have adverse results and limited stability margins.

In the direction of support from the distribution side, a corrective (distributed) and a preventive (centralized) optimization framework are created. Both frameworks exploit the ability of the active distribution networks to change the active and reactive power flows at the point of common coupling with the transmission grid, thus supporting the transmission system when facing a voltage stability problem and maximize the voltage stability margins. In order to ensure that the control taken in the distribution grid is optimal for the support of the transmission system, sensitivities are used in the decentralized approach. Sensitivities drive the control taken in the active distribution network into the right direction by linearly associating the changes of both active and reactive power flows at the point of common coupling with the voltage stability margin of the transmission system. In the centralized optimization framework, the flexibility of the ADN is exploited. More specifically, active distribution networks estimate a region in the active and reactive power plane at the point of common coupling and send it to the transmission system operator that takes it into consideration when computing the stability margins of the power system. In that way, the flexibility region that is calculated by the active distribution networks, can be used in the form of additional constraints, in the voltage stability margin problem maximization directly.

The calculation of the flexibility region of an active distribution network is a separate challenge and various methods are examined and compared. An optimization based approach is proved to be the most efficient especially when dealing with complex feeders containing multiple decision variables. The optimization based approaches, first solved with non-linear programming solvers, prove to have some limitations. For that reason, further optimization methods are explored, such as the convex relaxation second order cone programming approach is examined in order to accelerate the calculation process.

Both frameworks and the flexibility region estimation are implemented in test systems and results show significant support, in terms of increasing the voltage security margins when a critical contingency occurs. Moreover, results are also evaluated using time-domain simulation using the quasi steady state approach and implementing the results that are extracted from the optimization frameworks. In all cases, the proposed frameworks are able to support the transmission system in terms of voltage stability and even tackle imminent voltage collapses.

Flexibility region estimation, can in more complex feeder configurations prove to be time consuming. For that reason, an alternative fast method is implemented for the computation of the flexibility region, using a relaxation of the optimization problem. This proves to improve simulation time and still be fairly accurate.

Last but not least, an incident in the Hellenic Interconnected System is analysed, using the optimization formulation for the voltage security margins. The implementation on a real system and real incident makes the findings of the thesis and the formulation implemented more concrete.

The thesis not only proves that active distribution networks can significantly support the transmission system in cases of voltage stability issues, but also proposes alternate support frameworks to facilitate and optimize the procedure both preventively and correctively.

Περίληψη

Η παρούσα διδακτορική διατριβή με τίτλο Μέθοδοι μεγιστοποίησης περιθωρίων ευστάθειας τάσεως με τη βοήθεια ενεργών δικτύων διανομής, όπως υποδεικνύει και ο τίτλος, εξετάζει την ικανότητα των δικτύων διανομής που δύναται να ελέγχουν τις συσκευές που βρίσκονται σε αυτά, να υποστηρίξουν το Σύστημα Μεταφοράς ηλεκτρικής Ενέργειας σε περιπτώσεις που εμφανίζεται αστάθεια τάσης.

Η συνεχώς αυξανόμενη διείσδυση των Ανανεώσιμων Πηγών Ενέργειας τόσο στο Σύστημα Μεταφοράς, όσο και στο δίκτυο διανομής, αλλά και άλλων συσκευών που συνδέονται μέσω ηλεκτρονικών ισχύος, οδηγεί σταδιακά στη μείωση των συμβατικών μονάδων παραγωγής που παραδοσιακά εξασφάλιζαν την παροχή επικουρικών λειτουργιών στο Σύστημα Μεταφοράς σε επισφαλείς καταστάσεις, όπως η ενδεχόμενη αστάθεια τάσης. Για αυτό το λόγο και μεγαλώνει η ανάγκη άντλησης επικουρικών υπηρεσιών από τα δίκτυα διανομής. Η διατριβή αυτή εξετάζει κατά πόσο μπορούν να συμβάλουν τα δίκτυα διανομής σε αυτές τις υπηρεσίες, αλλά κυρίως στο ποιος είναι ο βέλτιστος τρόπος να το κάνουν. Πιο συγκεκριμένα, εξετάζονται βέλτιστα σχήματα ώστε αρχικά να εξασφαλιστεί ότι ο έλεγχος που δε θα υλοποιηθεί στα δίκτυα διανομής δε θα έχει ανάποδα αποτελέσματα, δηλαδή πιθανή επιδείνωση της κατάστασης. Στη συνέχεια, εξετάζεται η μεγιστοποίηση της ενίσχυσης μέσω των ενεργών δικτύων διανομής, χωρίς παράλληλα να τίθεται σε κίνδυνο τόσο η ίδια η λειτουργία των δικτύων, όσο και του εξοπλισμού που συνδέεται σε αυτά. Για το λόγο αυτό, όπως θα εξηγηθεί και παρακάτω, εφαρμόζονται μέθοδοι βελτιστοποίησης, δηλαδή εφαρμογή του προβλήματος της Βέλτιστης Ροής Φορτίου τόσο για τον υπολογισμό των περιθωρίων ασφάλειας τάσης, όσο και για το βέλτιστο έλεγχο στα δίκτυα διανομής.

Στη συνέχεια της εκτεταμένης ελληνικής περίληψης, θα περιγραφούν συνοπτικά τα κεφάλαια από τα οποία αποτελείται η διατριβή.

Το πρώτο Κεφάλαιο αποτελεί την εισαγωγή της διδακτορικής διατριβής. Στο κεφάλαιο αυτό γίνεται μια εισαγωγή σε γενικότερες έννοιες στο ευρύτερο θέμα των συστημάτων ηλεκτρικής ενέργειας, στα διαφορετικά είδε ευστάθειας και πιο συγκεκριμένα στην ευστάθεια τάσεως συστημάτων ηλεκτρικής ενέργειας. Περιγράφονται επίσης βασικές έννοιες που θα χρησιμοποιηθούν στα υπόλοιπα κεφάλαια τις διατριβής, όπως οι Ανανεώσιμες πηγές ενέργειας, τα ενεργά δίκτυα διανομής κλπ. Τέλος, στο πρώτο κεφάλαιο περιλαμβάνεται η βιβλιογραφική ανασκόπηση που πραγματοποιήθηκε κατά τη διάρκεια του διδακτορικού έργου και η περαιτέρω συμβολή του συγκεκριμένου διδακτορικού στην συγκριτικά με την υπάρχουσα βιβλιογραφία.

Στο Κεφάλαιο 2, γίνεται η περιγραφή της μοντελοποίησης του Συστήματος Μεταφοράς καθώς και ορίζεται το πρόβλημα βέλτιστης ροής φορτίου για τον υπολογισμό των περιθωρίων ευστάθειας τάσεως. Αρχικά, περιγράφονται αναλυτικά όλες οι εξισώσεις του Συστήματος, καθώς και οι περιορισμοί που εγείρονται από τα στοιχεία που συνδέονται στο Σύστημα ηλεκτρικής ενέργειας. Αρχικά, διατυπώνονται οι εξισώσεις ισορροπίας μόνιμης κατάστασης,

που αντιστοιχούν στις εξισώσεις ροής ισχύος. Για τη διατύπωση αυτών των εξισώσεων χρησιμοποιείται η καρτεσιανή μορφή. Στη συνέχεια, περιγράφεται η υλοποίηση του διεσπαρμένου ζυγού αναφοράς. Η χρήση διεσπαρμένου ζυγού αναφοράς στο πρόβλημα βέλτιστης ροής φορτίου πραγματοποιείται ώστε να προσομοιάσει τη λειτουργία της αυτόματης ρύθμισης παραγωγής, ώστε η αύξηση (ή μείωση του φορτίου) να διανέμεται σε πολλές γεννήτριες ανάλογα με συντελεστή συμμετοχής της καθεμίας. Στη συνέχεια, διατυπώνονται οι περιορισμοί που αφορούν τις σύγχρονες γεννήτριες και αντιστοιχούν σε περιορισμούς ρεύματος πεδίου (δρομέα) και στάτη, καθώς και περιορισμούς ενεργού ισχύος (ικανότητα παραγωγής). Αντίστοιχα, προκύπτουν και οι περιορισμοί ρεύματος που αντιστοιχούν στα όρια ρεύματος των μετατροπέων ηλεκτρονικών ισχύος. Αυτοί οι περιορισμοί αναφέρονται κυρίως σε Ανανεώσιμες πηγές ενέργειας που συνδέονται στο Σύστημα, αλλά μπορούν να επεκταθούν και σε άλλες συσκευές, όπως οι συστοιχίες μπαταριών. Αναφέρεται επίσης σε αυτό το σημείο η συμπληρωματική σχέση μεταξύ της τάσης των γεννητριών με το όριο ρεύματος τους. Πιο συγκεκριμένα, η συμπληρωματική σχέση υπονοεί ότι μία εκ των δυο μεταβλητών στο σημείο βελτίστου, θα πρέπει να ισούται με το άνω (μέγιστο) όριο. Αυτό μπορεί να εξασφαλιστεί με την προσθήκη επιπλέον μεταβλητών, ωστόσο δεν κρίνεται απαραίτητο, αφού η επίλυση των προβλημάτων δείχνει ότι η φύση του προβλήματος εγείρει αυτή τη συμπληρωματικότητα. Τέλος, ορίζονται οι υπόλοιποι λειτουργικοί περιορισμοί που αφορούν στα όρια τάσεως λειτουργίας, στα θερμικά όρια των γραμμών και καλωδίων καθώς και στα θερμικά όρια των μετασχηματιστών τάσης. Δεδομένου ότι έχουν περιγραφεί όλες οι εξισώσεις και περιορισμοί που ορίζουν την μόνιμη κατάσταση του συστήματος και τις συνθήκες ισορροπίας αυτού, θα οριστεί το πρόβλημα βέλτιστης ροής φορτίου για μεγιστοποίηση των περιθωρίων ασφάλειας τάσης. Το πρόβλημα ορίζεται ως η μεγιστοποίηση μιας αντικειμενικής συνάρτησης που περιγράφει τη γραμμική αύξηση του συνολικού φορτίου (ή του φορτίου μιας περιοχής) προς μια συγκεκριμένη κατεύθυνση, υπό τους περιορισμούς και τις εξισώσεις που περιγράφηκαν νωρίτερα. Η επίλυση του προβλήματος αυτού, λαμβάνοντας υπόψη και πιθανά σενάρια απώλειας εξοπλισμού (σενάρια N-1), θα δώσει ως αποτέλεσμα το περιθώριο ασφάλειας τάσης καθώς και τους πολλαπλασιαστές Λαγρανγε που χρησιμοποιούνται στο πρόβλημα, όπως και τις τιμές όλων των υπόλοιπων μεταβλητών του προβλήματος. Εφόσον, έχει διατυπωθεί πλήρως το πρόβλημα, θα εφαρμοστεί τόσο σε ένα απλό σύστημα δύο ζυγών όσο και σε ένα πιο σύνθετο σύστημα. Τα αποτελέσματα του προβλήματος βελτιστοποίησης συγκρίνονται επίσης και με τα αποτελέσματα χρονικής προσομοίωσης, που υλοποιείται με τη χρήση λογισμικού οιονεί μόνιμης κατάστασης, όπου μοντελοποιούνται και τα ΣΑΤΥΦ.

Στο Κεφάλαιο 3, παρουσιάζεται η επίδραση που μπορούν να έχουν οι ανανεώσιμες πηγές ενέργειας στο σύστημα και στα περιθώρια ασφάλειας τάσης, μέσω του ρεύματος (ενεργού και αέργου) που μπορούν να εγχύσουν στο σημείο που συνδέονται με το σύστημα. Σύμφωνα με τους Ευρωπαϊκούς Νόμους και κανονισμούς, υπάρχουν καμπύλες τάσης ρεύματος βάσει των οποίων οι ανανεώσιμες πηγές ενέργειας, οι οποίες συνδέονται μέσω μετατροπέων ηλεκτρονικών ισχύος, μπορούν να εγχύσουν γρήγορα άεργο ρεύμα στην περίπτωση που συμβεί κάποιο σφάλμα. Στο Κεφάλαιο αυτό μελετάται αρχικά η επίδραση που μπορεί να έχει ένα πάρκο σε ένα ακτινικό διάδρομο μεταφοράς σε συνάρτηση με τη θέση που βρίσκεται αλλά αι τη διαθέσιμη αιολική παραγωγή. Στη συνέχεια, για κάθε πιθανή σχέση, υπολογίζονται τα περιθώρια ευστάθειας τάσης με την εφαρμογή των ευρωπαϊκών κανονισμών για έγχυση αέργου ρεύματος, για διάφορες τιμές των παραμέτρων, στα διάφορα σημεία (ζυγούς) του ακτινικού συστήματος. Όπως παρατηρείται τόσο η ενίσχυση, όσο και η τιμή των παραμέτρων επηρεάζουν διαφορετικά τα περιθώρια ευστάθειας τάσης, ανάλογα με το σημείο κοινής σύνδεσης της μονάδας στο σύστημα. Για αυτό το λόγο και το κεφάλαιο κλείνει με τον υπολογισμό των βέλτιστων εγχύσεων ενεργού και αέργου ρεύματος γα κάθε πιθανό σημείο σύνδεσης. Όλα

τα αποτελέσματα υπολογίζονται με τη χρήση του προβλήματος βέλτιστης ροής ισχύος που παρουσιάστηκε και εξηγήθηκε στο δεύτερο κεφάλαιο.

Το Κεφάλαιο 4 ασχολείται με τη μοντελοποίηση των Ενεργών Δικτύων Διανομής καθώς και με την ευελιξία που μπορούν να παρέχουν. Αρχικά, γίνεται εκτενής περιγραφή του συνόλου των εξισώσεων που αφορούν το δίκτυο διανομής καθώς και των στοιχείων που συνδέονται σε αυτά. Τα στοιχεία που συνδέονται στα Ενεργά Δίκτυα Διανομής και μπορούν να συμβάλουν στην ευελιξία είναι τα εξής: οι διεσπαρμένες πηγές ενέργειας που συνδέονται στο δίκτυο μέσω ηλεκτρονικών ισχύος (αντιστροφέων), το Σύστημα Αλλαγής Τάσης Υπό Φορτίο (ΣΑΤΥΦ) που βρίσκεται στους μετασχηματιστές τάσης, τα φορτία τα οποία εξαρτώνται από την τάση και τα εγκάρσια στοιχεία συστοιχιών πυκνωτών ή αυτεπαγωγών. Οι διεσπαρμένες πηγές μπορεί να περιέχουν είτε ανανεώσιμες πηγές ενέργειας, είτε μονάδες αποθήκευσης (μπαταρίες). Εφόσον έχει γίνει πλήρης περιγραφή όλων των στοιχείων, καθώς και των εξισώσεων που περιγράφουν ένα ενεργό δίκτυο διανομής, ορίζεται ένα γενικό πρόβλημα βελτιστοποίησης, με γενική συνάρτηση που αφορά στις ανταλλαγές ισχύος στα όρια με το Σύστημα ηλεκτρικής ενέργειας, δηλαδή, στο Σημείο κοινής σύνδεσης της γραμμής διανομής με το σύστημα μεταφοράς ηλεκτρικής ενέργειας. Ακολούθως, παρουσιάζονται τρία δοκιμαστικά ενεργά δίκτυα διανομής που θα χρησιμοποιηθούν στη συνέχεια. Έπειτα, ορίζεται η έννοια της ευελιξίας των ενεργών δικτύων διανομής και περιγράφονται τρεις διαφορετική μέθοδοι για τον υπολογισμό της περιοχής ευελιξίας. Η περιοχή ευελιξίας αποτελεί το δισδιάστατο χώρο στο επίπεδο που ορίζει η ενεργός και η άεργος ανταλλαγή ισχύος του συγκεκριμένου δικτύου με το σύστημα ηλεκτρικής ενέργειας. Οι μέθοδοι για τον υπολογισμό της περιοχής ευελιξίας είναι οι εξής: 1) Μέθοδος Μόντε Κάρλο, η οποία βασίζεται στην παραγωγή τυχαίων σετ μεταβλητών ελέγχου για τη γραμμή διανομής και στην συνέχεια αξιολόγηση των αποτελεσμάτων της ροής ισχύος. Αν τα σημεία που υπολογίζονται, σέβονται όλους τους περιορισμούς που έχουν οριστεί, τότε αποτελούν σημεία της περιοχής ευελιξίας. Σε άλλη περίπτωση απορρίπτονται. 2) Εύρεση σημείων πολλαπλών ενεργών περιορισμών. Τα σημεία πολλαπλών περιορισμών ορίζουν σημεία που συνήθως αλλάζει ο περιορισμός που είναι ενεργός. 3) Ακτινική Σάρωση των ορίων της περιοχής ευελιξίας. Η μέθοδος αυτή βασίζεται στην επίλυση προβλημάτων βέλτιστης ροής ισχύος για πολλαπλές γωνίες στο επίπεδο που ορίζει η ενεργός και η άεργος ανταλλαγή ισχύος του συγκεκριμένου δικτύου με το σύστημα. Με αυτό τον τρόπο υπολογίζονται πολλαπλά σημεία τα οποία βρίσκονται στα όρια της περιοχής ευελιξίας. Και οι τρεις μέθοδοι βασίζονται στην εύρεση σημείων μέσα ή στα όρια της περιοχής ευελιξίας. Γι΄ αυτό το λόγο αναπτύσσεται ένας αλγόριθμος σχηματισμού ενός κυρτού πολυγώνου ενώνοντας γραμμικά σημεία που έχουν ευρεθεί. Με αυτό τον τρόπο γίνεται προσέγγιση της περιοχής ευελιξίας καθώς και δίνεται η δυνατότητα αναπαράστασης της μέσω γραμμικών περιορισμών.

Εφόσον στο Κεφάλαιο 2 έχει γίνει η περιγραφή του προβλήματος μεγιστοποίησης των περιθωρίων ασφάλειας τάσης, στο Κεφάλαιο 5 θα αξιοποιηθεί το πρόβλημα αυτό ώστε να δημιουργηθούν δύο μέθοδοι ενίσχυσης της ευστάθειας τάσης του Συστήματος Μεταφοράς από τα ενεργά δίκτυα διανομής. Πιο συγκεκριμένα περιγράφεται μια διορθωτική μέθοδος, η οποία εφαρμόζεται αμέσως μετά το συμβάν (διαταραχή) και μια προληπτική μέθοδος, η οποία εφαρμόζεται όταν ανιχνευθεί ότι μπορεί κάποιο συμβάν να οδηγήσει το Σύστημα σε μη ασφαλή λειτουργία (αστάθεια τάσης). Η πρώτη μέθοδος (διορθωτική) αποτελεί μέθοδο αντιμετώπισης με διεσπαρμένη υλοποίηση. Από το κεντρικό πρόβλημα βελτιστοποίησης υπολογίζονται οι ευαισθησίες των εγχύσεων στους ζυγούς στους οποίους συνδέονται τα ενεργά δίκτυα διανομής, οι οποίες αποτελούν την ευαισθησία της ενεργού και αέργου κατανάλωσης στο σημείο κοινής σύνδεσης με το σύστημα, ως προς το περιθώριο ασφάλειας τάσης. Στη συνέχεια σε κάθε ενεργό δίκτυο διανομής, επιλύεται ένα ξεχωριστό πρόβλημα

βελτιστοποίησης, αξιοποιώντας τις ευαισθησίες που υπολογίστηκαν. Η διορθωτική μέθοδος αντιμετώπισης εφαρμόζεται σε ένα δοκιμαστικό Σύστημα μεταφοράς στο οποίο θεωρείται ότι συνδέονται πέντε ενεργά δίκτυα διανομής. Τα αποτελέσματα της μεθόδου επιβεβαιώνονται με τη χρονική προσομοίωση. Οι τιμές των παραμέτρων που υπολογίζονται στη βελτιστοποίηση, χρησιμοποιούνται ως τιμές αναφοράς στη χρονική προσομοίωση. Η δεύτερη μέθοδος, που αναφέρεται ως προληπτική μέθοδος, βασίζεται τόσο στο κεντρικό πρόβλημα βελτιστοποίησης του Κεφαλαίου 2, όσο και στην εύρεση της περιοχής ευελιξίας των ενεργών δικτύων διανομής και την αναπαράσταση της με γραμμικούς περιορισμούς που παρουσιάστηκε στο Κεφάλαιο 4. Στην προληπτική μέθοδο μεγιστοποίησης των περιθωρίων ασφάλειας τάσης, το κεντρικό πρόβλημα βελτιστοποίησης επιλύεται με τον ίδιο τρόπο, με την προσθήκη των περιορισμών που προκύπτουν από τις περιοχές ευελιξίας των ενεργών δικτύων διανομής. Ως αποτέλεσμα, η επίλυση του προβλήματος, επιστρέφει το νέο αυξημένο περιθώριο ασφάλειας τάσης, καθώς και τις βέλτιστες εγχύσεις στα σημεία κοινής σύνδεσης των ενεργών δικτύων διανομής με το Σύστημα Μεταφοράς ηλεκτρικής ενέργειας. Οι βέλτιστες εγχύσεις/καταναλώσεις πρέπει να επιτευχθούν από το κάθε ενεργό δίκτυο διανομής μέσω μεταβολής των στοιχείων που μπορούν να ελέγξουν. Για τον υπολογισμό των τιμών των μεταβλητών ελέγχου για τις οποίες θα προκύψει η βέλτιστη κατανάλωση που ζητείται από το Σύστημα μεταφοράς, επιλύεται ένα ακόμα πρόβλημα βελτιστοποίησης σε κάθε ενεργό δίκτυο διανομής. Το πρόβλημα αυτό έχει ως αντικειμενική συνάρτηση την ελαχιστοποίηση της Ευκλείδειας απόστασης μεταξύ της κατανάλωσης ενεργού και αέργου ισχύος στο σημείο κοινής σύνδεσης και των βελτίστων που υπολογίστηκαν από το κεντρικό πρόβλημα βελτιστοποίησης. Η προληπτική μέθοδος βελτιστοποίησης εφαρμόζεται αντίστοιχα στο ίδιο σύστημα, με αντίστοιχα αποτελέσματα, ενώ παρουσιάζεται και το τελευταίο πρόβλημα βελτιστοποίησης εφαρμογής των τιμών αναφοράς στο δίκτυο διανομής, σε ένα πιο απλό ακτινικό σύστημα μεταφοράς, στη μέση του οποίου συνδέεται ένα σύνθετο ενεργό δίκτυο διανομής.

Η μέθοδος που προτείνεται στο Κεφάλαιο 4, για υπολογισμό των περιοχών ευελιξίας των Ενεργών Δικτύων Διανομής, παρέχει μια πολύ καλή προσέγγιση του χώρου ευελιξίας. Ωστόσο, λόγω της φύσης του προβλήματος, το οποίο αποτελεί ένα μη-γραμμικό και μη κυρτό πρόβλημα, η επίλυση πολλαπλών προβλημάτων βελτιστοποίησης σε πιο σύνθετα δίκτυα διανομής με πολλές μεταβλητές, μπορεί να αποδειχθεί χρονοβόρα, ιδιαίτερα αν υπάρχει ανάγκη αυτός ο υπολογισμός της ευελιξίας να γίνεται ανά τακτικά διαστήματα. Για αυτό το λόγο, στο Κεφάλαιο 6, προτείνεται μια εναλλακτική μέθοδος υπολογισμού της περιοχής ευελιξίας κάνοντας μια αλλαγή στην διατύπωση του προβλήματος, και χαλάρωση (μετατροπής από ισότητα σε ανισότητα) ενός εκ των περιορισμών. Από τη χαλάρωση αυτή, το πρόβλημα βελτιστοποίησης μετατρέπεται σε πρόβλημα προγραμματισμού κώνων δευτέρας τάξης, το οποίο εξασφαλίζει ότι το πρόβλημα θα είναι κυρτό και η επίλυση θα είναι ταχύτερη. Για την εξασφάλιση εύρεσης σημείων τα οποία θα αντιστοιχούν σε πραγματικές λύσεις του προβλήματος ροής φορτίου, γίνεται μια μετατροπή του προβλήματος που ορίζεται στο Κεφάλαιο 4. Η εφαρμογή της μεθόδου στα δοκιμαστικά ενεργά δίκτυα διανομής που εξετάστηκαν και στο Κεφάλαιο 4, δείχνει ότι η μέθοδος μπορεί να προσεγγίσει σε πολύ ικανοποιητικό βαθμό τις περιοχές ευελιξίας που υπολογίστηκαν από τη μη-γραμμική προσέγγιση, και σε μικρότερο χρόνο.

Στο Κεφάλαιο 7, αναλύεται ένα σχετικό πραγματικό συμβάν που προέκυψε στο Ελληνικό Σύστημα Μεταφοράς Ηλεκτρικής Ενέργειας. Για την ανάλυση χρησιμοποιείται το κεντρικό πρόβλημα βελτιστοποίησης που περιγράφτηκε στο Κεφάλαιο 2, ώστε να εξεταστεί το περιθώριο ασφάλειας τάσης μετά τη διαταραχή που προέκυψε, σε μια συγκεκριμένη περιοχή. Αντίστοιχα, τα αποτελέσματα μελετώνται και με τη χρήση χρονικής προσομοίωσης. Η α-

νάλυση στο πραγματικό σύστημα δείχνει ότι η μέθοδος είναι σε θέση να ανιχνεύσει πιθανά προβλήματα ευστάθειας τάσης και σε πραγματικά συστήματα. Παράλληλα, παρουσιάζεται και η δυνατότητα ενίσχυσης των περιθωρίων με την αξιοποίηση και έλεγχο των μεγάλων αιολικών πάρκων που συνδέονται μέσω αποκλειστικών γραμμών στο Σύστημα μεταφοράς της περιοχής. Στο Κεφάλαιο εξετάζονται δυο πραγματικά στιγμιότυπα που λήφθηκαν από τον εκτιμητή κατάστασης του Συστήματος Διαχείρισης Ενέργειας στο Κέντρο Ελέγχου Ενέργειας.

Το τελευταίο Κεφάλαιο αφορά στα συμπεράσματα που βγήκαν από τη διδακτορική διατριβή καθώς και ερευνητικά θέματα με ενδιαφέρον που εξετάστηκαν καθώς και προοπτικές για περαιτέρω έρευνα.

Contents

List of Tables

List of Figures

Chapter 1

Introduction

1.1 Power System Stability

1.1.1 Electric Power Systems

Electric power systems, also known as electric grids or electricity networks, play a crucial role in modern society by delivering electricity from power generation sources to end-users. These systems form the backbone of the infrastructure and enable the reliable distribution of electrical energy to homes, businesses, industries, and other institutions. As a result, it is crucial that the operation of the electric power systems is constant and uninterrupted.

Electric power is produced at generating stations and is transmitted to consumers through a complex network of components, including power lines, transformers, circuit breakers, relays, capacitors, and protective devices. These components work together to ensure a reliable supply of electricity and to protect the system from faults and overloads. The general structure of electric power systems, as also presented in Fig. 1.1, consists of the following subsystems:

- Transmission System
- Distribution Network

The transmission network operates at the highest voltage levels (150kV/220kV/400kV) and transmits power over significant distances to consumers spread over a wide area. The transmission system interconnects all major generating stations and main load centers in the system. Synchronous generating units operate between 10kV-30kV and are usually connected to the transmission grid through step-up transformers. Synchronous generating units usually include thermal and hydro power plants. Thermal power plants are also divided into coal and gas stations. Moreover, interconnections with neighboring power systems are formed at the transmission system level, thus creating vast synchronous areas. In addition, large consumers, such as the heavy industry, can be supplied directly from the transmission grid. The transmission system along with the power generating units is usually referred to as the bulk power system and is operated and monitored by a Transmission System Operator (TSO). A TSO is a crucial entity in the electricity industry responsible for the safe, reliable, and efficient operation of the high-voltage electricity transmission system.

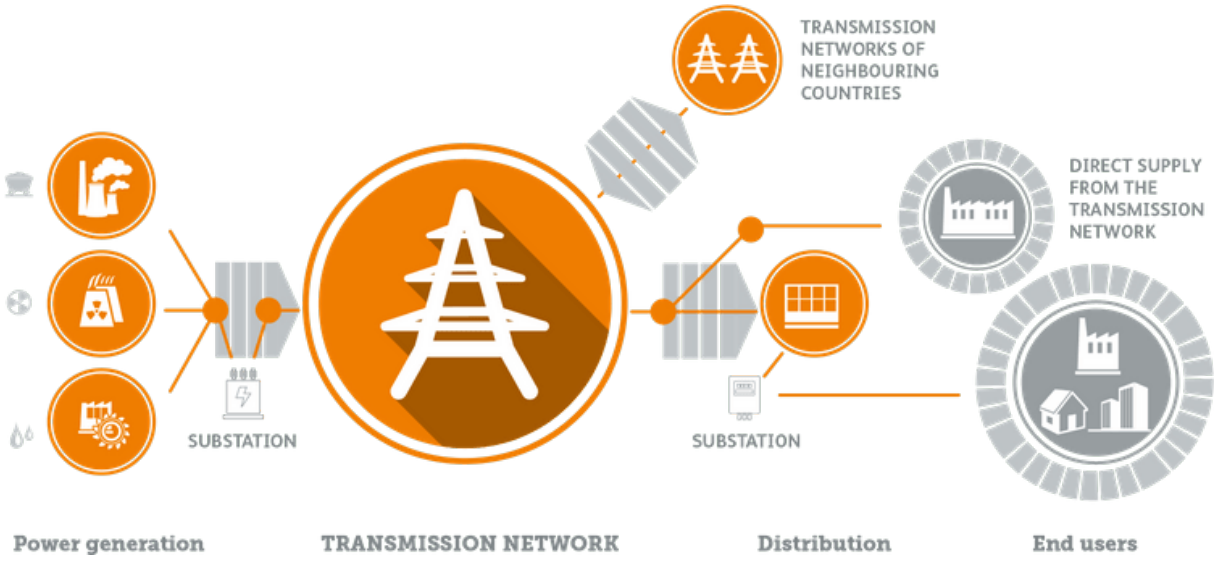

Figure 1.1: General Structure of Electric Power Systems

The main responsibilities of a TSO include operation and control. TSOs monitor and control the flow of electricity across the transmission network in real time. They ensure that the power system remains stable and secure, managing factors like voltage levels, frequency, and line capacities. Moreover, TSOs are responsible for ensuring a balance between electricity supply and demand. They need to anticipate fluctuations in demand and coordinate with power generators to adjust generation levels accordingly to prevent overloads or underloads on the transmission lines.

In many countries, TSOs are independent entities that operate the transmission network as regulated monopolies or under a specific regulatory framework to ensure fair and non-discriminatory access to the transmission infrastructure. They work closely with other entities in the electricity sector, such as Distribution System Operators (DSOs), power generator companies, regulators, and market operators, to ensure the overall functionality and reliability of the electricity supply chain.

In some countries, sub-transmission systems are also considered, usually operating in voltages between 40kV - 120kV.

The distribution network represents the final stage in the transfer of power to individual customers. Usually, distribution networks consist of primary and secondary distribution feeders. The primary distribution voltage level is usually around 11-33kV. At this level small industrial customers are also supplied. Finally, secondary distribution feeders supply residential and commercial customers at low voltage levels. The Distribution Network Operator (DNO) or Distribution System Operator (DSO) is responsible for the operation of the distribution network.

The power system at the moment is undergoing an important energy transition. The electrical energy transition refers specifically to the transformation of the electricity sector from fossil fuel-based power generation to cleaner and more sustainable sources. It is a critical component of the broader energy transition and plays a pivotal role in achieving global climate and environmental goals. The electrical energy transition aims to reduce greenhouse gas emissions, enhance grid flexibility and reliability, and promote the integration of renewable energy sources (RES).

The proliferation of RES and distributed generation (DG) or distributed energy resources (DER) in general is changing drastically the electric power system and its operation, as more and more generation is connected to the distribution network directly, thus also closer to the load demand. This consequently leads to gradual decommissioning of thermal power plants and overall operation of the transmission system. DG introduces new challenges and prospects to the ever changing operation of the electric power systems all around the world. Last but not least, load profile is also subject to big changes with the increase in electric vehicles (EV) that charge from lower voltage levels, adding to the total consumption.

In Fig. 1.2, a simple one line diagram is presented, containing all the voltage levels from the transmission grid and the power production to the low voltage consumers in the distribution network.

The complexity of the electric power system introduces several challenges, especially in modeling and analysis, such as stability, which require advanced mathematical tools to be analyzed.

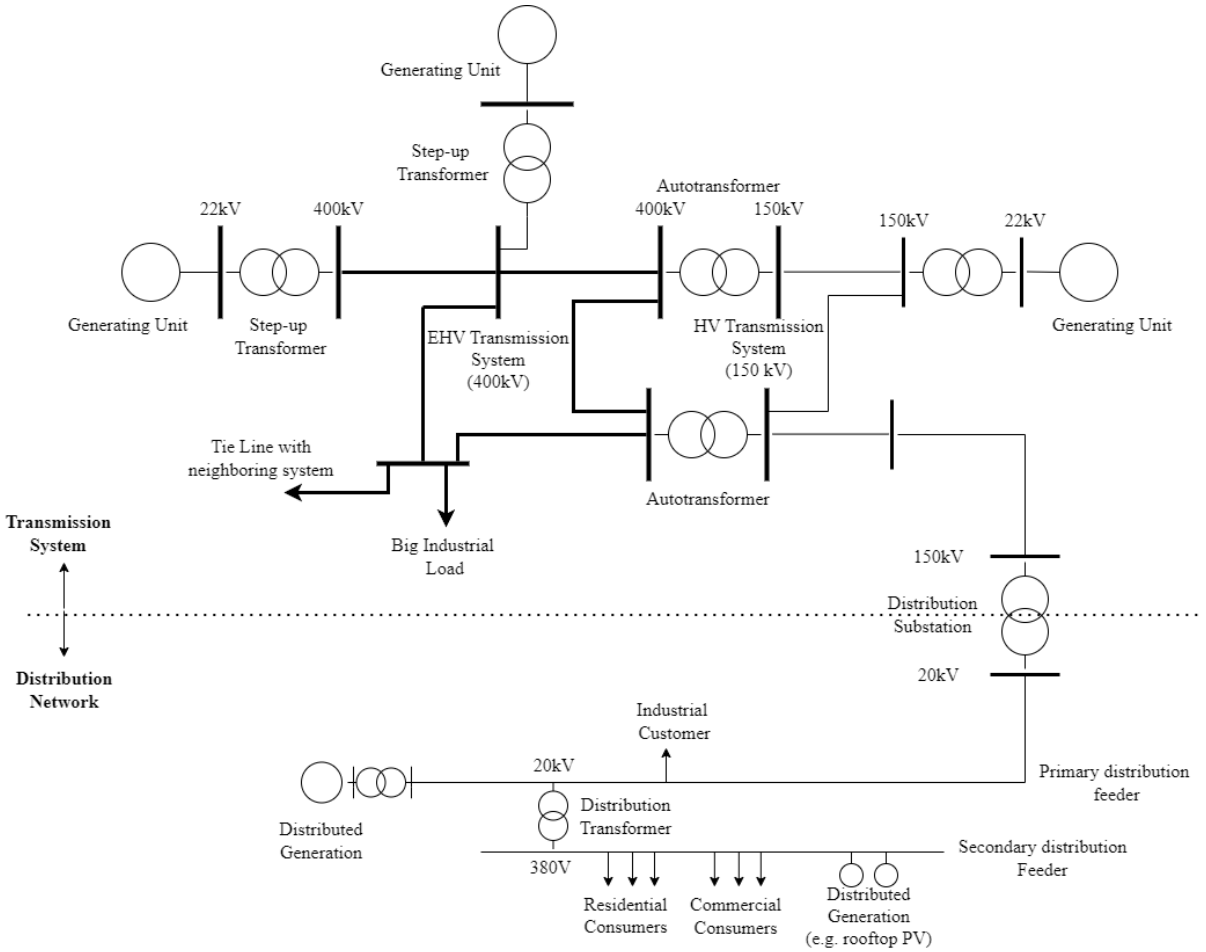

Figure 1.2: One line diagram of a complete Power System

1.1.2 Power System Stability Classification

Power system stability has been recognized as an important problem for secure system operation since the early 1920s. A formal definition for power system stability has been

proposed in [1]:

"Power system stability is the ability of an electric power system, for a given initial operating condition, to regain a state of operating equilibrium after being subjected to a physical disturbance, with most system variables bounded so that practically the entire system remains intact."

The power system is highly non-linear. Subjected to a disturbance, the stability of the system will depend on the initial operating point and the nature of the disturbance. Disturbances can range from small changes in the loading conditions to losses of transmission lines or loss of power generating units, short-circuit faults, etc.

The classification of power system stability proposed here is based on the following considerations [2]:

- The physical nature of the resulting mode of instability as indicated by the main system variable in which instability can be observed.
- The size of the disturbance considered, which influences the method of calculation and prediction of stability.
- The devices, processes, and time span that must be taken into consideration in order to assess stability.

An updated classification including higher frequencies and electronic inverters can be found in [3], with the addition of resonance stability and converter driven stability.

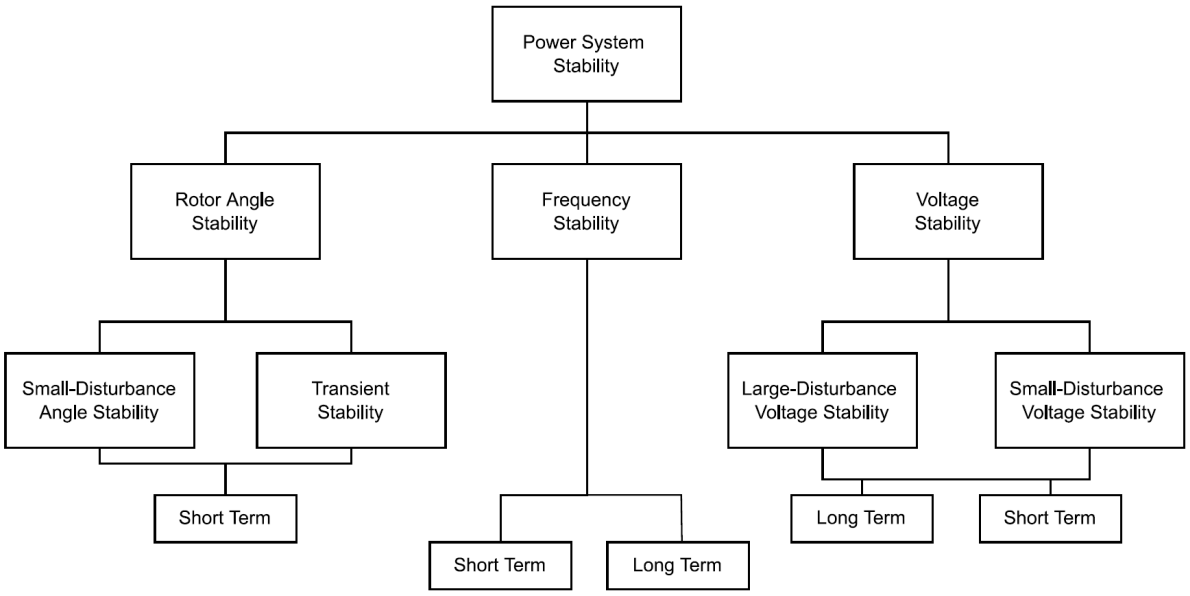

Figure 1.3: Power System Stability Classification

Fig. 1.3 gives the overall picture of the classical power system stability problem, identifying its categories and subcategories. The following are descriptions of the corresponding forms of stability phenomena:

- **Rotor angle stability** refers to the ability of synchronous machines of an interconnected power system to remain in synchronism after being subjected to a

disturbance. This kind of stability depends on the ability to maintain or restore equilibrium between electromagnetic torque and mechanical torque of each synchronous machine in the system. Rotor angle stability is divided into two main subcategories:

  - Small-disturbance (or small-signal) rotor angle stability is concerned with the ability of the power system to maintain synchronism under small disturbances. The disturbances are considered to be sufficiently small that linearization of the system equations is permissible for purposes of analysis.
  - Large-disturbance rotor angle stability, or transient stability, as is commonly referred to, is concerned with the ability of the power system to maintain synchronism when subjected to a severe disturbance, such as a short circuit on a transmission line. The resulting system response involves large excursions of generator rotor angles and is influenced by the non-linear power-angle relationship.

- **Frequency stability** refers to the ability of a power system to maintain steady frequency following a severe system upset resulting in a significant imbalance between generation and load. It depends on the ability to maintain/restore equilibrium between total system generation and load, with minimum unintentional loss of load. Instability that may result occurs in the form of sustained frequency swings leading to tripping of generating units and/or loads.

- **Voltage stability** refers to the ability of a power system to maintain steady voltages at all buses in the system after being subjected to a disturbance from a given initial operating condition. It depends on the ability to maintain/restore equilibrium between load demand and load supply from the power system. Instability that may result occurs in the form of a progressive fall or rise of voltages of some buses. A possible outcome of voltage instability is loss of load in an area or tripping of transmission lines and other elements by their protective systems leading to cascading outages. The loss of synchronism of some generators may result from these outages or from operating conditions that violate the field current limit [4].

1.1.3 Voltage Stability

Voltage stability problems are normally related to heavily stressed operation of the power system, meaning possible high demand and/or significant events such as loss of generation or significant transmission corridors. In some cases, voltage stability may lead to voltage collapse. Some of the principal factors that may contribute to voltage instability and subsequent voltage collapse, include the generators reactive power/voltage control limits, load characteristics, reactive compensation devices and voltage control devices such as transformers with on-load tap changers (LTC).

Voltage stability can be further classified into short- and long-term voltage stability:

- **Short-Term Voltage Stability** involves dynamics of fast acting load components such as induction motors, electronically controlled loads, and HVDC converters. The study period of interest is on the order of several seconds, and analysis requires solution of appropriate system differential equations; this is the same time scale as

that of rotor angle stability. Dynamic modeling of loads is often essential and short circuits near loads are important disturbances.

- **Long-Term Voltage Stability** involves slower acting equipment such as tap-changing transformers, thermostatically controlled loads, and generator current limiters. The study period of interest may extend to several minutes and long-term simulations are required to analyze the dynamic performance of the system. Stability is usually determined by the resulting outage of equipment, rather than by the severity of the initial disturbance. Instability is due to the loss of long-term equilibrium (e.g., when loads try to restore their power beyond the capability of the transmission network and connected generation), post-disturbance steady-state operating point being small-disturbance unstable, or a lack of attraction toward the stable post-disturbance equilibrium (e.g., when a remedial action is applied too late). The disturbance could also be a sustained load buildup (e.g. morning or evening load increase). In many cases, static analysis can be used to estimate stability margins, identify factors influencing stability, and screen a wide range of system conditions and a large number of scenarios. Where timing of control actions is important, this should be complemented by quasi-steady-state time-domain simulations.

In this thesis, the main interest revolves around long-term voltage stability.

1.2 Power System Modelling

1.2.1 Differential-Algebraic Equations

The electric power system is a complex dynamical system, so it needs to be modelled as such. Most dynamical systems can be analyzed using a set of n ordinary differential equations, written in the form:

$$\dot{\boldsymbol{x}} = \boldsymbol{f}(\boldsymbol{x}) \tag{1.1}$$

where $\boldsymbol{x}$ is a n x 1 vector and f_i, is a non-linear function of all $x_i, (i = 1, 2, ..., n)$.

The time response of a physical system is linked to a solution of the ordinary differential equations (ODEs) (1.1) for an initial condition giving the state vector at time t = 0:

$$x(0) = x_0 \tag{1.2}$$

The conditions under which there exists a solution of the nonlinear system (1.1), are outlined in the theorem of existence and uniqueness of solutions [4], [5].

Complex dynamical systems such as the electric power system, are described by a set of differential equations, which also include a number of algebraic variables and are subject to a set of algebraic constraints, essentially forming a Differential-Algebraic Equations (DAE) system. The differential-algebraic systems are described by a set of n differential and m algebraic equations, which are assumed smooth throughout this analysis:

$$\dot{\boldsymbol{x}} = \boldsymbol{f}(\boldsymbol{x}, \boldsymbol{y}, \boldsymbol{p}) \tag{1.3}$$

$$\mathbf{0} = \boldsymbol{g}(\boldsymbol{x}, \boldsymbol{y}, \boldsymbol{p}) \tag{1.4}$$

where, $\boldsymbol{x}$ is the vector of n state variables, $\boldsymbol{y}$ is the vector of m algebraic variables, and $\boldsymbol{p}$ are the k parameter variables. The m algebraic equations (1.4), define a manifold of dimension $n + k$, called constraint manifold, in the $n + m + k$ space of $\boldsymbol{x}, \boldsymbol{y}, \boldsymbol{p}$.

Differential-algebraic systems are studied using the implicit function theorem. Consider a point $\boldsymbol{x}, \boldsymbol{y}, \boldsymbol{p}$ for which the algebraic Jacobian $\boldsymbol{g_y}(\boldsymbol{x}, \boldsymbol{y}, \boldsymbol{p})$ is nonsingular. According to the implicit function theorem, there exists a locally unique, set of n smooth functions $\boldsymbol{F}$ of the form:

$$\dot{\boldsymbol{x}} = \boldsymbol{F}(\boldsymbol{x}, \boldsymbol{p}) \tag{1.5}$$

from which the algebraic variables have been eliminated. Since $\boldsymbol{F}$ can be defined and is smooth at all points where $\boldsymbol{g_y}$ is nonsingular, we know from the existence theorem that there exists a unique time solution of the differential-algebraic system for all these points.

For a fixed value of $\boldsymbol{p}$ the equilibrium points are solutions of the algebraic system:

$$\boldsymbol{f}(\boldsymbol{x}, \boldsymbol{y}, \boldsymbol{p}) = \mathbf{0} \tag{1.6}$$

$$\boldsymbol{g}(\boldsymbol{x}, \boldsymbol{y}, \boldsymbol{p}) = \mathbf{0} \tag{1.7}$$

The stability of equilibrium points can be determined by linearizing (1.6)-(1.7) around the equilibrium:

$$\begin{bmatrix} \boldsymbol{\Delta \dot{x}} \\ \mathbf{0} \end{bmatrix} = \boldsymbol{J} \begin{bmatrix} \boldsymbol{\Delta x} \\ \boldsymbol{\Delta y} \end{bmatrix} \tag{1.8}$$

where $\boldsymbol{J}$ called the unreduced Jacobian of the DAE system:

$$\boldsymbol{J} = \begin{bmatrix} \boldsymbol{f_x} & \boldsymbol{f_y} \\ \boldsymbol{g_x} & \boldsymbol{g_y} \end{bmatrix} \tag{1.9}$$

Assuming $\boldsymbol{g_y}$ is nonsingular at the equilibrium we can eliminate $\boldsymbol{\Delta y}$ from (1.8):

$$\boldsymbol{\Delta \dot{x}} = \left[\boldsymbol{f_x} - \boldsymbol{f_y} \boldsymbol{g_y^{-1}} \boldsymbol{g_x}\right] \boldsymbol{\Delta x} \tag{1.10}$$

and thus, obtain the state matrix $\boldsymbol{A}$ of the linearized system:

$$\boldsymbol{A} = \boldsymbol{F_x} = [\boldsymbol{f_x} - \boldsymbol{f_y} \boldsymbol{g_y^{-1}} \boldsymbol{g_x}] \tag{1.11}$$

The small-signal stability of an equilibrium point of the DAE system for a given value of $\boldsymbol{p}$ depends on the eigenvalues of the state matrix $\boldsymbol{A}$. As $\boldsymbol{p}$ varies, the DAE system may experience bifurcations as a simple ODE system.

1.2.2 Quasi steady state simulation

The system of DAE may describe phenomena that occur in different time scales. As a result, it is difficult to use all DAE in a model that describes the whole system and all involved phenomena. To overcome this problem, an approximation used is to assume that in fast transient phenomena the slow variables are practically constant, while in slow

transient phenomena the fast variables are already in equilibrium. In that way, the system of equations can be divided into subsystems with different time scales.

When this is possible, reduced-order models can be used, to describe each time scale. This is done using the singular perturbation analysis [4], [6]. In that kind of systems, a small parameter ϵ multiplies one or more of the derivatives of the state variables. The system is thus described from the following expression:

$$\dot{\boldsymbol{x}} = \boldsymbol{f}(\boldsymbol{x}, \boldsymbol{y}, \epsilon) \tag{1.12}$$

$$\epsilon\dot{\boldsymbol{y}} = \boldsymbol{g}(\boldsymbol{x}, \boldsymbol{y}, \epsilon) \tag{1.13}$$

where, $\boldsymbol{x}$ is the n x 1 vector of state variables with slow dynamic response, and $\boldsymbol{y}$ is the m x 1 vector of state variables with fast dynamic response.

Due to the term ϵ, an acceptable approximation for the description of slow dynamical systems is to assume that $\epsilon = 0$ in (1.13). That is the definition of the *quasi-steady state (QSS)* approximation of the slow dynamic system. The QSS model can be described from the following equations:

$$\dot{\boldsymbol{x}} = \boldsymbol{f}(\boldsymbol{x_s}, \boldsymbol{y_s}) \tag{1.14}$$

$$\boldsymbol{0} = \boldsymbol{g}(\boldsymbol{x_s}, \boldsymbol{y_s}) \tag{1.15}$$

where x_s are the state variables of the slow subsystem and y_s are algebraic variables corresponding to fast dynamic equilibrium while x_f, y_f are the fast components of state variables of the fast subsystem, with:

$$\boldsymbol{x} = \boldsymbol{x_s} + \boldsymbol{x_f} \tag{1.16}$$

$$\boldsymbol{y} = \boldsymbol{y_s} + \boldsymbol{y_f} \tag{1.17}$$

The QSS system is used for analysis in the long-term time scale, thus the short-term dynamics are considered to be in equilibrium.

Long - term voltage stability, which is the main interest in this thesis, is a slow dynamic phenomenon which can be studied using the QSS analysis. A big advantage of the QSS simulation analysis is the fast computational time.

A special simulation tool has been developed in NTUA for QSS simulation [7], in which in recent years remedial control schemes, as well as IBR and RES have been added [8],[9]. This software tool will be used in various cases in this thesis for comparison and evaluation of the developed optimization schemes.

1.2.3 Power Flow Equations

Power flow or load flow studies are of great importance in planning and designing the future expansion of power systems as well as in determining the best operation of existing systems. Load flow analysis refers to the calculation of voltages and voltage angles in all

buses of a power system, as well as the power flows in all branches for a specific operating point, that is defined by the respective consumption of loads, active power generation and voltage setpoints of generating units. Load flow analysis is essential for the operation planning of a power system for different reasons, such as:

- Monitoring whether voltages and flows are within operational limits
- Analysis of possible contingencies (e.g. loss of a transmission line)
- For long-term analysis of power system expansion and planning

As also explained in Section 1.2, the power system in the steady state can be described by a set of algebraic equations. These algebraic equations mainly refer to the power flow or power balance equations. Power flow formulation and solutions have been extensively studied in the literature, thus only a brief description will be mentioned here.

Let N be the number of buses of the system, then the voltage at bus k is:

$$\tilde{V_k} = V_k \angle \delta_k = V_k(cos\delta_k + jsin\delta_k) \tag{1.18}$$

where as V we represent the value of voltage and as $\tilde{V}$ or $V\angle\delta$ the voltage phasor. Then, the current injected into bus k, according to Kirchhoff's law, will be:

$$\tilde{I_k} = Y_{k1}\tilde{V_1} + Y_{k2}\tilde{V_2} + ... + Y_{kN}\tilde{V_N} = \sum_{n=1}^{N} Y_{kn}\tilde{V_n} \tag{1.19}$$

where, elements Y_{kn} correspond to the respective elements of the complex admittance matrix $Y = G + jB$.

If p_k, q_k denote the net active and reactive power entering the network at bus k, then:

$$s_k = \tilde{V_k}\tilde{I_k}^* \tag{1.20}$$

so,

$$s_k = p_k + jq_k = \tilde{V_k}\sum_{n=1}^{N} Y_{kn}^*\tilde{V_n}^* = Y_{kk}^* V_k^2 + \tilde{V_k}\sum_{n=1}^{N} Y_{kn}^*\tilde{V_n}^* \tag{1.21}$$

where, the injection s_k in a bus of the system will be equal to the total complex generation S_{gk} minus the total load S_{dk} in the bus:

$$s_k = S_{gk} - S_{dk} \tag{1.22}$$

Taking real and imaginary parts, and by combining (1.18), (1.21) and (1.22), the power balance equations for both the active and reactive power power in each bus k are written in polar form:

$$P_{gk} - P_{dk} = V_k^2 G_{kk} - V_k \sum_{n=1}^{N} V_n[-G_{kn}cos(\delta_k - \delta_n) - B_{kn}sin(\delta_k - \delta_n)] \tag{1.23}$$

$$Q_{gk} - Q_{dk} = -V_k^2 B_{kk} - V_k \sum_{n=1}^{N} V_n[G_{kn}sin(\delta_k - \delta_n) + B_{kn}cos(\delta_k - \delta_n)] \tag{1.24}$$

It should be noted that S_{gk} and S_{dk} are not necessarily constant, as they can be also functions of bus voltages and/or generation equations (functions of currents etc.). A lot of numerical approaches have been formulated for solving the classical power flow problem, including the Newton-Raphson method.

Power flow solution is also used for initialization in dynamic simulations or QSS analysis.

1.3 Bifurcation Analysis

Bifurcation theory deals with the emergence of sudden changes in nonlinear system response arising from smooth, continuous parameter variations [10]. The term bifurcation originates from the concept of different branches of equilibrium points intersecting each other, and thus bifurcating.

Hence, bifurcation analysis is usually associated with the study of equilibria of the nonlinear system model. In power systems, saddle-node bifurcations (SNBs) and some types of limit-induced bifurcations (LIBs) are basically characterized by the local merging and disappearance of power flow solutions as system parameters p, which correspond to system demand, slowly change, hence this phenomenon has been associated with voltage stability problems. These kinds of bifurcations are also referred to in the technical literature as fold bifurcations or turning points. There are also other type of bifurcations, associated with oscillatory instabilities (Hopf bifurcations) and singularity induced bifurcations.

Saddle-node bifurcations

A SNB point is where two branches of equilibria meet, meaning a stable and an unstable point coalesce. At the bifurcation the equilibrium becomes a saddle-node, hence the name of the bifurcation. A necessary condition for a saddle-node bifurcation of the DAE system is the singularity of the unreduced Jacobian $\boldsymbol{J}$.

Since the necessary SNB condition of a system is the singularity of the state Jacobian, this will both address to the short-term and the long-tern subsystems (resulting from the QSS approximation). Thus, the necessary condition for a saddle-node bifurcation of the long-term dynamics is the singularity of the unreduced long-term Jacobian. The unreduced long-term Jacobian is also the Jacobian of the algebraic equations, forming the long-term equilibrium constraints. Thus, in this case:

$$\phi_u = \boldsymbol{J}_l \tag{1.25}$$

so it can be concluded that the long-term loadability limits are met in general at a saddle-node bifurcation of long-term dynamics, where $\boldsymbol{J}_l$ is the Jacobian of the long-term dynamics, and ϕ is the vector of smooth functions.

Limit-Induced bifurcations

Limit-induced bifurcations, analysed in detail firstly in [11], are usually tied with limits of other constraints of the power systems such as reactive power limits of generators. This kind of bifurcations lead to a sudden disappearance of the operating point and result in reduced loading margins compared to the SNBs.

For both SNBs and LIBs, optimization methods can be used for the identification, as it will be seen in the following chapters.

1.4 PV Curves and Loadability Limits

1.4.1 Two-bus System

PV curves are used to represent the relationship between the load power consumption of a load or an area load and the bus voltage (or a representative bus of the area). This relationship stems from the long-term algebraic equations as explained before, for different values of the load parameter.

For example, in the lossless two-bus system of Fig. 1.4, the load bus voltage can be given by the following equation:

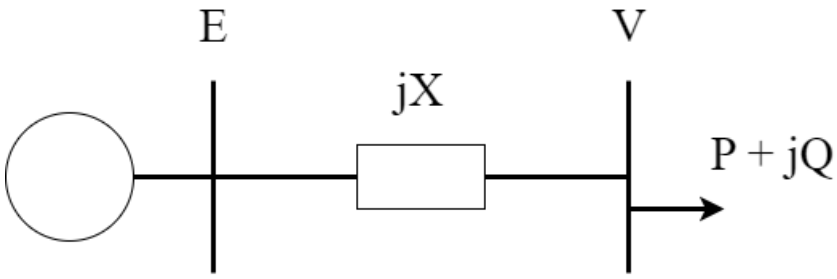

Figure 1.4: Lossless two-bus system

$$\tilde{V} = \tilde{E} - jX\tilde{I} \tag{1.26}$$

The apparent power consumed by the load is:

$$\begin{aligned} S = P + jQ = \tilde{V}\tilde{I}^* = \tilde{V}\frac{\tilde{E}^* - \tilde{V}^*}{-jX} \\ = \frac{j}{X}(EVcos\theta + jEVsin\theta - V^2) \end{aligned} \tag{1.27}$$

As a result the system of equations is as follows:

$$P = -\frac{EV}{X}sin\theta \tag{1.28}$$

$$Q = -\frac{V^2}{X} + \frac{EV}{X}cos\theta \tag{1.29}$$

and by eradicating θ from equations (1.28), (1.29) we get:

$$(V^2)^2 + (2QX - E^2)V^2 + X^2(P^2 + Q^2) = 0 \tag{1.30}$$

For the existence of at least one solution, the discriminant must be non-negative, so:

$$-P^2 - \frac{E^2}{X}Q + (\frac{E^2}{2X})^2 \geq 0 \tag{1.31}$$

Assuming that equation (1.31) can be satisfied, the two roots of equation (1.30) are given by the following equation:

$$V = \sqrt{\frac{E^2}{2} - QX \pm \sqrt{\frac{E^4}{4} - X^2P^2 - XE^2Q}} \tag{1.32}$$

In the three dimensional (P,Q,V) space, equation (1.32) creates a two-dimensional surface, where the upper part corresponds to the positive root of the equation while the negative corresponds to the lower part. The projection in the two-dimensional space (P,V) gives the PV curves. In Fig. 1.5, multiple curves are drawn for different load power factors, where $Q = Ptan\phi$.

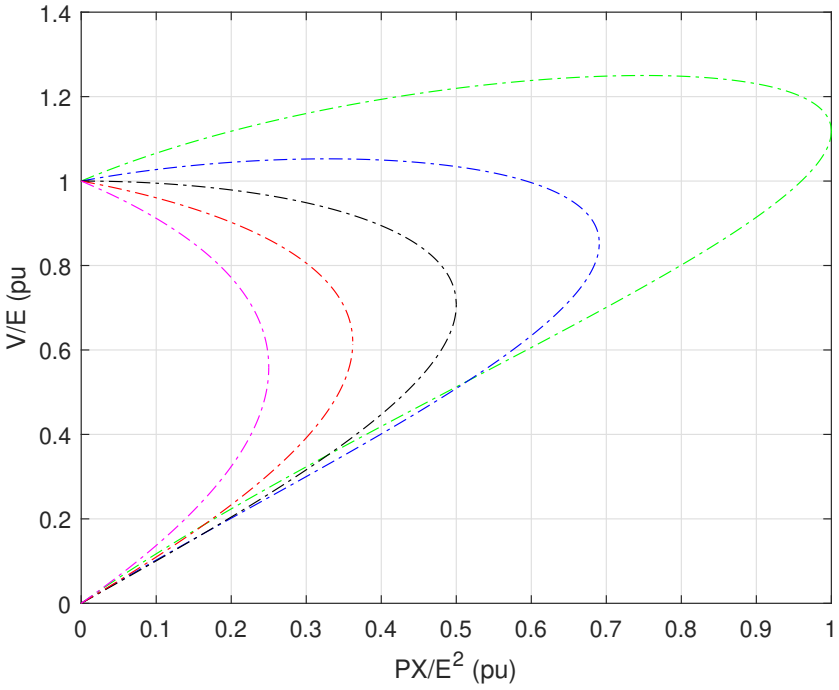

Figure 1.5: PV curves for different power factors

1.4.2 Loadability Limits

As described before, the points at which significant changes occur in the voltage stability of the power system are the bifurcation points of the nonlinear system model. These points also correspond to the loadability limits of the power system.

Assuming that the power system can be described in steady state by a set of n algebraic equilibrium equations in n algebraic variables which are denoted by the vector $\boldsymbol{u}$:

$$\boldsymbol{\phi}(\boldsymbol{u}, \boldsymbol{p}) = \boldsymbol{0} \tag{1.33}$$

where $\boldsymbol{\phi}$ is a vector of smooth functions, $\boldsymbol{p}$ is an n_p -dimensional vector of parameters.

Assuming that (1.33) describes the steady state of the power system and the set of network equations with both short-term and long-term state variables considered at equilibrium, then $\boldsymbol{\phi}$ corresponds to the set of equations $\boldsymbol{f}$ and $\boldsymbol{g}$, and (1.16)- (1.17) become (1.33).

Loadability limit is defined as the point where the independent demand parameters reach a maximum value, after which there is no solution of (1.33). If the load is considered as constant power the loadability limit corresponds to the maximum deliverable power to a bus, or a set of buses.

There is an infinite number of ways to reach a loadability limit, each "combination" of variables yielding a different particular limit. A loadability limit corresponds to the maximum of a scalar function ζ of $\boldsymbol{p}$, subject to equations (1.33):

$$\begin{array}{ll} \underset{p,u}{max} & \zeta(p) \\ subject & to \quad \boldsymbol{\phi(u,p)=0} \end{array} \tag{1.34}$$

The solution of the optimization problem satisfies the optimallity conditions known as the Karush-Kuhn-Tucker conditions [4]. The Lagrangian is defined as:

$$\mathcal{L} = \zeta(\boldsymbol{p}) + \boldsymbol{w^T \phi(u,p)} = \zeta(\boldsymbol{p}) + \sum_i w_i \phi_i(\boldsymbol{u,p}) \tag{1.35}$$

where $\boldsymbol{w}$ is the vector with the Lagrange multipliers. Then the derivatives of $\mathcal{L}$ with respect to $\boldsymbol{w, p, u}$ are set to zero, thus obtaining the following necessary, first-order optimality conditions:

$$\nabla_w \mathcal{L} = 0 \quad \Leftrightarrow \quad \boldsymbol{\phi(u,p)=0} \tag{1.36}$$

$$\nabla_p \mathcal{L} = 0 \quad \Leftrightarrow \quad \nabla_p \zeta + \boldsymbol{\phi_p^T w} = 0 \tag{1.37}$$

$$\nabla_u \mathcal{L} = 0 \quad \Leftrightarrow \quad \boldsymbol{\phi_u^T w} = 0 \tag{1.38}$$

where $\boldsymbol{\phi_u}$ and $\boldsymbol{\phi_p}$ are the Jacobians of $\boldsymbol{\phi}$ with respect to u and p, and $\nabla_p \zeta$ is the gradient of the scalar function ζ with respect to the vector $\boldsymbol{p}$. If $\nabla_p \zeta \neq 0$, ϕ_u is singular and solution of (1.34) corresponds to a SNB [12].

1.4.3 Loadability Surface

Let us consider a weak area that is prone to voltage instability and is fed from a larger healthy system through a transmission corridor. In this case, it has been shown [4], [13] that in an unstable scenario involving a load demand increase, the total consumption in the weak area will reach a maximum and will start decreasing with increased load demand before the actual stability limit is reached. This is shown graphically in the load power space of Fig. 1.6. This property is similar to a result proven in [14] using only power flow equations, according to which before a point of maximum power transfer at least one line feeding the receiving area will start reducing its active power transfer.

In the load power space of Fig. 1.6 both the consumed active power (varying with time) and the load demand are shown. The system is at equilibrium if the consumption is equal to the demand. The vertical axis represents the sum of active power in the affected area, while the horizontal axis is the sum of load active power in the remainder of the system. The points that constitute loadability limits (maximum power transfer points) form the dotted curve L, bounding the area of the load power space where solutions of the equilibrium equations exist and thus consumption can meet demand. The active power demand increase is plotted in Fig. 1.6 as a dashed line meeting the loadability curve at

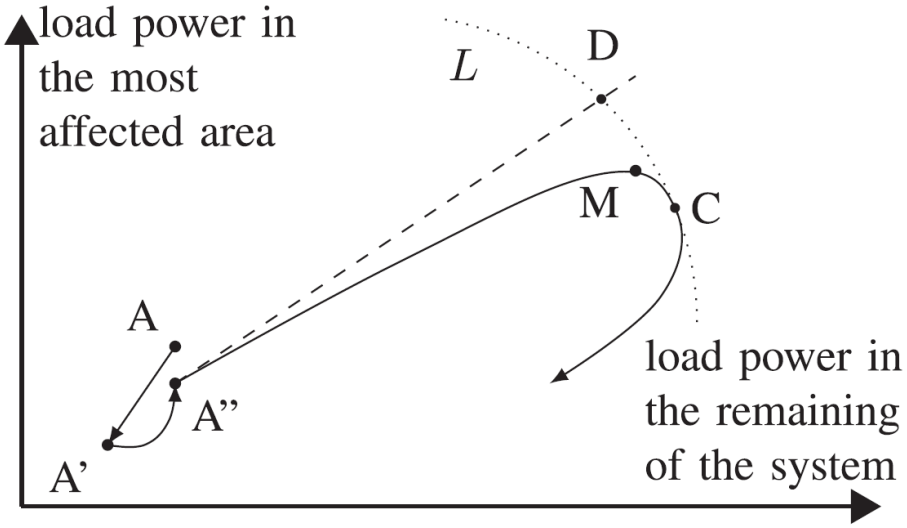

Figure 1.6: Loadability limits in load power space

point D, while the actual consumption is shown by a solid line hitting the loadability curve tangentially at point C and turning back since there are not solutions outside the loadability curve L. Clearly the consumption in the affected area reaches a maximum at point M before the instability limit (point C). After point M, the total active power consumption of the weak area will be reduced for further demand increase.

1.5 Voltage Security Margins

Power system security can be defined as the ability of the system to withstand without serious consequences a list of "credible incidents" or contingencies.

1.5.1 Contingencies

As mentioned VSM can computed taking also into account possible contingencies. For long-term voltage stability analysis, relevant contingencies are usually outages of transmission or generation facilities, especially under high loading conditions. Multiple contingencies may also represent a credible event, if they relate to a common cause of occurrence.

In accordance with Article 75 of Commission Regulation (EU) 2017/1485 of 2 August 2017 establishing a guideline on electricity transmission system operation, ACERs decision on the methodology for Coordinating operational security analysis (CSAM) classifies contingencies as follows:

1. Ordinary Contingencies
    - loss of a single line/cable
    - loss of a single transformer
    - loss of a phase-shifting transformer
    - loss of a single voltage compensation device
    - loss of a single component of a HVDC system such as a line or a cable or a single HVDC converter unit

- loss of a single power generation unit
- loss of a single demand facility

2. Exceptional Contingencies

   - loss of network elements having common fault mode, meaning that a single fault (such as a fault on a busbar, HVDC grounding system, circuit breaker, measurement transformer etc.) will lead to the loss of more than one network element
   - loss of overhead lines built on same tower
   - loss of underground cables built in same trench
   - loss of grid users having common process mode, meaning that the total or partial sudden loss of one grid user will lead to the total or partial loss of the others (for example: Combined cycle units etc.)
   - loss of network elements/users simultaneously disconnected as a result of the operation of a Special Protection Scheme
   - loss of multiple generation units (including solar and wind farms) disconnected because of a voltage drop on the network or system frequency deviation

3. Out-of-range Contingencies

   - loss of two or more independent lines
   - loss of two or more independent cables
   - loss of two or more independent transformers or phase shifter transformers
   - loss of two or more independent grid users (power generating unit or demand facility)
   - loss of two or more independent voltage compensation devices
   - loss of two or more independent busbars
   - loss of two or more independent components of a HVDC system such as lines, cables or HVDC converter units

1.5.2 Definition and problem statement

Even when the system state is voltage secure for a given operating point (base case), it is desirable to know how far the system can move away from the current operating point and still remain secure and stable. Thus, security margins can be calculated taking into account possible contingencies. Given a direction of stress, Loading Margin (LM) or stability margin indicates how much the system must be stressed to reach an unstable point or loadability limit. Voltage Security Margins (VSM) can be computed on the current operating conditions, in order to assess the system's ability to face a possible load increase, taking also into account the possible contingencies that may affect the systems stability point.

The change in parameter vector p along a stress direction is:

$$\boldsymbol{p} = \boldsymbol{p^0} + \lambda \boldsymbol{d} \tag{1.39}$$

so (1.33) can be rewritten as:

$$\boldsymbol{\phi}(\boldsymbol{u}, \lambda) = 0 \tag{1.40}$$

The optimization problem (1.34) can be rewritten including also the set of inequality constraints h, that relate to the operational limits and the generator capabilities, and will be detailed later:

$$\begin{aligned} \max \quad & \lambda && (1.41)\\ \text{subject to} \quad & \boldsymbol{\phi}(\boldsymbol{u}, \lambda) = 0 && (1.42)\\ & h(\boldsymbol{u}, \lambda) \leq 0 && (1.43) \end{aligned}$$

The concept is illustrated in the PV curves below, where load is assumed to restore to constant power. In Fig. 1.7, both pre-contingency and post-contingency margins are shown. In this case the margins represent the load increase from an initial operating point, with and without taking into account a possible contingency. It should be noted that in several cases, the post-contingency margin can be negative, meaning that the initial operating point is unstable under a specific contingency, as shown in Fig. 1.8.

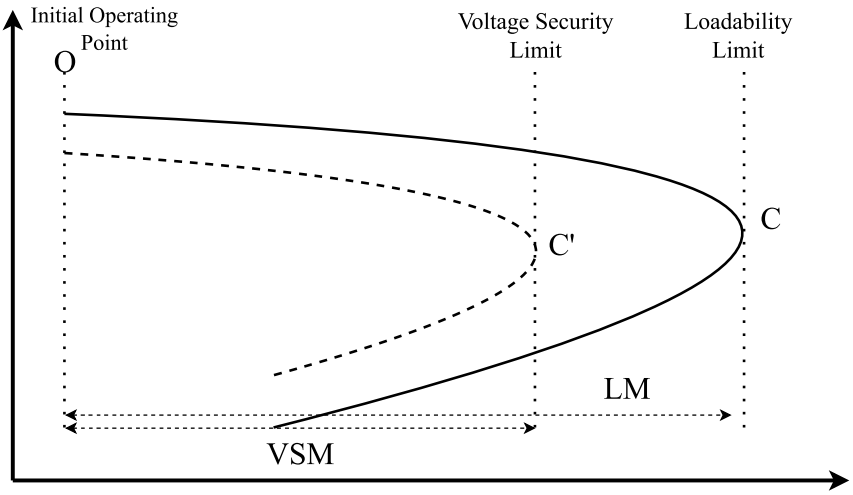

Figure 1.7: PV-curve of a positive post contingency loadability limit

It is important to notice that in the second case, the base operating point after the contingency is infeasible, meaning that the classic power flow solution would be unsolvable. However, the optimization problem of (1.42)-(1.43), will restore the solvability of the system, by determining the control actions needed or reduce the stress resulting in a negative VSM.

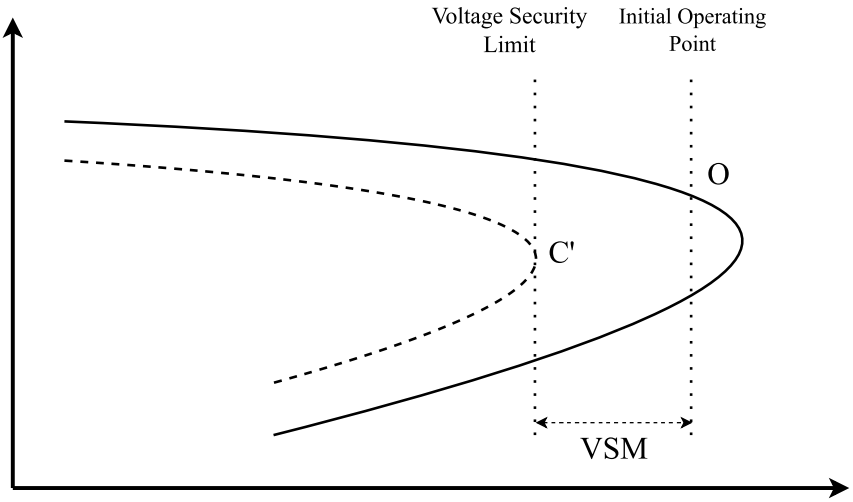

Figure 1.8: PV-curve of a negative post contingency loadability limit

1.6 Optimal Power Flow

In this thesis, the OPF will be used for voltage stability analysis, as well as for the optimization of the ADNs, so different formulations will be built for the transmission and the distribution network. The full AC OPF non-convex formulation will be used, as well as a convex relaxation of the OPF, mainly for the distribution network analysis.

The general problem of Optimal Power Flow (OPF) subject to equality and inequality constraints was formulated in 1962 [15], and later further extended [16]. In [17] a history of the OPF and its formulations is presented while in [18], a state of the art is presented regarding the OPF and its extension, the security-constrained OPF (SCOPF). The OPF model represents the problem of determining the best operating levels for electric power plants in order to meet demand, usually with the objective of minimizing operating cost. In addition, operational and security constraints can be incorporated to ensure secure system operation.

The OPF problem is a fundamental and complex optimization challenge in power systems engineering. It aims to find the most economic and efficient operating conditions for a power system, subject to various physical and operational constraints. The goal of the OPF problem is most commonly to minimize the overall cost of generation while ensuring that the system meets all operational and security constraints.

The OPF problem involves determining the optimal settings for control variables, such as generator output levels, transformer tap ratios, and reactive power settings, to usually achieve one of the following objectives:

- Minimize Generation Costs: The primary objective of the OPF problem is to minimize the total cost of generating electricity in the power system. This cost includes the fuel costs for thermal generators and the cost of purchasing power from external sources.

under some of the following constraints:

- Maintain Power Balance: The power generated by the generators should be equal to the total power consumed by the loads in the system to maintain power balance

and ensure that supply matches demand. This constraint is ensured by including the power flow equations of section 1.2.3 as equality constraints.

- Respect Equipment and System Limits: The solution must satisfy a wide range of constraints, including generator capacity limits, voltage limits, transformer tap changer limits, line thermal limits, and other operational and security constraints. These limitations are expressed in the OPF problems as inequality or bound constraints.

Mathematically, the OPF problem is formulated as a nonlinear, non-convex optimization problem. The objective function typically represents the total cost of generation, while the constraints incorporate the power balance equations, voltage limits, and other operational constraints. Other objectives of the OPF problem may include losses minimization, voltage control, voltage stability margin calculations etc. The constraints can be linear or nonlinear, depending on the complexity of the problem and the models used for various components.

Solving the OPF problem involves sophisticated optimization techniques, such as interior-point methods, gradient-based methods, or mixed-integer linear programming (MILP) solvers. Due to the non-convex nature of the problem and the large-scale nature of power systems, finding the global optimal solution can be challenging and computationally expensive. Therefore, heuristic and approximation methods are often used to find near-optimal solutions within acceptable time frames for real-world applications. Relaxations of the OPF have been also recently introduced to convexify the problem and increase solution speed and scalability.

The OPF problem plays a critical role in power system operation, planning, and market operation. It helps ensure the efficient and secure utilization of power system resources while promoting economic operations and grid stability. Additionally, with the increasing integration of renewable energy sources and the growth of smart grid technologies, the OPF problem becomes even more complex and crucial for the optimal functioning of modern power systems.

1.7 Active Distribution Networks

1.7.1 Definition

An active distribution network (ADN) is an emerging concept in the field of power systems, representing a paradigm shift from traditional passive distribution systems to more dynamic and intelligent infrastructures.

The proliferation of distributed energy resources (DER) has changed drastically the profile of the distribution network. Moreover, load profiles are significantly changing, especially with the introduction of Electric Vehicles (EVs). As a result, in order to increase the RES penetration as well as the load consumption, the distribution system must become active, meaning that it will be able to exploit the available control in the feeder. In that regard, distribution networks become Active Distribution Networks (ADN). One of the many definitions proposed is given by CIGRE WG C6.11 [19] as follows:

"Active distribution networks (ADNs) have systems in place to control a combination of DERs, defined as generators, loads and storage. Distribution system operators (DSOs)

have the possibility of managing the electricity flows using a flexible network topology. DERs take some degree of responsibility for system support, which will depend on a suitable regulatory environment and connection agreement."

ADN integrate DERs and advanced control technologies to actively manage electricity generation, distribution, and consumption at the distribution level. DERs include RES like solar photovoltaic (PV) panels, wind turbines, and small-scale hydro plants, as well as energy storage systems and demand response capabilities. The integration of these resources enables greater flexibility, efficiency, and resilience in the distribution grid, fostering a more sustainable and reliable energy supply. One of the primary features of ADNs is the ability to facilitate bidirectional power flows. Unlike traditional distribution systems, where electricity flows one-way from the central generation to consumers, ADNs allow for the injection of excess power from distributed resources back into the grid. This capability not only supports grid balancing but also encourages the growth of renewable energy adoption, reducing greenhouse gas emissions and enhancing energy sustainability. However, the integration of diverse DERs into the distribution grid introduces various technical and operational challenges. For instance, the intermittent nature of renewable energy sources poses uncertainties in power generation, leading to potential voltage fluctuations and stability issues. Additionally, the increased complexity of managing bidirectional power flows necessitates advanced control and communication systems to maintain grid stability and avoid overloading distribution lines.

Despite these challenges, active distribution networks offer numerous benefits for both utilities and end-users. For utilities, ADNs present opportunities for grid optimization and load management, reducing peak demand and deferring costly infrastructure upgrades. The implementation of smart grid technologies, such as advanced metering infrastructure (AMI) and distribution automation, further enhances grid visibility and control, improving overall operational efficiency.

For end-users, active distribution networks empower greater energy control and participation. Consumers can become prosumers, actively generating electricity and selling excess power back to the grid. Moreover, demand response programs allow consumers to adjust their energy consumption patterns in response to price signals or grid conditions, promoting energy conservation and cost savings.

In order for ADNs to be able to control their active components, at least some control system needs to be assumed in the form of some local controller. This local controller will be operated by some entity that can be either the distribution network operator (DNO) or an aggregator and will be responsible for the monitoring of the ADN and the actuation of the controls. In Fig. 1.9, a simple schematic of ADN is presented, where DG can be found, battery energy storage systems, EVs or EV charges and loads.

Lastly, the responsible entity will have to be in coordination with the respective transmission system operator and be able to exchange at least minimum information. In that respect, it is important for countries to adopt and implement proper legislation in order to fully exploit the distribution network. The Swiss TSO for example, already provides incentives for reactive power provision from the distribution side under certain circumstances [20]. Minimum requirements are also stated in VDE-AR-N 4141-1 [21] for TSO/DSO coordination.

In this thesis, since the time scale of interest is the one required for long-term voltage stability analysis, for all components used also in the distribution network, fast dynamic

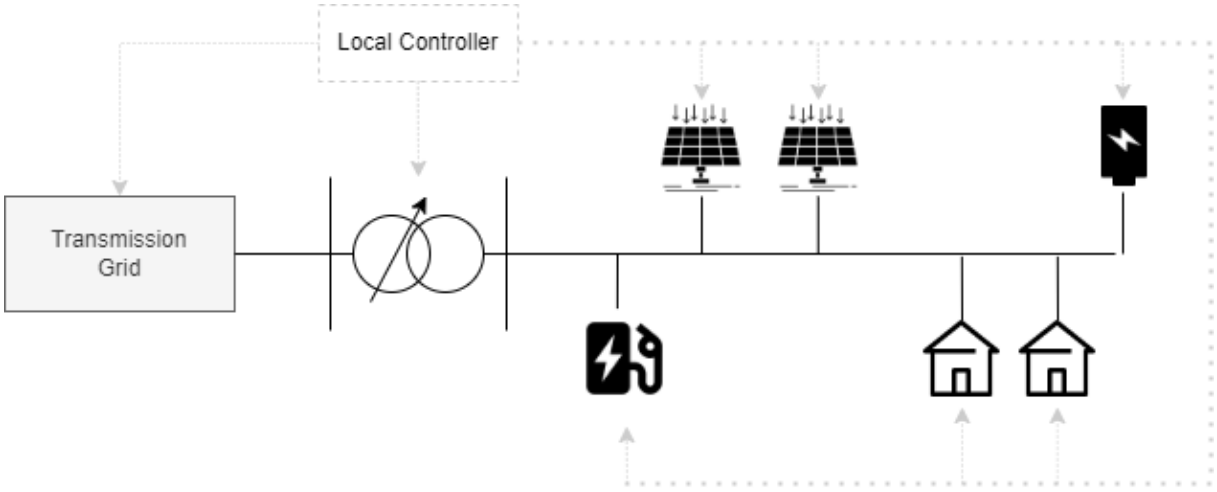

Figure 1.9: Active Distribution Network

responses will be neglected.

1.7.2 Inverter based resources

Inverter based resources (IBR) refer to all appliances that are connected to the utility grid through inverters. Terms like Converter Interfaced Generation (CIG) or Inverter based generation (IBG) are also used in the literature and usually refer to distributed or dispersed generation (DG) connected to the grid through power electronics. In this thesis the term IBR will be mainly used in order to include all kind of resources that can be connected through inverters such as distributed generating units and battery energy resources, or in some cases both.

Inverter-based resources encompass a wide range of distributed energy technologies, including solar photovoltaic (PV) systems, wind turbines, battery energy storage systems (BESS), and electric vehicle (EV) chargers. The distinctive feature of IBRs is their use of power electronic inverters to convert DC electricity from renewable sources or batteries into AC electricity compatible with the grid. This enables seamless integration of these resources into the distribution network, allowing for bidirectional power flows, voltage regulation, and grid support capabilities.

An IBR is a key component of active distribution networks and plays a crucial role in the integration of renewable energy sources and energy storage systems. This thesis paragraph delves into the significance, challenges, and advantages of inverter-based resources in the context of modern power systems.

The integration of inverter-based resources brings several benefits to the power system. Firstly, IBRs significantly increase the share of renewable energy in the energy mix, fostering sustainability and reducing dependence on fossil fuels. Solar PV systems and wind turbines generate clean energy, mitigating greenhouse gas emissions and combating climate change. Secondly, the deployment of battery energy storage in IBRs enhances grid resilience by providing backup power during outages and balancing supply-demand fluctuations. Batteries can store excess renewable energy during periods of high generation and release it during peak demand, thereby improving grid stability and reliability.

Despite these advantages, the proliferation of inverter-based resources also poses chal-

lenges to power system operation. The intermittency of solar and wind resources leads to variability in power generation, necessitating effective forecasting and control mechanisms to manage the grid's dynamic conditions. The voltage fluctuations caused by sudden changes in IBR output require advanced voltage regulation schemes to ensure grid stability and quality of supply. Furthermore, the integration of a high number of IBRs raises concerns about grid protection, islanding, and the potential for grid resonance issues. Addressing these challenges requires sophisticated control and coordination strategies. Advanced power electronics and control systems are essential to manage the bidirectional power flows and maintain grid stability. Additionally, grid operators and utilities need to develop robust energy management systems that can effectively monitor, predict, and control the behavior of inverter-based resources in real-time.

As mentioned before, power electronics have very fast response as they operate at switching frequency. In that sense, regarding voltage stability studies it is safe to assume that fast dynamics are at equilibrium between steady state points. More specifically, for the QSS approximation it can be assumed that their active and reactive power output is at steady state equilibrium in every step of the simulation. For the load flow and consequently for the OPF, they can be represented by PV buses, taking also into consideration current limits.

As seen in Fig. 1.10, IBR considered in this thesis may include wind farms (WF) or photovoltaics (PV) with or without battery energy storage systems (BESS). It is assumed that in case there is storage alongside with generation, both are connected to the grid through the same bi-directional converter, meaning that the converter is capable of both absorbing and injecting power to the grid. In most cases, power electronics consist of DC/DC boost converters, mainly for voltage step-up, and a DC/AC inverter for the connection the grid. Some types of wind tourbines like doubly-fed induction motors (DFIG) are connected through an AC/DC and a DC/AC converter.

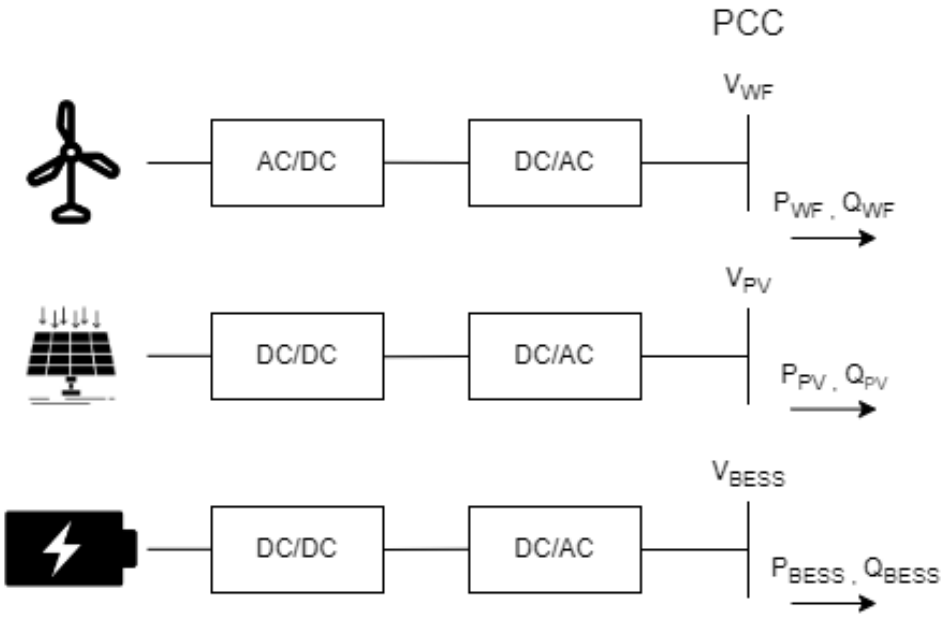

Figure 1.10: Inverter Based Resources

IBRs and the services that they are able to provide have been studied a lot in the recent literature. Several control schemes have been reported mainly for voltage control in the

distribution networks [22] and [23]. In [24], the authors propose a voltage-frequency control in order to improve the dynamic response of the system.

In conclusion, inverter-based resources play a vital role in the transformation of power systems towards active distribution networks. Through their ability to convert and control renewable energy sources and storage systems, IBRs contribute to sustainability, grid flexibility, and customer empowerment. However, the integration of inverter-based resources requires overcoming technical and operational hurdles to ensure the secure and efficient functioning of modern power systems. By addressing these challenges and capitalizing on the advantages offered by IBRs, power systems can pave the way for a greener, more resilient, and customer-centric energy future.

In this thesis, IBRs will be widely exploited in order to support transmission's system needs and mainly voltage stability problems. Moreover, the flexibility provision will be studied on the side of the distribution grid.

1.8 Literature Survey

In this section, the extensive literature review that has been conducted is presented, covering subjects that extend from system stability issues and mainly voltage stability, to the distribution networks and their flexibility. The literature is divide into three main subjects:

- Optimal Power flow for Voltage Stability Margins
- Voltage Stability and Optimization in Presence of Distributed Generation and Energy Transition
- Active Distribution Networks and ancillary services, TSO-DNO coordination
- On Flexibility and Feasibility of Active Distribution Networks

1.8.1 Optimal Power flow for Voltage Stability Margins

The Voltage Stability Problem also explained in Section 1.5, is a continuing concern for every Transmission System Operator (TSO) and is covered in [4], [25].

The voltage stability problem, has also been expressed as a maximization problem of the system loadability, as a variant of the classic OPF, firstly presented in [16]. Use of the OPF problem for voltage stability and bifurcation points estimation has been investigated in the literature [26] [27] [28] [29] and has been compared to other methods such as the continuation power flow. The equivalence of a maximum power transfer condition to a static bifurcation has been established in [4] [12] and [30]. As also explained in [31], the main advantage of optimization methods is that they are capable to include both economic and technical aspects of voltage instability mitigation.

Paper [31] uses the OPF formulation to maintain post contingency voltage security in the presence of voltage depended demand-response, taking also into consideration the cost minimization. In [31], the solution of the optimal Voltage Security Cost is examined, taking into account voltage dependency of loads, meaning that on-load tap changing transformers (OLTCs) are assumed locked, to prevent worsening the system condition. However, that would mean low voltage conditions on the distribution side as well. In this

thesis, full load restoration is assumed by the LTCs, and thus in the transmission system, loads are considered as constant power. In that way, it is possible to decouple and study separately the transmission and the distribution network.

1.8.2 Voltage Stability in the Presence of Distributed Generation

With the proliferation of Converter Interfaced Generation (CIG) [32], TSOs will also need to take into consideration the uncertainty that is incorporated in the Renewable Energy Resources (RES). On the other hand, fast response of converters, through which RES are usually connected, offers new chances for distributed control and support for all types of stability problems, including voltage stability.

Technical Report [33], explains how the penetration of DERs can have an impact on the overall steady state and dynamic behaviour of the bulk power system. Also, how increased generation in the distribution networks can cause reverse power flows and overvoltages. A DN with high penetration of DERs responds dynamically to system disturbances and therefore affects overall power system stability and dynamic behavior. DER, when properly controlled can provide support to the upstream network by supporting the reactive power needs of the loads (at the distribution level) and flow reduction in case of congestions by supplying the demand at the distribution level. Control can be basically exercised by exploiting the power electronic converters used to interconnect most types of DER.

Paper [34] investigates the effect of reactive support by Wind Farms (WF) on the maximum power transfer, and thus the voltage stability limit of a transmission system. Converter current limits, as well as the overvoltage limitations on the MV feeder, are taken into consideration in assessing the effect of the WF support.

Thesis [35] examines the impact that the converter of the wind parks, connected to the system through dedicated medium voltage distribution feeders, can have on the voltage stability of the bulk power system. The stochastic nature of wind generation is also examined. The work validates the theoretical results on the Greek power system for a specific test case. Contrary to [35], in this thesis the effect of the loads connected to the same feeder with DER is included in the modelling.

1.8.3 ADNs and ancillary services, TSO-DNO coordination

Introduction of active distribution networks has also driven a lot of research in the management and control of the distribution grids [36], [37]. Moreover, interest is growing in exploiting ADNs for the purpose of supporting the transmission system. For example, [38] introduces a non-intrusive voltage emergency control scheme based on the synchronization of distributed generating units (DGU) and the load tap changer of the corresponding distribution transformer. The conclusions are derived from time-domain simulations using an extended version of the IEEE Nordic test system for voltage stability assessment. Moreover, [9] evaluates the CIG impact on instability onset and determine the performance of a voltage instability monitoring method, as well as of three protection scheme variants. Different CIG connection topologies, as well as reactive control modes are examined. Conclusions drawn show significant impact of CIGs and demonstrate the need for specific countermeasures design that account for CIG interaction with traditional protection measures. While both works seem to support the system in case of emergencies,

neither guarantees that the actions taken are always in the right direction or fully exploit the available assets.

In [39], a case study is examined, where a distribution network with high integration of dispersed generation is used to deal with a long-term voltage instability. The reported simulations show the impact of distribution network voltage restoration, as well as the benefit of load voltage reduction actuated by the dispersed generators.

In [40], an OPF problem is formulated on an ADN to ensure dynamic voltage security after possible islanding and provide resilience to the power system. Last but not least, A co-optimization model of transmission and distribution systems is examined in [41], for optimal day-ahead battery energy storage scheduling under voltage security constraints.

Active distribution networks highlight the need for even more coordinated operation between the Transmission and the Distribution System. Authors in [42], perform a review on the status-quo regarding the TSO-DSO coordination models and presenting advantages and disadvantages. In [20], it is pointed that some TSOs (such as the Swiss TSO), already provide incentives for reactive power provision from the distribution side under certain circumstances. Minimum requirements are also stated in VDE-AR-N 4141-1 [21] for the TSO/DSO coordination. In [43], a scheme is presented to regulate flows at the interconnection between the TSO and the DSO.

1.8.4 On Flexibility and Feasibility of Active Distribution Networks

The terms 'smart grids' and 'active distribution networks' are heavily used in the most recent literature and mainly rely on the flexibility that can be provided from the distribution network. This flexibility stems from the controllable components that are ever increasing and form the future distribution grids.

The term operational flexibility or flexibility region of ADNs has been introduced in the recent literature to describe the amount of the regulating capacity that ADNs can provide in terms of active and reactive power, while satisfying their own operational constraints. Operational flexibility or flexibility region is translated into the active and reactive power exchange in the point of common coupling (PCC) between the transmission and the distribution network and the ability of each ADN to control these flows through it's own resources. Operational flexibility is translated into the active and reactive power exchange in the point of common coupling (PCC) between the transmission and the distribution network and the ability of each ADN to control these flows through it's own resources. Alternatively the same service is referred to as Reserve [44], or Ancillary Service [45] Provision. Authors of [44], propose a method to define a convex reserve provision capability area of an ADN by creating a linear scenario-based optimization problem and searching in multiple directions, starting from a base operating point.

The authors in [46] and [47] make a distinction between the terms 'feasibility' and 'flexibility'. More specifically, feasibility is described as the feasible operating region of the distribution network, which is considered as a virtual power plant (VPP). On the other hand, the temporal ability of the VPP to move between two set points inside the feasible operating region, is described as flexibility. Different flexibility regions are assumed depending on the service provisions they offer and the time horizon they can be activated.

In [48] authors see operational flexibility as a link between diverse operational require-

ments and the flexible adjustment capabilities of controllable resources. Also, they distinguish the operational flexibility into the Flexibility Provision and the Flexibility Availability. Flexibility provision is defined as the regulating capacity that ADNs can provide, subject to operational requirements while satisfying constraints. Flexibility availability is defined as the available regulating capacity that ADNs can further provide, while secure constraints and diverse operational requirements are both satisfied. FA is a portion of the flexibility provision. Authors use a Monte Carlo approach to estimate the flexibility regions they defined.

Authors in [49] propose a framework in order to estimate the time-variant flexibility of an ADN to provide ancillary services across voltage levels by the regulation of the power flow over the transmission-distribution interface. It is shown that the flexibility region can be approximated by a polygon and uncertainty is taken into account for future time-intervals. The flexibility region is estimated by generating random control scenarios for the decision variables of the ADN.

The work in [50], proposes an optimization-based method to provide a practical answer to the flexibility estimation problem – where the concept of distributed flexibility includes the margins of decision offered by aggregators in the electricity market, non-firm connection contracts, as well as OLTCs and the DSO reactive power compensation devices. The authors compare the simulation results with a random sampling algorithm showing that they identify bigger flexibility regions and in shorter times.

While [51] mainly focuses on a dynamic reduced order equivalent of an ADN, it also poses the very significant question of convexivity of the flexibility region of the ADN and attempts to find a convex core of the region.

More specifically, in [48], authors try to define and quantify this operational flexibility provision and availability of ADNs using the linearized DistFlow model and Monte Carlo simulations. The time-dependent flexibility in order to control the TSO-DSO interconnection power flows is calculated in [49], by determining a feasible operating region with a random number sampling approach. Authors of [44], propose a method to define a convex reserve provision capability area of an ADN by creating a linear scenario-based optimization problem and searching in multiple directions, starting from a base operating point. The works in [50], [45] also define the flexibility area in the PQ plane, but using non-linear OPF formulations, with the former one also including different levels of flexibility costs. In the aforementioned works, authors ensure implicitly or explicitly the convexity of the flexibility region but that is not always the case. In [51], the authors address this issue and define a core of the non-convex flexibility region.

1.9 Objective and outline of the thesis

1.9.1 Research Gap

This thesis seeks to address some issues that have been left out of the literature. For example, while contribution of dedicated feeders with wind farms to voltage stability of the transmission system has been examined, only a few papers consider extended distribution networks that host multiple DGs and loads. Due to the fact that the power generation in the distribution side is ever increasing, ADN contribution becomes all the more relevant. One very important problem when dealing with voltage stability issues is to ensure that

corrective actions taken will not have adverse effects, thus making the problem more severe. In that sense, while some recent literature has addressed the effect of ADNs in the stability of a power system, and some heuristic rules of thumb have been proposed, little references have been found where the proposed control is optimized, ensuring that the control taken in the distribution network will help the transmission system as much as possible. This thesis deems to fill that gap by creating an optimization frameworks to maximize systems stability limits. Last but not least, different methods for computing the ADN flexibility region are examined in the thesis. While some of them have already been proposed in recent bibliography, in the thesis the selected methods are compared and implemented in different feeders. Moreover, flexibilities are applied in the formulation of centralised problems for voltage stability support of the transmission system, which is an approach not studied in the literature, to the author's knowledge. As a result, including Flexibility Regions in centralized Optimization problems for voltage stability issues is a novel contribution of this Thesis. Moreover, regarding the fast estimation of the flexibility regions of ADNs, a convex relaxation of the OPF is proposed, that has not been used in previous literature.

1.9.2 Objective

As discussed above, the main scope of this Thesis is to establish ways in order to achieve support from the distribution network to the transmission system in terms of voltage stability, usually following a grid disturbance such as the loss of an important transmission line, or other major contingency. A first thesis objective is to examine existing regulations and directives on fast current injections for system-connected RES with emphasis on how this control (which is originally proposed for short-circuit current contribution) can impact voltage stability margins of the transmission system, in cases where a voltage stability contingency induces the low-voltage, instead of a fault.

Other thesis objectives refer to the distribution system side. In general, coordination between TSOs and DNOs is limited, so determining ways to obtain support from the distribution system can be quite challenging. For this reason, two different approaches are proposed in this thesis, relying on both distributed and central optimization. Both approaches solve the transmission and distribution problems separately. The two problems are coupled through limited data exchange for the support of the transmission system between the Control Centre at the transmission level (Energy Management System-EMS) and the local controllers of the respective active distribution networks. The distributed optimization approach aims at solving a central problem at the EMS level, without including data from the ADNs, except for the active and reactive power injections at the HV side of the substations. Then, sensitivities are distributed to the ADNs with request to support the system, in case of an emergency. This approach ensures that the control actions taken from the ADNs will be in the correct direction in terms of supporting the system which is undergoing a voltage stability emergency situation. In that sense, the distribute optimization approach is considered as a corrective control measure. The second optimization approach that will be developed in the thesis, assumes more data exchange between the TSO and DNO, as the ADNs are requested to provide flexibility regions around their current operating point, defining their ability to change their active and reactive power flows at the PCC. These flexibility regions can then be used at the EMS level to solve a VSM optimization problem. This approach can be considered as a preventive control measure. Both schemes are applied on test systems, in order to

evaluate the provided support in terms of voltage stability margin extension offered by the ADNs. The support optimization schemes are simulated using a time domain QSS simulator (WPSTAB), in order to evaluate their impact.

A real system incident form the Hellenic interconnected System is also examined and analyzed with the techniques that were developed in this thesis.

1.9.3 Outline

In the next Chapters the modelling used in this thesis is presented for both the transmission and the distribution system and the VSM problem for the transmission system is explicitly formulated. Then the above different approaches in order to support the transmission system in terms of voltage stability, from the distribution network and its assets are detailed and compared. More specifically, the thesis is structured as follows:

This first chapter explains briefly some of the basic concepts that are relevant to the research, some mathematical background related to the modelling of power systems as sets of differential-algebraic equations and the stability issues that occur, with emphasis on the voltage stability problem and the long-term equilibrium conditions. Moreover, it introduces the terms of active distribution networks and the inverter-based resources connected to them. Finally, it provides an extensive literature review on the existing bibliography, mainly around the subjects of voltage stability in Power Systems, OPF, Active Distribution Networks and flexibility of ADNs.

Chapter 2 aims at describing the modelling used for the transmission system and extensively describes the OPF formulation of the transmission system for the calculation of the Voltage Stability Margins, including the modelling of equipment such as generators, shunts, etc, with the objective of calculating the transmission system voltage security margins. The formulation is applied on a simple transmission corridor and to a more complex transmission test system and compared to the WPSTAB (QSS) simulations.

The third chapter examines the effect of current RES injections on the VSM. Based on the European regulations for fast current injections the OPF for the VSM of chapter 2 is reworked to include the current injections of system-connected RES on the formulation after a contingency. Results include optimal parameterization on a simple test feeder.

In the fourth chapter, the modelling of the active distribution networks is described and a constrained optimization problem is formulated with the objective of modifying the flows at the point of common coupling (PCC) with the transmission system. Moreover, three different test feeders are introduced, including a simple dedicated wind park feeder, a 30-bus test feeder and a real 20kV distribution rural feeder in the Greek region. Last but not least, in this chapter the term of flexibility region is introduced and three different approaches are developed to calculate it. For the flexibility region, a novel polygon approximation method is proposed.

Chapter 5 describes the two approaches used for the support of the transmission system in terms of the voltage stability margin, by the ADNs. A corrective (distributed) and a preventive (centralized) approach are formulated. The corrective approach is distributed optimization approach to maximize the VSM, in emergency conditions, after a critical contingency has occurred. The approach relies on a two-stage optimization framework, formulating two separate OPF problems that are coupled together via sensitivities. The framework is also applied in a test transmission system, which is then also simulated

using time-domain simulations. The second, preventive approach is a central optimization problem, taking into account flexibility of ADNs. More specifically, the ADNs calculate their flexibility regions, using one of the approaches of Chapter 4, and then provide them to the central optimization problem of VSM. Optimal reference values are then calculated for the active and reactive power absorptions at the PCC of each ADN. The optimal values are then sent back to the ADN controllers so that the suitable controls are taken. A final optimization problem is formed for that reason, as controls that achieve optimal setpoints are not obvious.

Chapter 6 proposes a fast method to approximate the flexibility region of Active Distribution Networks by formulating a relaxation of the OPF of Chapter 4, using a Second Order Cone Programming OPF formulation. The formulation is used on the same feeders as in chapter 4.

Finally, Chapter 7 implements the VSM formulation of the OPF in order to examine a real incident on the Hellenic Interconnected System. Moreover, an optimization on the possible RES injections is performed to examine the increase in the VSM. The conclusion of the Thesis and the main points, as well as prospects for future area are presented in the final 8th Chapter of the Thesis.

Chapter 2

Transmission System Modelling and Optimal Power Flow for Voltage Stability Margins

2.1 Overview

In this chapter, the Optimal Power Flow (OPF) for the Voltage Stability Margin (VSM) determination will be formulated for the transmission system, including all constraints taken into consideration.

As described in Section 1.1.3, voltage stability stems from the attempt of the load dynamics to restore power consumption beyond the capability of the combined transmission and generation system [4]. OPF formulations have been used to identify the loadability or voltage stability limits and margins of power systems. As also explained in section 1.3, loadability limits are met in general at a saddle-node bifurcation of long-term dynamics. In [30] it is proven that the optimality conditions of the solution points of the OPF problem for the VSM, yield the transversality conditions of the bifurcation points of the non-linear set of equilibrium equations.

As a result, loadability margin (LM) can be defined as the solution of an optimization problem, where the system load is increased considering a specific stress direction to its maximum, subject to the long term equilibrium conditions. At the solution point, the dynamical system (load restoration) undergoes a static bifurcation. In this case equilibrium corresponds to the power flow equations, assuming full load restoration in the long-term, as seen by the HV buses of bulk delivery substations. In practice, P and Q load restoration is achieved indirectly by LTCs restoring the distribution side voltage, regardless of the short-term load sensitivity to voltage (if deadband effect and tap range limits are neglected). This formulation assumes that the transmission system ends at the HV side of the HV/MV transformers and the loads are seen as equivalent active and reactive power absorptions.

Let $\mathcal{N}$ be the set of buses and G the subset of generators. Starting from a given initial operating point, a stress direction is assumed, along which load and generation is increasing

with one degree of freedom according to:

$$p_{dk} = p_{dk0} + \lambda d_{pk}, \quad k \in \mathcal{N} \tag{2.1}$$
$$q_{dk} = q_{dk0} + \lambda d_{qk}, \quad k \in \mathcal{N} \tag{2.2}$$

where $\boldsymbol{d}_p$ and $\boldsymbol{d}_q$ are vectors defining the active and reactive power stress direction, and λ is a scalar corresponding to the level of stress. Generation pattern is discussed in Section 2.4.

2.2 Objective function

As already mentioned, VSM is obtained by solving the optimization problem for maximizing the total load increase from the current operating point:

$$\Delta P = \lambda \sum_{k \in \mathcal{N}} d_{pk} \tag{2.3}$$

subject to long-term equilibrium constraints. Since (2.3) has no unconstrained maximum, the maximization corresponds to the point where the long-term equilibrium point disappears, i.e. where the system undergoes a static bifurcation. Thus, ΔP_{max}, corresponds to the VSM along the specified stress direction. The static bifurcation point may correspond to a saddle node or a limit-induced bifurcation point depending on the condition violated at the solution.

It should be noted, that the stress direction can correspond to the total load of the system or specific area loading patterns, depending on the case. Also, as explained in 1.5, the margin can correspond to either pre-contingency state (LM) or to a post-contingency situation (Voltage Security Margin).

2.3 Power balance equations

The power balance or power flow equations equations as described in (1.23), (1.24), stem from Kirchhoff's laws and can be also written either in polar form or rectangular form (Cartesian coordinates). The bus voltage phasor for bus k expressed in rectangular coordinates and its magnitude squared are expressed as:

$$\tilde{V_k} = e_k + j f_k, \quad k \in \mathcal{N} \tag{2.4}$$

$$y_k = e_k^2 + f_k^2 = V_k^2 \tag{2.5}$$

while, active power generation is equal to:

$$p_{gk} = p_{gk0} + \Delta p_{gk}, \quad k \in G \tag{2.6}$$

for buses where there is a generating unit, while for the rest buses, if:

$$p_{gk} = 0, \quad k \notin G, \quad k \in \mathcal{N} \tag{2.7}$$

Superscript '0' refers to the steady state (long-term equilibrium) conditions of the transmission system either pre- or post-contingency.

As in (1.22), the net active and reactive power injection at each transmission bus is given by:

$$p_k = p_{gk} - p_{dk}, \quad k \in \mathcal{N} \tag{2.8}$$
$$q_k = q_{gk} - q_{dk}, \quad k \in \mathcal{N} \tag{2.9}$$

and the equilibrium conditions of the network are given by the power flow equations, where the vectors $\boldsymbol{g_k}$, $\boldsymbol{b_k}$ are the real and imaginary parts respectively of the k^{th} column of the bus admittance matrix where:

$$\boldsymbol{Y_k} = [\boldsymbol{g_k} + j\boldsymbol{b_k}], \quad k \in \mathcal{N} \tag{2.10}$$

so, following the formulation of equations (1.23), (1.24) in Chapter 1,

$$\boldsymbol{h}(x) = \begin{bmatrix} \boldsymbol{h_p}(x) \\ \boldsymbol{h_q}(x) \end{bmatrix} = \begin{bmatrix} p_k - e_k(\boldsymbol{g_k}^T\boldsymbol{e} - \boldsymbol{b_k}^T\boldsymbol{f}) - f_k(\boldsymbol{b_k}^T\boldsymbol{e} + \boldsymbol{g_k}^T\boldsymbol{f}) \\ q_k + e_k(\boldsymbol{b_k}^T\boldsymbol{e} + \boldsymbol{g_k}^T\boldsymbol{f}) - f_k(\boldsymbol{g_k}^T\boldsymbol{e} - \boldsymbol{b_k}^T\boldsymbol{f}) \end{bmatrix} = 0 \tag{2.11}$$

Equations (2.11) will serve as the equality constraints of the optimization problem corresponding to the power balance equations.

2.4 Distributed slack bus

The objective of the optimization problem as described in 2.3, is the change in the loading of the system, which corresponds also to a change in the generation that has to be dispatched to each generating unit.

In order to realistically distribute the shift in load among the generators of the system, a distributed slack bus approach is introduced. This approach approximates the automatic generation control (AGC), or the primary frequency control in the absence of AGC and is based on participation factors of individual generators. Generator participation factors are grouped in vector K_k and are normalized to sum up to 1,

$$\sum_{k \in G} K_k = 1 \tag{2.12}$$

The total shift in active generation must cover the change in the total load (2.3), as well as additional transmission losses that are due to the increasing system stress. Consider initial system losses:

$$L = \sum_{k \in G} p_{gk0} - \sum_{k \in N} p_{dk0} \tag{2.13}$$

which during the stress, will change by ΔL:

$$\Delta L = \sum_{k \in G} p_{gk} - \sum_{k \in N} p_{dk} - L = \sum_{k \in G} \Delta p_{gk} - \sum_{k \in N} \Delta p_{dk} \tag{2.14}$$

Using ΔL as a slack variable, the change of each generator's (2.6) active power is given by:

$$\Delta p_{gk} = K_k(\Delta L + \lambda \sum_{k \in \mathcal{N}} d_{pk}) \tag{2.15}$$

Clearly by adding up all shifts in generators Δp_{gk} of (2.15), results in (2.14). Thus, the latter is not an independent equation and is not part of the optimization problem. The slack variable ΔL is balanced by arbitrarily setting one f_k to zero for the reference bus.

Generators obviously are limited in terms of active power by the nominal active power of their turbine p_n. As a result, the first constraint regarding the active power generation is:

$$p_{gk}^{min} \leq p_g \leq p_{gk}^{max}, \quad k \in G \tag{2.16}$$

In case an active power generation reaches its upper or lower limit, the vector K_k needs to be re-defined so that (2.12) still stands. Here this is solved by checking p_{gk} constraints at the solution point and resolving the problem iteratively, when necessary.

2.5 Synchronous generator Q constraints

The VSM is heavily affected by the reactive capabilities of synchronous generators and it is crucial to properly represent in the constraints of the optimization problem both armature and field current limits for every synchronous machine $k \in G$. For simplicity of the presentation the subscript k is omitted in the following subsection. Obviously, active power limits are also taken into consideration, as explained above. In this thesis under-excitation limits are not considered, as in most cases under-excitation limits are not met in operation related to voltage drop and voltage stability, where generators tend to be over-excited.

2.5.1 Armature Current Limits

If I_n is the maximum rated current, then from the definition of apparent power:

$$I_n = \frac{S_n}{V_n} \tag{2.17}$$

So, the active current limit inequality constraint is written as:

$$q_g \leq q_a(p_g, V_g) = \sqrt{(V_g I_n)^2 - p_g^2} \tag{2.18}$$

or,

$$q_g^2 + p_g^2 \leq (V_g I_n)^2 \tag{2.19}$$

2.5.2 Field Current Limits - Saturated Machine

Again the reactive power limit, taking into account the emf corresponding to the field current limit E_{lim} and magnetic saturation, is a function of generated active power and voltage. Saturation is expressed with the use of saturation factor $K < 1$ given by [4]:

$$K = \frac{1}{1 + mV_l^n} \tag{2.20}$$

where m, n are saturation coefficients and the air-gap emf V_l is a function of generator voltage and loading:

$$\hat{V}_l = V_g + jX_l \frac{p_g - jq_g}{V_g} \tag{2.21}$$

where X_l is the leakage reactance and stator reactance is neglected. Note that from the above complex equation only the magnitude of $\hat{V}_l$ needs to be calculated.

Saturation factor K is affecting both saturated emf and saturated d-axis reactance. Thus at the rotor current limit:

$$E_{qs} = KE_{lim} \tag{2.22}$$
$$X_{ds} = X_l + KX_{ad} \tag{2.23}$$

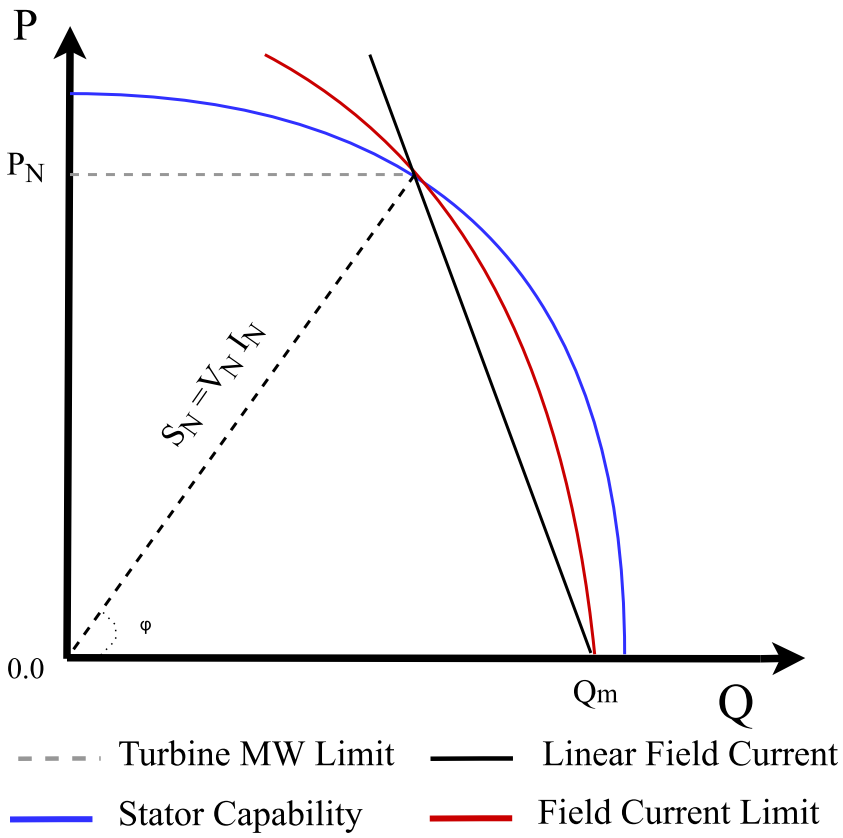

Figure 2.1: Synchronous Round Rotor Machine Capability Curve

In Fig. 2.1, the generator capability curve is shown for nominal voltage V_N. The rotor current limit is approximated in this work with a linear approximation joining the stator current limit for $p = p_N$ with the point of maximum reactive power generation Q_m for $p = 0$ considering the level of saturation of the machine. Thus Q_m is defined as:

$$Q_m = \frac{V_g}{X_{ds}}(E_{qs} - V_g) \tag{2.24}$$

and the linear approximation of the field current limit is given by:

$$q_r(p_g, V_g) = Q_m - \gamma p_g \tag{2.25}$$

with the slope γ given as:

$$\gamma = \frac{Q_m - \sqrt{(V_g I_n)^2 - p_n^2}}{p_n} \tag{2.26}$$

Equations (2.18) (2.25) shape up the inequality constraints of the optimization problem, regarding the reactive power limits of the synchronous machines. In essence, it is a set of 5 extra non-linear equations that are added to the set of equality constraints of the optimization problem.

2.6 IBR injection constraints

Constraints for the IBR injections are also taken into consideration, as it is quite common for RES with high installed capacity, to be directly connected to the high voltage transmission system through converters.

Converters cannot violate over-current limitations, even for a short amount of time. The maximum permissible current has to cover nominal apparent power S_n under nominal voltage V_n. As a result, the limit for the current of the converter is set as:

$$I_n = \frac{S_n}{V_n} \tag{2.27}$$

Since, IBRs may operate in off nominal voltage, the reactive power constraint is given by the following equation:

$$q_g = \sqrt{(I_n V_g)^2 - p_g^2} \tag{2.28}$$

In Fig. 2.2, the IBR capability curves for nominal and off-nominal voltage are presented. Of course, if there are power factor limitations, the capability curve can be even more limited.

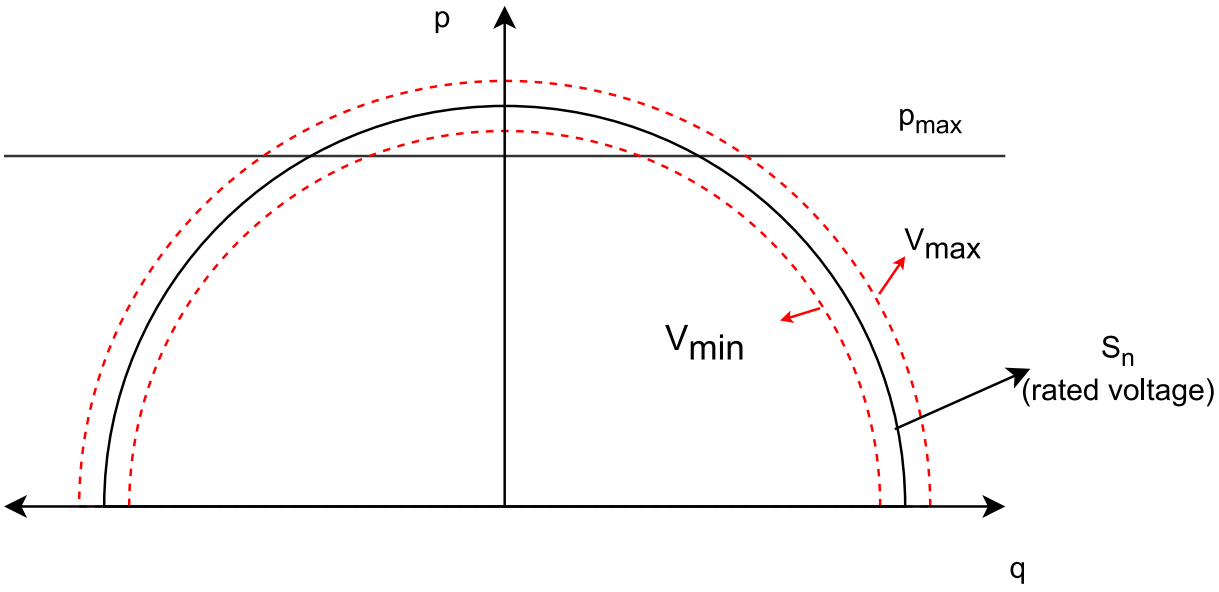

Figure 2.2: IBR Capability Curve

2.7 Voltage Control Complementarity Constraints

As the load increases, reactive power demand generally increases as well, and thus, reactive power limits of generators or other voltage-regulating devices may be reached. When the

limits are met, devices change behaviour. For example in the classic load flow system representation, a PV bus will turn into a PQ bus when the machine will reach its reactive power limits. For this reason, in the optimization problem formulation, the machine should either be at the reference voltage setpoint, or at its maximum reactive power, meaning that at least one of the two inequality constraints needs to hold as an equality. The authors in [52] introduced the use of complementarity constraints to model this change of behaviour.

With the introduction of two slack positive variables V_{gka} and V_{gkb}, the voltage is allowed to increase or decrease from the setpoint depending on whether the machine has reached the maximum or minumum reactive power limit. The complementarity constraints are modelled as follows:

$$0 \leq (q_{gk} - q_{gk}^{min}) \perp V_{gka} \geq 0 \Rightarrow (q_{gk} - q_{gk}^{min}) V_{gka} = 0 \tag{2.29}$$

$$0 \leq (q_{gk}^{max} - q_{gk}) \perp V_{gkb} \geq 0 \Rightarrow (q_{gk}^{max} - q_{gk}) V_{gkb} = 0 \tag{2.30}$$

$$V_{gk} = V_{gk}^{ref} + V_{gka} - V_{gkb} \tag{2.31}$$

Including (2.29)- (2.31), ensures that at the solution point, the machine will be either at the reference voltage setpoint or at it's reactive power limits.

It should be noted that the specific OPF formulation in this thesis refers to the maximization of load power. In most cases, load maximization ensures that the free variable of generator voltage will usually be at the highest possible value (which is the reference value), unless a maximum reactive power constraint is met, meaning that at least one of equations (2.32), (2.33) will hold as an equality. The bus voltage is limited by the reference value, as a maximum bound, but there is no lower limit imposed, as expressed in (2.32).

$$V_{gk} \leq V_{gk}^{ref} \tag{2.32}$$

$$q_{gk} \leq q_{gk}^{max} \tag{2.33}$$

As a result, complementarity constraints can be omitted from the optimization problem, as the inclusion of (2.29) will make the problem unnecessarily more time-consuming. It is easier instead, to be checked at the solution, that at least one of the reactive power or the voltage setpoint inequality constraints holds as equality.

2.8 Operational Constraints

2.8.1 Bus Voltage Constraints

In this specific problem operational constraints that correspond to the power system's normal operation are usually omitted, in order to identify optimal solution points that correspond to actual bifurcation points of the dynamical system.

For example, bus voltage constraints for buses without generation connected are not taken into consideration because they would limit the solution space to normal operating conditions and power limits would not correspond to bifurcation points (SNB or LIB).

Thus, for load buses, no constraints are imposed.

However, over- and under-voltage constraints may be imposed to ensure operation inside the desired voltage limits, in which case, the power limit obtained corresponds to the specific voltage limit and not maximum loadability of the system.

For example, under normal operation, grid codes define secure operational conditions for transmission voltages inside a ±8% voltage deviation for 150kV buses and ±5% for 400kV buses.

2.8.2 Branch Flow Constraints

Branch flow limits are not taken into consideration for voltage-stability constrained systems. Usually, voltage stability limit is due to a large impedance between generation and load, thus the line ampacity limits are not encountered before maximum loadability is reached.

However, in cases where a security limit is due to the overloading that can lead to cascaded line overload trippings, these limits can be included in the constraints as follows:

Let L be the set of line from/to buses (i, j). Then:

$$p_{ij} = (e_i^2 + f_i^2)g_{ij} - (e_i e_j + f_i f_j)g_{ij} + (e_i f_j - e_j f_i)b_{ij}, \quad \forall (i,j) \in L \tag{2.34}$$

$$q_{ij} = -(e_i^2 + f_i^2)(b_{ij} + b_{sij}) + (e_i e_j + f_i f_j)b_{ij} + (e_i f_j - e_j f_i)g_{ij}, \quad \forall (i,j) \in L \tag{2.35}$$

where p_{ij}, q_{ij} represent the active and reactive flow on every line of the system, g_{ij},b_{ij} are the line series admittance and susceptance respectively and b_{sij} is one half of the line charging susceptance.

Assuming that the thermal or steady state limit of line (i, j) is s_{ij}^{lim}, then the branch flow constraints are as follows:

$$p_{ij}^2 + q_{ij}^2 \leq (s_{ij}^{lim})^2, \quad \forall (i,j) \in L \tag{2.36}$$

2.8.3 Transformer Flow Constraints

Similarly, flow limits in transformers and auto-transformers can be constrained by including the tap ratio r in equations 2.34 and 2.35. The one-line diagram of the transfomer is presented in Figure 2.3. If the set of i, j buses is L^{trf} the equations are formed as follows:

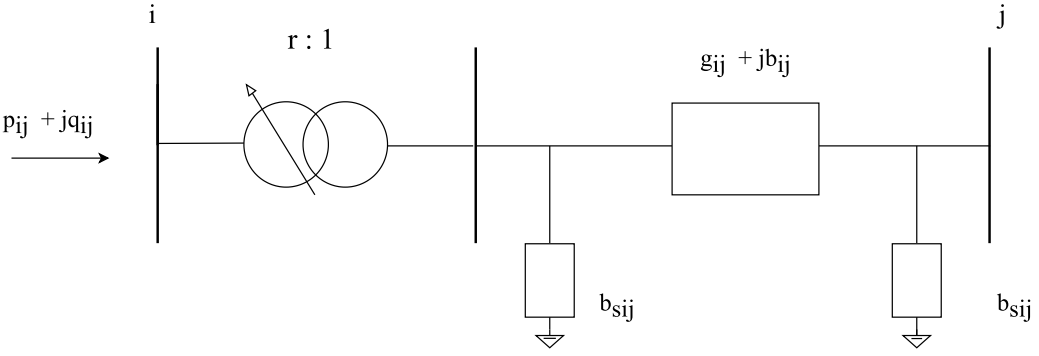

Figure 2.3: Transformer one line

$$p_{ij}^{trf} = (1/r^2)(e_i^2 + f_i^2)g_{ij} - (1/r)(e_i e_j + f_i f_j)g_{ij} + (1/r)(e_i f_j - e_j f_i)b_{ij}, \quad \forall (i,j) \in L^{trf} \tag{2.37}$$

$$q_{ij}^{trf} = -(1/r^2)(e_i^2 + f_i^2)(b_{ij} + b_{sij}) + (1/r)(e_i e_j + f_i f_j)b_{ij} + (1/r)(e_i f_j - e_j f_i)g_{ij}, \quad \forall (i,j) \in L^{trf} \tag{2.38}$$

Assuming that the thermal or steady state limit of transformer (i,j) is $s_{ij}^{trf,lim}$, then the transformer flow constraints are as follows:

$$(p_{ij}^{trf})^2 + (q_{ij}^{trf})^2 \leq (s_{ij}^{trf,lim})^2, \quad \forall (i,j) \in L \tag{2.39}$$

2.9 VSM computation

2.9.1 Problem Formulation

Taking into consideration all the above, the OPF formulation for the calculation of the Voltage Security Margins, neglecting operational constraints (as discussed before), starting from a post-contingency point, is the following:

$$\zeta = -\Delta P = -\lambda \sum_{k \in \mathcal{N}} d_{pk} \tag{2.40}$$

$$\text{VSM} = \min_{\boldsymbol{e},\boldsymbol{f},\Delta \text{L},\lambda} \zeta \tag{2.41}$$

subject to :

$$\boldsymbol{h}(e, f, \Delta L, \lambda) = 0 \tag{2.42}$$

$$\Delta p_{gk} = K_k(\Delta L + \lambda \sum_{k \in \mathcal{N}} d_{pk}) \tag{2.43}$$

$$p_{gk}^{min} \leq p_{gk} \leq p_{gk}^{max}, \forall k \in G \tag{2.44}$$

$$q_{gk} \leq q_{ak}(p_{gk}, V_k), \forall k \in G \tag{2.45}$$

$$q_{gk} \leq q_{rk}(p_{gk}, V_k), \forall k \in G \tag{2.46}$$

$$V_{gk} \leq V_{gk}^{ref}, \forall k \in G \tag{2.47}$$

where (2.42) is the set of long-term equilibrium equations assuming load restoration to constant power (through e.g. LTC restoration of distribution voltage). Thus, $\boldsymbol{h}$ correspond to the (quadratic) power balance equations (2.11) in rectangular coordinates $\boldsymbol{e}, f$. p_{gk} and q_{gk} are the active and reactive power generation, V_{gk}^{ref} is the voltage setpoint and V_{gk} is the voltage magnitude of generator k:

$${V_{gk}}^2 = {e_k}^2 + {f_k}^2 \tag{2.48}$$

Active power generation constraints are defined in (2.44) and are checked at the solution. If the constraints are violated, the limited generators are replaced by constant P injections and the parameters of vector $\boldsymbol{K}$ of (2.15) are updated and the problem is solved

again. Constraints (2.45), (2.46) represent the generators' reactive power limits, where $q_{ak}(p_{gk}, V_k)$ corresponds to the armature current limit and $q_{rk}(p_{gk}, V_k)$ to the rotor (field) current limit. Both q_{ak} and q_{rk} are functions of active power p_{gk} and voltage magnitude V_{gk} and are defined in subsection 2.5. For each generator either (2.47) or one of (2.45),(2.46) must hold as equality. However, as explained in 2.7 there is no need to add the complementarity constraint, since the load maximization ensures that at the solution the free variable of generator voltage will be at its highest possible value. Again this is checked at the solution.

It is noted that the network equations $\boldsymbol{h}$ terminate at the primary side of HV/MV transformers feeding ADNs, which are considered as the Points of Common Coupling (PCC) for connected ADNs. Load restoration to constant power is taking place by LTCs not explicitly modelled in $\boldsymbol{h}$.

Finally, as stated before, the above equations refer to a post-contingency condition of the system. The same problem without contingency will give the maximum pre-contingency LM.

2.9.2 Lagrange multipliers and sensitivities

The Lagrangian function for an equality constrained optimization problem in its general form is:

$$\mathcal{L}(x, w) = \zeta - w^T h(x) \tag{2.49}$$

where x is the vector of decision variables of the optimization problem and w the Lagrange multipliers. Function ζ is the objective and h the set of equality constraints. The inequality and bound constraints (2.44)-(2.47) can also be included in (2.49) but in this case are neglected. The reason for this is that only the Lagrange multipliers (sensitivities) that correspond to the equality constraints (2.42) are of interest in the following chapters.

For the equality constrained optimization problem (2.40)-(2.42) the objective function is the maximization of function ζ, which is in essence the minimization of the function ζ:

$$\min \zeta \tag{2.50}$$

s.t. equations (2.11):

$$h_{p_k} = p_k - e_k(\boldsymbol{g_k}^T \boldsymbol{e} - \boldsymbol{b_k}^T \boldsymbol{f}) - f_k(\boldsymbol{b_k}^T \boldsymbol{e} + \boldsymbol{g_k}^T \boldsymbol{f}) = 0, \quad k \in \mathcal{N} \tag{2.51}$$

$$h_{q_k} = q_k + e_k(\boldsymbol{b_k}^T \boldsymbol{e} + \boldsymbol{g_k}^T \boldsymbol{f}) - f_k(\boldsymbol{g_k}^T \boldsymbol{e} - \boldsymbol{b_k}^T \boldsymbol{f}) = 0, \quad k \in \mathcal{N} \tag{2.52}$$

Thus, the Lagrangian function is expressed as follows:

$$\mathcal{L} = \zeta - \boldsymbol{w_p}^T \boldsymbol{h_p} - \boldsymbol{w_q}^T \boldsymbol{h_q} \tag{2.53}$$

According to the Karush Kuhn Tacker (KKT) optimality conditions, the gradient of the Lagrangian function with respect to the violations of the equality constraints are equal to zero, so:

$$\begin{aligned} \nabla_{p_k}\mathcal{L} = 0 \Rightarrow \frac{\partial\zeta}{\partial p_k} - w_{p_k} = 0 \\ \Rightarrow w_{p_k} = \frac{\partial\zeta}{\partial p_k} = -\frac{\partial\Delta P_{max}}{\partial p_k}, \quad k \in \mathcal{N} \end{aligned} \tag{2.54}$$

$$\begin{aligned} \nabla_{q_k}\mathcal{L} = 0 \Rightarrow \frac{\partial\zeta}{\partial q_k} - w_{q_k} = 0 \\ \Rightarrow w_{q_k} = \frac{\partial\zeta}{\partial q_k} = -\frac{\partial\Delta P_{max}}{\partial q_k}, \quad k \in \mathcal{N} \end{aligned} \tag{2.55}$$

The Lagrange multipliers corresponding to active and reactive power balance equations of (2.42), $\boldsymbol{w_p}$ and $\boldsymbol{w_q}$ and express the sensitivity of the security margin to the violation of the respective consumption p_k, q_k respectively assuming these as independent variables [4]. The negative sign derives from the minimization of the objective function. Also, it should be noted that for active and reactive flows, a positive load convention is taken into consideration, as also shown in the equations. In the following chapter these sensitivities are linked to the controlled active and reactive power absorptions at the ADN's PCC.

Equations (2.54), (2.55) correspond to the sensitivity of the change in the VSM, with respect to the active and reactive power injections of a specific bus. Sensitivities can be computed at the HV side of the HV/MV transformers where the distribution feeders are connected, meaning that its possible to use these sensitivities in order to control the distribution network to provide support to the VSM, as it will be shown in the next chapter.

2.9.3 Solution Method and Implementation

The constrained optimization problem (2.40) - (2.47) is a problem containing both non-linear equality and inequality constraints. It contains both non linear equality and inequality constraints, which makes the solution of the problem quite challenging, as it is non-convex.

For this thesis, a MATLAB [53] program has been created including all the equations of the optimization problem. The program consists of several different functions in order to formulate and solve the problem.

The MATLAB program consists of the following:

- System Input data: The data of the system studied is imported. The input data can be given in MATPOWER [54] case struct format or .raw format.
- Data Clearing: This function checks for errors or missing data in order to ensure the quality of the input data. It is more important when dealing with real system data, rather than benchmarks and test systems.
- Initialization : Based on the input data, a power flow is solved using a standard Newton-Raphson (NR) load flow algorithm. The results of the NR load flow is provided as initial point for the optimization. As a result, vector $\boldsymbol{x_0}$ contains all the initial values of the decision variables of the optimization.

- Problem formulation: The system of equations regarding all the constraints of the optimization is written as well as the objective function. The problem is properly constructed to fit the formulation required by the Non-Linear Programming solver that will be used.
- Solver: The problem is solved using MATLAB's internal routine called *fmincon*. The solver used is a sequential quadratic programming (sqp) solver that can handle non-linear optimization problems.
- Output: The MATLAB program will directly provide the value of the objective of the problem which corresponds to the VSM. Moreover, it will calculate all the values of the decision variables at the solution points and pass them back to the MATPOWER case struct which can be exported to .raw format as well. As byproducts of the optimization, all Lagrange multipliers are available at the solution point, corresponding to both equality and inequality constraints.

Sequential Quadratic Programming [55] [56] [57] (SQP) is a numerical optimization technique used to solve nonlinear constrained optimization problems. It falls under the category of nonlinear programming methods and is particularly well-suited for solving problems where both the objective function (the function to be minimized or maximized) and the constraints are nonlinear. SQP is an iterative method that seeks to find the optimal solution by approximating the problem with a series of quadratic subproblems. SQP is considered a quasi-Newton method.

A basic overview of how SQP is as follows:

1. Initialization: SQP begins with an initial guess for the solution. This guess could be a starting point or an estimate of the optimal solution.
2. Quadratic Approximation: At each iteration, SQP constructs a quadratic approximation of the objective function and constraints in the vicinity of the current solution.
3. Solving the Subproblem: The quadratic approximation is solved to find an update to the current solution. This update is expected to improve the objective function while satisfying the constraints as much as possible. This is done by solving a quadratic programming subproblem, which is generally easier and faster to solve than the original nonlinear programming problem.
4. Update: The current solution is updated based on the results of the subproblem solution.
5. Convergence Check: The algorithm checks for convergence, meaning it examines whether the current solution satisfies certain optimallity and feasibility conditions. If these conditions are met, the algorithm terminates. If not, it goes back to step 2 and repeats the process.

In Figure 2.4, a schematic representation of the main idea of an SQP algorithm is presented, where d corresponds to the search direction of the algorithm that is computed at each QP sub problem instead of a Newton step.

All problems are solved with a PC with the following specifications: a GPU Core i9, 3.8 GHz and 16 GB RAM.

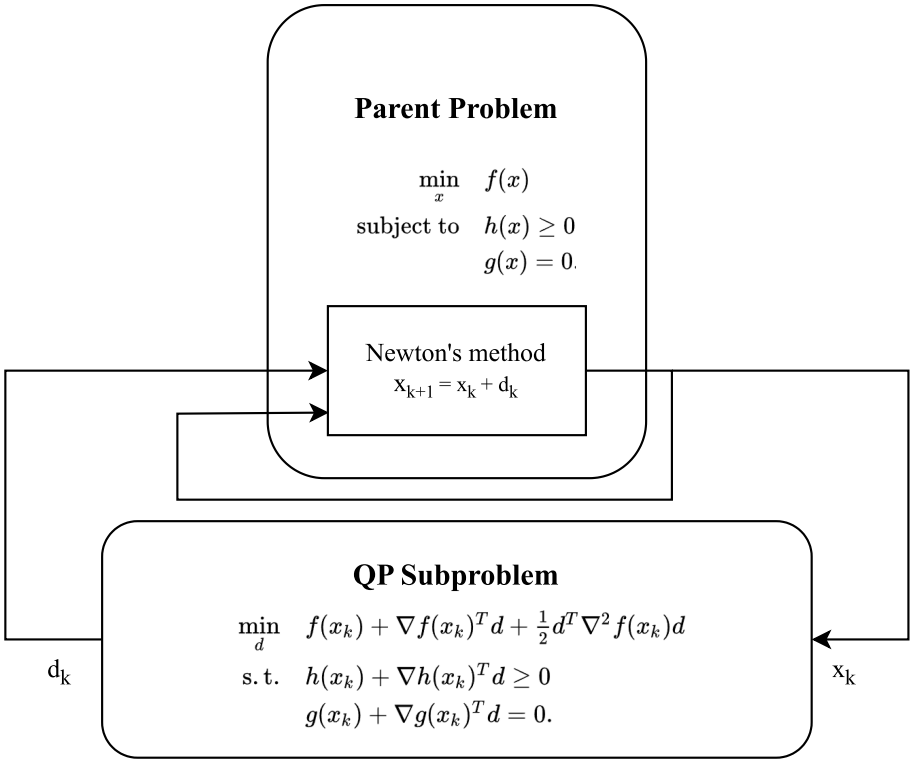

Figure 2.4: SQP flowchart

2.10 Radial Test System

2.10.1 System Description

The 2-bus transmission system of Figure 2.5 is a lossless line ($R = 0$) with an active power load at one bus and an infinite bus on the other bus. The system data are provided in Table 2.1. The infinite bus is also the reference bus.

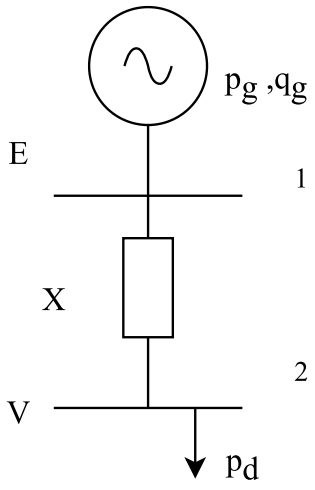

Figure 2.5: Radial 2-bus Transmission System

For the 2-bus lossless system it is easy to write the full equations according to the formulation of the problem.

Table 2.1: Data of Radial 2-bus Transmission System

E(pu)	R (pu)	X (pu)	base MVA
1	0	0.4	100

For the infinite bus, which is also a reference bus:

$$E = e_1 + jf_1 = 1pu \Rightarrow e_1 = 1, f_1 = 0 \tag{2.56}$$

and for the load bus:

$$V = e_2 + jf_2 \tag{2.57}$$

The real and imaginary parts respectively of the k^{th} column of the bus admittance matrix are:

$$g = \begin{bmatrix} g_{11} & g_{12} \\ g_{21} & g_{22} \end{bmatrix} = \begin{bmatrix} 0 & 0 \\ 0 & 0 \end{bmatrix} \tag{2.58}$$

and

$$b = \begin{bmatrix} b_{11} & b_{12} \\ b_{21} & b_{22} \end{bmatrix} = \begin{bmatrix} -2.5 & 2.5 \\ 2.5 & -2.5 \end{bmatrix} \tag{2.59}$$

Only an active power load is considered in the test system which is initially zero. As a result $p_{d2_0} = 0$ and the stress direction:

$$d_{p_k} = \begin{bmatrix} 0 \\ 1 \end{bmatrix} \tag{2.60}$$

Finally, generation is only considered on the infinite bus, so $p_{g2} = 0, q_{g2} = 0$.

As a result, equality constraints (2.42) are written as follows:

$$\begin{aligned} p_{g1} - p_{d1} = e_1(\boldsymbol{g_1}^T\boldsymbol{e} - \boldsymbol{b_1}^T\boldsymbol{f}) + f_1(\boldsymbol{b_1}^T\boldsymbol{e} + \boldsymbol{g_1}^T\boldsymbol{f}) \Rightarrow \\ p_{g1} = -2.5f_2 \end{aligned} \tag{2.61}$$

$$\begin{aligned} q_{g1} - q_{d1} = -e_1(\boldsymbol{b_1}^T\boldsymbol{e} + \boldsymbol{g_1}^T\boldsymbol{f}) + f_1(\boldsymbol{g_1}^T\boldsymbol{e} - \boldsymbol{b_1}^T\boldsymbol{f}) = 0 \Rightarrow \\ q_{g1} = 2.5e_2 \end{aligned} \tag{2.62}$$

$$\begin{aligned} p_{g2} - p_{d2} = e_2(\boldsymbol{g_2}^T\boldsymbol{e} - \boldsymbol{b_2}^T\boldsymbol{f}) + f_2(\boldsymbol{b_2}^T\boldsymbol{e} + \boldsymbol{g_2}^T\boldsymbol{f}) \Rightarrow \\ -p_{d2_0} - \lambda d_{p_2} = -2.5e_2f_2 + 2.5f_2^2 \end{aligned} \tag{2.63}$$

$$\begin{aligned} q_{g2} - q_{d2} = -e_2(\boldsymbol{b_2}^T\boldsymbol{e} + \boldsymbol{g_2}^T\boldsymbol{f}) + f_2(\boldsymbol{g_2}^T\boldsymbol{e} - \boldsymbol{b_2}^T\boldsymbol{f}) = 0 \Rightarrow \\ e_2^2 + f_2^2 = e_2 \end{aligned} \tag{2.64}$$

2.10.2 Optimization Implementation and Results

Since the test system is a simple corridor, no contingency is taken into consideration and the resulting maximization will provide the LM:

$$\text{LM} = \min_{\text{e}_2,\text{f}_2,\text{p}_{\text{g1}},\text{q}_{\text{g1}},\lambda} \zeta \tag{2.65}$$

Based, on equations (2.61)- (2.64), the OPF formulation for the calculation of the LM (2.41)- (2.47), is written as follows:

$$\min_{e_2,f_2,p_{g1},q_{g1},\lambda} -\lambda \tag{2.66}$$

$$\text{subject to :}$$

$$p_{g1} = -2.5 f_2 \tag{2.67}$$

$$q_{g1} = 2.5 e_2 \tag{2.68}$$

$$-\lambda = -2.5 e_2 f_2 + 2.5 f_2^2 \tag{2.69}$$

$$e_2^2 + f_2^2 = e_2 \tag{2.70}$$

$$\tag{2.71}$$

It can be observed that in this case there are no inequality constraints, due to the simplicity of the system and some constraints are neglected (such as the distributed slack additional constraints). LM optimization problem (2.66)-(2.70) is solved using the program and solver described in the previous sub section 2.9.3.

The results are presented in Table 2.2, where $V_{2,maxP}$ is the voltage value at the LM point, and P_{max} is the loading margin of the system, which in this case is equal to the stressed load of the bus load p_{d2}.

The results of the optimization can be verified by equations in Section 1.4, where for $Q = 0$, the maximum P and corresponding V are :

$$P_{max} = \frac{E^2}{2X} = 0.125pu = 125MW \tag{2.72}$$

and

$$V_{maxP} = \sqrt{\frac{E^2}{2}} = 0.707107pu \tag{2.73}$$

Table 2.2: LM results on Radial 2-bus Transmission System

$V_{2,maxP}$ (pu)	P_{max} (MW)
0.707107	125

In Figure 2.6, the iterations needed for the optimization problem to be solved, are presented, along with the objective function value. The value of the objective function is negative, as the problem is formulated as a negative minimization of the stress of the system.

The simplicity and the size of the system make this problem computationally easy, so it is computed in about a second using the MATLAB *fmincon* function.

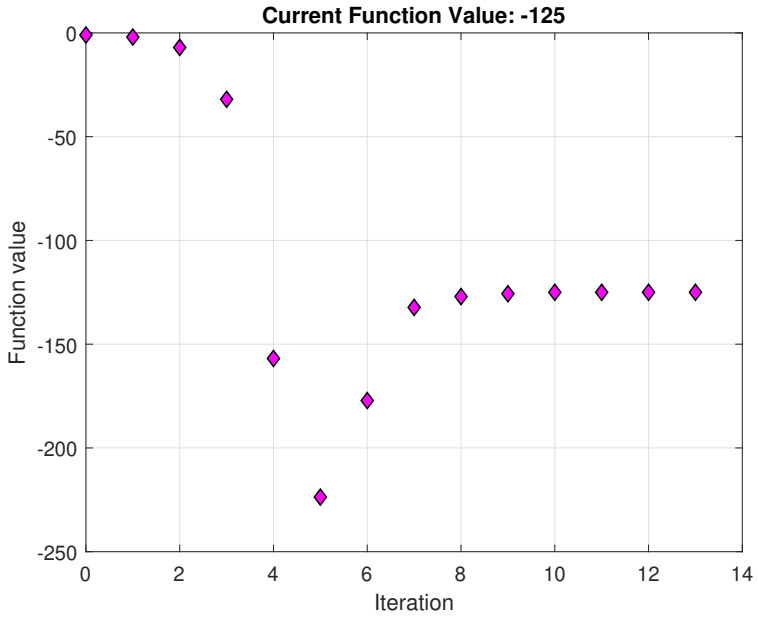

Figure 2.6: Iterations and objective function value $\zeta = -\lambda$

2.10.3 QSS Simulation and Comparison

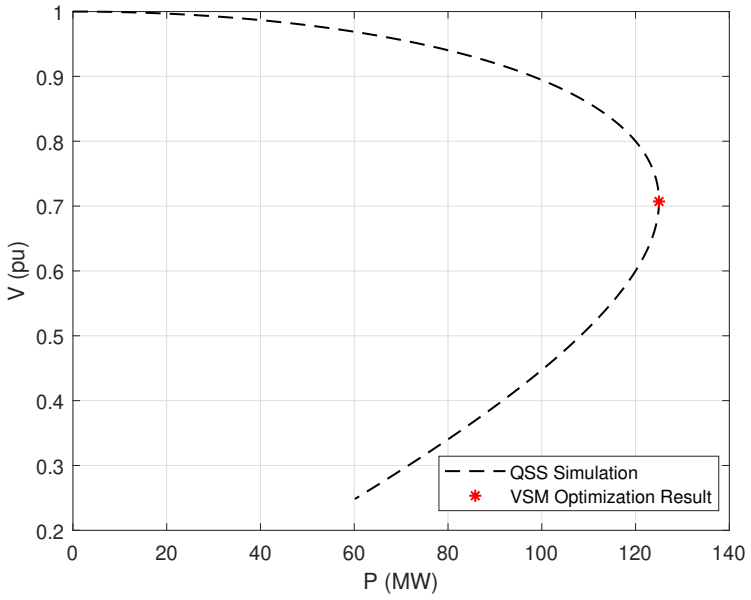

Figure 2.7: QSS simulation results vs LM OPF

As explained, the objective function value in this case corresponds to the LM of the transmission system. It is effectively the maximum power transfer possible and corresponds to the SNB point of the dynamic system.

The test system is also simulated using WPSTAB [7] and QSS simulation explained in Section 1.2.2. WPSTAB performs time-domain QSS simulation. In this simulation, starting from the initial point where the loading of the system is zero, the conductance of the load is increasing with a steady rate (ramp). The ramp increase of the conductance is

presented in Figure 2.8 and the total load in Figure 2.9.

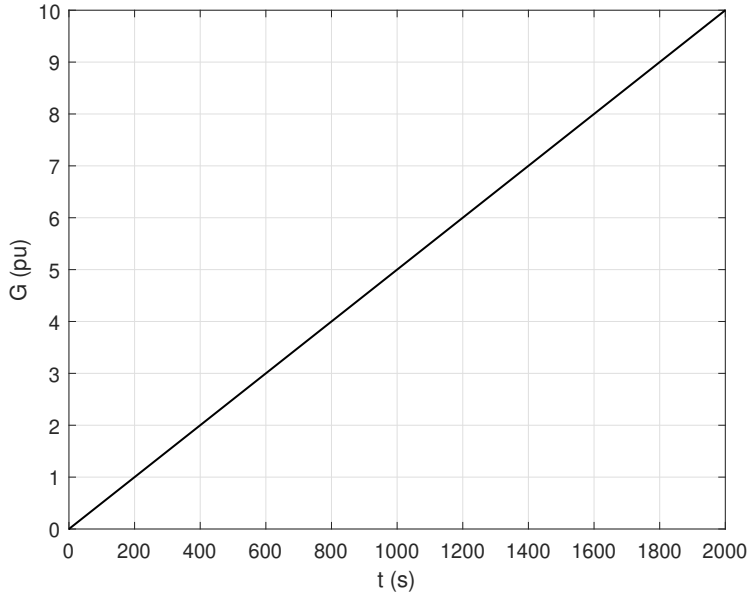

Figure 2.8: Conductance ramp rate (pu)

The load bus voltage in time is presented in Figure 2.10.

Finally, in Figure 2.7, the P-V characteristic is plotted for the load bus voltage and active power load together with the point calculated from the LM optimization. It can be seen that the result of the LM OPF corresponds to the maximum power transfer. In this case, the optimization method and the simulation are effectively identical problems (no assumptions are made), so the results are the same.

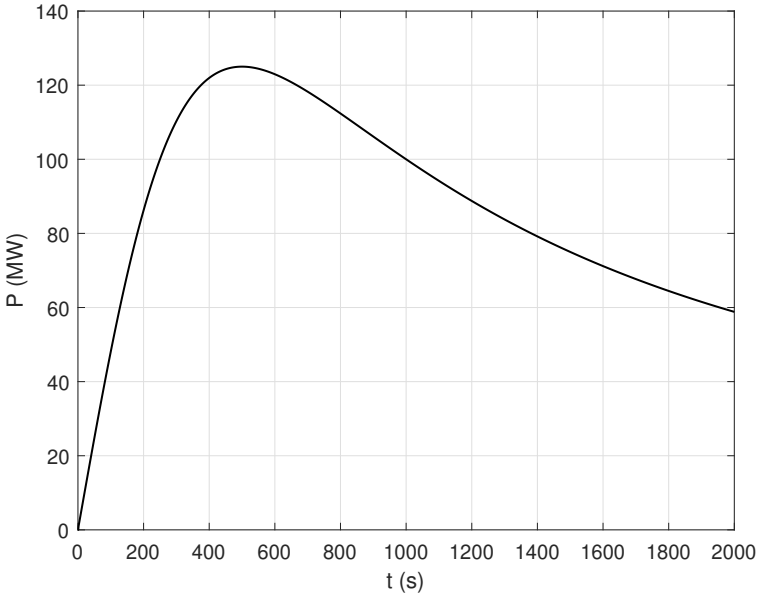

Figure 2.9: Total Load in time (MW)

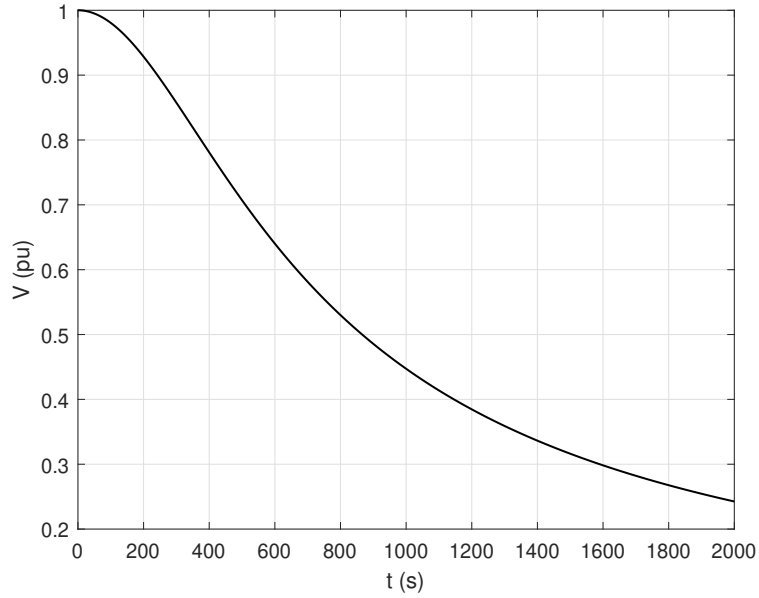

Figure 2.10: Load bus voltage in time (pu)

2.11 Nordic Test System

2.11.1 System Description

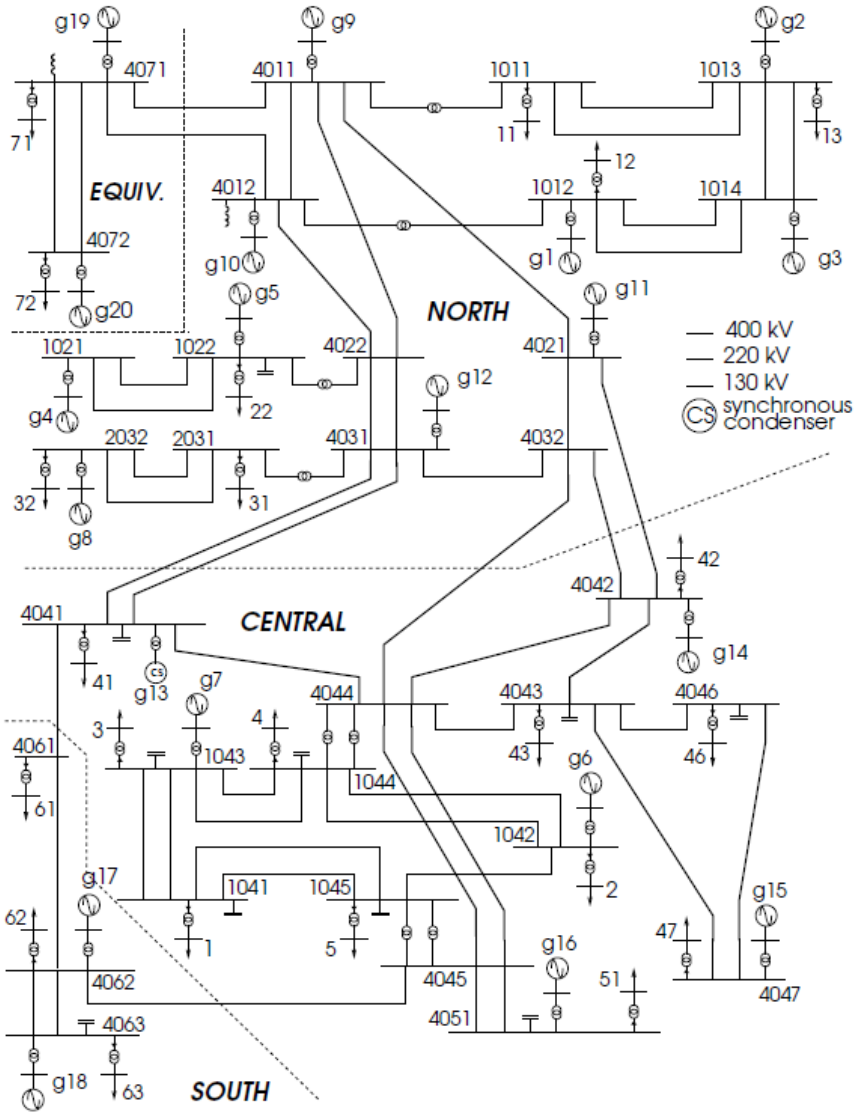

Figure 2.11: Online diagram of the IEEE Nordic Test System

The VSM optimization problem (2.41)-(2.47) is solved for the IEEE Nordic Test System [58] of Fig. 2.11. The IEEE Nordic Test System is an updated version of the Nordic32 system. It is a fictitious system that is based on the Swedish and Nordic real transmission systems. System data are presented in 2.12.

This test system has been used widely for voltage stability studies. As shown in the one-line diagram, the test system consists of 3 different areas (North, Central, South) and an equivalent generator that represents an interconnection with another system. The test system is prone to voltage instability due to the high transfer of power from the north to the central area, as the majority of the load is located in the central and south area and generation in the northern area. The share of load and generation among the different areas is presented in 2.3.

IEEE Nordic test system data.

	Nordic
Nominal frequency (Hz)	50
No. of buses	74
No. of lines	50
No. of transformers	52
No. of generators	19
No. of synchronous condensers	1
No. of loads	22
No. of (switched) shunts	11
Total generation (M\V)	11506
Toial load (MW)	11060

Figure 2.12: Data of the IEEE Nordic Test System

Table 2.3: Area load and generation

area	generation (MW)	load (MW)
North	4629	1180
Central	2850	6190
South	1590	1390
Equiv	2437	2300

In this thesis, the reduced version of the test system, consisting only of the EHV and HV transmission buses (130kV, 220kV, 400kV), is used. Thus, loads are transferred to the high voltage side of LTC transformers as P and Q injections equal to that of the initial operating point A of [58]. The reduced version is validated with the initial load flow solution to confirm that voltages in transmission buses are identical.

2.11.2 Loading and voltage security margins

As explained in 1.5, starting from a base operating point, post-contingency (VSM) and pre-contingency (LM) margins can be computed in order to evaluate how secure is the current operating point in terms of voltage stability.

For this reason, a specified list of contingencies is examined for each operating point. Contingency lists can contain all data according to sub-section 1.5.1, or can be limited to pre-specified lists.

Applying the optimization problem (2.41)- (2.47) for different contingencies, the VSM for each contingency can be estimated, and the most critical ones can be identified. The problem is solved using the Non-Linear programming function of MATLAB (fmincon) and the solver used is a sequentially quadratic programming (sqp) solver, as already explained in Section 2.9.3. The problem is solved in around 30 seconds in a PC with CPU 3.8 GHz and RAM 16 Gb for each contingency.

The direction of the stress is a uniform load increase in the Central area only, where $\mathcal{C} \subset \mathcal{N}$ the set of buses in the central area. Thus:

$$d_{p_k} = p_{dk0}, \quad k \in \mathcal{C} \tag{2.74}$$

$$d_{q_k} = q_{dk0}, \quad k \in \mathcal{C} \tag{2.75}$$

As a result, the VSM calculated refers to the maximum load consumption of the central area and the associated stability limit, for each specific contingency.

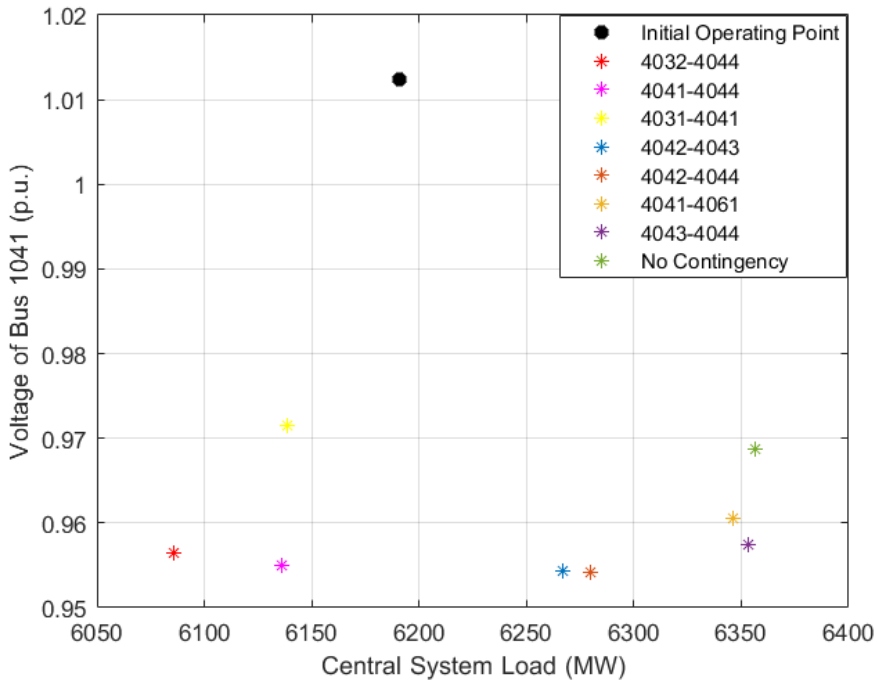

Figure 2.13: Load against voltage for different N-1 scenarios

In Table 2.4, central area maximum system load, along with the stress level and the VSM are presented for several N-1 contingencies which consist of loss of transmission lines, mainly between the northern and the central area. Negative stability margins indicate that the system will not be able to restore the pre-contingency loading point and thus may result in system collapse. Contingencies with negative margins are considered as critical contingencies and there is need for remedial actions and emergency support, should they occur.

Table 2.4: Stress level for different N-1 scenarios

N-1	**Central Area System Load**	**Stress Level**	**VSM (MW)**
Initial Loading	6190	-	-
4032-4044	6086	-0.0169	-104
4041-4044	6136	-0.0088	-54
4031-4041 ck.1	6139	-0.0083	-51
4042-4043	6267	0.0125	77
4042-4044	6280	0.0145	90
4041-4061	6346	0.0253	156
4043-4044	6353	0.0264	163
No Contingency	6356	0.0268	166

In Fig. 2.13, the voltage of a 130kV bus (1041) in the central area, is plotted against the System Load of the Central Area for various N-1 scenarios, indicating positive and negative VSMs for each examined contingency.

It should be noted that a small positive margin can be still threatening for the operation of the power system. Usually, TSOs define a secure operation margin heuristically based on the experience of their systems, e.g. a $VSM \geq 100MW$.

2.11.3 Critical Contingency Analysis

Hereafter, the analysis refers to the most critical contingency of Table 2.4, loss of transmission line 4032-4044, as is the one with the most negative VSM.

For the most critical contingency, the optimization problem (2.41)- (2.47) is solved in 5 iterations as shown in Fig. 2.14, where the objective function value is the negative minimization of the stress for the load located in the central area.

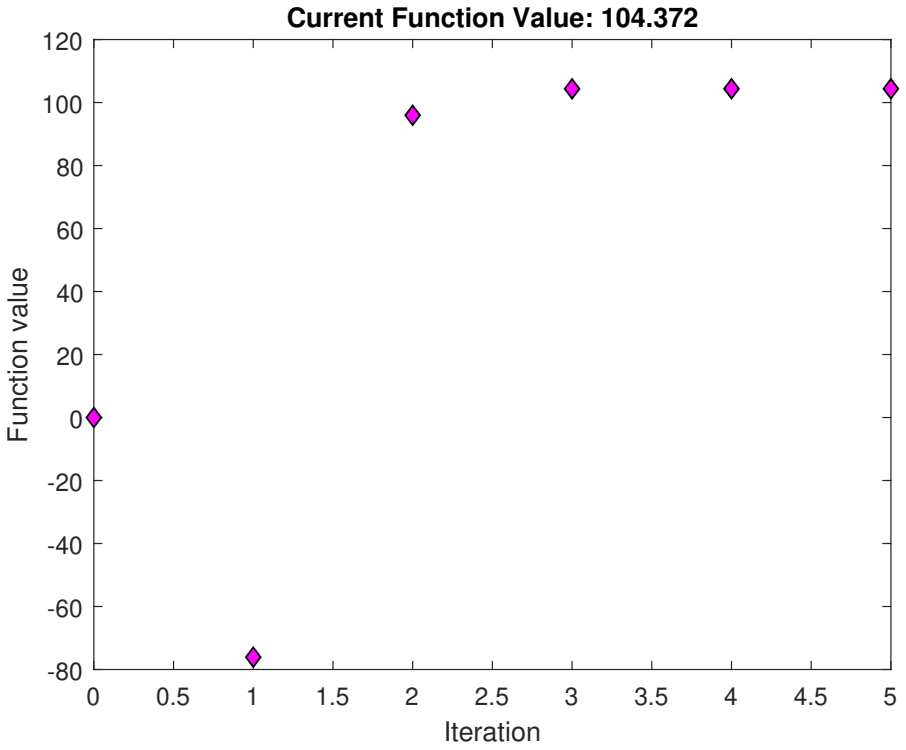

Figure 2.14: Iterations and objective function value $\zeta = -\lambda \sum_{k \in C} d_{p_k}$

In Table 2.5, the voltages in the central area are shown for the pre-contingency initial operating conditions and at the maximum loading point for the most critical contingency. As expected, a significant decrease in the voltages is observed in both 130kV and 400kV. Voltage drop is a sign of imminent voltage collapse.

In Table 2.6, the voltages of the generating units are shown in both the initial and the VSM point. As also explained in subsection 2.7, the problem formulation drives the voltages of machines at the highest possible value which is the reference value. When either the stator or the field current limit is met, then the voltage will start dropping. As seen in the results, for the most critical contingency, only Generator 14, which is located on bus 4042 reaches its reactive capability limit, thus resulting in a drop in its voltage. Results of Table 2.6 also provide an insight on how each generator affects the resulting VSM.

Table 2.6 confirms that the complementary relationship between voltage and current limits

Table 2.5: Bus voltages of central area pre and post contingency

Bus	**Initial point**	$\boldsymbol{V_{maxP}}$
1041	1.0124	0.9564
1042	1.0145	0.9977
1043	1.0274	0.9778
1044	1.0066	0.9490
1045	1.0110	0.9605
4041	1.0506	0.9937
4042	1.0428	0.9766
4043	1.0370	0.9822
4044	1.0394	0.9793
4045	1.0533	1.0019
4046	1.0357	0.9893

Table 2.6: Generator reactive power and voltage setpoints

Bus	Q_g^0	V_g^0	Q_g	V_g
g6	138.58	1.0084	181.93	1.0084
g7	60.43	1.0141	124.98	1.0141
g13	50.13	1.0170	215.44	1.0170
g14	295.88	1.0454	467.68	1.0190
g15	377.93	1.0455	628.30	1.0455
g16	222.65	1.0531	359.46	1.0531

holds at the solution point, as at least one of the two hold as an equality constraint.

2.11.4 QSS Simulation of Critical Contingency

Similarly to the radial transmission system of Section 2.10, time domain simulation is performed on the test System to evaluate the results of the VSM Optimization for the most critical contingency. The simulation is performed with WPSTAB as described also in 2.10.3.

The simulation is performed for the most critical contingency that was identified in Section 2.11.2, which is the loss of transmission line between buses 4034-4044. The simulation starts from the initial operating point described also in 2.11.1, and the said contingency is introduced 10 seconds into the simulation.

Note that there are some important differences, between the VSM formulation and the QSS simulation. Firstly, in the QSS the model of the power system includes the distribution feeders and the LTC transformers, meaning that the load restoration mechanism is included explicitly including the deadband and tap limits.The loads are modeled using the following voltage dependent models:

$$p_{dk} = p_{dk}^0 (\frac{V_k}{V_k^0})^a \quad \forall k \in \mathcal{N} \tag{2.76}$$

$$q_{dk} = q_{dk}^0 (\frac{V_k}{V_k^0})^b \quad \forall k \in \mathcal{N} \tag{2.77}$$

In this simulation the values used for $a = 1$ and $b = 2$. As a result, there is the possibility of exhausting available tap position. In Fig. 2.15 the voltages of a distribution and a transmission bus are presented along with the tap ratio and the deadband of the controlled voltage. It is shown that the tap ratio will try to maintain the voltage of the MV bus inside the deadband, but due to fast decrease in the transmission voltage this is not possible.

In this case the system collapses before the LTC tap range is exhausted. In Fig. 2.16 the load consumption of the MV bus is presented. It is shown that the LTC attempts to restore the active power consumption to the pre-contingency levels but it is not possible due to the fast voltage drop.

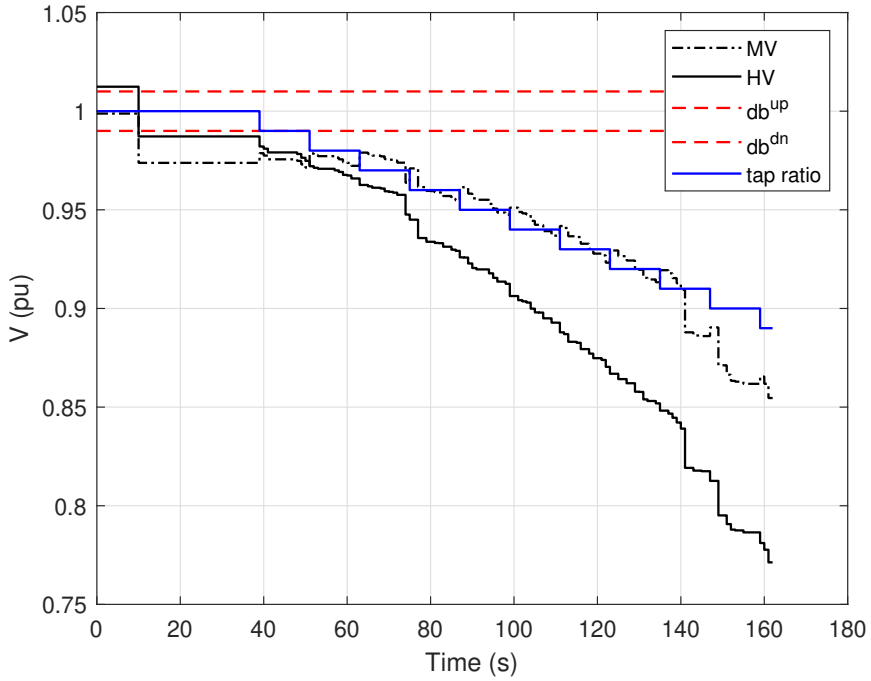

Figure 2.15: Distribution and Transmission Voltages with tap ratio

In Fig. 2.17, the total active power consumed in Central Area is plotted together with the voltage of bus 1041 in the form of a PV curve. It can be seen that the post contingency central area load is lower than the initial loading point, indicating that the load cannot be restored to its pre-contingency consumption, as already indicated from the negative VSM solution. It should be highlighted that the OPF VSM solution is close to the maximum loading of the QSS simulation (after the contingency) but it is not the same, for the reasons explained above.

The voltage instability is obvious from Figure 2.17 as the pre-contingency load cannot be restored and voltages collapse. Also the VSM solution point (shown with red dot) is quite close to the maximum point of the PV curve. In case the load demand were reduced by changing the deadbands or by freezing the LTC operation, the collapse could be avoided and the system would operate with a total consumption close to the operating point obtained by the solution of the optimization.

The voltages of several buses across the central area are shown in Fig. 2.18. As expected, there is a voltage drop, which continues until the system collapses at 162 seconds of the simulation.

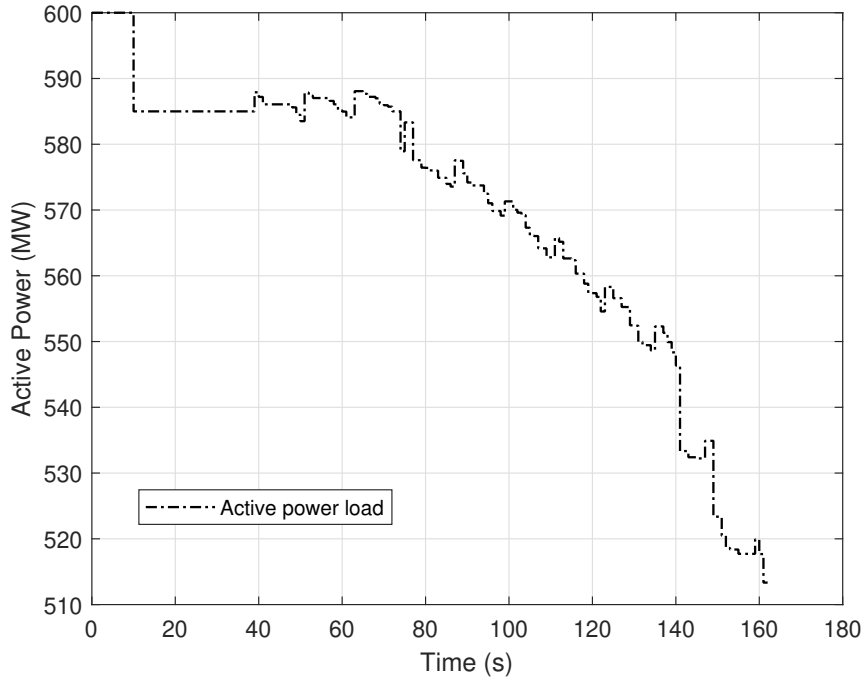

Figure 2.16: Active power load of a bus

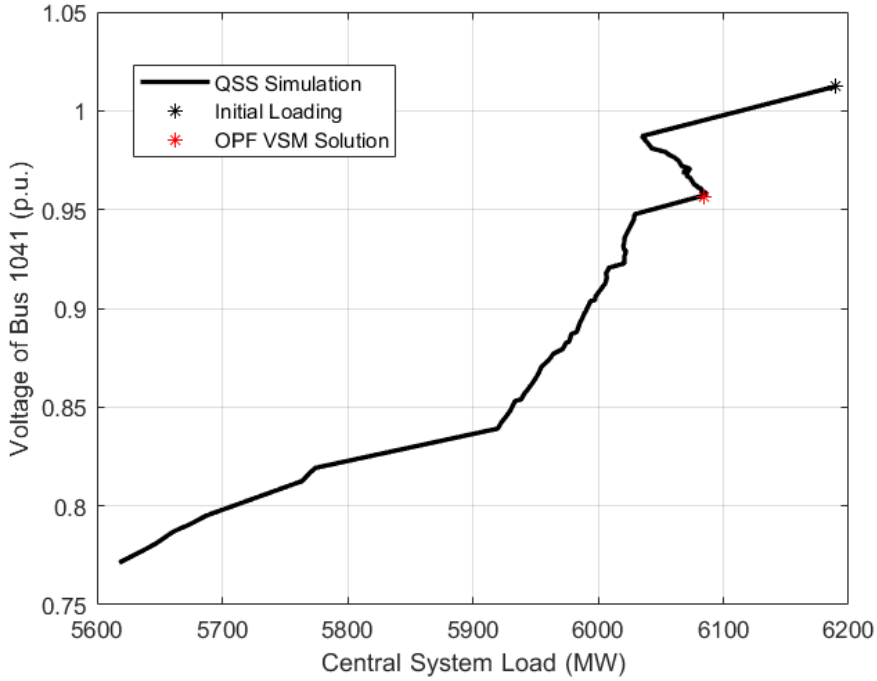

Figure 2.17: Post Contingency PV Curve for bus 1041 and Central Load

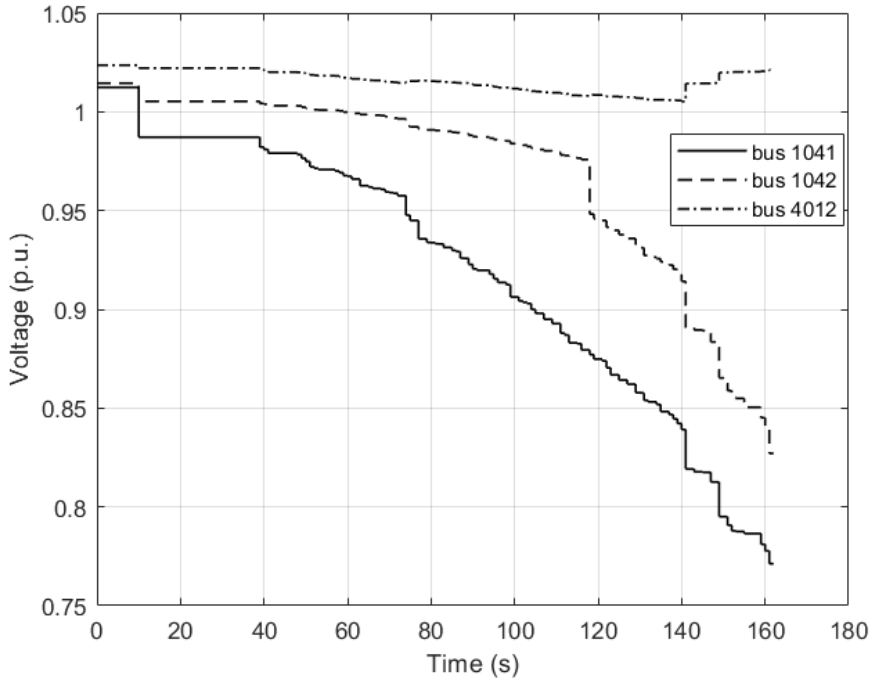

Figure 2.18: Transmission Voltages

In Fig. 2.19, the load voltages are shown in different distribution feeders at the 20kV level. It is obvious that distribution voltage cannot be restored successfully by the LTC.

Finally, in Fig. 2.20, the reactive power generation is plotted for Synchronous Generators 6,7 and 14 which are in the Central Area. In the QSS simulation, the exact rotor current limits are considered for the synchronous generators, while in the OPF, an approximation is considered. It is noted that apart from generator g14 which was the only one limited in the optimization VSM solution, generators g6 and g7 also reach the over excitation limits in the QSS simulation. The limitation of g6 is essentially the reason for the voltage collapse.

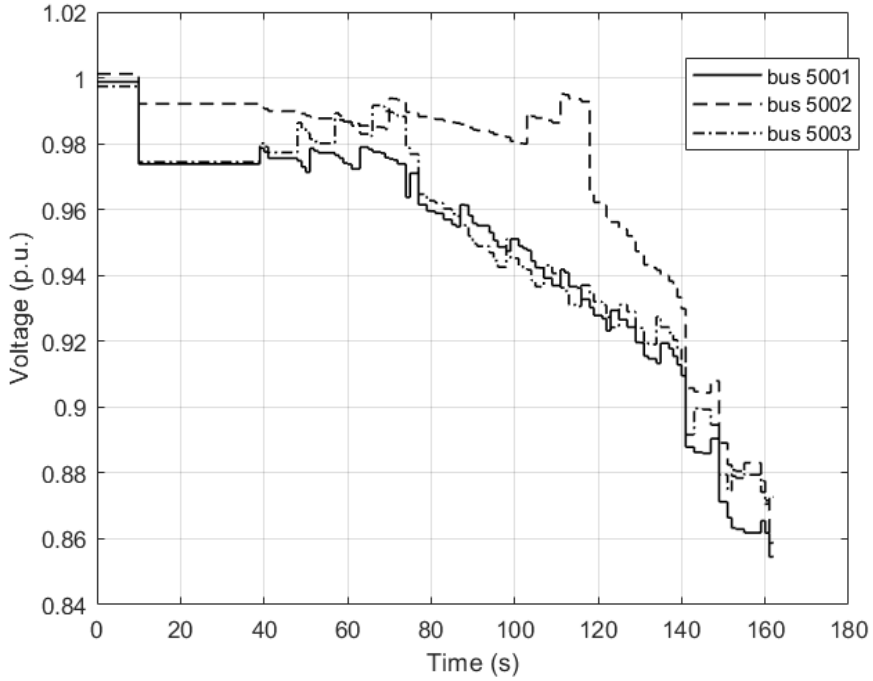

Figure 2.19: Distribution Voltages

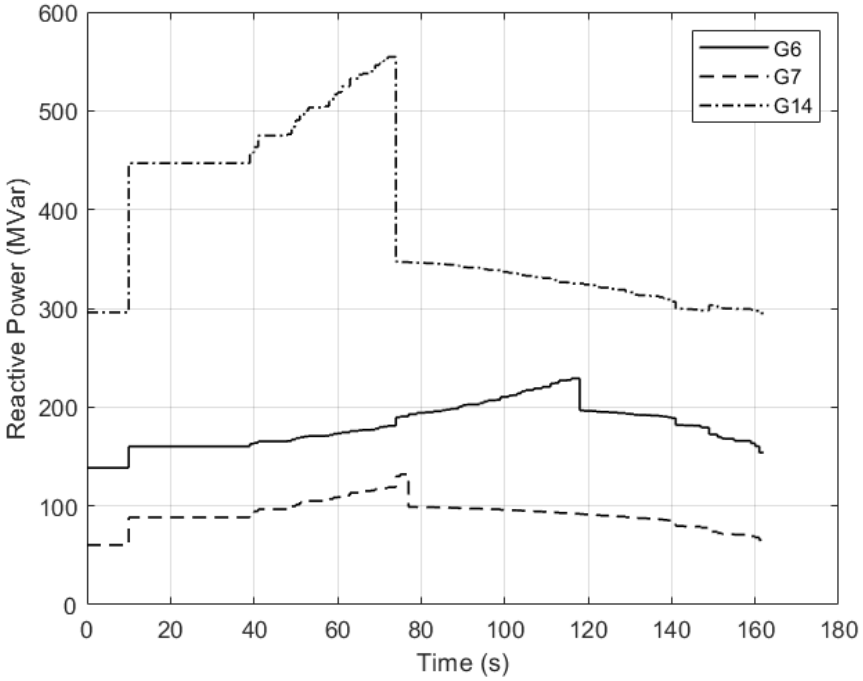

Figure 2.20: Synchronous Generators Reactive Power

Chapter 3

Effect of RES current injection requirements on Voltage Stability Margin

3.1 Ancillary services from RES

Following the formulation of the system equations for the Voltage Security Margin Optimal Power Flow in Chapter 2, in this chapter the effect of RES injection in transmission systems will be explored.

The increasing penetration of renewable energy resources (RES) connected to the grid via inverters (inverter-based resources – IBR), is drastically changing power system dynamics and control. When first introduced most IBRs would not provide any ancillary services, following a 'fit and forget' practice.

The decommissioning of conventional (mostly thermal) power plants creates a necessity for IBRs to replace them in terms of ancillary services, such as voltage/frequency regulation and balancing needs including emergency support in case of system instabilities or faults. For voltage stability problems in particular, the reactive power provided by synchronous generators is essential [4] and should be replaced when these units are withdrawn.

In 2016 EU released regulation 631 [59] with the objective to establish a network code that stipulates grid connection requirements for new power generating modules. Although the regulation differentiates to some extent the requirements for synchronous machines and IBRs, it sets a general framework with requirements concerning the operation of power generating modules in steady state as well as during system disturbances. More specifically, it stipulates that when necessitated by the responsible TSO, all new transmission-connected generating modules shall be capable of supporting the transmission system by providing frequency related or voltage related ancillary services. This may take place during either continuous system operation, or under sudden disturbances that may threaten system stability.

Focusing on voltage related services under abnormal system conditions, article 20 of the regulation elaborates on the so-called fast fault current injection (FFCI) capability for providing voltage support under system disturbances.

Previous works as in [60] and [61] have considered the impact of active and reactive current

injection on short-term system stability. More specifically, [60] examines the effect of the so-called K-factor introduced in the German grid code [62]. In this Chapter we focus on the effect of the same parameters on long-term voltage stability, as a low voltage at the point of common coupling (PCC) can result also from a severe contingency leading to long-term voltage instability and collapse.

Also, previous research has shown that IBRs can enhance voltage stability by providing reactive power, see for instance [63] and references therein. The provision of voltage stability control services by active distribution networks is also proposed in [64] and [65].

3.2 Regulations for Power Generating Modules

The fast fault current injection capability (FFCI) is defined in [59] and [62] as an incremental reactive current that must be injected by RES during events that result in considerable voltage deviations at their PPC, such as system faults. Supporting voltages during abnormal system conditions is a vital system service that has been traditionally provided by synchronous machines, that allows fault identification by system protection, while it assures better voltage restoration profile after fault clearance.

Considerable freedom is given to TSOs to specify FFCI parameters. In particular, article 20 of [59] stipulates that each TSO decides on whether FFCI is activated by a voltage deviation at the IBR grid connection point, or at its terminals. In addition, the definition of voltage deviation is left open, leaving plenty of room for determining the onset and termination of FFCI injection.

FFCI activation is based on a specified voltage threshold. When a transmission system operates under stressed conditions (e.g. with small voltage stability margin), a contingency may cause voltages to drop below this voltage threshold activating FFCI service. Thus, the operation of the IBR will change providing the required reactive current and possibly reducing its active power. However, the degree to which active and reactive current injection help in avoiding voltage instability is not known a priori, and thus a careful selection has to be made of parameters to ensure that the FFCI is towards the most appropriate direction to increase voltage stability.

Figure 3.1 shows the voltage-reactive current injection diagram corresponding to the FFCI requirement for transmission-connected RES according to [59] and [62].

In this diagram V_0 is the pre-fault voltage and V_{thr} the voltage threshold, below which the FFCI service is triggered. The reactive support is suspended when voltage returns back to V_{thr}. The vertical axis shows the requirement of additional reactive current injection Δi_q:

$$\Delta i_q = i_q - i_{q0} \tag{3.1}$$

where i_{q0} is the initial reactive current. Active and reactive currents are defined assuming $\tilde{V}$ as the phasor reference, and the current phasor:

$$\tilde{I} = i_p + j i_q \tag{3.2}$$

Active and reactive power are thus given by:

$$p = V I_p \tag{3.3}$$

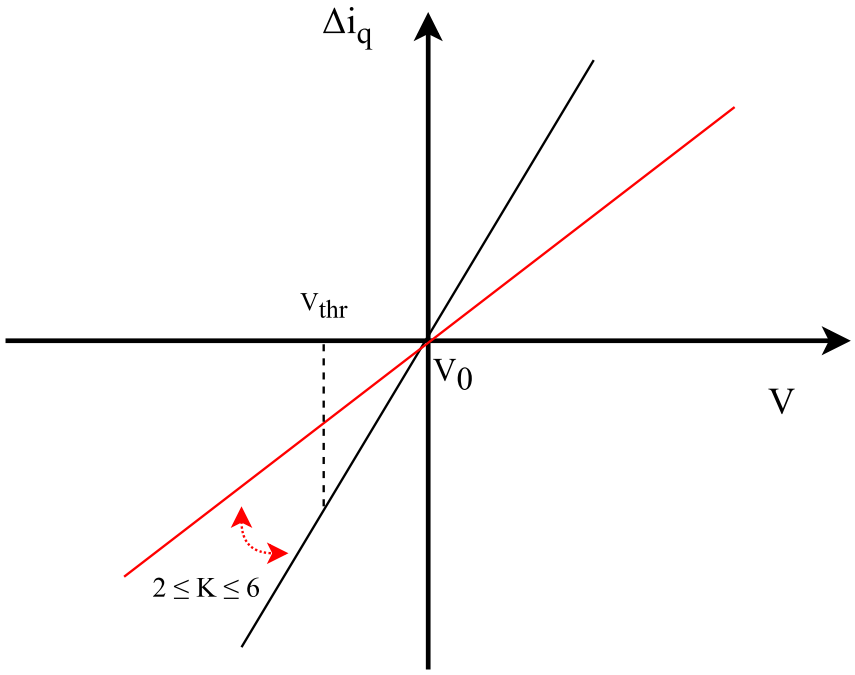

Figure 3.1: FFCI voltage-reactive current injection diagram

$$q = -VI_q \tag{3.4}$$

Thus negative i_q provides positive Q injection.

$$\tilde{I} = i_p + ji_q \tag{3.5}$$

The K-factor defines the required reactive current support as:

$$\Delta i_q = K(V - V_0) \tag{3.6}$$

In Fig. 3.1 the values of K-factor range between 2 and 6 according to the grid-code requirements.

3.3 Security Margin Determination using OPF

The formulation of the OPF for VSM of Section 2.9, (2.40) - (2.48), is used for determining the loadability limits. Let $\mathcal{N}$ be the set of buses and G the subset of generators, which in this chapter are assumed to be IBRs (no synchronous machines). Similarly to the problem of Section 2.10, the result of the optimization corresponds to the loading margin (LM) of the system, since no contingency is taken into consideration.

The OPF formulation to define the LM is the following:

$$\text{LM} = \max_{\boldsymbol{e},\boldsymbol{f},\lambda} \Delta\text{P} \tag{3.7}$$

where:

$$\Delta P = \lambda \sum_{k \in \mathcal{N}} d_{pk} \tag{3.8}$$

subject to power flow constraints (2.11) and:

$$p_{gk}^{min} \leq p_{gk} \leq p_{gk}^{max}, \forall k \in G \tag{3.9}$$

$$p_{gk}^2 + q_{gk}^2 \leq (e_k^2 + f_k^2) I_{Nk}^2, \forall k \in G \tag{3.10}$$

where p_{gk} and q_{gk} are the active and reactive power generation, and i_{Nk} is the rated current corresponding to nominal apparent power S_{Nk} under nominal voltage V_N. In (3.9), the left part of the inequality represents the ability of the IBR to curtail active power, while for the the right part p_{gk}^{max} is the power available from the primary energy source at the examined operating point.

Assuming for instance that the primary energy source is wind, then the available wind power P_w will be equal to the maximum of p_{gk}:

$$p_{gk}^{max} = P_{wk}, \quad \forall k \in G \tag{3.11}$$

3.4 Two Bus Transmission Test System

The test system used in this chapter is a simple radial transmission corridor (based on the radial 2 bus transmission system of Section 2.10) consisting of an infinite bus feeding a load, as presented in Fig. 3.2. At the load bus a capacitor bank is connected for voltage support. The impedance between the source (bus 1) and the load (bus $n+1$) is divided into n equal segments, thus defining intermediate buses 2 to n. In one of these buses, shown as bus k, a single IBR is connected representing a wind farm (WF). It is assumed that the IBR can control its active and reactive power injection at bus k.

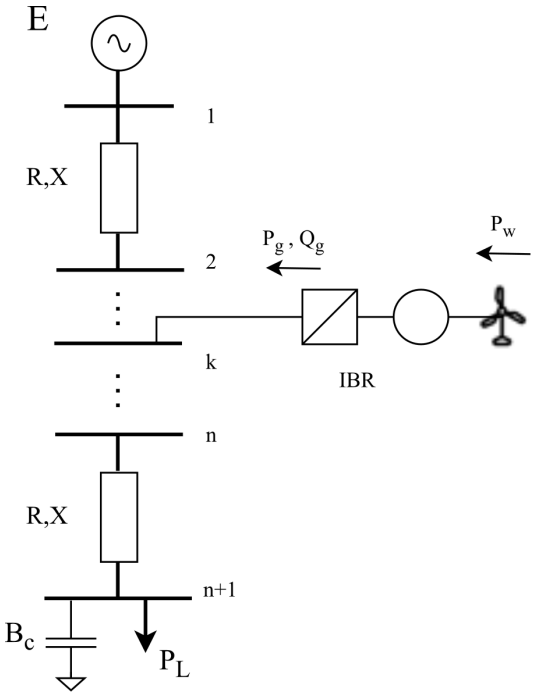

Figure 3.2: Test transmission line

Connecting the WF to one intermediate bus at a time gives rise to $n-1$ different system configurations, in each of which the IBR is at a different distance from the load. In this

way, the support provided by the IBR is evaluated as a function of its proximity to the load area.

In this study, $n = 10$. The power factor of the load is taken equal to 1. The rated apparent power of the IBR $S_N = 30\ MVA$, and the power available from the wind is denoted as P_w. In Table 3.1 the total impedance of the line is given together with all other data of the test system.

Table 3.1: Transmission System Data

nR (pu)	nX (pu)	B_c (pu)	E_{th} (pu)	n	S_N (MVA)
0.1	0.4	0.2	1.05	10	30

For each of the n-1 configurations (IBR connected at bus 2 up to bus n) the maximum active power that can be transferred to the load is calculated with the OPF method of the previous Section 3.3. Assuming a no-load initial condition, this corresponds to the voltage stability or loading margin. In the following Section the LM for different reactive current injection strategies by the IBR are compared. When FFCI is considered, it is assumed that a contingency (such as a sudden load increase) takes the system very close to its limit and if the voltage drops below V_{thr} the IBR will deliver the required current instantly, thus affecting the LM.

3.5 Case Study and Results

In this section, the optimization formulation of Section 3.3 is used to calculate the LM with three different assumptions regarding the IBR current injection. First, the IBR operates under unity power factor and constant active power equal to P_w. Next, the FFCI service explained in Section 3.2 is assumed with different gains K. Finally, the optimal IBR injections that maximize the VSM are calculated. In the two last cases, the active power can be curtailed.

In all cases, the test feeder presented in Section 3.4 is used with the IBR connected alternatively to each intermediate bus, 2 up to 4.

It is noted that the LM of the test system without any RES injection is equal to 114.98 MW.

3.5.1 Constant IBR injection with unity PF

The LM is computed using the formulation presented in Section 3.3. In this case, no control is assumed to be available from the IBR, meaning that the IBR is operating under unity power factor (UPF) and there is no possibility for active power curtailment. Thus, active power p_{gk} is equal to the one available from the wind P_w and inequality constraints (3.9) and (3.10) are transformed into equality constraints:

$$p_{gk} = P_w, \quad \forall k \in G \tag{3.12}$$

$$p_{gk}^{min} = p_{gk} = p_{gk}^{max}, \quad \forall k \in G \tag{3.13}$$

$$q_{gk} = 0, \quad \forall k \in G \tag{3.14}$$

Table 3.2 presents for each IBR connection bus, the calculated LM, the active and reactive generation and the voltage at bus k at the limit, when the IBR operates at constant unity power factor with $P_w = 18MW$. From Table 3.2 it becomes obvious that active power injections closer to the load have a greater effect on extending the LM. At the same time, the voltage at the PCC becomes lower the closest it is to the load, as expected. The value of factor E_{P_w} represents the percentage of the increase in the LM (compared to the case without any RES injections, $LM = 114.98MW$) with respect to the wind power available.

$$E_{P_w} = \frac{\Delta LM}{P_W} 100\% \tag{3.15}$$

Table 3.2: VSM for different RES locations under UPF

	k	LM (MW)	p_g (MW)	q_g (Mvar)	$V_{k,maxP}$ (pu)	$E_{P_w}(\%)$
Infinite Bus	1					
|	2	115.44	18.00	0.00	1.0041	3
|	3	116.09	18.00	0.00	0.9609	6
|	4	116.97	18.00	0.00	0.9205	11
|	5	118.12	18.00	0.00	0.8831	17
|	6	119.60	18.00	0.00	0.8486	26
|	7	121.45	18.00	0.00	0.8169	36
|	8	123.71	18.00	0.00	0.7876	48
|	9	126.41	18.00	0.00	0.7608	63
↓	10	129.53	18.00	0.00	0.7369	81
Load bus	11					

In Table 3.3, the effect of the IBR on VSM can be seen for three different active power generation P_w values. For all cases, the reactive power generation is zero, according to (3.14).

Table 3.3: VSM for different active power generation on each bus

		VSM (MW)		
	k	$P_w = 9MW$	$P_w = 18MW$	$P_w = 25MW$
Infinite Bus	1			
|	2	115.21	115.44	115.62
|	3	115.54	116.09	116.51
|	4	115.99	116.97	117.71
|	5	116.58	118.12	119.28
|	6	117.34	119.60	121.30
|	7	118.28	121.45	123.75
|	8	119.42	123.71	126.46
|	9	120.77	126.41	129.60
↓	10	122.31	129.53	133.17
Load bus	11			

As seen in Table 3.3, when only active power is available, the support to the VSM is greater when more power is injected, and when the IBR is located closer to the load area, as it relieves the system from transferring P_w from the remote bus. This can be also

Table 3.4: LM increase factor

	VSM (MW)			
	k	$E_{Pw9}(\%)$	$E_{Pw18}(\%)$	$E_{Pw25}(\%)$
Infinite Bus	1			
|	2	2.60	2.56	2.55
|	3	6.25	6.16	6.10
|	4	11.22	11.04	10.90
|	5	17.78	17.45	17.21
|	6	26.18	25.66	25.28
|	7	36.66	35.94	35.08
|	8	49.37	48.50	45.91
|	9	64.36	63.48	58.48
↓	10	81.42	80.82	72.77
Load bus	11			

observed in Figure 3.3, where the VSM grows larger for more active power generation from the IBR the closer it gets to the load area. In Table 3.4, the factor E_{P_w}, is presented for each case of wind power available.

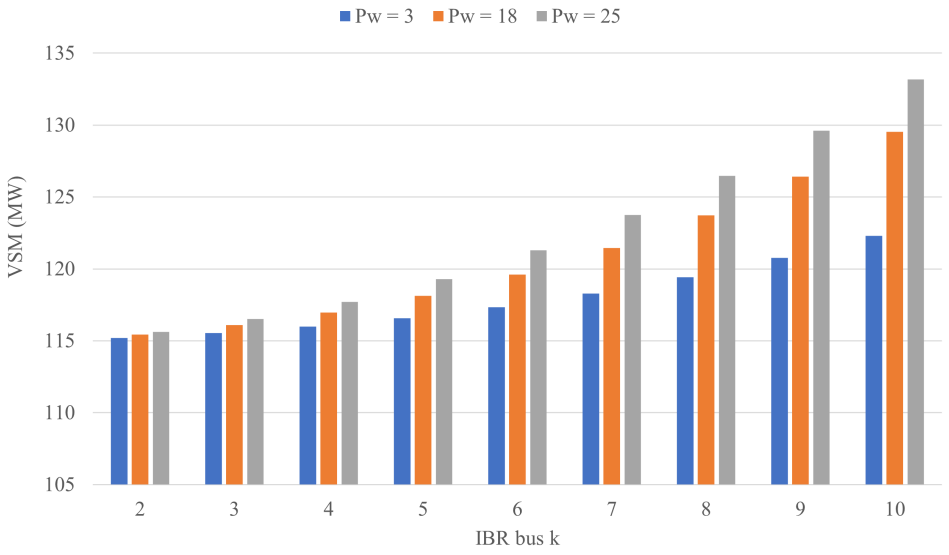

Figure 3.3: VSM for different active power generation

3.5.2 Implementation of assumed FFCI service

During stressed conditions, as also observed in Table 3.2, voltages may decrease significantly along the buses of the transmission system, thus triggering the activation of the FFCI service for the IBRs, if a contingency brings the system close to the stability limit. In this case, the IBRs will provide reactive current support according to the deviation of the voltage at the PCC. The reactive current injection requirement is active only while the voltage at the PCC is below the voltage threshold V_{thr}, which in this case is taken equal to 0.85 pu according to [59]. From Table 3.2, it becomes clear that for $P_w = 18MW$, when the WF is connected to one of the buses between 2-5, there will be no actions, since the threshold is not violated.

A high reactive current injection from the IBR may bring the current close to its rated value, thus causing a limitation of the active current. Therefore, for high wind conditions the IBR may have to curtail active power generation, in order to meet the requirements of Fig. 3.1.

To address these issues some modifications are necessary in the OPF formulation (3.7)-(3.10). In order to include the reactive current injection requirements two inequalities are added to the OPF formulation, which apply only if the voltage without control is below the threshold at the LM:

$$q_{gk} \leq KV_k(1 - V_k), \quad \forall k \in G \tag{3.16}$$

$$V_k = \sqrt{e_k^2 + f_k^2} \leq V_{thr} \tag{3.17}$$

where, (3.16) stems from the reactive current voltage-deviation linear equation (3.6) assuming $i_{q0} = 0$ and $V_0 = 1$, while (3.17) ensures that the voltage of the RES will be under the desired threshold, for the control to be active. Note that (3.16) will not hold as equality in two cases: either when (3.17) holds as equality and further injection is not required, or when (3.9) is active even with $p_{gk} = 0$ and thus the current limit is reached and no further reactive support is possible.

As stated above, since the trigger for the FFCI support is the voltage threshold, the LM is recalculated only for the cases where the value of the voltage at the PCC at the LM is below $V_{thr} = 0.85pu$ in the cases with $p_g = P_w$ under UPF. Thus, for cases 2-5, (3.16)-(3.17) do not apply.

For example, for the results of Table 3.2, with active power generation $P_w = 18$MW, the new formulation needs only to be applied for connection of the RES to buses 6 to 10, as for the other buses the system reaches its stability limit without violating the voltage threshold and no FFCI control is triggered.

Table 3.5: VSM for P_w=18MW with FFCI and K=2

	k	VSM (MW)	p_g (MW)	q_g (Mvar)	$V_{k,maxP}$ (pu)	$E_{S_N}(\%)$
|	6	123.09	18.00	7.65	0.8500	27.03
|	7	126.34	18.00	8.98	0.8169	37.87
|	8	130.02	18.00	10.12	0.7853	50.12
|	9	133.96	18.00	11.04	0.7568	63.27
↓	10	137.92	18.00	11.71	0.7340	76.46
Load Bus	11					

Table 3.6: VSM for P_w=18MW with FFCI and K=4

	k	VSM (MW)	p_g (MW)	q_g (Mvar)	$V_{k,maxP}$ (pu)	$E_{S_N}(\%)$
|	6	126.29	18.00	15.30	0.8500	37.70
|	7	130.77	18.00	17.11	0.8278	52.62
|	8	134.47	17.44	17.48	0.8231	64.98
|	9	137.67	16.85	17.85	0.8182	75.65
↓	10	140.56	17.16	17.66	0.8207	85.28
Load bus	11					

Similarly to the UPF case, the value of factor E_{S_n} represents the percentage of the increase in the LM (compared to the case without any RES injections, $LM = 114.98MW$) with respect to the nominal apparent power of the WF.

$$E_{S_N} = \frac{\Delta LM}{S_N} 100\% \tag{3.18}$$

Results in Tables 3.5 and 3.6 respectively, present the increased VSM when the FFCI is applied for different parameters K. It can be observed that, compared to the constant IBR injections with unity PF, the VSM is significantly increased. Moreover, for larger K factor, the stability margin increases more. Thus a first conclusion is that FFCI can be beneficial for long-term voltage stability, when activated by a contingency that brings the system close to the LM.

It is important to highlight that for $K = 4$, if the IBR is close to the load and higher voltage deviations are experienced, then the reactive current injection comes at the expense of active power, as shown in the rows where k is 8, 9 and 10, for which $p_{gk} < P_{wk}$. This implies that the result may or may not be optimal, as the curtailed active power could be more valuable than the reactive injection.

Sensitivity of the LM with respect to the active power injections is greater the closer the IBR gets to the load. As a result, curtailing active power injections for reactive current injections may prove to be sub-optimal, when the IBR is located relatively close to the load.

Table 3.7: VSM with FFCI for different K and P_w = 18MW

	k	K=2	K=3	K=4	K=5	K=6
|	6	123.09	124.72	126.29	127.54	127.74
|	7	126.34	128.64	130.77	131.60	131.58
|	8	130.02	132.98	134.47	134.72	134.17
|	9	133.96	137.00	137.67	137.41	136.26
↓	10	137.92	140.44	140.56	139.92	138.10
Load bus	11					

In table 3.7 and also displayed in Figure 3.4, the LM is shown for different values of K for the IBR positioned in buses between 6 and 10. It can be observed that depending on the location of the IBR, different values of K achieve the highest VSM. As the RES gets closer to the load, lower values of K are needed to obtain the largest VSM. Higher values of K imply a larger active current curtailment in order to respect the inverter current limit. In buses close to the aggregated load, the sensitivity of VSM with respect to the injected active power increases and thus curtailment of active power proves ineffective.

3.5.3 Optimal RES injections

While the implementation of the FFCI has increased the LM in all cases, as observed in the previous subsection, Table 3.7 reveals that depending on the proximity of the IBR bus to the aggregate load, different values of parameter K achieve the largest VSM, thereby indicating the need for further investigation.

For that reason, in this subsection, the initial OPF formulation is solved again, without

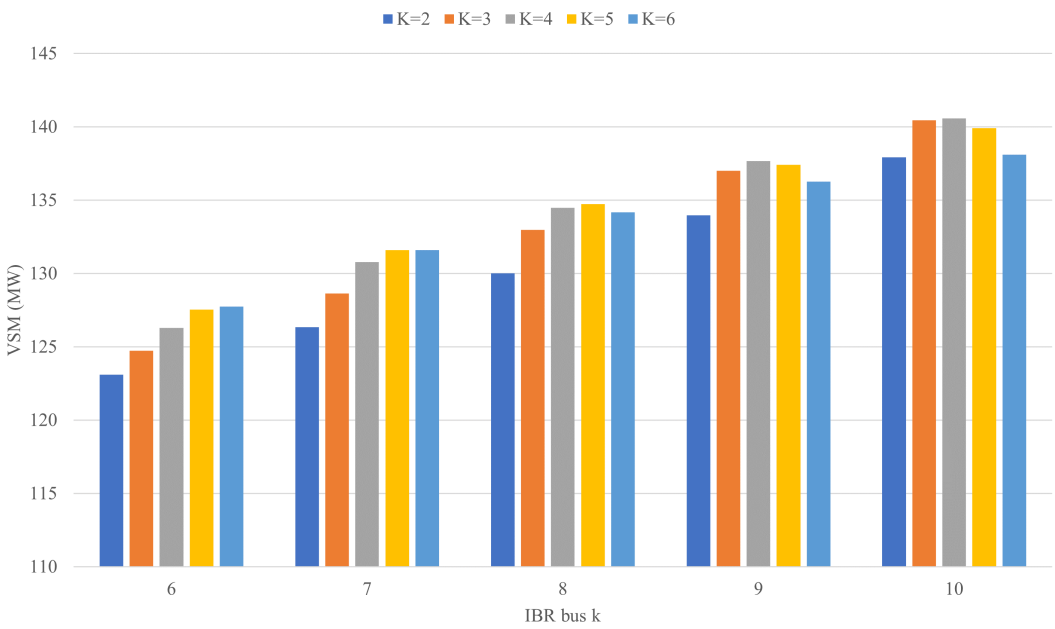

Figure 3.4: VSM with FFCI for different K

constraint (3.16). In this case, variables p_{gk} and q_{gk} are only restricted by the maximum wind power available $P_w = p_{gk}^{max}$ and by the inverter maximum current constraint (3.10). Thus, the LM is calculated with p_g, q_g as free decision variables and the problem is written again here:

$$\text{LM} = \max_{\boldsymbol{e,f,p_g,q_g},\lambda} \Delta\text{P} \tag{3.19}$$

s.t.

$$\boldsymbol{h}(e, f, p_g, q_g, \lambda) = 0 \tag{3.20}$$

$$V_{gk} \leq V_{thr}, \forall k \in G \tag{3.21}$$

$$p_{gk}^{min} \leq p_{gk} \leq p_{gk}^{max}, \forall k \in G \tag{3.22}$$

$$p_{gk}^2 + q_{gk}^2 \leq (e_k^2 + f_k^2) I_{Nk}^2, \forall k \in G \tag{3.23}$$

As a result, for the IBR placed on each bus k, where $V_k \leq V_{thr}$ at the optimal LM without any control (Section 3.5.1). For the other configurations, application of the K-factor is irrelevant as the voltage remains above the threshold V_{thr} at the LM. At the solution point, the optimal active and reactive power injections are computed, for which the LM is maximized. Based on these results, the optimal value for parameter K_{opt} can be computed in each configuration based on the optimal value of q_g injection and voltage at the stability limit.

In Tables 3.8 and 3.9, the optimal injections are presented for maximum VSM and the resulting optimal values of parameter K, calculated from (3.16), with the values obtained from the OPF solution (3.19)-(3.23) for available active power P_w = 18MW. It can be observed, that closer to the load the active power curtailment is decreased with respect to the previous subsection, as the sensitivity of the VSM to the active power injections is greater. Also, it is obvious that optimal values of parameter K depend not only on the proximity of the IBR to the load, but also on the available active power P_w. When

Table 3.8: Calculation of optimal K for $P_{gk}^{max} = 18MW$

k	VSM (MW)	p_g (MW)	q_g (Mvar)	V_k (pu)	K_{opt}	$E_{S_N}(\%)$
6	127.78	12.76	22.08	0.8500	5.77	42.67
7	131.75	14.18	21.19	0.8500	5.54	55.90
8	134.73	15.45	19.82	0.8378	4.86	65.83
9	137.68	16.65	18.13	0.8205	4.10	75.67
10	140.66	17.88	16.39	0.8085	3.53	85.60

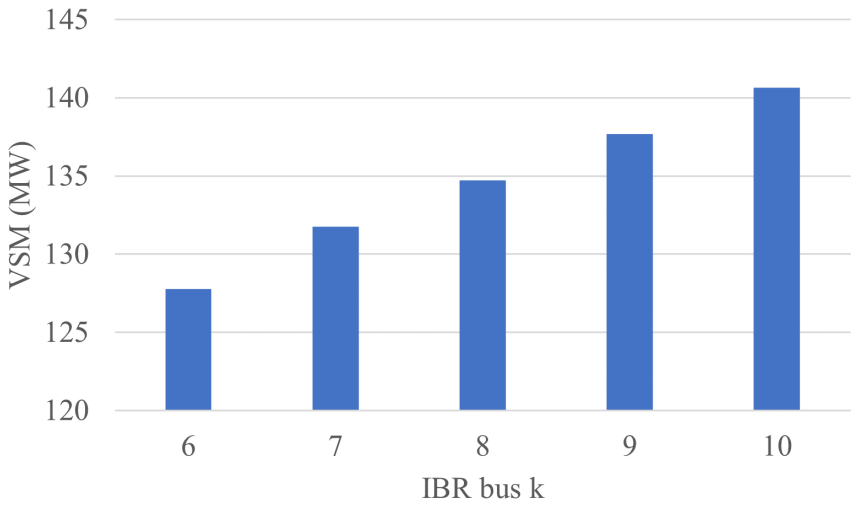

Figure 3.5: VSM for optimal RES injections per bus

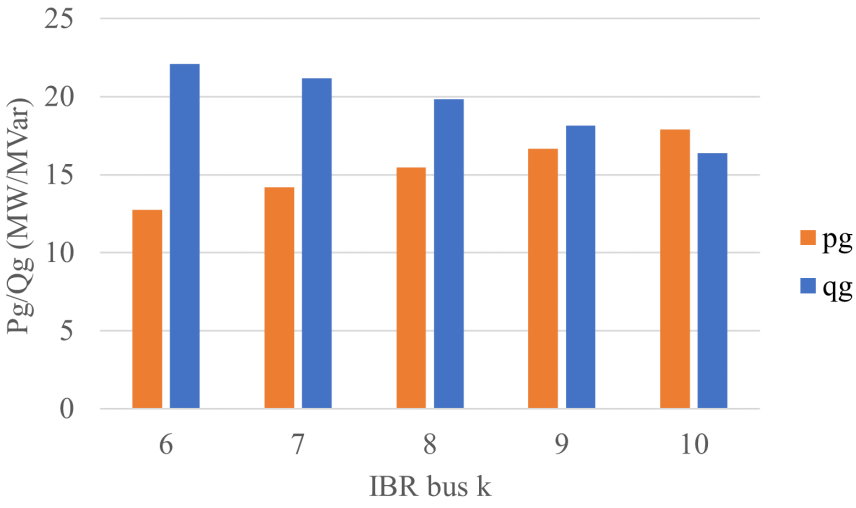

Figure 3.6: Optimal RES injections for each bus k

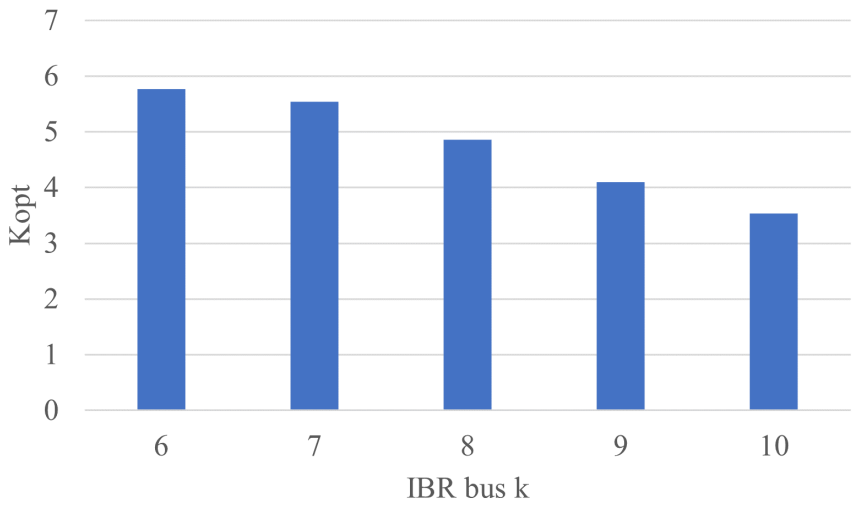

Figure 3.7: Optimal K parameter per bus

less active power is available, more reactive current injections can be provided without violating inverter current constraints (3.10), thus optimal value of K is higher.

Respectively, in Figures 3.5, 3.6 and 3.7 the VSM, active and reactive power injections and K parameter per bus k are presented.

Finally, in Table 3.9, the same results are presented for available active power equal to $P_w = 9$MW. In this case it can be observed that, due to low available active power from wind, the optimal parameters can be achieved without active power curtailment, as current limits are not exceeded.

Table 3.9: Calculation of optimal K for $P_{gk}^{max} = 9MW$

IBR bus	VSM (MW)	p_g (MW)	q_g (Mvar)	V_g (pu)	K_{opt}
6	127.62	9.00	23.86	0.8500	6.24
7	131.29	9.00	23.86	0.8500	6.24
8	133.78	9.00	23.38	0.8351	5.66
9	135.97	9.00	22.80	0.8170	5.08
10	137.79	9.00	22.41	0.8049	4.76

3.6 Conclusions

This chapter investigated the impact of current-injection requirements for transmission-connected RES on the long-term voltage stability of a simple radial transmission system. This impact is illustrated by comparing the system maximum power transfer (VSM) for different IBR control schemes and for IBR locations with varying distance to the load. The aim is to extract some general conclusions and guidelines for the selection of appropriate gain parameters for the reactive current injection control.

Three control schemes were compared:

- (i) constant unity power factor at the PCC

- (ii) fast fault current injection service as specified in EU regulation 2016/631 [66]
- (iii) optimal active/reactive power control to maximize VSM

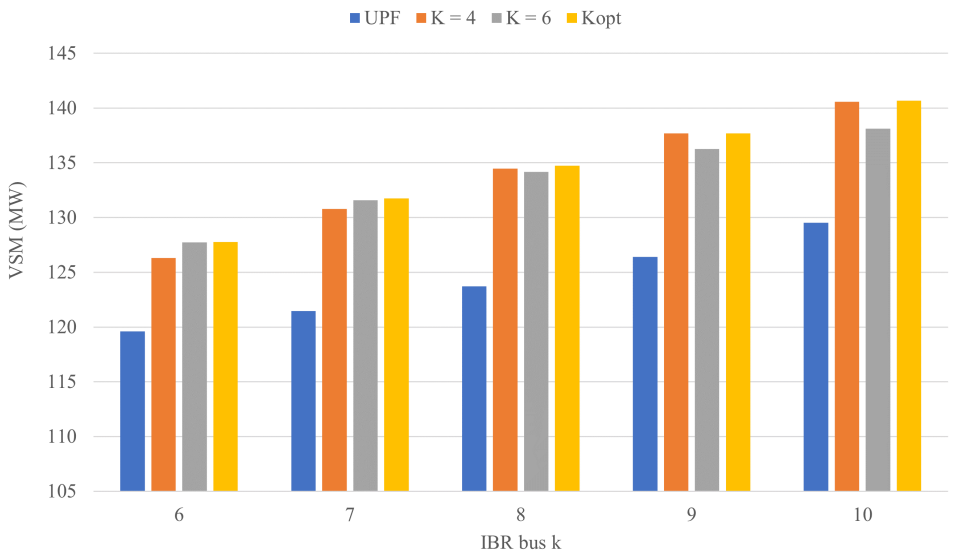

Figure 3.8: VSM compared between different control schemes

A first and rather expected conclusion was that injection of active power by the RES is increasing VSM, especially when the injection is closer to the load. In the studied system the VSM increase can go above 70% of the injected active power when close to the load.

The second conclusion drawn was that when the FFCI requirement is activated due to the low voltage induced after a contingency, the stability margin is increased, which is an encouraging sign, as this type of control, designed to help protection operation and voltage recovery, is also supporting long-term voltage stability. The further VSM increase with small gain K to that provided by only the active power injection ranges depending on the proximity to the load from 11%-28% of the nominal apparent power of the IBR (30 MVA in the example). For a medium value K=4 this increase can go up to 37% of the IBR rating. However, if the gain K increases further, the VSM is actually reducing. This is a result of the required reduction of active power to keep the reactive support. Clearly the net result depends on the sensitivity of the margin to active versus reactive injection at each IBR location.

The obtained results on the test system showed that the closer the IBR is located to the load, the more important the active power injection becomes with respect to the reactive power, thereby indicating that a smaller K is required for maximizing VSM. Thus the need for optimization which showed that away from the load and for lower active power injection the gain could go to its maximum value of K=6, while close to the load and for higher active injections by the RES the optimal value of the gain K is reduced. A visual representation of the comparison between the different control schemes is shown in Figure 3.8.

Clearly, for a real system deeper investigations on selecting K_{opt} are necessary for each RES location and contingency considered, in order to improve system robustness. However, the general rules suggested in this chapter can facilitate the FFCI gain selection

process at a time where conventional synchronous machines are being gradually decommissioned, thereby raising the need for further ancillary services from IBRs to preserve system stability margins.

Chapter 4

Distribution Network Modelling and Flexibility

In this chapter, the modeling of the distribution network is described. The distribution network is studied separately, decoupled from the transmission system. In some cases, however, it may include an equivalent Thevenin of the transmission system assuming that the secondary bus of the distribution transformer maintains a constant voltage.

4.1 Active distribution network modelling

The components that form an Active Distribution Network (ADN) include distributed generation (DG), or in general, inverter based resources (IBR) with or without battery energy storage systems (BESS), the load tap changer (LTC), voltage depended loads, shunt capacitors or reactances and the distribution lines or cables.

For the estimation of the distribution network consumption limits, a constrained optimization problem will be formulated, similarly to Chapter 2 for the transmission system equations.

Using the OPF formulation of the ADN, the P and Q flexibility region will be introduced and will be computed, using different methods and comparing methods that already exist in the recent literature presented in Chapter 1.

P, Q represent the active and reactive power flow at the point of common coupling (PCC) between the transmission system and the distribution feeder. The general layout is presented in Figure 4.1.

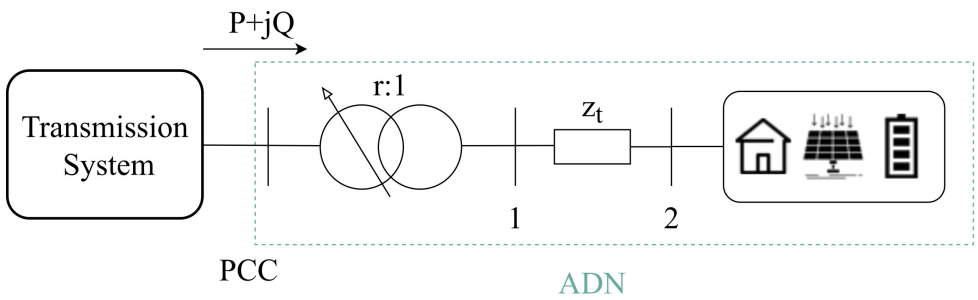

Figure 4.1: Active and Reactive power at the PCC

In the following subsections, the modelling of the active distribution network will be presented, including the following components:

- Inverter based resources (IBR)
- Load Tap changers (LTC)
- Shunts
- Distribution lines/cables

Finally, the optimization problem to determine the P,Q flexibility will be defined.

4.1.1 Inverter based resources

IBR or CIG refer to the distributed energy resources connected at the lower voltage levels through power electronics, consisting of DC/DC, AC/DC and DC/AC converters, depending on the energy source that is used. The most common IBRs are photovoltaic power plants (PV) and wind parks or winds farms (WF). Wind farms are usually connected to the transmission system through their own dedicated feeders, while photovoltaics are connected to the distribution network close to the load demand.

A big advantage of IBRs is that converters can control separately active and reactive power at the point of common coupling (PCC) with the power grid. Control can be achieved very fast, so in the time-scale of long-term voltage stability, it is assumed that control and reference values are achieved practically instantaneously, assuming converter short-term stability.

Unlike synchronous machines, converters have limited over-current ability, even for a short time. The maximum permissible current has to cover nominal apparent power S_n under nominal voltage V_n. As a result, the limit for the current of the converter is set as:

$$I_n = \frac{S_n}{V_n} \tag{4.1}$$

Since, IBRs can operate in off nominal voltage, the reactive power limit is given by the following inequality:

$$p_g^2 + q_g^2 \leq (V_g I_n)^2 \tag{4.2}$$

Of course, simultaneously with (4.2), the active power must also respect the maximum permissible value.

$$p_g^{min} \leq p_g \leq p_g^{max} \tag{4.3}$$

Depending on the requirements of the system, further limitations can be applied, like minimum and maximum values for the power factor of the inverter at the PCC, thus limiting further the capability curve of the inverter. European legislation [66] addresses the requirements for generators in order to connect to the grid, applying also to inverter based generation. In this thesis, it is assumed that the inverter can operate in the full region represented by equations (4.2)- (4.3).

Based on the inverters limits:

Moreover, converters voltages are also bound by upper and lower voltage constraints:

$$V_g^{min} \leq V_g \leq V_g^{max} \tag{4.4}$$

Battery energy storage systems (BESS) are not explicitly modelled. It is assumed that BESS can be connected to the same bi-directional converter as the distributed generator as seen in Fig. 4.2, thus the limits of (4.3) can be extended to negative values.

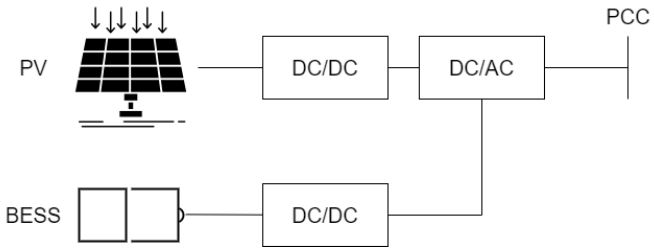

Figure 4.2: Solar panel with BESS

For the time duration that will be needed in case of a voltage stability emergency, the storage combined with the distributed generation can provide active power inside the full range of the IBRs active power capability.

If no BESS is assumed, then upper and lower active power limits coincide with the input of the IBG source, $p_g^{min} = p_g = p_g^{max}$. As a result p_g is constant when no BESS is assumed, or it is a decision variable when BESS is assumed.

4.1.2 Load tap changer

The step-down transformers installed in the HV/MV substations are regulating the distribution voltage inside a specified dead-band by performing discrete changes of their tap ratio. The equivalent circuit of Figure 4.3, is widely used for representation of two-winding transformers in power flow and stability studies [2]. The IEEE common format for exchange of solved power flow cases uses this representation [67]. This equivalent circuit can be used to represent a transformer with a fixed tap on one side and an on-load tap changer (OLTC) on the other side.

The equivalent circuit of 4.3, is then reduced to the form of a π network as presented in 4.4.

The corresponding admittance terms y_1, y_2, y_3 are calculated as follows:

$$y_1 = \frac{Y_t}{r} \tag{4.5}$$

$$y_2 = \frac{Y_t}{r^2} - \frac{Y_t}{r} \tag{4.6}$$

$$y_3 = \frac{(r-1)Y_t}{r} \tag{4.7}$$

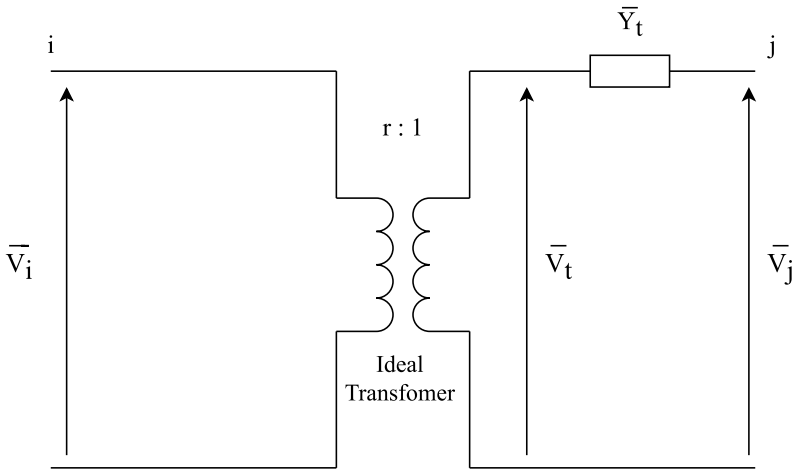

Figure 4.3: Standard equivalent circuit for a transformer

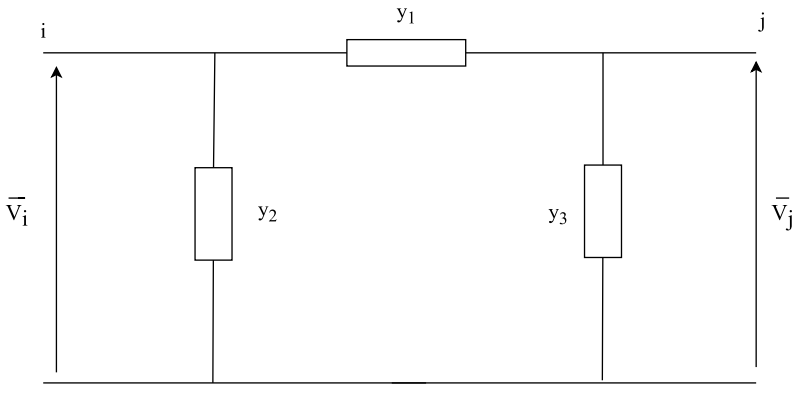

Figure 4.4: Equivalent π circuit

As a result, the branch admittance matrix Y_{ij} for a transformer of ratio $r:1$, connected between buses i, j is as follows:

$$Y^{trf} = \begin{bmatrix} \frac{Y_t}{r^2} & -\frac{Y_t}{r} \\ \frac{Y_t}{r} & Y_t \end{bmatrix} \tag{4.8}$$

If the voltage of the medium voltage side of the HV/MV substation is $V_j = V_d$, then for a specified deadband d and a voltage setpoint V_{ref}, the voltage is regulated in the range:

$$V_{ref} - \frac{d}{2} \leq V_d \leq V_{ref} + \frac{d}{2} \tag{4.9}$$

From (4.8), it is observed that the tap r can be included in the power balance equations, through the admittance matrix, as a continuous decision variable and is bound between the upper and the lower limit of the tap ratio:

$$r^{min} \leq r \leq r^{max} \tag{4.10}$$

When the distribution feeder is considered decoupled, the LTC may be neglected and not explicitly represented. In this case, the regulated voltage V_d of the secondary side of the HV/MV transformer is one of the decision variables. Flows P,Q are calculated at the primary (transmission bus) side to include reactive power losses on the leakage reactance of the transformer X_t (transformer is assumed lossless). For the decision variable V_d, (4.11) defines its limits.

$$V^{min} \leq V_d \leq V^{max} \tag{4.11}$$

This assumption is plausible as long as the LTC tap range is not exhausted, so that it can regulate the distribution side voltage close to its setpoint.

4.1.3 Loads

The loads in the ADN are considered as voltage sensitive and are modelled as exponential functions of voltage with exponents a and b for active and reactive power respectively. In the examples of this thesis active load is considered as constant current ($a = 1$) and reactive load as constant admittance ($b = 2$).

$$p_d = p_{d0}(\frac{V}{V_0})^a, \tag{4.12}$$

$$q_d = q_{d0}(\frac{V}{V_0})^b, \tag{4.13}$$

Voltage dependency of loads, as presented in (4.12) and (4.13) offers the opportunity of indirect load modification through voltage control.

If specific loads are considered dispatchable, following demand-response (DR) signals, i.e. that they can actively control their demand upon a request from the control centre, these will be treated as controlled injections, similar to DG/BESS. In that case:

$$p_d^{min} \leq p_d \leq p_d^{max} \tag{4.14}$$

4.1.4 Active and Reactive Shunts

Shunt reactors and capacitors are included in the bus admittance matrix, as parts of the diagonal elements of the corresponding buses. The same applies to constant admittance loads. Shunt conductance g_{ii} (or susceptance b_{ii}) connected to bus $i \in N$, are added to the diagonal elements of the Y matrix. In distribution networks, usually capacitor banks are installed near the HV/MV transformer.

4.1.5 Distribution Line Limits

Distribution feeders are designed so that line limits are not met in normal operating conditions. Nonetheless, with the increase of distributed generation and reverse power flows, there is a necessity to monitor the thermal limits of the lines at any point.

Similarly to Chapter 2 and (2.34), (2.35), let L be the set of line from/to buses (i, j). Then:

$$p_{ij} = (e_i^2 + f_i^2)g_{ij} - (e_i e_j + f_i f_j)g_{ij} + (e_i f_j - e_j f_i)b_{ij}, \quad \forall (i,j) \in L \tag{4.15}$$

$$q_{ij} = -(e_i^2 + f_i^2)(b_{ij} + b_{sij}) + (e_i e_j + f_i f_j)b_{ij} + (e_i f_j - e_j f_i)g_{ij}, \quad \forall (i,j) \in L \tag{4.16}$$

where p_{ij}, q_{ij} represent the active and reactive flow in every line of the system, g_{ij},b_{ij} are the line series admittance and susceptance respectively and b_{sij} is one half of the line charging susceptance.

Assuming that the thermal or steady state limit of line (i, j) is s_{ij}^{lim}, then the branch flow constraints are as follows:

$$p_{ij}^2 + q_{ij}^2 \leq (s_{ij}^{lim})^2, \quad \forall (i,j) \in L \tag{4.17}$$

4.1.6 Constrained optimization problem formulation

Let $\mathcal{A}$, be the subset of nodes of the transmission system, in which ADNs are connected. Each ADN is considered separately. The ADN is absorbing power P, Q, as shown if Fig. 4.1 from the primary side of a distribution transformer, while the voltage of the secondary transformer bus is regulated by the transformer LTC. The ADN includes voltage sensitive loads, IBGs, and possibly storage. Let $\mathcal{N}_A$ be the set of the considered ADN buses and G_A the set of buses with IBGs and/or BESS (IBRs).

For an initial absorption P_0, Q_0 objective function $\zeta(\Delta P, \Delta Q)$ is a linear combination of absorption changes ΔP, ΔQ that refer to the change in the active and reactive power flow at the PCC, from the operating point P,Q.

$$P = P_0 + \Delta P \tag{4.18}$$

$$Q = Q_0 + \Delta Q \tag{4.19}$$

Subject to the power balance and ADN operational constraints leads to the problem formulation:

$$\max_{e,f} \quad \zeta(\Delta P, \Delta Q) \tag{4.20}$$

$$\boldsymbol{g_A}(e,f) = 0 \tag{4.21}$$

$$V_k^2 = e_k^2 + f_k^2, \forall k \in \mathcal{N}_A \tag{4.22}$$

$$V_k^{min} \leq V_k \leq V_k^{max}, \forall k \in \mathcal{N}_A \tag{4.23}$$

$$p_{gk}^2 + q_{gk}^2 \leq (V_k i_{Nk})^2, \forall k \in G_A \tag{4.24}$$

$$p_{gk}^{min} \leq p_{gk} \leq p_{gk}^{max}, \forall k \in G_A \tag{4.25}$$

where, $\boldsymbol{g_A}$ is the set of power balance equations:

$$p_k = p_{gk} - p_{dk0}(\frac{V_k}{V_{k0}})^a, \quad \forall k \in \mathcal{N}_\mathcal{A} \tag{4.26}$$

$$q_k = q_{gk} - q_{dk0}(\frac{V_k}{V_{k0}})^b, \quad \forall k \in \mathcal{N}_\mathcal{A} \tag{4.27}$$

including also the voltage dependency of loads, as explained in Section 4.1.3, and:

$$p_k = e_k(\boldsymbol{g_k}^T \boldsymbol{e} - \boldsymbol{b_k}^T \boldsymbol{f}) + f_k(\boldsymbol{b_k}^T \boldsymbol{e} + \boldsymbol{g_k}^T \boldsymbol{f}), \quad \forall k \in \mathcal{N}_\mathcal{A} \tag{4.28}$$

$$q_k = -e_k(\boldsymbol{b_k}^T \boldsymbol{e} + \boldsymbol{g_k}^T \boldsymbol{f}) + f_k(\boldsymbol{g_k}^T \boldsymbol{e} - \boldsymbol{b_k}^T \boldsymbol{f}), \quad \forall k \in \mathcal{N}_\mathcal{A} \tag{4.29}$$

It should be noted, that absorptions P, Q are included also in (4.28), (4.29) as:

$$p_1 = P \tag{4.30}$$

and

$$q_1 = Q \tag{4.31}$$

Equations (4.23) represent the voltage constraints for every bus of the ADN. Branch flow limits are neglected in this formulation for simplicity, but they can be included, if considered necessary. Function ζ has no unconstrained maximum or minimum points, so the optimal points are determined by the active (or binding) operational constraints.

The problem formulation (4.20)-(4.25) is used as the basic formulation for the optimization problems that will be described later in this chapter, on the test feeders that will be presented in Section 4.2.

4.2 Test Feeders

For the analysis and implementation of the methodologies, three different ADN test feeders are considered in this thesis. The first one is a simple 2-bus feeder with aggregate load and a WF, the second one is a 30-bus test feeder with multiple loads and IBGs (PVs) and the third test feeder is a real rural distribution network from the network from North Eastern Greece.

4.2.1 2-bus feeder

The 2-bus feeder represents a Wind Farm (WF) dedicated distribution feeder and an aggregate load placed in the MV bus. The WF is connected to the system through a bi-directional inverter, allowing for battery storage. In the next chapters, five different 2-bus feeders are used, representing different WFs connected through dedicated feeders. The data for one such test feeder are presented in 4.1, the initial absorption of the feeder is shown. Also, initial load consumption and generation are included. It is noted that for this feeder, generation from RES is constant, meaning that $p_g = p_g^{min} = p_g^{max}$.

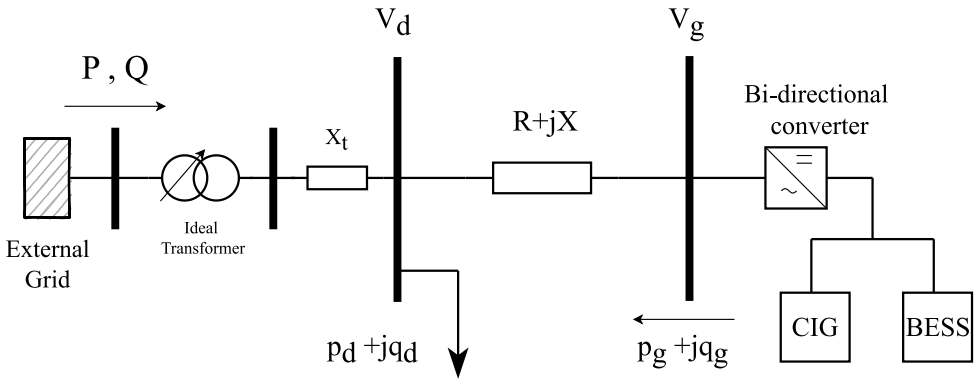

Figure 4.5: 2-bus feeder

The feeder is connected to the grid through a 150kV/20kV transformer with LTC as presented in Figure 4.5.

Table 4.1: Two Bus ADN Data

$P_0(MW)$	$Q_0(Mvar)$	$p_{d0}(MW)$	$q_{d0}(Mvar)$	$p_g(MW)$	$q_g(Mvar)$
600	180	696.784	142.471	97.2	0

$R(pu)$	$X(pu)$	$X_t(pu)$
0.00441	0.0608	0.0015

4.2.2 30-bus feeder

The 30-bus ADN feeder is taken from [40] and is slightly modified by replacing synchronous generation with IBRs. The distribution network is limited to the 20kV level and is hosting 5 CIGs and multiple loads. It is also connected to the grid through a 150kV/20kV transformer with LTC. The R/X ratio of the feeder is close to 0.35. Full data for this feeder are presented in the Appendix. The one line diagram of the 30-bus feeder is presented in Fig. 4.6.

4.2.3 Rural distribution feeder

This distribution feeder is a real feeder from the distribution network of North-Eastern Greece and specifically from the area of Xanthi and the single line diagram is presented in Fig. 4.7.

It consists of approximately 100 buses and is connected to the transmission system through a 150kV/20kV transformer with LTC. Two PVs are connected to the ADN as well as a

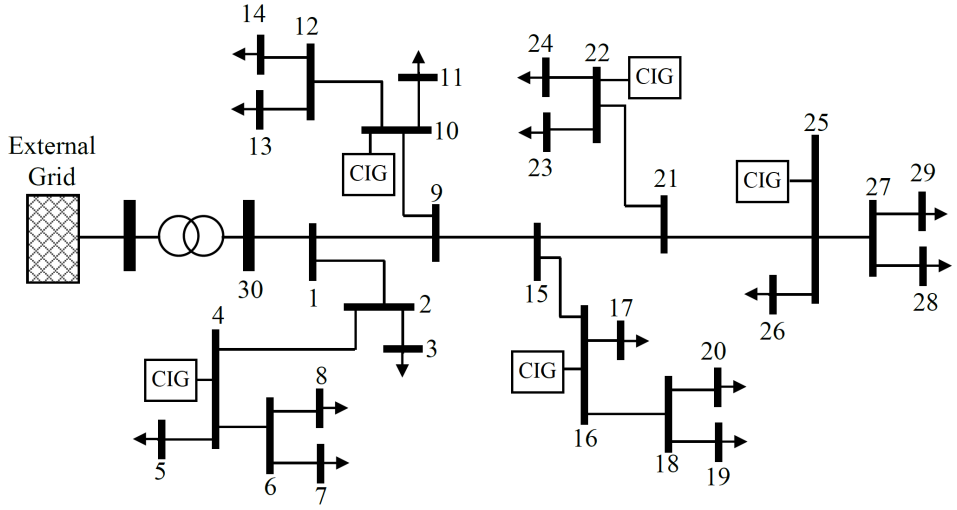

Figure 4.6: 30-bus feeder

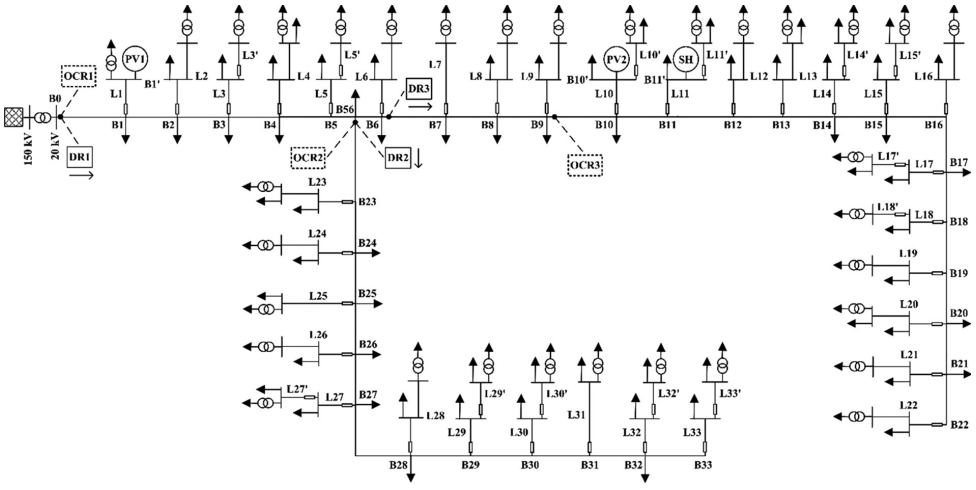

Figure 4.7: Rural Feeder from the area of Xanthi

Small Hydro Power plant, which in the simulations of this thesis is represented as a CIG. The network has multiple loads connected to the 20kV level as well as the low voltage level through secondary transformers. In this work all loads are modelled in the 20kV side.

Data for the feeder were acquired from [68] and are fully presented in the Appendix. The R/X ratio of the feeder is close to 2.55.

4.3 Active Distribution Network Flexibility Calculation

4.3.1 Flexibility Region Definition

Realistic distribution feeders can be long and complex, consisting of Medium (MV), as well as Low (LV) Voltage levels. As a result, hundreds of feeders would create a very demanding computational problem, if modelled and simulated together with the transmission system. Moreover, in most cases TSOs don't have access to the distribution network data. As a result, distribution feeders are usually treated from the transmission point of view as equivalent active and reactive power consumptions at the High Voltage (HV) side of HV/MV substations. The information exchange between the ADNs and the control center can be limited to the active and reactive power consumptions at the PCC of each ADN as shown in Fig. 4.8. Flow is considered from the transmission system to the ADNs (positive values for load assumption).

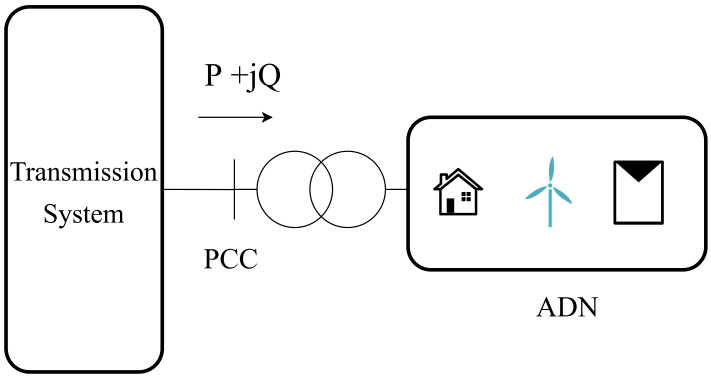

Figure 4.8: Active and Reactive power at the PCC of the ADN

Using the controllable assets that are connected in the ADN (presented in the previous sections) it is possible to control the power exchange at the PCC. In order to calculate how much the ADN can alter this power exchange, using its own resources, we introduce the 'flexibility region' (FR) of an ADN. A typical FR is shown in Fig. 4.9, where ζ is defined as:

$$\zeta = a\Delta P + b\Delta Q \tag{4.32}$$

The FR of ADN is defined as the area in PQ consumption space (at the PCC), for which all operating constraints within the ADN feeder are satisfied.

This includes voltage and current constraints in nodes and branches and all controller limits. The boundary of the FR is determined in this thesis as the solution of an optimization

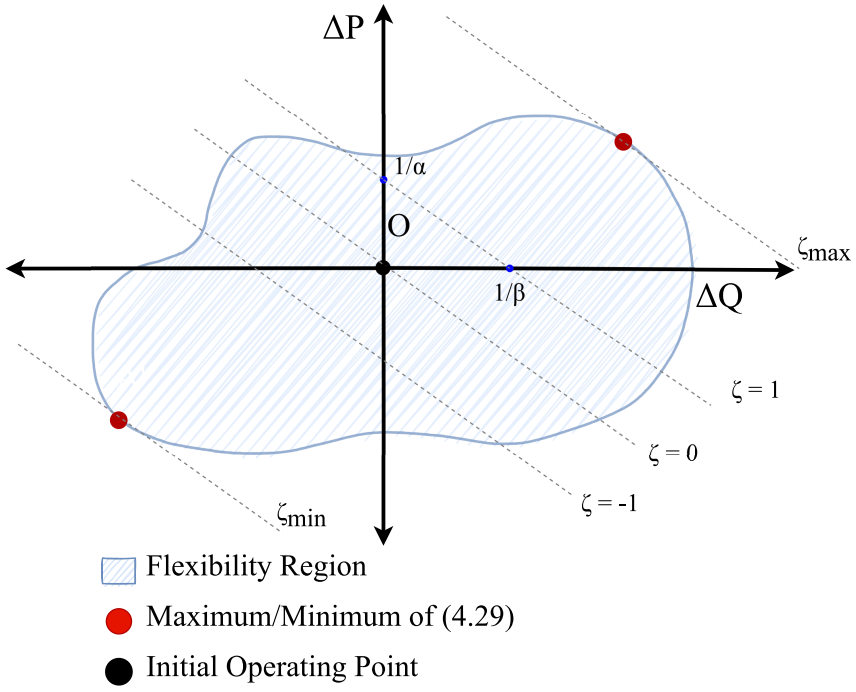

Figure 4.9: Typical FR of an ADN

problem, the objective of which is the maximum deviation from an initial operating point in PQ injection space. This problem is solved by the local ADN controller separately at periodic intervals.

As discussed in Section 1.8, various methods and formulations have been proposed in the literature to identify and calculate ADN flexibility.

Three alternative approaches are proposed in this thesis for determining the FR of each ADN, based also on [50] [44]:

- Monte Carlo simulations
- Multiple binding constraints
- Radial boundary scan

The first relies on Monte Carlo simulations, achieving different setpoints for the decision variables of the ADN.

In the second method, the points of multiple binding operational constraints in the distribution feeder are identified and are used to define the boundary of the FR.

In the third approach, a radial scan is performed, in order to maximize the distance from the initial operating point in multiple directions subject to all operational constraints, similarly to [44]. The above three methods are tested in the feeders presented in the previous section.

4.3.2 Feeder Control Variables

Variables of the general formulation of the problem (4.20)-(4.25), can be divided into two categories, feeder control variables and free variables. Feeder control variables refer to the

variables that represent actual control setpoints, such as the voltage of LTC controlled bus, or the active power generation of an IBR. Free variables correspond to the variables that will be calculated from the system equations, such as the voltages of load buses etc.

Specifically for generator buses, either the voltage or the reactive power can be a control variable along with the active power generation, as there exists a complementary relationship between the two.

The vector of feeder control variables $\boldsymbol{x}$ is the following:

$$\boldsymbol{x} = [V_d, p_{gk}, q_{gk} \perp v_{gk}], \quad \forall k \in G_A \tag{4.33}$$

It is noted here, that for a specific vector $\boldsymbol{x}$ corresponds a single P,Q power consumption at the PCC. On the other hand, a single P,Q consumption of the ADN can be achieved via different vectors $\boldsymbol{x}$.

4.3.3 Monte Carlo Simulations

The first way examined to approximate the FR, is by performing multiple power flows with Monte Carlo Simulations. This approach is used in [46] and [47].

This approach relies on creating multiple vectors $\boldsymbol{x}$ for the feeder control variables of (4.33) which will be used as setpoints on a load flow problem.

For the control variables of (4.33), vectors of setpoints are generated using a uniform distribution. The uniform distribution is considered as a good choice, in the sense that is expected to provide results in multiple parts of the FRs. On the other hand, a normal distribution would provide results closer to the centre of the control variable bounds.

Let s be the random variable $\in [0, 1]$, with a uniform distribution function. Then, for the control variable vector $\boldsymbol{x}$, for sample i the control variable will be:

$$x_i = (x_i^{max} - x_i^{min})s + x_i^{min}, \quad s \in [0, 1] \tag{4.34}$$

For example, voltage setpoints of IBRs can range from V_g^{min} to V_g^{max}. As a result, the voltage setpoint for k IBR with:

$$V_g^{min} = 0.95pu \tag{4.35}$$

$$V_g^{max} = 1.05pu \tag{4.36}$$

is calculated as:

$$V_{gk} = (V_{gk}^{max} - V_{gk}^{min})s + V_{gk}^{min} = 0.1s + 0.95, \quad s \in [0, 1], \quad \forall k \in G_A \tag{4.37}$$

The following procedure is followed to determine whether a point found is acceptable or not. The solution of the AC Power flow (ACPF) problem defined by (4.28),(4.29), using the randomly generated set of variables $\boldsymbol{x}$ as setpoints for the feeder control variables, will provide the rest of the free variables, including the consumption P, Q at the solution point. The solution of the ACPF needs to satisfy equations (4.23)-(4.25), meaning that the free variables calculated by the load flow will need to be inside the limits. More specifically, voltages of load buses and current limits of IBRs need to be respected.

If the solution satisfies the constraints, then the P, Q of the bus at the PCC is considered as acceptable and part of the FR. If one or more of the aforementioned equations is violated then the resulting solution P,Q point is unacceptable and is not part of the FR.

Moreover, it should be noted that if the setpoints result in insolvable AC problems, they are also not taken into consideration since P,Q points cannot be calculated. This is not the same as points deemed as unacceptable due to equations (4.23)-(4.25), where the ACPF problem is solvable but the solution violates one of the inequalities.

In the following Figure the feasible points will be plotted in the PQ plane with green dots and the ones that are violating equations (4.23)-(4.25) with red dots. For this technique, the voltage V_d controlled by the LTC was changed by a step of $0.01p.u.$ and for each step a sample of 10000 setpoints was generated for each decision variable, creating a total of 110000 solutions of the AC power flow problem. The monte-carli approach will be implemented in the three test feeders of Section 4.2.

2-bus feeder

The Monte-Carlo method is applied on the 2-bus feeder presented in Section 4.2.1, in Fig. 4.5 with the data of Table 4.1. The results are shown in Fig. 4.10.

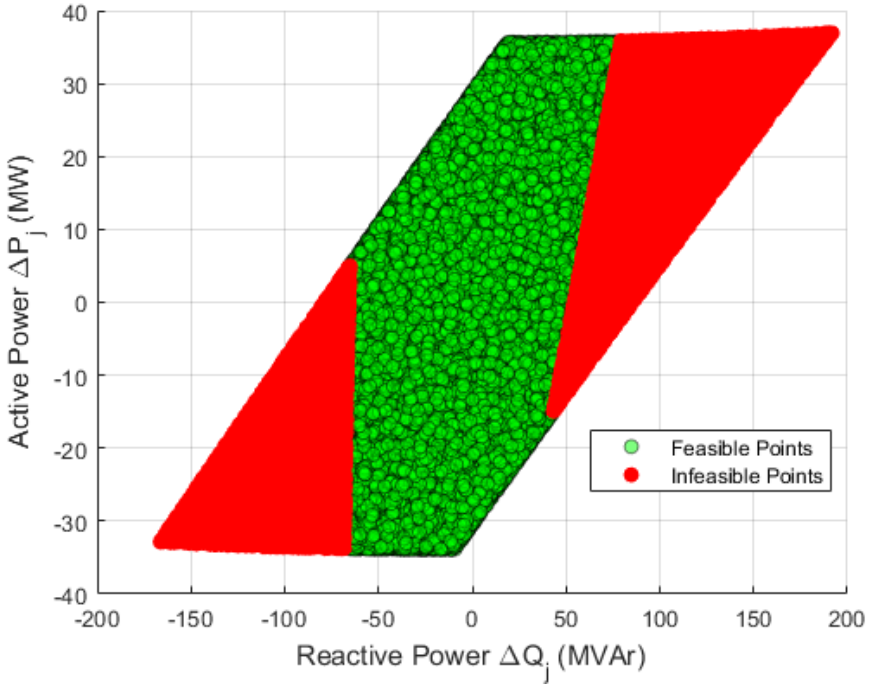

Figure 4.10: Monte Carlo Simulations of 2-bus feeder

Here it can be seen that the boundaries of the region are very clear. The reason is that the flows at the PCC of the 2-bus feeder are unique for each set of voltage setpoint created. It should be noted that in this specific case, active power of the IBR connected in the 2-bus feeder is considered constant. Bus voltage V_d is selected to take values between V^{min} and V^{max} according to (4.23). For each value of V_d, N values are generated for V_g within the respective operating limits. A slack bus and a PV bus give a unique solution (assuming solvability) for P,Q (including the reactive losses on X_t).

Inversely, a set of P,Q values requires one more variable to determine a power flow (4.21). If active power generation p_g is constant (as in this case) each P and Q correspond to a single set of V_d and V_g even if its computation is not obvious as there is no slack bus (no voltage is determined). However, since P and Q have been determined by a value of V_d , this and only this is the one giving the desired p_g at the IBR bus.

As a result, in this case only, each random vector corresponds to a single solution and each solution will correspond to a single random vector, as the PQ plane is the two-dimensional projection of a two-dimensional flow problem.

30-bus feeder

Uniqueness of P,Q solution is not guaranteed in other feeders, e.g. for the 30 bus feeder. As shown in Fig. 4.11, a lot of unacceptable points appear between the acceptable P,Q consumptions. This makes sense, as the PQ plane is just a two-dimensional projection of the flows, of a multi-dimensional problem. As a result, P,Q points inside the feasible region may correspond to both acceptable and unacceptable operating points for both the control and free variables.

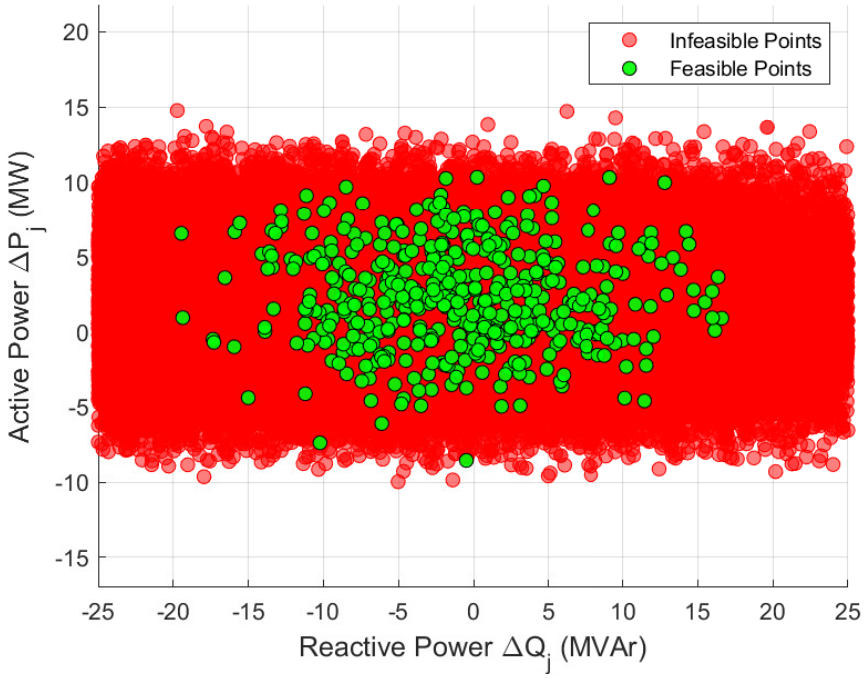

Figure 4.11: Monte Carlo Simulations of 30-bus feeder

Clearly, in this case the same P,Q consumption corresponds to multiple operating points (multiple feeder control variable vectors), some of which may be acceptable and others unacceptable. Thus, this requires one more step to check whether a P,Q point considered as when resulting from a set of setpoints $\boldsymbol{x_i}$, can actually be acceptable with a different set of setpoints. Assuming this test is performed, one can consider as FR the area bounded by the points of maximum distance from the initial operating point.

Rural distribution feeder

For the more complex ADN of Xanthi 4.2.3, 110000 simulations were not enough to identify adequate feasible solution points in order to form an FR. As a result, the scalability of this approach in longer feeders is questionable and requires very long computational time.

As a result, we conclude that the MC method is not the best suitable for identifying the FR of realistic ADN feeder.

4.3.4 Multiple Binding Constraints (2-bus feeder)

The clear-cut polygon shape of the FR of the 2-bus feeder (Fig. 4.10), gives rise to the second approach to determine the FR of simple ADN configurations. This is based on identifying the points on the PQ plane where multiple operational constraints are simultaneously met. The operational constraints correspond to equations (4.21)-(4.25) of the OPF formulation for the FR.

Points of multiple binding constraints, or corner points (CP) are also examined in [69] in order to identify switching loadability limits, also known as limit induced bifurcations in the case of voltage instability analysis. Corner points can be associated with local optima. Depending on the system of equations and the decision variables it is possible to identify the number of active constraints needed for the system of equations to be fully determined. In this section, the corner points are considered as vertices of a polygon in PQ space that bounds the FR.

The ADN configuration of Fig. 4.5, also used in [9], consists of an aggregate voltage depended load placed on the secondary bus of the HV/MV transformer and an IBR at the remote bus. In this section, as in the previous one, no BESS is considered and the active power generation P_g of the IBR is constant. The decision variables are thus, the two bus voltages, V_d of the distribution transformer secondary and V_g of the IBR, which are both subject to (4.23) for minimum and maximum voltage. Another constraint to be considered is (4.24) for which both a q^{max} and a q^{min} limit can be met as the limit depends on q^2. It is noted that if any two of the three variables V_d, V_g, q_g are determined, the power consumption P, Q is derived from the PF equations (4.28),(4.29) and thus the change of consumption $\Delta P, \Delta Q$ on the PQ plane.

With constant p_g, active power flexibility depends on V_d, thus the limit values of voltage determine the ΔP extreme values. Similarly, ΔQ extremes are linked with V_g or q_g limits. Each of the two extreme values of V_d can be combined with maximum or minimum of either V_g or q_g, whichever will occur first. This gives 2x2=4 corner points. Two further corner points correspond to V_g and q_g being simultaneously at their maximum or minimum. Thus six corner points can be determined in general in the two-bus ADN feeder.

For the 2-bus feeder of subsection 4.2.1, the above six corner points are summarized in Table 4.2 and are shown in PQ space in Fig. 4.12. These are computed as load flow solutions withe the parameters V_d, V_g and q_g determined as above.

The corner points in Fig. 4.12 are joined with linear segments so as to form a polygon. Each line segment represents a linear constraint where the line equation of each vertice from corner point $(\Delta Q_i, \Delta P_i)$ to corner point $(\Delta Q_{i+1}, \Delta P_{i+1})$ is given by the following equation, for a total number of n corner points:

Table 4.2: Points of Multiple Binding Constraints on the two bus ADN

Point	Set of Binding Constraints
A	V_d^{max}, V_g^{max}
B	$V_d^{max}, -Q_g^{max}$
C	$V_g^{min}, -Q_g^{max}$
D	V_d^{min}, V_g^{min}
E	V_d^{min}, Q_g^{max}
F	V_g^{max}, Q_g^{max}

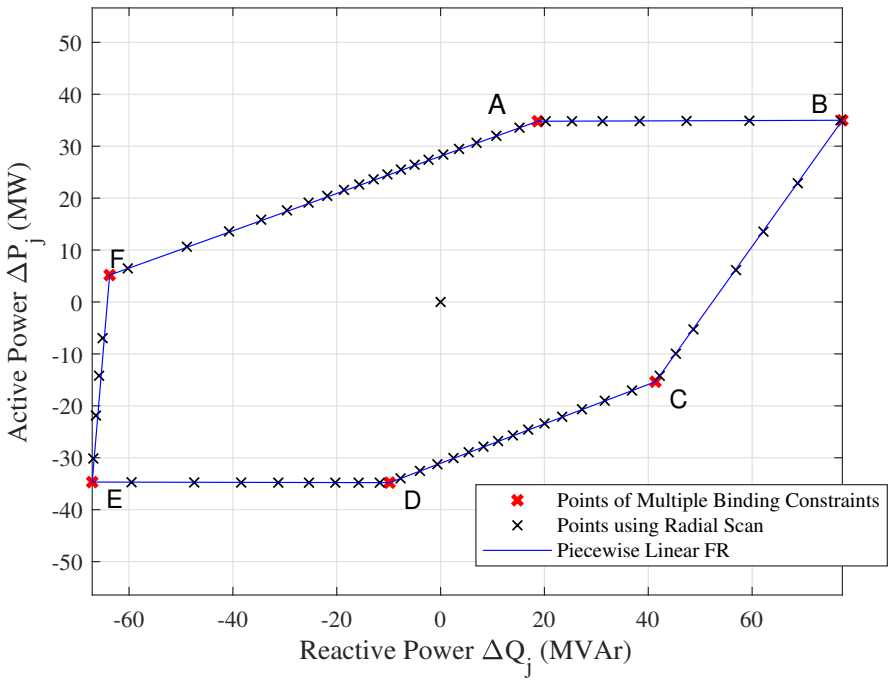

Figure 4.12: Flexibility Region Boundary of 2-bus ADN using Multiple Binding Constraints

$$\alpha_i \Delta P + \beta_i \Delta Q = 1, \quad i \in N \tag{4.38}$$

for which the coefficients α and β are determined by the following equations, where $\Delta P_{n+1} = \Delta P_1$ and $\Delta Q_{n+1} = \Delta Q_1$:

$$\alpha_i = \frac{\Delta P_{i+1} - \Delta P_i}{\Delta P_i \Delta Q_{i+1} - \Delta P_{i+1} \Delta Q_i}, \quad i = 1, ..., n \tag{4.39}$$

$$\beta_i = \frac{\Delta Q_i - \Delta Q_{i+1}}{\Delta P_i \Delta Q_{i+1} - \Delta P_{i+1} \Delta Q_i}, \quad i = 1, ..., n \tag{4.40}$$

It is noted that depending on the two-bus feeder data it is possible that a corner point is infeasible or two corner points may be identical. In these cases, only the feasible points are used to form the FR boundary in the PQ plane.

Clearly, this method is efficient, but can be applied only to simple 2-bus feeders and again only if p_g is given. Introduction of one more decision variable will complicate this approach considerably. On the other hand, the limitation considered in 4.3.3 for the MC method, i.e. multiple operating point for each pair of P, Q values, has also to be considered.

Thus, a more general method to determine the FR boundary is introduced in the next section.

4.3.5 Radial boundary scan

This approach estimates the FR by maximizing the distance from the initial operating point in the PQ plane along multiple search directions finding points that are on the boundary of the feasible region. For each search direction, two points are calculated, one for maximizing and one for minimizing the change in the active and reactive power flow at the PCC of each ADN, similar to the method proposed in [44] and [50].

The constraints of the optimization problem ensure that each solution will be feasible. In Fig. 4.13, points A,N and A',N' represent points on the boundary of the FR for different directions θ for positive and negative values.

For the 30 bus test feeder and the initial operating point, for a specific angle in the $\Delta P, \Delta Q$ plane, e.g.$\theta = 45^o$, the points that are found for minimum and maximum $\Delta P, \Delta Q$ are shown in Fig. 4.14 (i.e. $\Delta P = \Delta Q$).

For multiple angles, depending on the desired granularity, different points on the boundary of the FR are calculated, thus forming the FR region around the initial operating point of the ADN.

The optimization problem to be solved in each search direction is similar to the problem formulation (4.20)-(4.25). The objective function corresponds to the maximization of change in the power absorption of the PCC in both positive and negative direction and is defined as follows:

As described also in Section 4.1.6, for an initial absorption P_0, Q_0 objective function $\zeta(\Delta P, \Delta Q)$ is a linear combination of absorption changes ΔP, ΔQ that refer to the change in the active and reactive power flow at the PCC, from the operating point P,Q:

$$P = P_0 + \Delta P \tag{4.41}$$

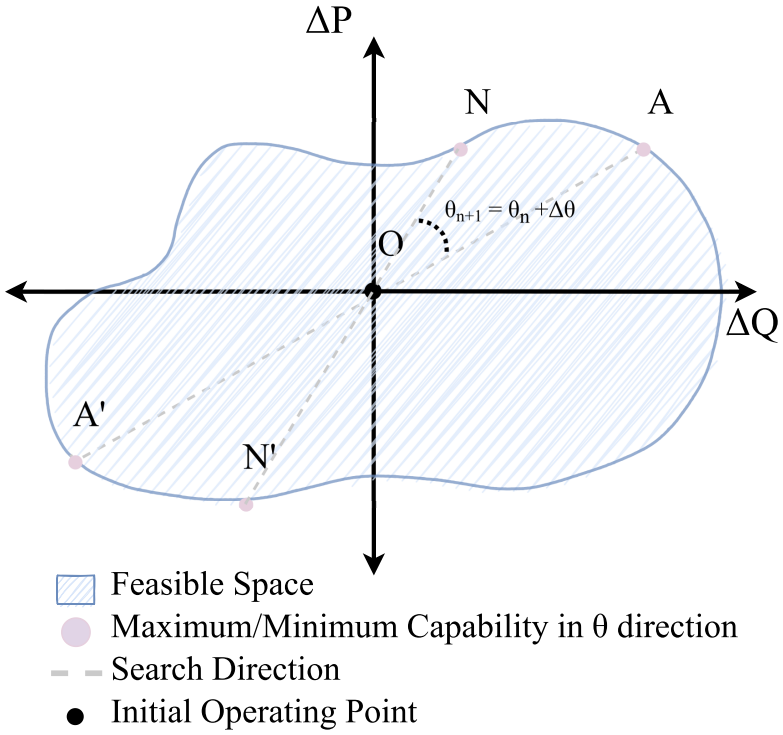

Figure 4.13: Feasibility Region Determination using the Radial Scan

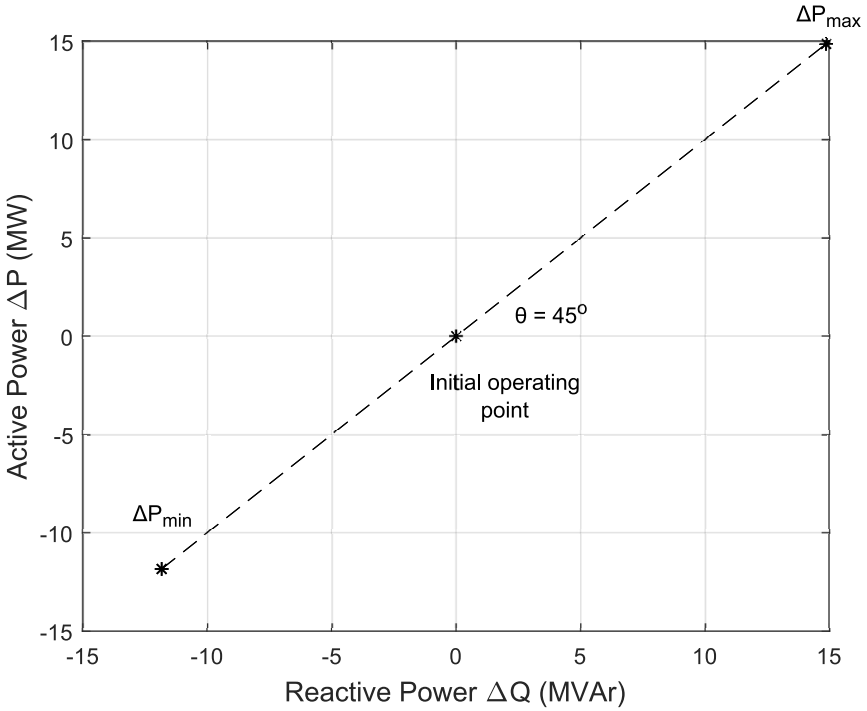

Figure 4.14: Minimum and maximum ΔP for $\theta = 45^o$

$$Q = Q_0 + \Delta Q \tag{4.42}$$

for function ζ:

$$\zeta = a\Delta P + b\Delta Q \tag{4.43}$$

then for $a = \pm 1$ and $b = 0$, the OPF formulation for the radial boundary scan OPF formulation is defined as follows:

$$\max_{e,f} \quad \pm\Delta P \tag{4.44}$$

$$\text{subject to :}$$

$$\Delta Q = \Delta P tan(\theta) \tag{4.45}$$

$$\boldsymbol{g_A}(e, f) = 0 \tag{4.46}$$

$$V_l^2 = e_k^2 + f_k^2, \forall k \in \mathcal{N}_A \tag{4.47}$$

$$V_k^{min} \leq V_k \leq V_k^{max}, \forall k \in \mathcal{N}_A \tag{4.48}$$

$$p_{gk}^2 + q_{gk}^2 \leq (V_k I_{Nk})^2, \forall k \in G_A \tag{4.49}$$

$$p_{gk}^{min} \leq p_{gk} \leq p_{gk}^{max}, \forall k \in G_A \tag{4.50}$$

$$\tag{4.51}$$

The algorithm for finding the points on the FR boundary is as follows:

1. The ADN is initialized based on the current operating point with absorption P_0, Q_0. We assume that the starting point in the PQ plane is inside the FR, meaning that the initial operating point satisfies constraints (4.48)-(4.50).

2. The direction of change as seen in the PCC is determined by the angle θ as shown in (4.45). For each value of θ, the optimization problem (4.44)-(4.50) is solved. Depending on the desired granularity, a step in angle θ between the active and reactive power is chosen. Application on the test systems shows that a small angle step of $\Delta\theta = 3^o - 5^o$ provides reasonable granularity to define the FR. Finer granularity is more time consuming but provides more accurate results. The step is chosen heuristically to properly define the FR without wasting time. The optimization problem (4.44)-(4.50) is solved for both positive (maximization) and negative (minimization) a, providing two points on the boundary of the feasible region of each θ.

3. The obtained boundary points can be connected with line segments to create a linear FR as will be explained in Section 4.4.

4.3.6 Solution method and Implementation of Radial Boundary Scan

The aforementioned approach for the determination of the FR boundary is used for the three test systems that were presented in 4.2. The initial consumptions at the PCC for each feeder are presented in the Appendix.

Similarly to the implementation of the VSM OPF of Chapter 2, the algorithm is created in MATLAB environment. The test system data are imported as Matpower case structs. All the optimization problems are solved with MATBLAB's *fmincon* function, using the *sqp* solver. All problems are solved with a PC with the following specifications: a GPU Core i9, 3.8 GHz and 16 GB RAM.

The algorithm consists of a main program that calls separate functions. Functions include, input of data, matrix formulation and initialization of the test system, formulation of the optimization problem (constraints, objective function), solution of the OPF and output of the results of the optimization. Figures of the FR are also exported.

The following color coding has been established in the FR boundary points, which is tied to the constraints that are active at the solution point of the specific optimization problem. More specifically, the color of the point in the PQ plane is defined depending on the voltage and current constraints which are active. Asterisk are related to voltage constraints while cirles represent IBR current constraints. Of course it is possible that both active and voltage constraints are active.

The color coding is defined as follows:

- Red Asterisk: At least one voltage is at the maximum (upper) limit.
- Blue Asterisk: At least one voltage is at the minimum (lower) limit.
- Orange Asterisk: At least one voltage is at the maximum (upper) limit and at least one voltage is at the minimum (lower) limit.
- No asterisk: No voltage constraint is active.
- Circle: At least one IBR current constraint is active

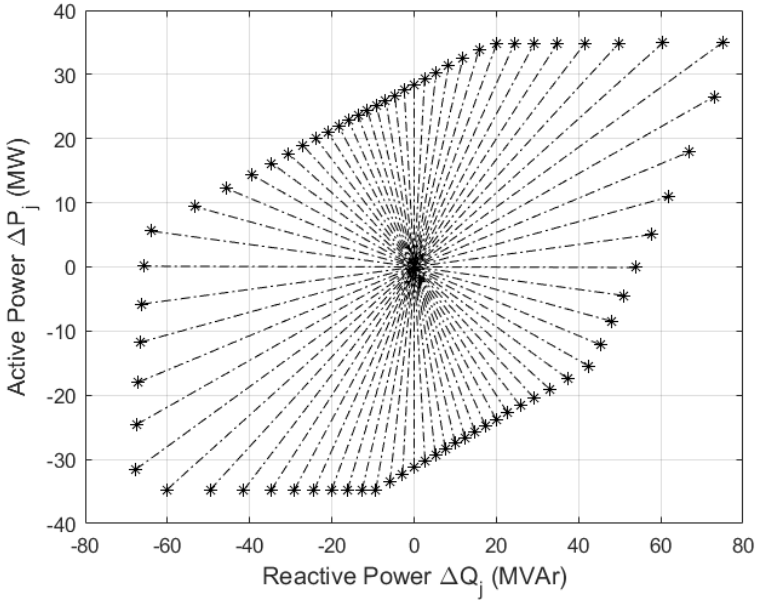

Figure 4.15: FR Boundary Points of 2-bus ADN

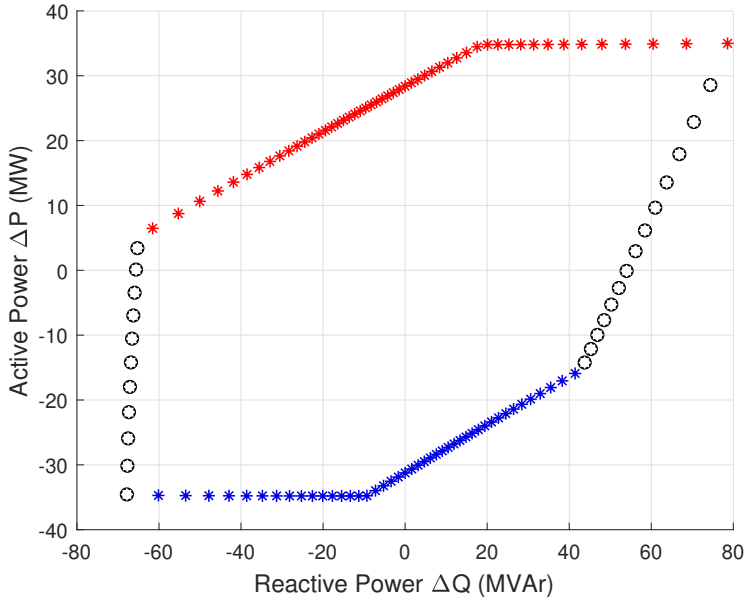

Figure 4.16: Boundary point active constraints of 2-bus ADN

As observed in Fig. 4.15, for the 2-bus feeder, while there is no BESS assumptions and the active power generation is considered constant, there is great capability in changing the active power at the PCC. This capability is due to the very high aggregated load and its voltage sensitivity. In terms of the reactive power at the PCC, the IBR contributes significantly, together with the reactive part of the load and it's voltage sensitivity.

From Fig. 4.16, the active constraints are shown for the 2-bus system. In this test system, as already discussed in subsection 4.3.4, it is quite clear which constraints are active on the corner points. As observed, the upper part of the FR is associated with high voltages, as at least one upper voltage constraint is active, while the lower part is associated with lower voltage active constraints. The points in the two sides are associated with active IBR current constraints. It can be seen clearly in this case, that the vertices of the clear-cut polygon FR, are points where the active constraints change, as explicitly explained in subsection 4.3.4.

As observed in Fig. 4.17, for the 30-bus test system, the impact of the IBRs is more dominant, since the installed capacity can almost cover the load. The range of the change in the reactive power at the PCC is also quite significant. In this case, the range in the active power change is mainly attributed to the BESS assumption.

The active constraints are shown in Fig. 4.18. In the 30-bus ADN, it is harder to distinguish between the active constraints. In almost all points found on the boundary of the FR, with the exception of the lower part, the IBR current limits are met on at least one of the IBRs. Moreover, on the right part of the FR, there are points where both upper and lower voltage limits are active. This makes sense in longer feeders, where distant buses may encounter upper limits, while closer to the PCC buses may at the lower limits.

In Fig. 4.19, the resulting FR for the ADN of Xanthi is shown and it can be observed that it has similar attributes to that of the 30-bus ADN. The installed capacity of IBRs is close to the total load and the range of active and reactive power change at the PCC

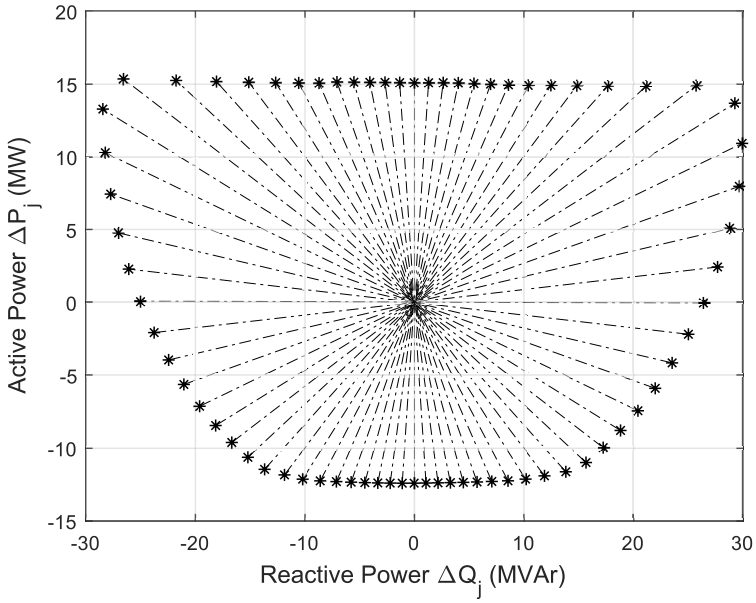

Figure 4.17: FR Boundary Points of 30-bus ADN

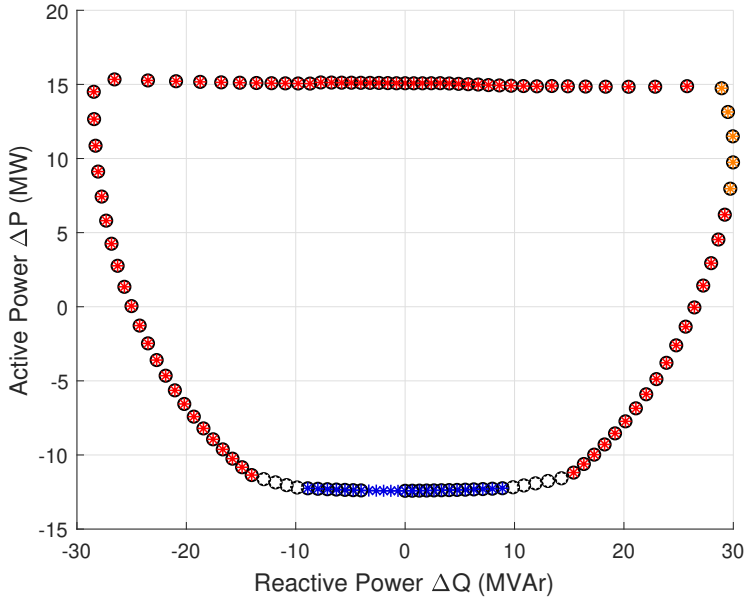

Figure 4.18: Boundary point active constraints of 30-bus ADN

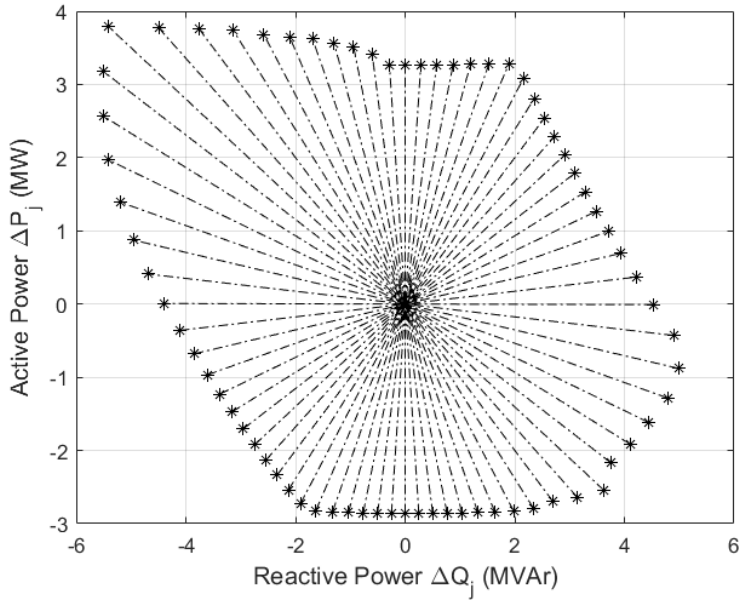

Figure 4.19: FR Boundary Points of Xanthi ADN

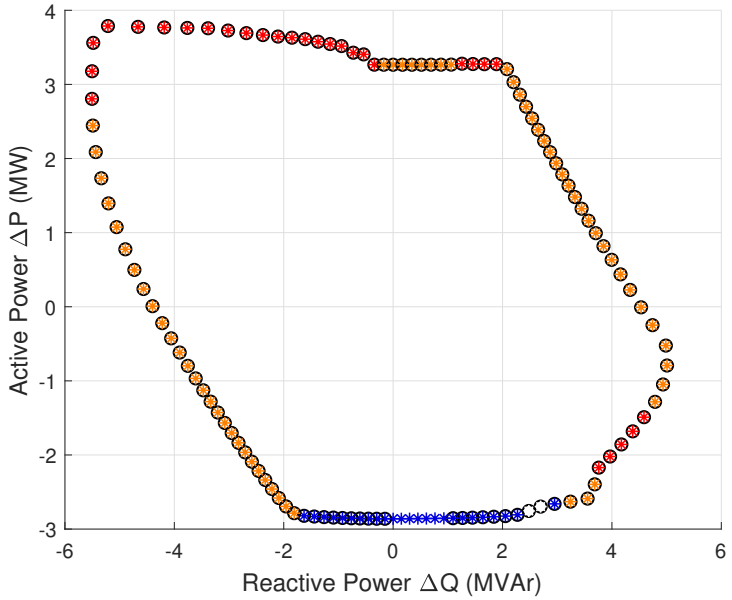

Figure 4.20: Boundary point active constraints of 99-bus ADN

is quite close.

The active constraints for the Xanthi ADN are presented in Fig. 4.20. Similarly, in most boundary points found, at least one IBR current constraint is active. Moreover, in the top of the FR upper voltage limits are met, while in the bottom part lower voltage limits are met.

4.3.7 Comparison

All simulations are performed in the same PC again, with an angle step $\Delta\theta = 3^o$. The time required for the determination of each ADN is presented in Table 4.3. It can be observed that the simulation time for the FR of the test systems grows exponentially, with the increase of buses (and as a result) variables of the optimization problem.

Table 4.3: Simulation time

Number of buses	time (s)	$\Delta\theta$ (^{o})
2	17	5
30	573	5
99	887	5

The superiority of the radial scan with respect to the Monte Carlo approach of subsection 4.3.3 is showcased in Fig. 4.21, where the FR of the 30 bus feeder is plotted using both the radial boundary scan, as well as the MC method. It is obvious that the radial scan is faster in terms of the computational time and is able to define a much wider FR compared to the points found from the MC simulations. This is no surprise, as it is expected that by producing random setpoints, it's highly unlikely that points on the boundary will be found, especially as the number of buses increases.

4.3.8 Normal and Expanded Flexibility Regions

Depending on the limits set on the operational constraints, different FRs can be obtained for the same ADN. In this section, two different operating regions will be defined for an ADN, one corresponding to normal operating conditions and one to expanded operating constraints. The two operating constraints are the following:

1. **Normal operating constraints** : All voltages including the bus of the MV substation are allowed to range inside the limits:

$$0.95 \quad p.u. \leq V_k \leq 1.05 \quad p.u. \tag{4.52}$$

2. Expanded operating conditions : In case emergency support is needed, the emergency operating constraints can allow voltage in the ADN to vary further:

$$0.90 \quad p.u. \leq V_k \leq 1.10 \quad p.u. \tag{4.53}$$

For all operating conditions, the current limits on the inverters are imposed in the same manner. For the three test feeders of section 4.2, the radial boundary scan is performed to identify the FRs around a specific operating point for both normal and emergency

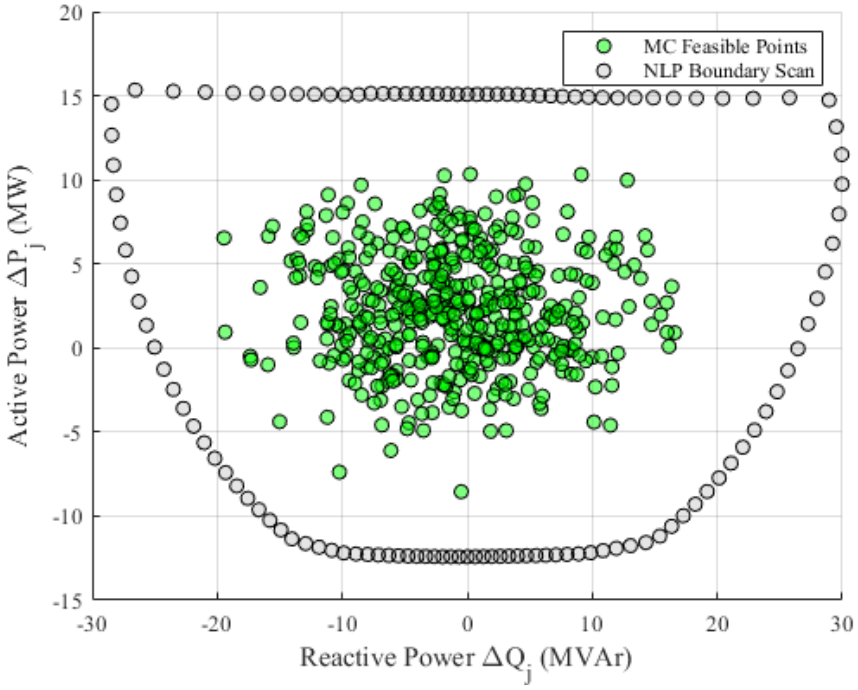

Figure 4.21: Radial Scan vs MC on 30 bus feeder

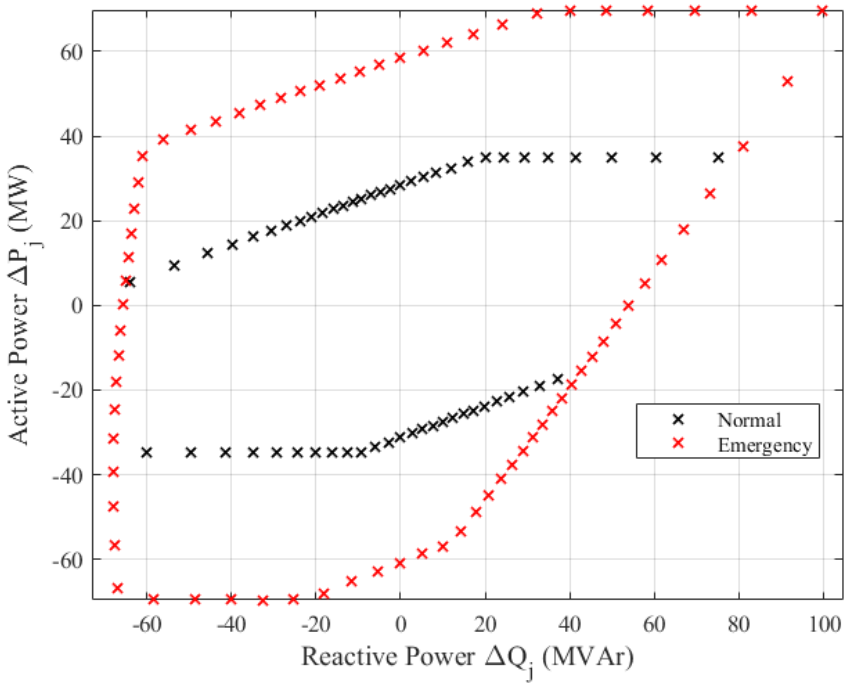

Figure 4.22: 2bus ADN

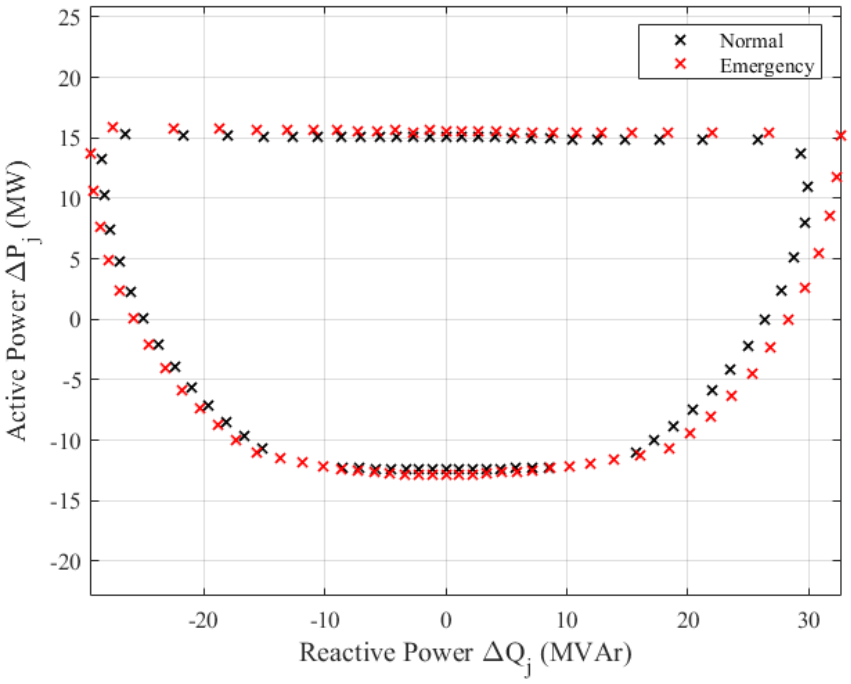

Figure 4.23: 30bus ADN

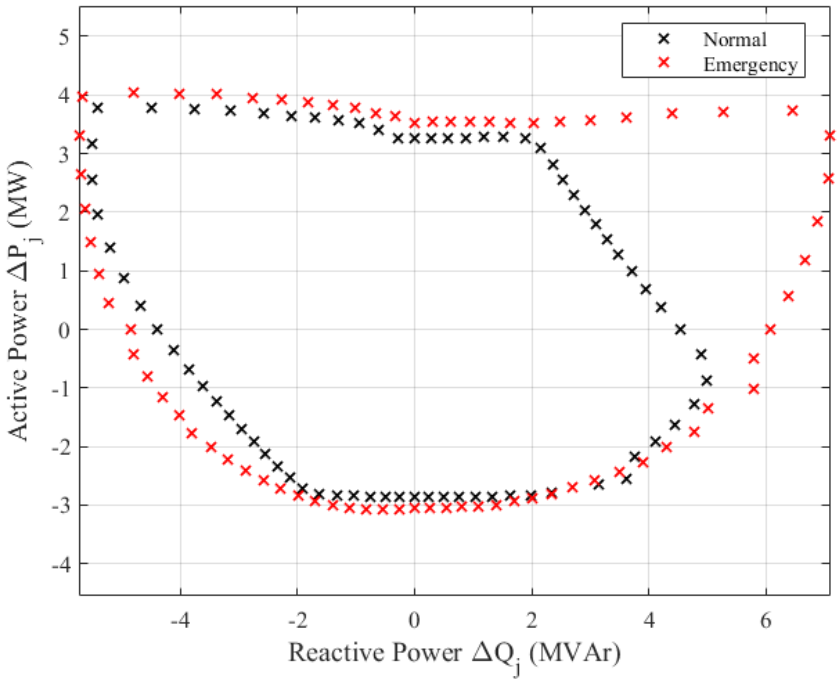

Figure 4.24: Xanthi ADN

operating constraints. For each feeder the two aforementioned FRs are plotted in figures 4.22, 4.23, 4.24.

As shown in the figures, extended voltage limits may affect differently the FR of each ADN.

In some cases, such as the 2-bus ADN, wider voltage limits affect the FR in greater manner due to the voltage dependency of the loads. Extension of the FR heavily relies on the constraints that are active in each ADN.

For example, for the 30 bus feeder the extension of the FR is quite small for the emergency operating constraints. This is due to the fact that active constraints for both normal and operating conditions for almost all the points of the boundary, are the currents of the IBRs.

For the case of Xanthi ADN, presented in Fig. 4.24, it can be observed that the extension of the voltage limits is unsymmetrical, giving considerably larger limits for reactive absorption while only slightly enlarging the FR in terms of reactive power injections. The change in the range of the active power at the PCC is only slightly altered due to the voltage dependency of the loads.

4.4 Polygon Approximation of the FR boundary

Depending on the granularity chosen by the search direction step, several boundary points of the FR can be found. Using all these points in the FR description to be sent to a central controller would require a large number of linear constraints between successive boundary points. To overcome this, an algorithm is developed in order to keep only a few points that will approximate the FR and also ensure that it will be convex. The FR boundary is then created by linearly connecting these points. This section presents the algorithm developed for the polygon approximation.

Initially, three boundary points are selected. It is crucial that the initial operating point $[0, 0]$ is inside the triangle that is formed by the three points. The points used are those for which ΔQ is maximum or minimum and the point where ΔP is maximum (ΔQ^{min},ΔQ^{max},ΔP^{min}). Selection of 3 points ensures that the resulting FR will be convex, as the points added will be external to the first convex triangle.

The polygon approximation of the FR is defined by the following set of inequality constraints:

$$\alpha_i \Delta P + \beta_i \Delta Q + 1 \geq 0, \quad i = 1, .., n \tag{4.54}$$

Each line segment represents a linear constraint where the line equation of each vertice from corner point $(\Delta Q_i, \Delta P_i)$ to corner point $(\Delta Q_{i+1}, \Delta P_{i+1})$ is given by the following equation, for a total number of n corner points, similarly to subsection 4.3.4 for which the coefficients α and β are determined by the following equations, where $\Delta P_{n+1} = \Delta P_1$ and $\Delta Q_{n+1} = \Delta Q_1$.

Initially, $n = 3$, as the polygon starts as a triangle.

Coefficients α and β correspond to the line equation i of the existing polygon and are calculated as follows:

$$\alpha_i = \frac{\Delta P_{i+1} - \Delta P_i}{\Delta P_i \Delta Q_{i+1} - \Delta P_{i+1} \Delta Q_i}, \quad i = 1, .., n \tag{4.55}$$

$$\beta_i = \frac{\Delta Q_i - \Delta Q_{i+1}}{\Delta P_i \Delta Q_{i+1} - \Delta P_{i+1} \Delta Q_i}, \quad i = 1, .., n \tag{4.56}$$

In order for the polygon to remain convex, the algorithm adds points that are outside the initial triangle approximate FR. So, for all initially calculated boundary FR points that are external to the polygon approximation, i.e. for which at least one of the constraints (4.54) is violated, the distance to the violated constraint is calculated. If M is the number of points violating the polygon approximation constraints, then for each external point m the distance to each violated constraint i is defined as:

$$d_{im} = \frac{|\alpha_i \Delta P_{im} + \beta_i \Delta Q_{im} + 1|}{\alpha_i^2 + \beta_i^2}, \tag{4.57}$$

Between the external points m calculated, the one with the largest distance d_i from the respective line segment is kept. The single point m is added to the three initial points. By adding one more point to the polygon, the number of points n is increased, so in the form of a programming assignment statement:

$$n = n + 1 \tag{4.58}$$

In this work six points are considered enough to approximate the FR, so the procedure is repeated until $n = 6$.

The polygon approximation on the 3 feeders is shown in Figures 4.25, 4.26 and 4.27 respectively. Black points are the points calculated by the radial FR boundary scan. The red dots correspond to the 3 initial points chosen, and purple are the additional points that are found by the algorithm in order to create a polygon with 6 vertices.

As shown by the figures, it can be claimed that the polygon approximation of the FRs is adequate with 6 points. It is obvious that selecting more points can lead to even more precise estimation of the FR.

Constraints (4.54), can be exported to the central controller (at the EMS level), so they can be included in an optimization problem that will determine the optimal reference values P^{ref},Q^{ref} in each ADN. This means that for the central optimization problem, in every bus where ADN is assumed to be connected, the equivalent injections will be able to vary inside the limits of the corresponding FRs, essentially adding 6 linear constraints to the optimization problem for each ADN. Addition of linear constraints is not very expensive in terms of computational speed.

The polygon approximation, as also shown in the figure, may leave out some points, or even exceed the feasible solution space in the PQ plane. Nonetheless, the approximation error is not very significant and can be accepted. Moreover, when implementing a possible setpoint sent from the EMS to a certain feeder, the feeder will seek to achieve this setpoint but always inside its feasible region. The implementation of the reference values back to the feeder will be presented in a following section. Improvement of accuracy can be achieved by increasing the number of polygon vertices

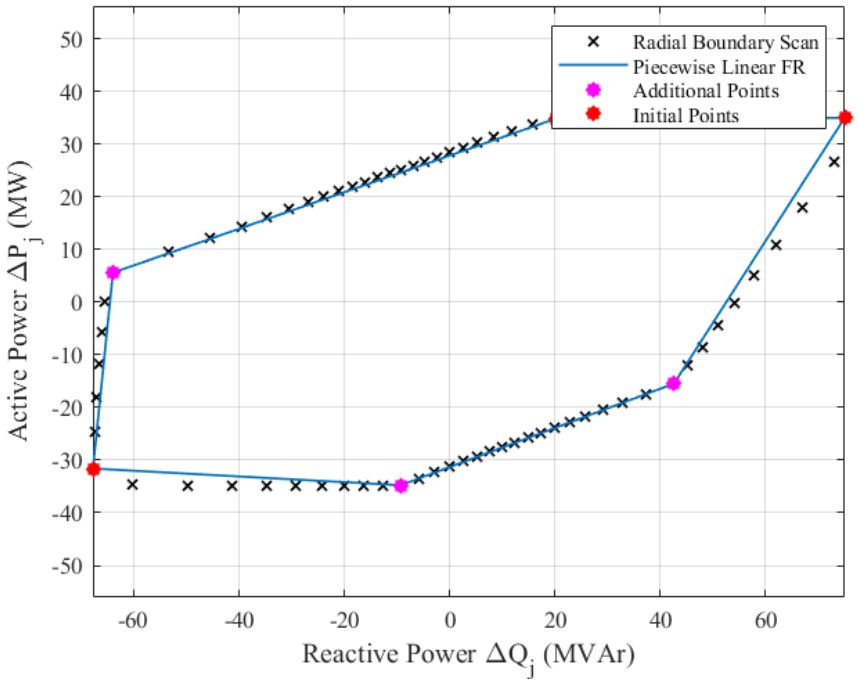

Figure 4.25: 2bus ADN

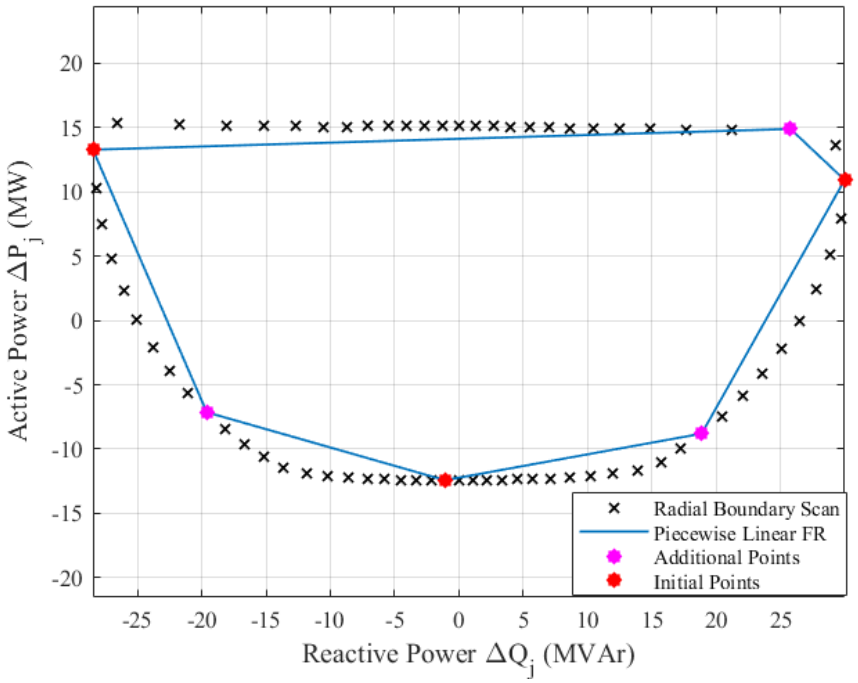

Figure 4.26: 30bus ADN

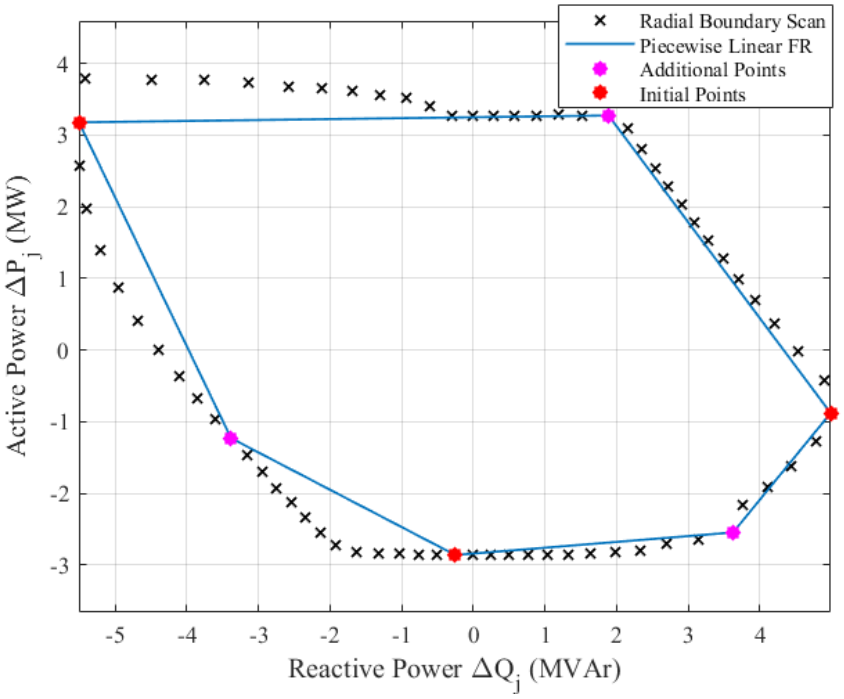

Figure 4.27: Xanthi ADN

Chapter 5

VSM Optimization using Active Distribution Networks

5.1 Corrective vs Preventive Control

Distribution Networks and in particular ADNs have considerable potential to support a Transmission System which is experiencing Voltage Stability Problems. In most cases Transmission Control Centers have limited information about the distribution network, other than the active and reactive power flows in the HV side of distribution transformers. As a result, in a state of emergency, it is not obvious how to request support from the distribution network. For instance, conventional load shedding by simply opening distribution feeders may entail the danger of disconnecting large amounts of distributed generation. Also, the approach of requesting maximum reactive power support may entail the danger of increasing consumption due to the load-voltage dependency. Thus, the need to establish optimal coordination between transmission control center and distributed resources is important.

In this chapter, two approaches are proposed for coordinating ADN support to optimize Voltage Security, without requirements from the TSO to have information about the configuration of the ADNs, other than the active and reactive power injections at the HV side of the HV/MV substations. A limited communication needs to be established, so that the control centre can send the security margin and sensitivity signals to the ADNs.

5.1.1 Corrective Control

The first approach is best suited for corrective control and is based on a distributed optimization of VSM for a specific contingency. The methodology consists of explicitly formulating and solving two separate optimization problems, one for the transmission system (central problem) and the other for each distribution feeder (local problem). The link between the central and the local optimization problems is the sensitivity of the centrally computed voltage security margin (VSM) to the consumptions of active and reactive power at the connection points of ADNs. Each local controller is then solving separately the second optimization problem to provide setpoints for optimal voltage stability support. The conceptual framework of the proposed methodology is presented in Fig. 5.1.

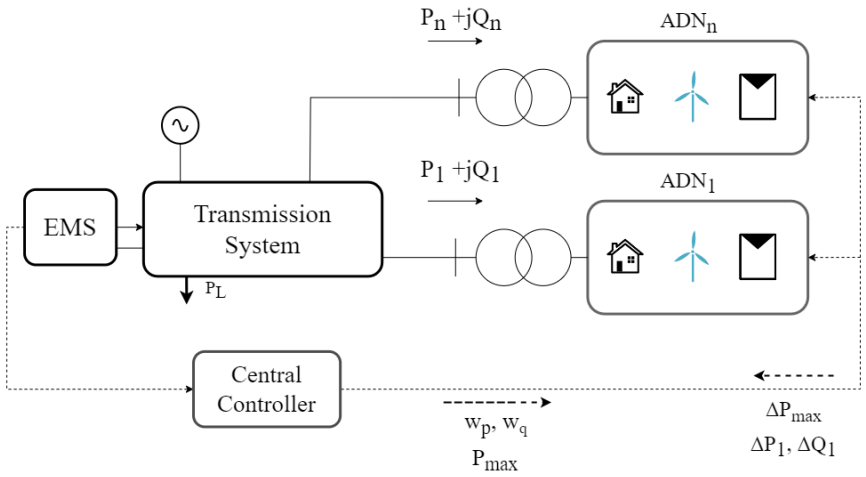

Figure 5.1: Conceptual Framework for Corrective Control

The upper-level optimization problem involves the determination of VSM for a number of selected contingencies starting from the State Estimator operating point. It is noted that VSM can be negative, meaning that the operating point may be insecure for the specific contingency. For each critical contingency with negative or small positive margins, sensitivities with respect to the HV bus power injections are calculated using Lagrange multipliers 2.9.2. Also, the equivalent Thevenin impedances in each substation where an ADN is connected are calculated and transmitted to the local controllers.

The above information for each critical contingency is received by each ADN controller, in order to solve the second-stage optimization problem of maximizing VSM by modifying the active and reactive power injections to the transmission system, using the available control variables in the feeder, such as the reactive control of IBRs, and the tap ratio of the LTC transformer. All calculations are made off-line and emergency control will be implemented only if one of the critical contingencies, for which it is designed, actually takes place. Both types of optimization problems are solved using a Sequential Quadratic Programming (SQP) solver where the power flow equations are written in Cartesian form.

5.1.2 Preventive Control

The second approach presented in this chapter is best suited for preventive control, i.e. it aims to increase security margins whenever these are deemed inadequate. The preventive control scheme is thoroughly presented in section 5.4. For this preventive control the flexibility region (FR) of each feeder is taken into account. Fig. 5.2 shows the conceptual framework of active and reactive power as well as communication exchange between the TSO and each ADN.

In particular, the FR of each ADN is locally determined and exported to the central controller, which is then maximizing VSM for a critical contingency by determining suitable P, Q consumption setpoints to ADN controllers, thus achieving a most efficient control. In other words, the central VSM is now taking into consideration the flexibility of the ADNs.

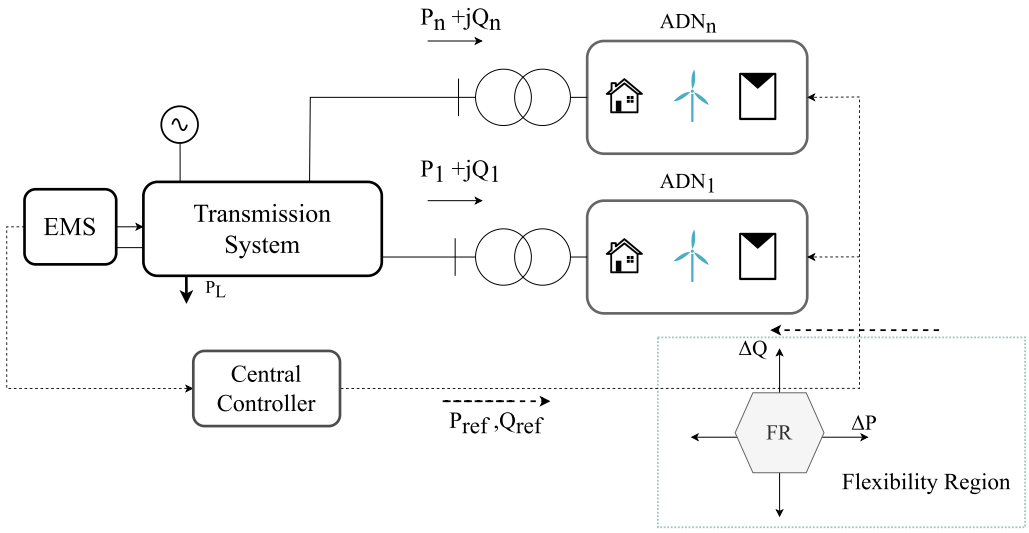

Figure 5.2: Conceptual Framework for Preventive Control

While, the transmission system is decoupled from the distribution feeders and different problems are solved, the voltage stability margins optimization problem will take into account the flexibility of the ADNs. This makes the approach more centralized and efficient in terms of exploiting the available resources.

The boundary of the FR of each ADN is determined periodically by its local controller and exported to the TSO control center in the form of linear constraints on P and Q consumption variations around the current operating point. These constraints are then added to the central OPF problem solved by the central controller, in order to maximize the voltage stability margin by varying the ADN P and Q consumptions within the specified limits.

The Central Controller at the TSO EMS level solves the VSM for each contingency and determines the most critical ones. It can then determine P,Q consumption setpoints to maximize the VSM for the most critical contingency(ies).

A third and final problem is the activation of ADN controls to achieve the desired setpoint determined by the central OPF problem. This is formulated as a local optimization problem which tries to minimize the Euclidean distance in PQ space of the actual power consumption at the PCC from the desired setpoint, by varying available ADN feeder controls which include IBG and Load Tap Changer (LTC) transformer secondary voltage setpoints, always subject to operational constraints. In the implementation stage the modified LTC setpoint is activated first, followed by a slow ramp modifying IBR voltage and reactive power as in [9], preventively, meaning that the setpoints are actuated before the contingency happens.

Both proposed methods are applied to the IEEE Nordic Test System. The test system is appropriately modified in order to include IBRs in the distribution feeders of the voltage stability sensitive area, without altering the initial operating point [9]. The results of both the preventive and the corrective control, are validated using the time-domain QSS simulation.

5.2 Distributed VSM optimization

5.2.1 Corrective VSM Optimization

At regular intervals, of around 5 minutes in most cases, the state estimator at the Transmission Control Centre is performing a state estimation of the transmission system, and provides a snapshot of the current operating point of the power system. The upper level optimization uses the most recent state estimation solution in order to perform a VSM calculation, by solving the following problem, already defined in Chapter 2 for each of a pre-specified list of credible contingencies. The VSM optimization problem (2.41)-(2.47) is rewritten here for convenience, with a slight change in the objective function, where P instead of ΔP is maximized, which represents the total system load or area load that is stressed:

$$\zeta = -P = -(p_{dk0} + \lambda \sum_{k \in \mathcal{N}} d_{pk}), \quad k \in \mathcal{N} \tag{5.1}$$

$$\min_{\boldsymbol{e},\boldsymbol{f},\Delta L,\lambda} \zeta \tag{5.2}$$

$$\text{subject to :}$$

$$\boldsymbol{h}(e, f, \Delta L, \lambda) = 0 \tag{5.3}$$

$$p_{gk}^{min} \leq p_{gk} \leq p_{gk}^{max}, \forall k \in G \tag{5.4}$$

$$q_{gk} \leq q_{ak}(p_{gk}, V_k), \forall k \in G \tag{5.5}$$

$$q_{gk} \leq q_{rk}(p_{gk}, V_k), \forall k \in G \tag{5.6}$$

$$V_{gk} \leq V_{gk}^{ref}, \forall k \in G \tag{5.7}$$

where $\boldsymbol{h}$ is:

$$h_{p_k} = p_k - e_k(\boldsymbol{g_k}^T \boldsymbol{e} - \boldsymbol{b_k}^T \boldsymbol{f}) - f_k(\boldsymbol{b_k}^T \boldsymbol{e} + \boldsymbol{g_k}^T \boldsymbol{f}) = 0, \quad k \in \mathcal{N} \tag{5.8}$$

$$h_{q_k} = q_k + e_k(\boldsymbol{b_k}^T \boldsymbol{e} + \boldsymbol{g_k}^T \boldsymbol{f}) - f_k(\boldsymbol{g_k}^T \boldsymbol{e} - \boldsymbol{b_k}^T \boldsymbol{f}) = 0, \quad k \in \mathcal{N} \tag{5.9}$$

where,

$$p_k = p_{gk} - p_{dk}, \quad k \in \mathcal{N} \tag{5.10}$$

$$q_k = q_{gk} - q_{dk}, \quad k \in \mathcal{N} \tag{5.11}$$

As already explained, the contingencies with a small positive or negative post contingency VSM are deemed as critical for the security of the power system operation in terms of voltage stability. This means that in the occurrence of one of the critical contingencies, the transmission system operator will need to take corrective remedial actions immediately, in order to instability and imminent voltage collapse.

At the solution point of the upper level optimization, as explained in 2.9.2, the Lagrange multipliers are also calculated, in addition to the VSM, thus providing the sensitivities of

the VSM with respect to the active and reactive power injections at the point of connection of each ADN. Let $\mathcal{N}_\mathcal{A}$ be the subset of buses where ADNs are located. Then, at each bus $k \in \mathcal{N}_\mathcal{A}$, sensitivities with respect to active and reactive power consumptions are the following:

$$\begin{aligned} \nabla_{p_k}\mathcal{L} = 0 \Rightarrow \frac{\partial\zeta}{\partial p_k} - w_{p_k} = 0 \\ \Rightarrow w_{p_k} = \frac{\partial\zeta}{\partial p_k} = -\frac{\partial P_{max}}{\partial p_k}, \quad k \in \mathcal{N}_A \end{aligned} \tag{5.12}$$

$$\begin{aligned} \nabla_{q_k}\mathcal{L} = 0 \Rightarrow \frac{\partial\zeta}{\partial q_k} - w_{q_k} = 0 \\ \Rightarrow w_{q_k} = \frac{\partial\zeta}{\partial q_k} = -\frac{\partial P_{max}}{\partial q_k}, \quad k \in \mathcal{N}_A \end{aligned} \tag{5.13}$$

The increase in the VSM, due to the changes in both active and reactive power consumptions p_k and q_k can be thus linearly approximated by the following equation:

$$\Delta P_{max} = -w_{pk}\Delta p_k - w_{qk}\Delta q_k \tag{5.14}$$

From (5.10), (5.11), it is implied that the convention for the sensitivities is positive for generation and negative for load. Later in this section, P,Q are treated as consumptions by the ADN, so there needs to be a change in the sign.

Different VSM sensitivities will occur for each contingency. For each specific contingency, it is possible to use the sensitivities in order to estimate the support that can be offered from each distribution feeder through altering the active and reactive power consumptions. The sensitivities (5.12) and (5.13) are provided then to each bus where ADN is connected. Then each ADN can use these sensitivities in order to control its power injections at the PCC in order to support the transmission system in terms of voltage stability.

5.2.2 Distributed optimization at each ADN

From the transmission system perspective, each feeder is represented by P and Q consumption at the high voltage (HV) side of distribution substations and is modelled as such in the upper level optimization problem.

Active distribution feeders contain multiple active components and as a result, can modify their P and Q consumptions by changing the voltage setpoints of the LTC and the IBRs within their allowed operational limits, or by exploiting their storage capabilities, if any. In this Section P, Q absorptions and the respective setpoints are modified by solving an optimization problem to maximize VSM, using the sensitivities that are distributed from the control centre, after the upper level optimization problem is solved.

For the solution of the local VSM maximization problem full knowledge of each ADN is assumed at each local controller, including LTC and any other available controls (e.g. capacitive compensation). However, the transmission network is not known, from the local controller's perspective. For this reason, along with the Langrange multipliers, a

post contingency Thevenin equivalent is provided by the control center to the ADN for each critical contingency.

Thus, at regular intervals together with the VSM solution the equivalent Z_{th} after each contingency is sent to the ADNs. The equivalent E_{th} can then be computed from the measured transmission voltage and P, Q consumptions at the time of the emergency control activation, which as stated earlier will be triggered only after the specified contingency has occurred. Clearly a predefined table of contingencies with corresponding Lagrange multipliers and Z_{th} will have to be made available in advance. In this thesis Z_{th} is calculated using the Z-bus approach, with use of the commercial power system simulation software PSSE [70].

The local controller of each ADN will have to solve its optimization problem containing also an equivalent Thevenin of the transmission network at the point where it is connected. The complete configuration, including the equivalent Thevenin, as well as the tap of LTC, as explained in 4.1.2, is presented in Fig. 5.3, for the 2-bus ADN of 4.2.1:

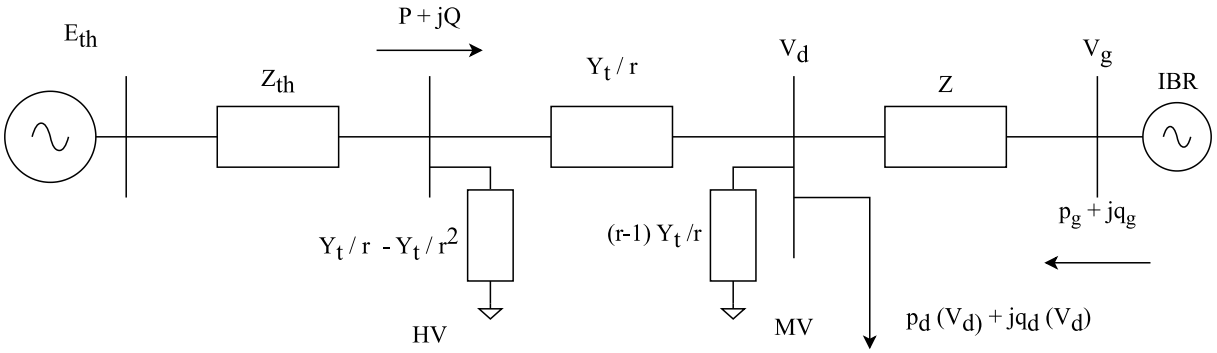

Figure 5.3: 2-bus ADN with Thevenin Equivalent

In this configuration, the available controls are the LTC tap ratio r and the IBR setpoint V_g. Using these controls and the sensitivities, the controller will seek to optimize P, Q absorptions in order to support the transmission system. The lower-level optimization performed in the ADN aims at computing the optimal setpoints for its controllable resources in order to maximize the VSM of the transmission system according to (5.14), by varying the P, Q consumptions. Several such resources can be considered including interruptible load shedding. In this specific application, we consider the setpoint of the LTC and the voltage of the IBRs as controllable parameters or decision variables.

Using the sensitivities (5.12), (5.13) calculated from the VSM problem (5.2)-(5.7), the objective function actually computes the linearized change in the maximum loading of the transmission system ΔP_{max}. The sings of (2.54),(2.55) are changed to match the consumption convention of P, Q as seen from the ADN side.

The operational constraints of the distribution network are included in the optimization so that no voltage or current limits are violated. This results in non-intrusive voltage stability support offered by the ADN, meaning that support comes at no operational cost of the ADN. Nonetheless, since this is a post-contingency corrective measure, a wider expansion can be allowed for distribution voltages.

The operational constraint of the feeders and the current limits of the IBRs are included as inequality constraints. The tap ratio of the LTC is treated as a continuous variable in the optimization problem. In the formulation tap r and voltage setpoint of the IBR are

the control parameters, in order to maximize VSM. Active IBR generation is considered constant and reactive generation is constrained by maximum converter current.

In order to keep consistency with the formulation of Chapter 4, subscript k denotes the buses of the ADN and P^0, Q^0 are the initial ADN consumptions, so that:

$$\Delta P = P^0 - P \tag{5.15}$$
$$\Delta Q = Q^0 - Q \tag{5.16}$$

Let $\mathcal{N}_A$ be the set of buses of each ADN, then the formulation of the OPF for each ADN is rewritten as follows:

$$\max_{e,f,r} \quad w_p \Delta P + w_q \Delta Q \tag{5.17}$$
$$\text{subject to :}$$
$$\boldsymbol{h_A}(e,f,r) = 0 \tag{5.18}$$
$$V_k^2 = e_k^2 + f_k^2, \forall k \in \mathcal{N}_A \tag{5.19}$$
$$V_k^{min} \leq V_k \leq V_k^{max}, \forall k \in \mathcal{N}_A \tag{5.20}$$
$$p_{gk}^2 + q_{gk}^2 \leq (V_k I_{nk})^2, \forall k \in G_A \tag{5.21}$$
$$p_{gk}^{min} \leq p_{gk} \leq p_{gk}^{max}, \forall k \in G_A \tag{5.22}$$
$$r^{min} \leq r \leq r^{max} \tag{5.23}$$

where $\boldsymbol{h_A}$ refers to the set of power balance equations similarly to (2.11), but in this case they are also a function of the LTC tap as well, since r is included in the admittance matrix as explained in 4.1.2.

$$h_{p_k} = p_k - e_k(\boldsymbol{g_k}(r)^T \boldsymbol{e} - \boldsymbol{b_k}(r)^T \boldsymbol{f}) - f_k(\boldsymbol{b_k}(r)^T \boldsymbol{e} + \boldsymbol{g_k}(r)^T \boldsymbol{f}) = 0, \quad k \in \mathcal{N}_A \tag{5.24}$$
$$h_{q_k} = q_k + e_k(\boldsymbol{b_k}(r)^T \boldsymbol{e} + \boldsymbol{g_k}(r)^T \boldsymbol{f}) - f_k(\boldsymbol{g_k}(r)^T \boldsymbol{e} - \boldsymbol{b_k}(r)^T \boldsymbol{f}) = 0, \quad k \in \mathcal{N}_A \tag{5.25}$$

V_k denotes the voltages of the buses of the ADN, and (5.20) defines the voltage limits. Equation (5.21) and (5.22) refer to the current and the active power limits of the IBRs respectively. Finally, (5.23) defines the limits of the LTC tap ratio.

5.3 Case Study: Nordic Test System - Corrective Control

5.3.1 Upper level OPF

The proposed framework is used on the transmission system that was presented in 2.11.1, for the most critical contingency that was identified. It is assumed that in five HV substations, the equivalent injections are actually ADN with the configuration of the 2-bus feeder, including a WF connected through a dedicated feeder and an aggregate load placed at the MV side of the HV/MV substation.

This extended version of the IEEE Nordic Test System was firstly used in [9], in order to include distributed generation. In this thesis, the same test system is used, including the WFs only in the 220kV buses 1041-1045. The data for the 5 feeders can be seen in Table 5.1. The active power generation of the WFs as well as the load consumption are modified in order to match the injection at the HV side of the initial operating point. As a result the solution of the power flow for the high voltage transmission system is identical.

Table 5.1: WF data connected to the system

WF	HV	P_{WF} (MW)	S_N (MVA)	P_{max} (MW)	R (pu)	X (pu)	r_{max}	r_{min}
1	1041	97.2	113.68	108	0.00441	0.0608	1.1	0.88
2	1042	99.3	110.05	104.55	0.04505	0.0916	1.1	0.88
3	1043	64.6	71.58	68	0.0779	0.14757	1.1	0.88
4	1044	90	100	90	0.0308	0.1396	1.1	0.88
5	1045	81	94.74	90	0.00529	0.07296	1.1	0.88

The sensitivities (Lagrange multipliers) for the critical contingency, which is the loss of 400kV transmission line 4032-4044 between the North and the Central area, as calculated from the upper level optimization problem, are shown in Table 5.2. Only the sensitivities for the 5 HV buses with connected ADNs in the Central Area are shown. These sensitivities are accurate for small changes in the injection, as can be verified by repeated runs of the optimization program. For large changes, however, the actual change of VSM may differ from the linear estimate.

Table 5.2: Post contingency data for each ADN bus

bus	w_p	w_q	V (pu)	P (MW)	Q (MVar)	$z_{th}(pu)$
1041	1.1835	0.446	0.9564	589.89	177.08	0.024+j0.032
1042	0.9268	0.1155	0.9977	324.44	88.43	0.028+j0.065
1043	1.0629	0.3868	0.9778	255.61	98.42	0.019+j0.031
1044	0.8892	0.457	0.9489	825.83	295.05	0.011+j0.012
1045	0.9459	0.4019	0.9605	707.86	226.45	0.012+j0.015

5.3.2 Lower Level - Distributed Optimal Control

As explained in section 5.2.2, the optimization on each distribution feeder aims at providing the optimal setpoints for the IBG, as well as the optimal tap position (or the voltage setpoint for the MV side) of the LTC transformer. In Table 5.3, the optimal setpoints computed with the methodology of Section 5.2.2 at each feeder and the estimated ΔP_{max} increase based on the sensitivity formula are presented.

As observed in Table 5.3, for buses 1041, 1042, 1044, 1045 the active limiting constraints of the optimization problem are the voltage limit of the MV bus of the transformers and the current limit of the IBR. For feeder 1043, the IBR has not reached its converter current limit, so the limiting constraint is the IBR maximum voltage. All MV feeder buses are inside the operational limits, making this scheme non-intrusive for the distribution network. Regarding the change in the active and reactive power at the PCC, ΔP and ΔQ, it can be observed that all are positive, denoting a decrease in the consumption of the ADN at the PCC for both active and reactive power. The positive change in consumption

Table 5.3: Optimal ADN setpoints and results

bus	V_g (pu)	r_{opt}	V_d (pu)	ΔP (MW)	ΔQ (MVar)	ΔP_{max} (MW)
1041	0.9908	1.034	0.95	44.02	73.27	84.7
1042	1.0387	1.100	0.95	25.81	57.61	30.4
1043	1.05	1.038	0.95	17.75	46.75	37
1044	1.04	0.996	0.95	34.17	68.49	61.7
1045	1.0261	1.016	0.95	43.10	65.82	67.2

in terms of active power is attributed to the indirect load shedding due to the voltage dependency. Regarding the positive change in the reactive power, it is attributed to both the reactive generation of the IBR as well as the decrease in reactive load consumption. That's the reason why in all cases the reactive power change is greater.

Assuming the critical contingency happens at the considered operating point, the system will become unstable. To avoid this a distributed emergency control is assumed that will enforce the optimal settings calculated to the five HV feeders. In Table 2.4 the loss of 400kV Transmission line 4032-4044, which is the same contingency applied in this section, has a negative VSM margin of -104 MW. The results of Table 5.3 show that the collective expected increase of stability margin from the implementation of the setpoints on the 5 ADN is more than enough to stabilize the system. However, this is based on linearization, therefore it has to be checked by simulation, which will be the subject of the next subsection.

5.3.3 QSS Time Domain-Simulation - Corrective Control

It has already been shown in 2.11.4 with simulation that the system becomes unstable under the loss of transmission line 4032-4044, which is the critical contingency considered above in subsection 5.3.1. In order to apply the acquired setpoints from the optimization framework that was described, the whole system is simulated in WPSTAB with full feeder representation, including the LTC and the 20kV buses, where the loads and IBR are located.

It should be noted at this point that the optimization approach relies on a static modelling of the system, thus the time required to achieve each separate setpoint is not taken into consideration. The converter can change its voltage and reactive power generation almost instantaneously, while changing a single LTC tap will take close to 10 seconds. For this reason, it is important to establish an appropriate scheme to apply the optimal setpoints in order to avoid adverse interactions.

For instance, by applying the IBR setpoints immediately after the contingency, may lead to an even faster collapse of the system [9]. This happens because of the increase in the load consumption of the system, before the LTC can act to lower load voltage. As also seen in 5.2, the system in the critical condition is more sensitive to the active power injections meaning that the increase in load consumption is more critical than the reactive support offered by the increased IBR voltage.

Following the above observations and since the optimal setpoints concerning each contingency have been identified for each ADN, the distributed emergency support scheme is implemented and simulated as follows:

- Step 1 : The corrective control starts immediately (1 second) after the occurrence of the contingency, since the contingency has already been identified as critical and voltage instability is imminent.

- Step 2 : The deadband of the LTC MV bus of each ADN is changed according to Table 5.3. The new deadband will be around the optimal value of V_d^{opt} :

$$V_{LTC} - \frac{db}{2} \leq V_d^{opt} \leq V_{LTC} + \frac{db}{2} \tag{5.26}$$

- Step 3 : Voltage setpoints of the IBGs from Table 5.3 are sent only after the LTC controlled MV bus gets inside the deadband.

This control sequence guarantees that the active power injection of each feeder will be lowered before the reactive power support is offered. The sequence and implementation of the setpoints is presented in the following Fig. 5.4:

In Figures 5.4(a)-(c), the two voltages V_d and V_g are plotted, which correspond to the voltage of the load bus (controlled by the LTC) and the voltage of the IBR bus. With red dashed lines, the deadband of the LTC according to (5.26) is included. Figures show that the required setpoints are achieved, in different time-frames for every ADN and in every ADN the operational voltage limits (0.95 pu- 1.05 pu are satisfied. As described in the three steps above, it can be seen that the voltage of the IBR bus V_g, achieves the setpoint implemented, only after the load bus voltage enters the desired deadband. This sudden voltage increase may drive the voltage of the load bus out of the deadband, in some of the ADNs, which is then restored again.

The reactive power of the WFs connected to each one of the ADNs modelled is presented in Fig. 5.5. Before the contingecy, all WFs are operating under unity power factor.

The voltages over time in some of the HV and the EHV buses of the central area are also presented in Fig. 5.6, 5.7. Despite the initial drop, right after the contingency, the support offered is able to restore stability in the system and keep voltages in normal values, in contrast to the red dashed lines, where the bus voltages are plotted, where no control is assumed, for the case examined in Section 2.11.4.

In Fig. 5.8, the net load of the central area is presented over time. Net load (or system load) is the sum of power at the HV side of the HV/MV substations, which is essentially the total load consumptions minus the distributed generation at the medium voltage level. It can be observed that the load is decreased due to the indirect load reduction caused by the change of the deadband of the LTC.

The amount of indirect load shedding in each feeder can be calculated as follows:

$$\Delta P_d = \frac{p_d^0}{V_0^a}(V_{min}^a - V_{fin}^a) \tag{5.27}$$

Where V_{min}^a is the lower limit of the initial deadband, V_{fin}^a is the load voltage at the end of the simulation and V_0^a is the initial voltage. In this case, the total load reduction in the Central area is $\Delta p_d^{tot} = 134$MW and the total reactive power generation offered by the IBGs is about 228 MVAr.

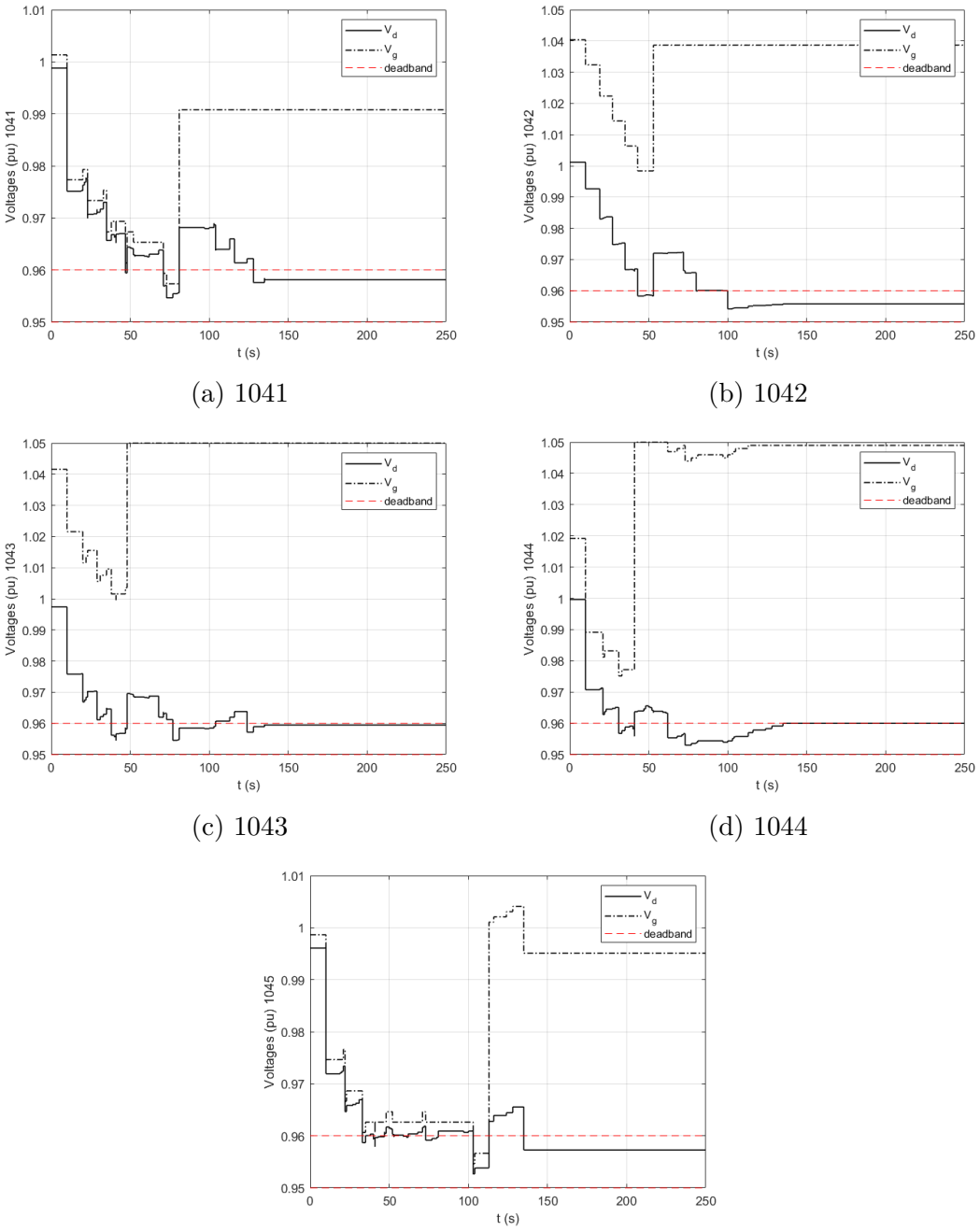

(a) 1041

(b) 1042

(c) 1043

(d) 1044

(e) 1045

Figure 5.4: Setpoint implementation in ADNs connected in the 5 HV buses

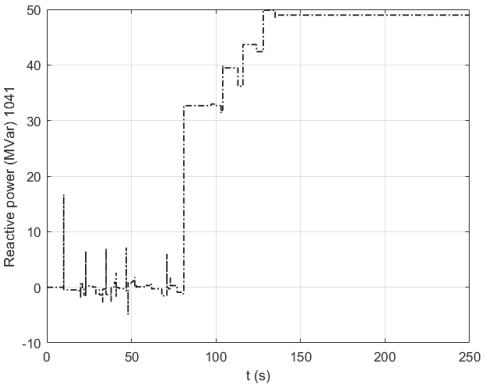

(a) 1041

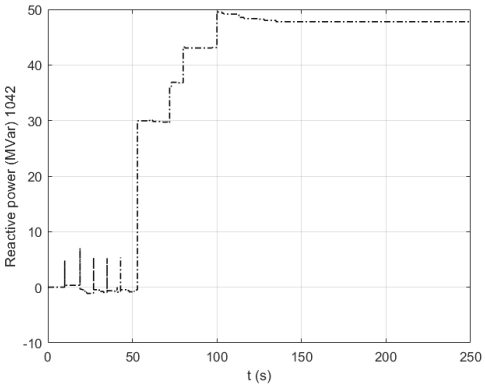

(b) 1042

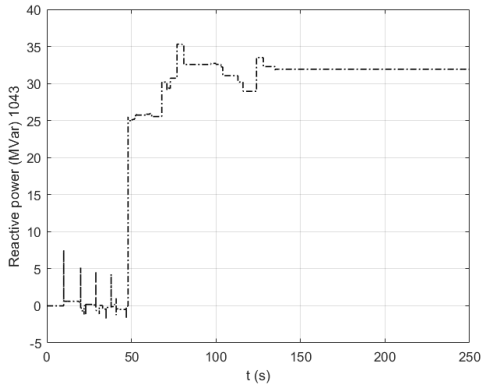

(c) 1043

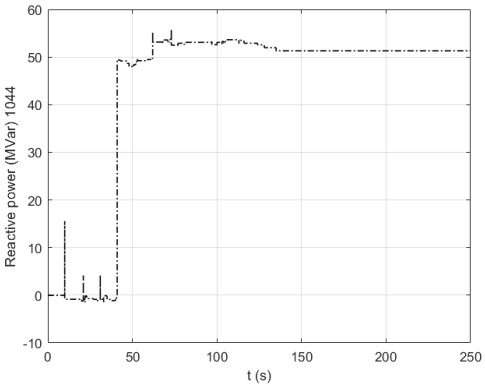

(d) 1044

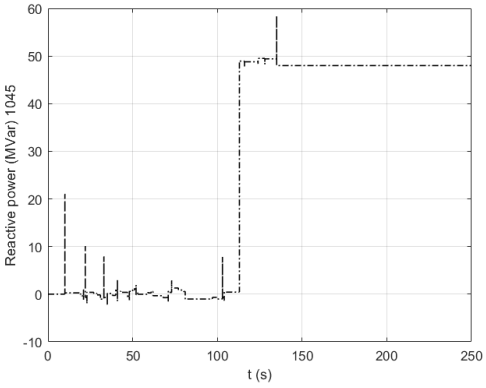

(e) 1045

Figure 5.5: Reactive power of WFs in the 5 ADNs

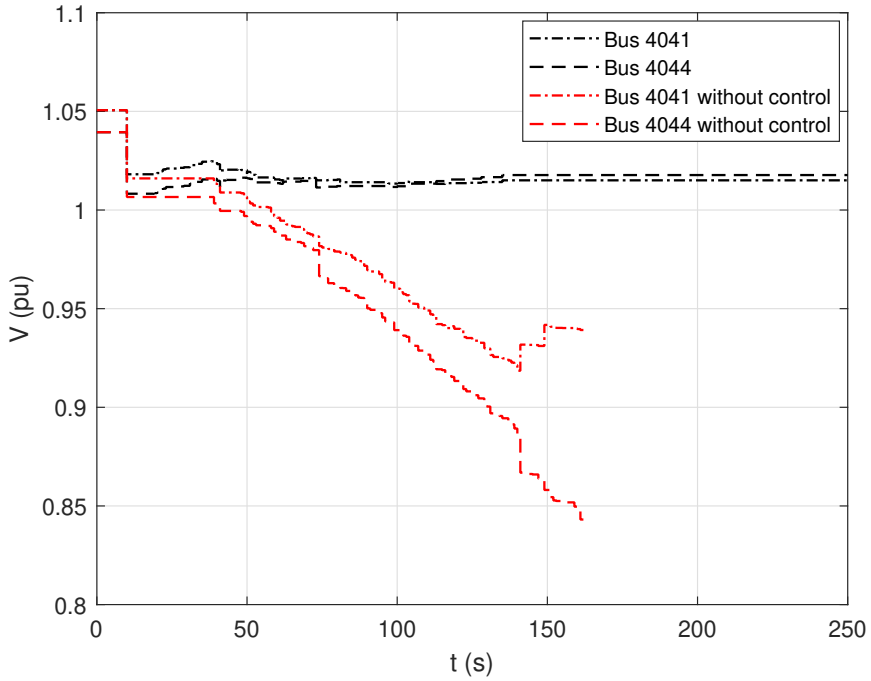

Figure 5.6: EHV buses 4041,4044

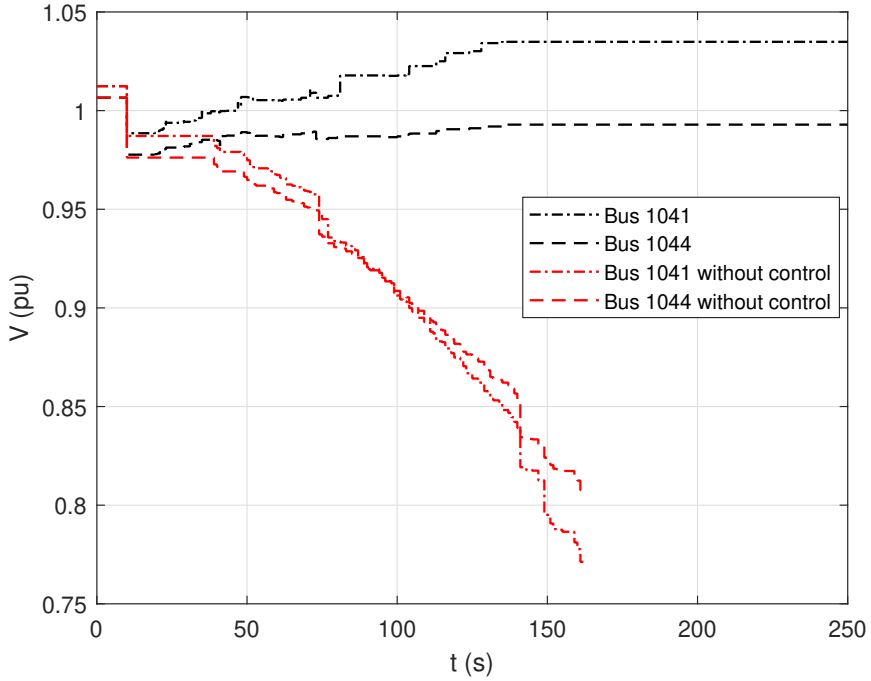

Figure 5.7: EHV buses 1041,1044

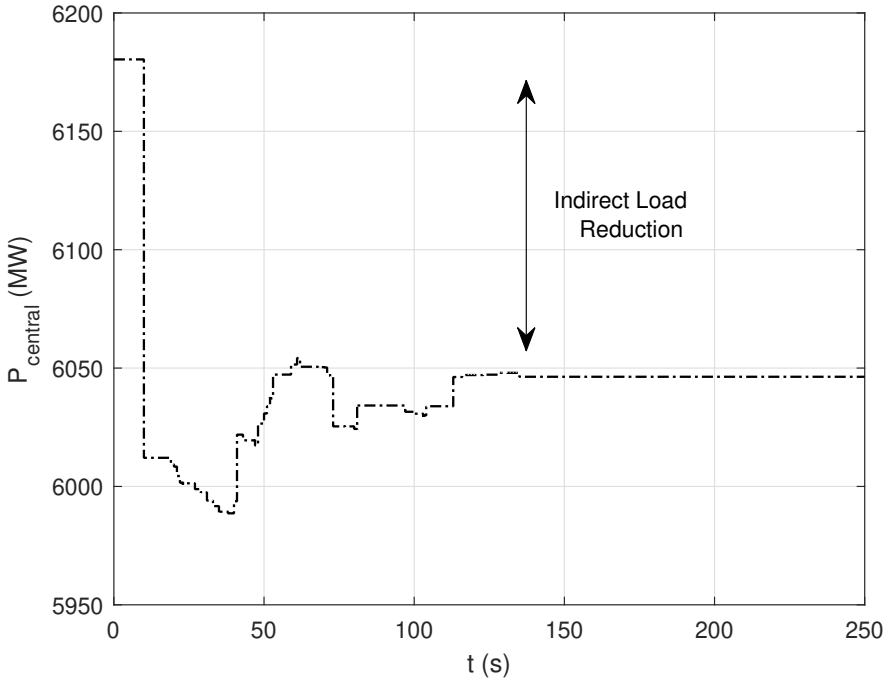

Figure 5.8: Central area net load

5.3.4 Comparison with EMRS

The EMRS approach was presented in [8] and stands for 'Emergency Reactive Support'. As it's name suggest, it aims at injecting maximum reactive power from the available WFs to support the transmission system. While reactive power is crucial to the stability of the voltages, in some cases, it may cause a sudden increase in the load and lead to even faster collapse.

More specifically, in dedicated WF feeders, it is straightforward that the maximum reactive power injection will support the system. However, in feeders where both load and IBRs are connected, the sudden voltage increase may lead to a sudden increase in load consumption, which may in turn fasten the system collapse.

For the same, most critical contingency examined in the cases above, which is the loss of 400kV transmission line 4032-4044, the EMRS approach is simulated, using the QSS simulation software WPSTAB. In this case, the EMRS is triggered when a pilot bus (bus 1041) drops below a specific voltage threshold. If that happens, EMRS is activated and all the IBRs of the area will inject maximum reactive power simultaneously.

In Figures 5.9a-5.9d, the QSS simulation results are presented for the EMRS approach. The critical contingency is applied 10 seconds in the simulation and the EMRS triggers at $t = 73s$. More specifically, in Fig. 5.9a, the voltages of the load and IBR bus are presented for the ADN connected in bus 1041. It is observed that the second EMRS is triggered, voltages increase significantly. The increase in the load voltages will also increase the load consumption for both the active power (Fig. 5.9b) and the reactive power (Fig. 5.9c) load. Finally, the load of the central area is presented in Fig. 5.9d, where it is shown that the load consumption almost matches the pre-contingency load consumption, which is proven to be unstable. This leads to the collapse of the system and the simulation ends

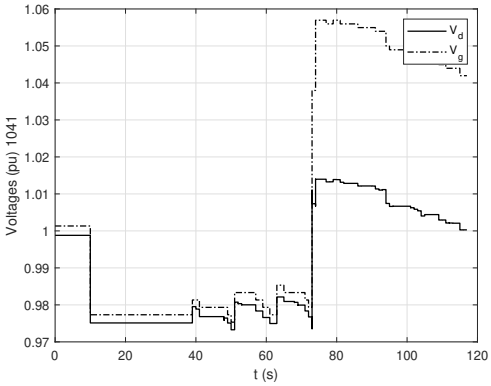

(a) Bus Voltages of ADN 1041

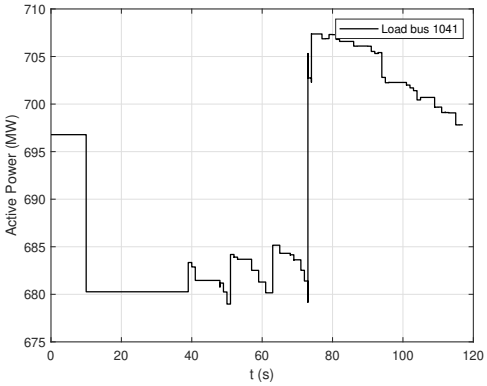

(b) Active Power Load 1041

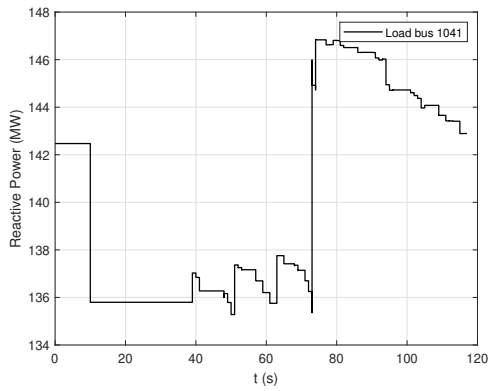

(c) Reactive Power Load 1041

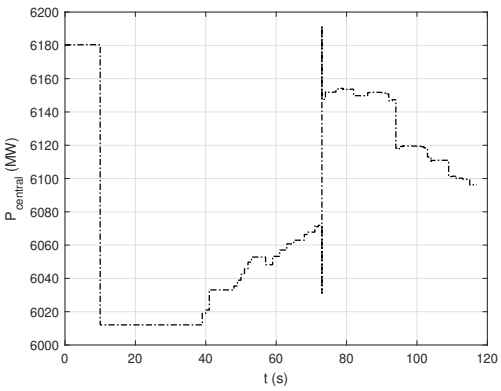

(d) Central Area Active Power Load

Figure 5.9: QSS Simulation Results using the EMRS approach

in only 117 seconds.

On the other hand, using the ADN distributed support approach, simulation results verified that the additional margins offered by the ADNs and calculated with the linearization offered by the Lagrange multipliers, are enough to keep the system stable in terms of voltages, after the contingency.

The results using the EMRS were mainly presented to also highlight that the sequence of implementation of the optimal setpoints, as calculated by the support scheme, plays a very critical role. As shown, while the EMRS will drive the system to higher voltages, which is desirable, the load consumption increase is an adverse result.

In 5.10, three cases, and their respective simulation results, are presented. Black solid line presents the case where no support is applied and the system collapses after some time (around . The red dashed line show the EMRS approach, where it can be seen that voltages are increased for some time but the system collapses for the reasons explained above. Finally, blue dashed line presents the ADN distributed optimal support immediately after the contingency. As shown, the voltages remain close to the initial voltages and the system reaches a new stable point.

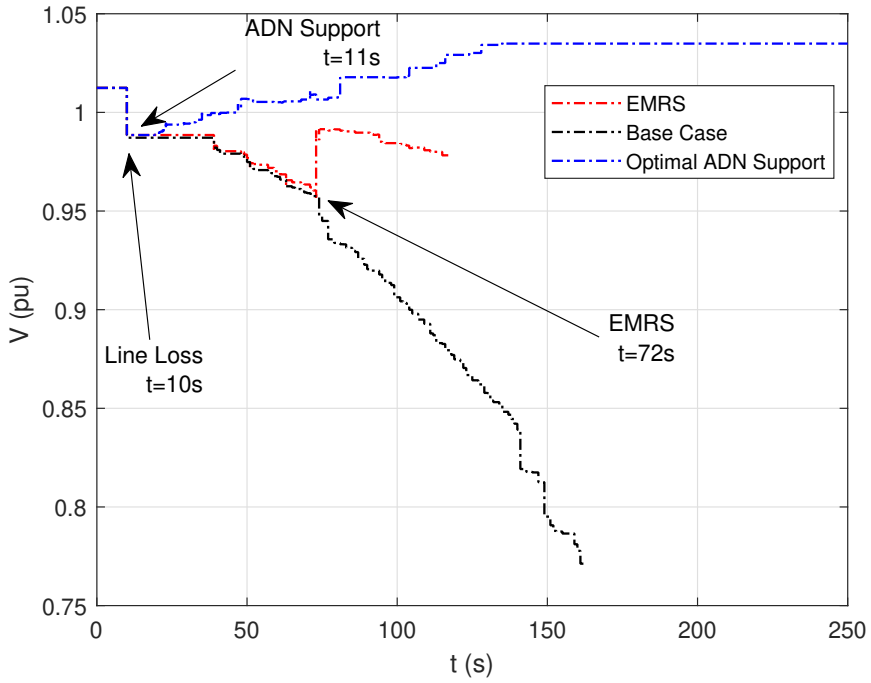

Figure 5.10: Bus 1041 voltage for Base Case, EMRS, Optimal ADN Support

5.4 Preventive VSM optimization using FR

In the previous sections, a corrective distributed optimization framework was proposed to support the transmission system in case of emergency. In that approach, the operator of the transmission system solves a problem for the VSM, without any information about the ADNs, and then distributes control signals to ask for support. The corrective support is applied immediately after the contingency and it is shown that it can support the system and avoid a possible voltage collapse.

The preventive control, as also described in Section 5.1, relies on the FRs provided by the ADN. The methodology for the computation of the FR presented in Chapter 4 is used to provide linear constraints for the consumption of the ADNs at their PCC with the transmission system, which then can be used in an upper level optimization to increase the VSM. This approach is centralized, since the VSM optimization takes into consideration the flexibility of the ADNs.

The flowchart of the proposed centralized corrective approach is presented in Fig. 5.11, where a period of ΔT is assumed for the ADNs to update their FRs. This periodic time ΔT could be hourly, or correspond to the dispatch periods of the balancing market. The said FRs are provided to the transmission level controller (possibly the EMS), which will include the FRs in the optimization problem for the VSM. If the optimization finds critical contingencies with negative (or small positive) VSM, then the resulting reference values are sent to each ADN. The last step of the flowchart is for the ADNs to actuate the reference values at their PCC, by implementing setpoints to their controllable assets.

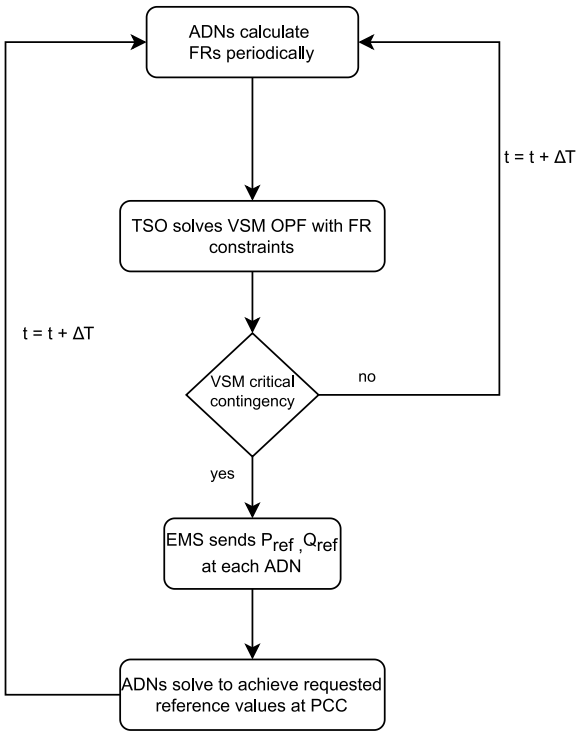

Figure 5.11: Flowchart of proposed scheme

The formulation of the centralized optimization problem is similar to (2.41)-(2.47), with the addition of the constraints (4.54) for each ADN connected to the transmission system. Let $\mathcal{N}$ be the set of buses of the transmission system and $\mathcal{A}$ the subset of buses where ADN is connected and G the subset of generator buses, the central VSM optimization problem with the inclusion of the FRs of the ADNs as linear inequality constraints, is formulated as follows:

$$\text{VSM} = \max_{\boldsymbol{e},\boldsymbol{f},\Delta\text{L},\lambda} \Delta\text{P} \tag{5.28}$$

$$\text{subject to :}$$

$$\boldsymbol{h}(e, f, V, \Delta L, \lambda, \Delta P, \Delta Q) = 0 \tag{5.29}$$

$$\Delta p_{gk} = K_k(\Delta L + \lambda \sum_{k \in \mathcal{N}} d_{pk}) \tag{5.30}$$

$$p_{gk}^{min} \leq p_{gk} \leq p_{gk}^{max}, \forall k \in G \tag{5.31}$$

$$q_{gk} \leq q_{ak}(p_{gk}, V_k), \forall k \in G \tag{5.32}$$

$$q_{gk} \leq q_{rk}(p_{gk}, V_k), \forall k \in G \tag{5.33}$$

$$V_{gk} \leq V_{gk}^{ref}, \forall k \in G \tag{5.34}$$

$$\alpha_i \Delta P_k + \beta_i \Delta Q_k + 1 \geq 0, \quad k = 1, .., N_k, \quad \forall k \in \mathcal{A} \tag{5.35}$$

where, $\boldsymbol{h}$ is the set of power balance equations, that stand as equality constraints. The power balance equations in this cases are also a function of the change in the consumptions at the PCC. Specifically for the ADN buses $k \in \mathcal{A}$, where there is no other load or generation connected ($p_{gk} = 0, q_{gk} = 0, p_{dk} = 0, q_{dk} = 0, \quad k \in \mathcal{A}$):

$$h_{p_k} = \Delta P_k - e_k(\boldsymbol{g_k}^T \boldsymbol{e} - \boldsymbol{b_k}^T \boldsymbol{f}) - f_k(\boldsymbol{b_k}^T \boldsymbol{e} + \boldsymbol{g_k}^T \boldsymbol{f}) = 0, \quad k \in \mathcal{A} \tag{5.36}$$

$$h_{q_k} = \Delta Q_k + e_k(\boldsymbol{b_k}^T \boldsymbol{e} + \boldsymbol{g_k}^T \boldsymbol{f}) - f_k(\boldsymbol{g_k}^T \boldsymbol{e} - \boldsymbol{b_k}^T \boldsymbol{f}) = 0, \quad k \in \mathcal{A} \tag{5.37}$$

Then, p_{gk},q_{gk} are the active and reactive power generation of machines connected to the transmission system, subject to the inequality constraints (5.31)-(5.33) and the voltage reference (5.34). Finally, (5.35) corresponds to the inequality constraints based on the FR of each ADN of $\mathcal{A}$.

The solution of the above optimization problem, provides the maximum stress that can be achieved by the power system, using optimally the flexibility that can be provided by the ADNs. As a result, the decision variables ΔP_k and ΔQ_k are also calculated. The new reference values for each ADN can then be sent back to the local controller of each ADN in order to achieve optimal control.

5.5 Case Study: Nordic Test System - Preventive Control

5.5.1 System Description

The central optimization problem, posed in 5.4, is applied to the IEEE Nordic Test System [58] of Fig. 2.11, which is modified similarly to [9], as in Section 5.3, but with only the five feeders connected to the sub-transmission HV buses of the Central Area replaced by ADNs. These ADNs are represented with the two-bus equivalent of Fig. 4.5 with the data and initial conditions given in [9] and the initial P, Q consumption shown in Table 5.4 and no storage capacity.

As also mentioned in section 2.11.1, the system is prone to voltage instability due to high power transfers from the north to the central area. While several critical contingencies

Table 5.4: Initial Consumption by ADNs

Bus	P_k (MW)	Q_k (MVar)
1041	600	180
1042	330	90
1043	260	100
1044	840	300
1045	720	230

that can result in voltage instability have been identified, as also presented in Table 2.4, in this section, only the most critical contingency will be examined, which is the loss of transmission line 4032-4044.

The direction of stress chosen for the VSM determination, is a uniform load increase in the central area only, with all generators participating resulting in an increase of power transfer to the Central Area which is generation deficient. Thus $d_{pk} = P_{0k}$ and $d_{qk} = Q_{0k}$ while all other elements of $\boldsymbol{d_p}$ and $\boldsymbol{d_q}$ are set to zero.

5.5.2 ADN Flexibility Regions

For the identification of the FRs of the five ADNs, any of the aforementioned methods can be used from 4.3. In this case the approach of multiple bindings constraints is used, due to the simplicity of the ADNs, presented in section 4.3.4. The FR is calculated for the five ADNs of Table 5.4. The initial power injections of the buses where ADNs are placed, are presented in Table 5.4, where the positive sign indicates flows from the transmission system to the feeders. For each ADN the FR is determined through the linear constraints (5.35), and the relevant coefficients α and β are presented in Table 5.5.

In Fig. 5.12, the FRs of the five ADNs are shown graphically. Depending on the ADN parameters, FRs are different for each case. Note that in some of the cases, some of the points corresponding to multiple binding constraints are infeasible, resulting in fewer linear constraints. The FRs could similarly be created using either the radial scan approach, or the Monte Carlo simulations and then the polygon approximation of section 4.4.

Table 5.5: Feeder coefficients α and β that form the linear constraints

1041		1042		1043		1044		1045	
α	β	α	β	α	β	α	β	α	β
0.009	-2.878	0.239	-5.084	0.379	-6.795	0.051	-2.193	0.008	-2.504
-1.910	1.365	-2.256	1.806	-3.712	3.352	-3.461	2.535	-2.600	1.781
-1.221	3.219	0.000	5.022	0.000	6.631	-2.518	3.102	-1.586	3.287
0.005	2.873	1.490	0.401	12.922	-33.018	0.009	2.172	0.005	2.498
1.558	-0.131	6.681	-19.200			1.468	-0.358	1.710	-0.383
1.279	-3.562					3.535	-4.483	1.428	-3.112

5.5.3 Centralized OPF results including FRs

The VSM optimization problem (5.28)-(5.35) is solved for the test system first without ADN flexibility, and then successively by introducing one by one the five ADN FRs. The

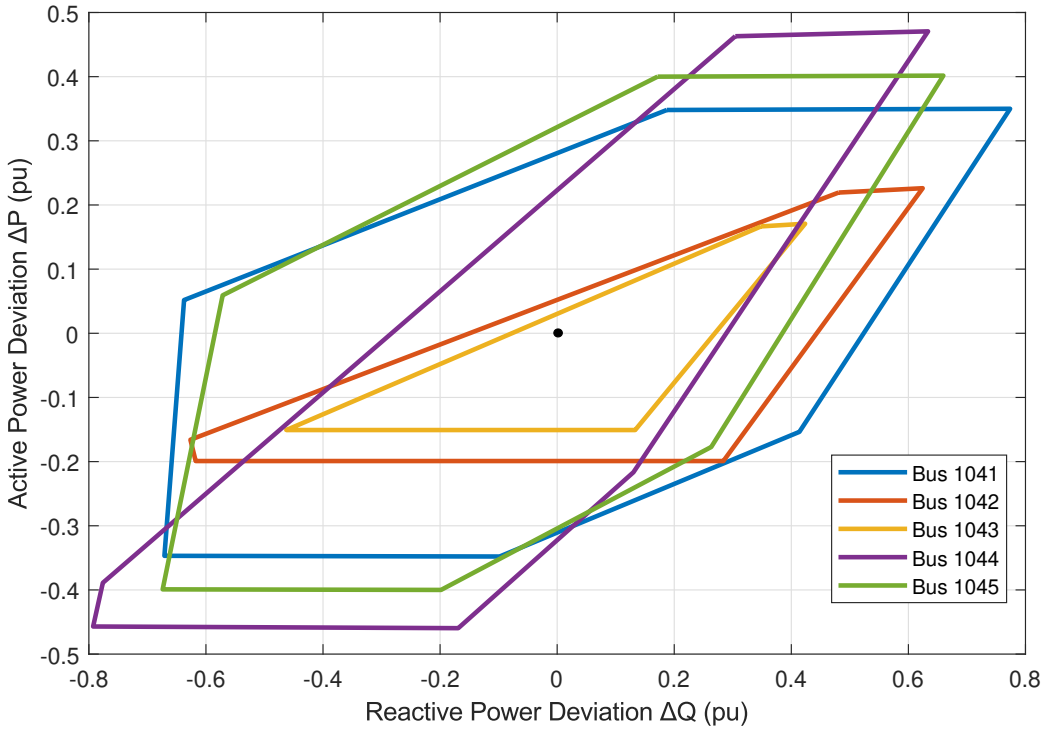

Figure 5.12: Flexibility Regions of 5 ADNs

corresponding maximum VSM and level of stress, along with the total load of the central area, after the most critical contingency are presented in Table 5.6. As expected, without ADN flexibility the system is insecure having a negative post-contingency margin of -105 MW. However, if the three first feeders are assumed to be flexible system security is restored, as the post-contingency VSM becomes positive. Making use of the flexibility of all five ADNs results in a relatively safe margin of 139 MW.

Table 5.6: VSM with and without ADN flexibility

	Central Area (MW)	max stress level λ	VSM (MW)
Initial Loading	6190	–	–
No ADN	6085	-0.0169	-105
1 ADN	6153	-0.0058	-37
2 ADN	6178	-0.0020	-12
3 ADN	6206	0.0027	16
4 ADN	6274	0.0135	84
5 ADN	6329	0.0255	139

For the last case, where all 5 feeders are flexible, the optimal consumption adjustments ΔP_k and ΔQ_k for each ADN$_k$ as provided by the solution of the optimization problem are presented in Table 5.6. In the optimal solution for all five ADNs the load bus voltage is minimized, while either the maximum voltage or the current limit constraint is active for the IBR bus. As expected, the results are similar to the results of the previous approach.

Thus, the optimal solution for each ADN corresponds to either point A, or E of Table 4.2. As a result, it is pretty straightforward to determine the optimal setpoints that need to

Table 5.7: Active and Reactive power change in each ADN at the VSM solution

Bus	ΔP (MW)	ΔQ (MVAr)
1041	-34.7	-70.8
1042	-19.9	-61.7
1043	-15.0	-46.4
1044	-45.7	-79.4
1045	-39.9	-67.7
Total	-155.3	-326.1

be applied to each feeder to achieve the changes presented in Table 5.6. It is noted that this optimal solution is the same with the intuitive approach employed in [9] and [38], where LTC voltage is minimized and reactive support from IBRs is maximized through a ramp.

5.5.4 QSS Time Domain-Simulation - Preventive Control

In this subsection, a long-term simulation is performed for the Nordic test system with WPSTAB software developed in NTUA, just like in subsection 5.3.3. The simulation includes control actions to achieve the optimal consumption adjustment for the five flexible ADNs. In this case, since the control is preventive, the new setpoints are implemented before the contingency. The control is applied 40s into the simulation, simultaneously to all five ADNs. The considered contingency (loss of transmission line 4032-4044) is applied 300s after the start of the simulation, when the preventive control has already been applied and the system has reached a new operating point.

More specifically, the preventive control scheme, that is based on the results of the VSM optimization of subsection 5.5.3 and the simulation of the critical contingency is as follows:

1. System is stable until t=40s of the simulation time

2. After 40 seconds the preventive control scheme is being applied. The setpoints of Table 5.8 are applied, which correspond to the points found on the FRs of Fig. 5.12. In each ADN, the voltages calculated in order to achieve the ΔP and ΔQ of Table 5.7 at each ADN are applied as setpoints to the LTC controlled voltage and the voltages of the IBRs.

Table 5.8: Optimal ADN setpoints

bus	V_g (pu)	V_d (pu)
1041	0.9872	0.95
1042	1.0368	0.95
1043	1.05	0.95
1044	1.0409	0.95
1045	0.9871	0.95

3. For the IBRs small steps are performed in the voltage setpoint so that the optimal

setpoints are achieved in 100 seconds. So the voltage step for each IBR is:

$$V_{step} = \frac{V_{gk}^{opt} - V_{gk}^{0}}{100} \tag{5.38}$$

4. The LTC starts changing it's reference value to the optimal V_d, at time t=40s. For each step of the LTC, ten seconds are required. The LTC adjustment may be affected by the voltage setpoint change of the IBRs, so additional steps may be needed to regulate the voltage of the load bus. In Table 5.8, the optimal value of V_d is presented, but in the simulation it is expressed as a deadband between 0.95 and 0.96 pu.

5. In t=300s, the critical contingency occurs and the simulation ends at t=800s, where the system has reached a new stable operating point.

In Figures 5.13(a)-(e), the voltages V_d of the secondary side of the HV/MV transformer and V_g of the IBR are shown for the 5 ADNs. It can be seen that the new setpoints are achieved before the contingency occurs (at t=300s). The resulting reactive power generation of the IBRs is plotted in Fig. 5.14. It is noted, that since the optimization takes into consideration the current limits, implementation of the setpoints should not trigger any current limits in the qss simulation.

Due to the voltage dependence of loads (4.12), (4.13), the reduction of the MV bus voltage indirectly reduces the active power flow in the PCC, so ΔP for each ADN is presented in Fig. 5.7. It can be observed that the change in consumption is negative, as expected, in order to support the transmission system. The change in the ΔP of each ADN is close to the one that is calculated from the VSM optimization presented in Table 5.7.

Finally, in Fig. 5.16 the voltages of EHV buses 4041 and 4044 of the central area are presented, with and without the implementation of the preventive actions on the flexible ADNs, in order to show how the voltage collapse is avoided. As can be observed, the implementation of the preventive control scheme will gradually increase the voltages of the transmission system, even in the EHV buses. Then, when the contingency occurs, the system remains stable and the voltages remain in normal levels, close to the initial voltages.

The amount of indirect load shedding in each feeder $\forall i \in \mathcal{A}$ can be calculated using the following equation [9]:

$$\Delta P_i = \frac{p_{di}^{0}}{V_{di}^{a}}(V_{min,i}^{a} - V_{fin,i}^{a}) \tag{5.39}$$

where, V_{dj}^{a} is the initial load bus voltage, $V_{fin,j}^{a}$ is the same voltage at the end of the simulation, and $V_{min,j}^{a}$ is the lower limit of the initial LTC deadband. The total indirect load reduction amounts to $\Delta P_{tot} = 142.5$ MW, as seen in the last row of Table 5.7. This is less than the one calculated by the VSM optimization, as the voltage of the load bus is not exactly equal to the specified setpoint due to the deadband. It is noted that the indirect load reduction is less than the one reported in [9] in the majority of the protection schemes that were used, while keeping both transmission and distribution voltages inside the operational limits.

In that respect if the voltage deadband of the LTC is wide, the VSM optimization may overestimate the amount of load reduction in the optimal solution.

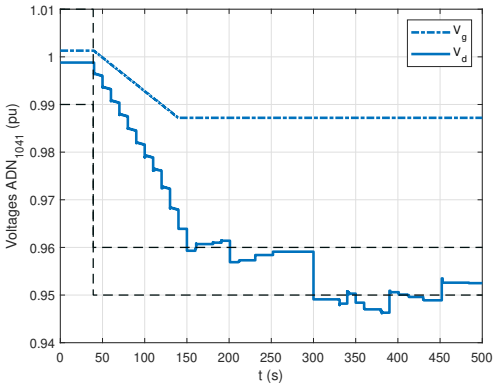

(a) 1041

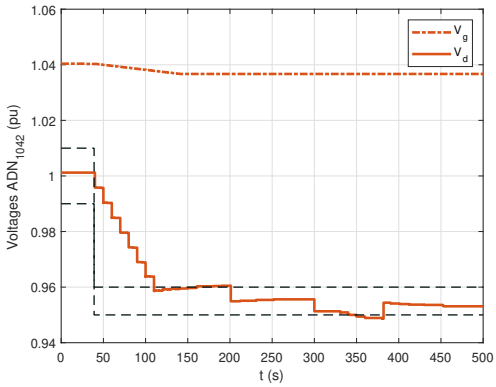

(b) 1042

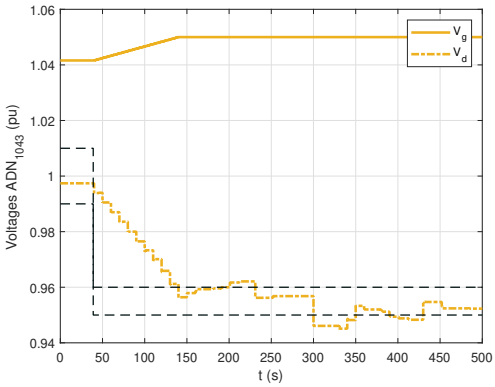

(c) 1043

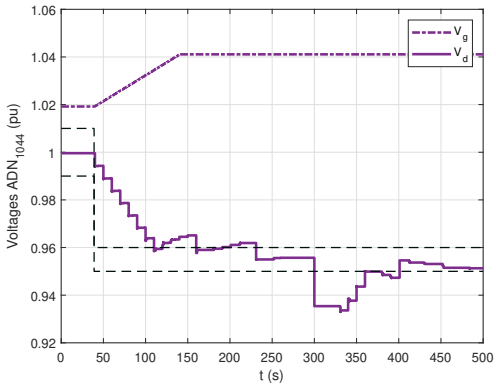

(d) 1044

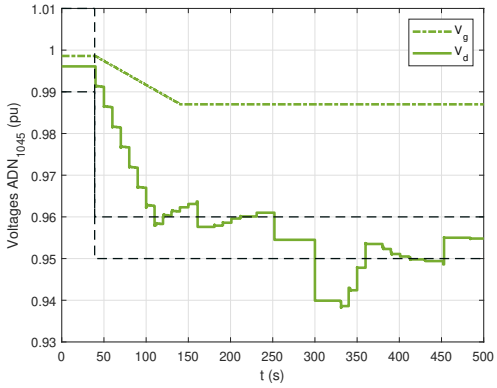

(e) 1045

Figure 5.13: Preventive implementation of Setpoints on ADNs

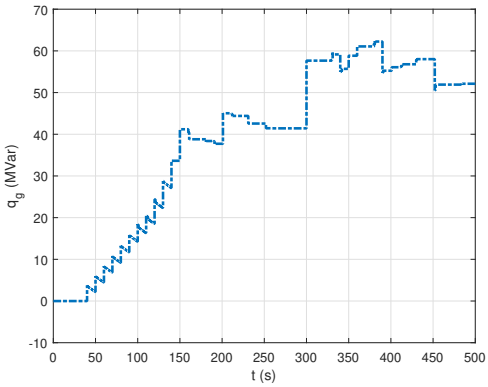

(a) 1041

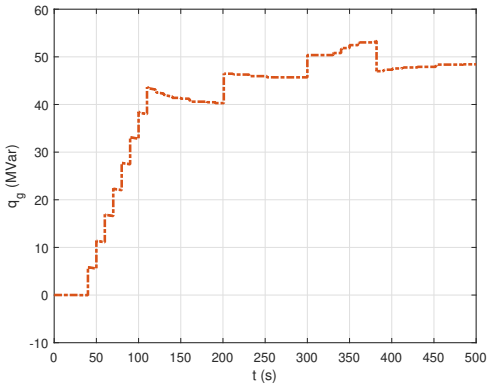

(b) 1042

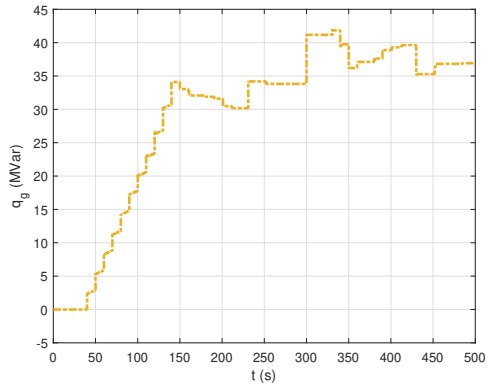

(c) 1043

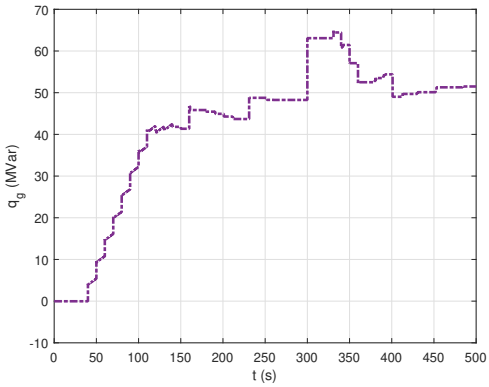

(d) 1044

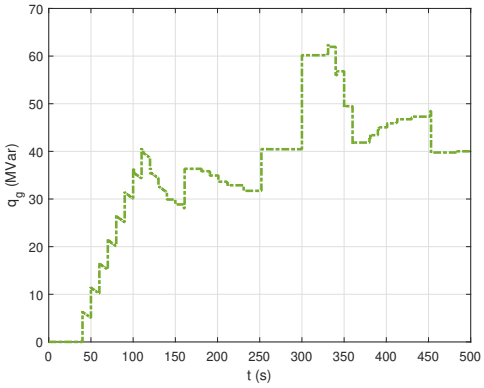

(e) 1045

Figure 5.14: Reactive Power generation of IBRs on each ADN

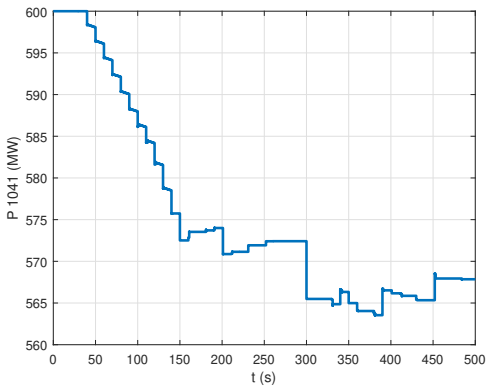

(a) 1041

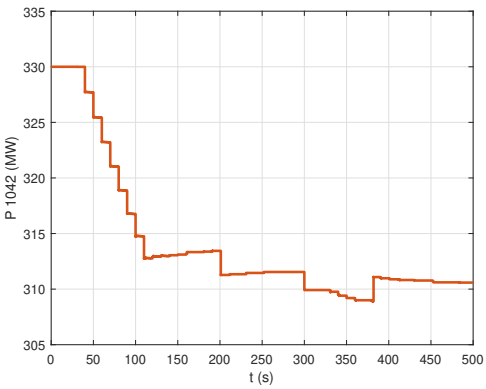

(b) 1042

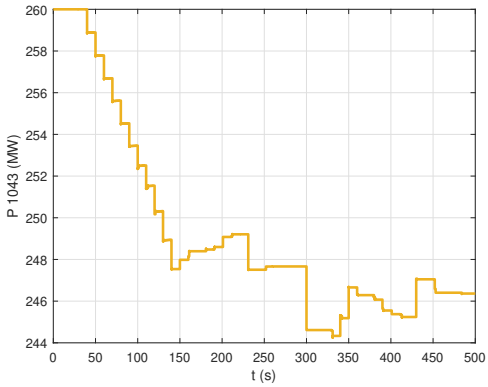

(c) 1043

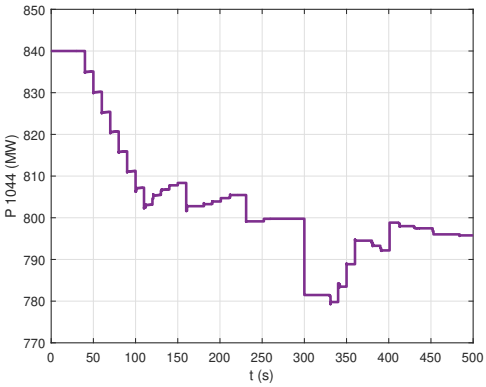

(d) 1044

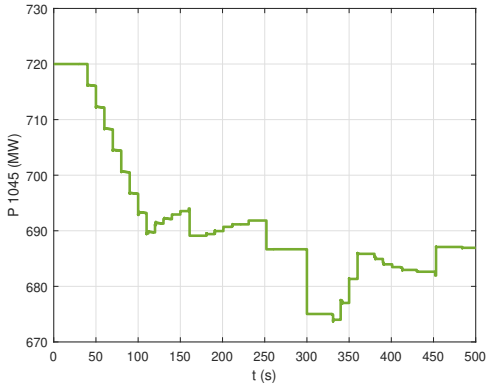

(e) 1045

Figure 5.15: Reactive Power generation of IBRs on each ADN

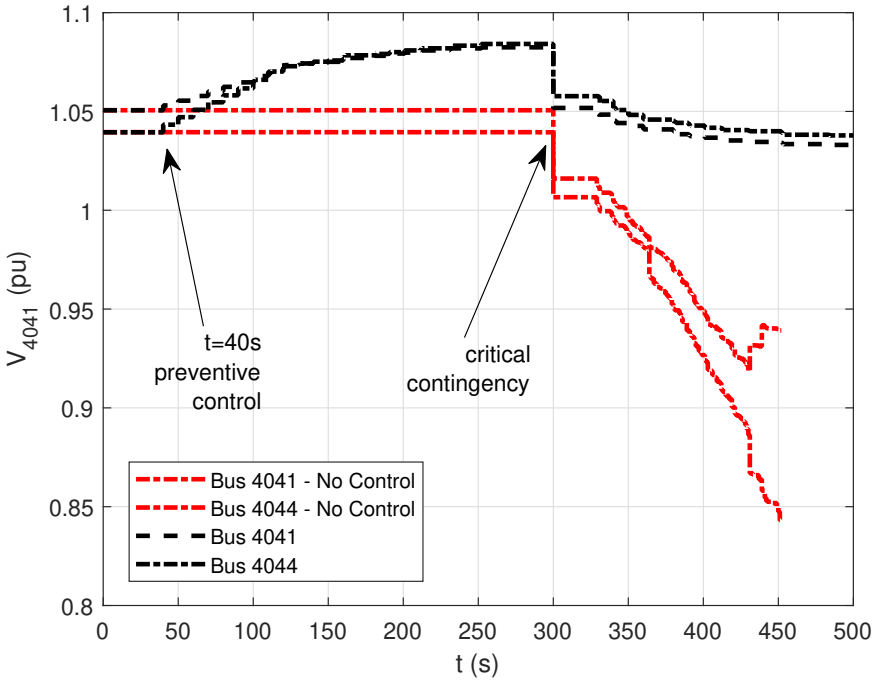

Figure 5.16: Voltages of buses 4041,4044 with and without the proposed preventive control

5.6 Application to Radial test system with 30-bus ADN

5.6.1 Test System description

In the previous section, because of the simple feeder configuration, it was easy to implement the reference values directly by sending the setpoints corresponding to the active (binding) constraints. In more complex feeder this is not so straightforward. In this Section the 30-bus feeder of Fig. 4.6 is considered connected to a simple radial test system, in order to demonstrate how to implement the optimal power adjustment setpoints in complex feeders.

The simple radial transmission test system considered is shown in Fig. 5.17 with the data provided in Table 5.9. The ADN presented in section 4.2 is connected in the middle of the radial transmission line of Fig. 5.17 which consists of two parts with identical R, X.

Table 5.9: Radial Transmission System Data (100MVA base)

R (pu)	X (pu)	B_c (pu)	E_{th} (pu)
0.05	0.2	2	1.05

For the ADN, in the base case, IBRs are operating with unity power factor. The initial consumption of the ADN is also provided in Table 5.10.

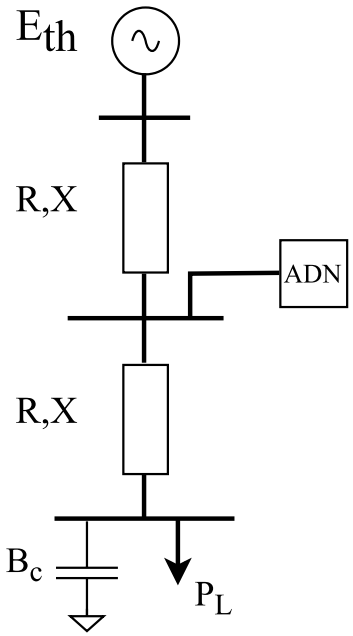

Figure 5.17: Transmission Corridor with ADN connected in the middle

5.6.2 VSM optimization

The VSM maximization problem (5.28)-(5.35) is used for the test system, with and without the polygon constraints of the 30-bus ADN. The problem is solved first for constant consumption from the distribution feeder (no flexibility), and then again allowing the ADN consumption to vary within the polygon FR approximation previously calculated in Fig. 4.26 (flexibility). The solution of the optimization provides the maximum power results, which in this case is the maximum active power P_L that can be transferred to the remote load bus, and the reference values calculated in the case where flexibility is provided and are shown in Table 5.10. For the reference values:

$$P_{ref} = P^0 + \Delta P \tag{5.40}$$
$$Q_{ref} = Q^0 + \Delta Q \tag{5.41}$$

Table 5.10: VSM Results

	ADN flexibility	No ADN flexibility
P^0 (MW)	-3.24	-3.24
Q^0 (MVAr)	5.29	5.29
ΔP (MW)	-6.85	-
ΔQ (MVAr)	-20.34	-
P_{ref} (MW)	-10.09	-
Q_{ref} (MVAr)	-15.05	-
VSM (MW)	124.59	113.34

Again, results show that VSM support is translated into decreasing ADN consumption both in terms of active and reactive power at the PCC. The change in the consumption

results in quite significant increase in the VSM, compared to the case where no flexibility is provided by the feeder and consumptions remain constant.

5.6.3 Setpoint implementation

As already discussed, a third OPF problem is formulated, in order to achieve P, Q consumption as close as possible to the reference values determined by the central optimization P_{ref},Q_{ref} for each ADN and also calculate the individual setpoints of each asset (IBRs and LTC).

The ADN operational constraints remain the same as in the flexibility determination phase (4.46)-(4.50), while the objective function to be minimized is the Euclidean distance between the reference point and the actual active and reactive power flows at the PCC. Thus, the new OPF problem is:

$$\min_{e,f,V} \sqrt{(P_{ref} - P)^2 + (Q_{ref} - Q)^2}) \tag{5.42}$$

$$\text{subject to :}$$

$$\boldsymbol{g_A}(e, f) = 0 \tag{5.43}$$

$$V_k^2 = e_k^2 + f_k^2, \forall k \in \mathcal{N}_A \tag{5.44}$$

$$V_k^{min} \leq V_k \leq V_k^{max}, \forall k \in \mathcal{N}_A \tag{5.45}$$

$$p_{gk}^2 + q_{gk}^2 \leq (V_k I_{Nk})^2, \forall k \in G_A \tag{5.46}$$

$$p_{gk}^{min} \leq p_{gk} \leq p_{gk}^{max}, \forall k \in G_A \tag{5.47}$$

$$\tag{5.48}$$

where, $\mathcal{N}_\mathcal{A}$ is the set of buses of the ADN, and G_A the subset of generator buses, (5.43) refers to the power balance equations of the ADN, (5.45) to the voltage bound constraints and (5.46)-(5.47) to the operational constraints of the IBRs.

The solution of problem (5.42)- (5.47) ensures that the ADN will reach the reference value, and if this is not achieved due to assumptions in the calculation of the FR, the consumption will move as close as possible to the reference point. The setpoints for the controllable voltages of LTC and IBRs in order to achieve these reference values are obtained solving the optimization problem (5.42)- (5.47) and are presented in Table 5.11. The results show that for this test system, the VSM is greater if the ADN is able to provide the maximum reactive power from its assets, while respecting (5.46).

Table 5.11: Optimal Setpoints for 30 Bus ADN

		Initial			Optimal		
Bus	S_{nom}	V_{set}	p_g	q_g	V_{set}	p_g	q_g
30	-	1.0000	-	-	1.0047	-	-
4	8.8	0.9961	4.0	0	1.0383	6.43	6.49
10	6.6	0.9906	3.3	0	1.0394	4.88	4.82
16	5.5	0.9873	2.0	0	1.0448	4.13	4.00
22	2.75	0.9876	2.0	0	1.0489	2.08	1.99
25	5.5	0.9861	3.0	0	1.0500	4.21	3.96

5.6.4 Quasi steady state simulation

The test system is simulated using long-term simulation with the WPSTAB software, in order to validate the results of the VSM optimization. The disturbance is a conductance load ramp at the remote bus past the maximum power transfer limit. When, voltage at the HV bus at the PCC falls below a certain value, the ADN support is activated. Similarly to the previous section 5.5.4, LTC setpoints and IBRs are activated separately. The LTC setpoint is applied immediately, while the IBR setpoints are activated with a ramp. In this case, in contrast with the previous one, active power setpoints are also activated, due to the fact that storage is also assumed. In that way, adverse results, such as temporary overvoltages at the ADN are prevented. In this case for every IBR, both voltage and active power setpoints are send in a form of ramp. In figures 5.18 and 5.19, the setpoints achieved are shown. It should be noted that compared to the optimal setpoints, small deviations may exist, mainly due to the discreet dynamics of the LTC.

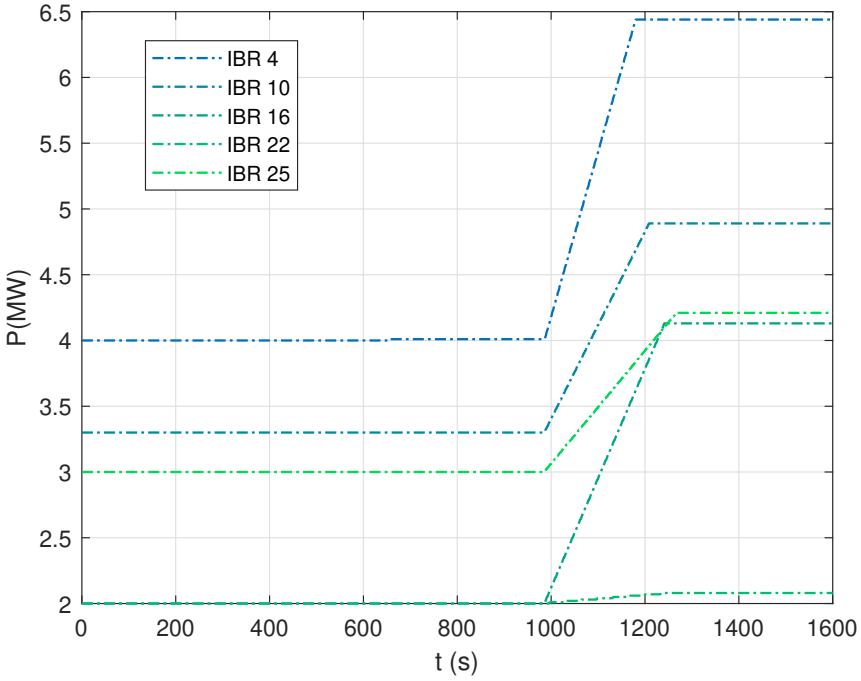

Figure 5.18: Active power of IBRs in the ADN

The resulting remote load PV curve is presented in Fig. 5.20, with and without implementing the optimal setpoints already shown in Table 5.11. The maximum loading points as shown in this figure are $C = 113.4MW$ and $C_{opt} = 123.2MW$, which are very close to the VSM solution reported in Table 5.10. While the increase in the VSM is rather small (about 11 MW), compared to the total capacity of the IBRs in the distribution feeder (29.15 MVA) it amounts to about 38 %, which is a signigicant percentage of the installed IBR capacity.

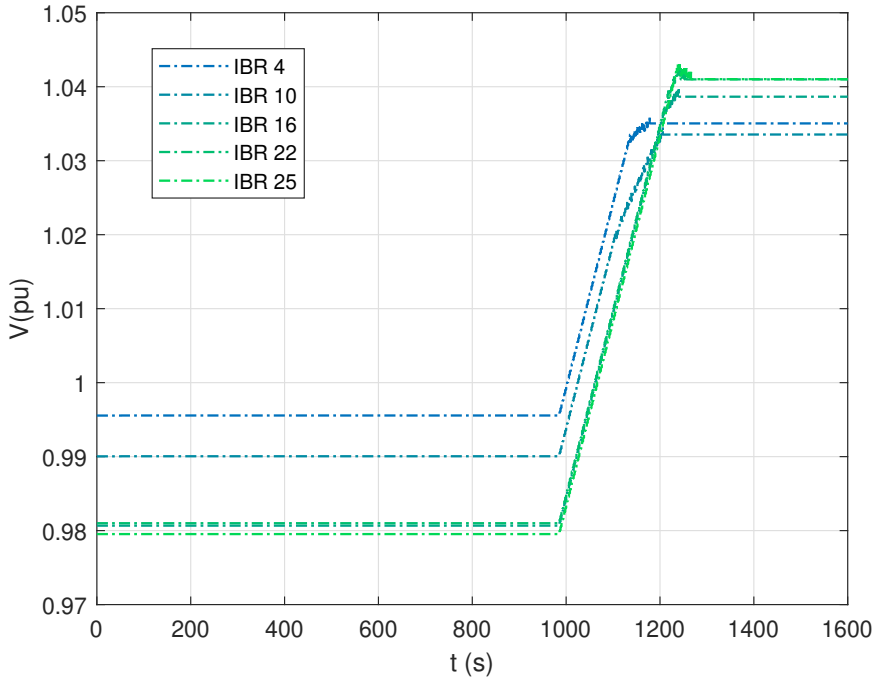

Figure 5.19: Voltage Setpoint of IBRs in the ADN

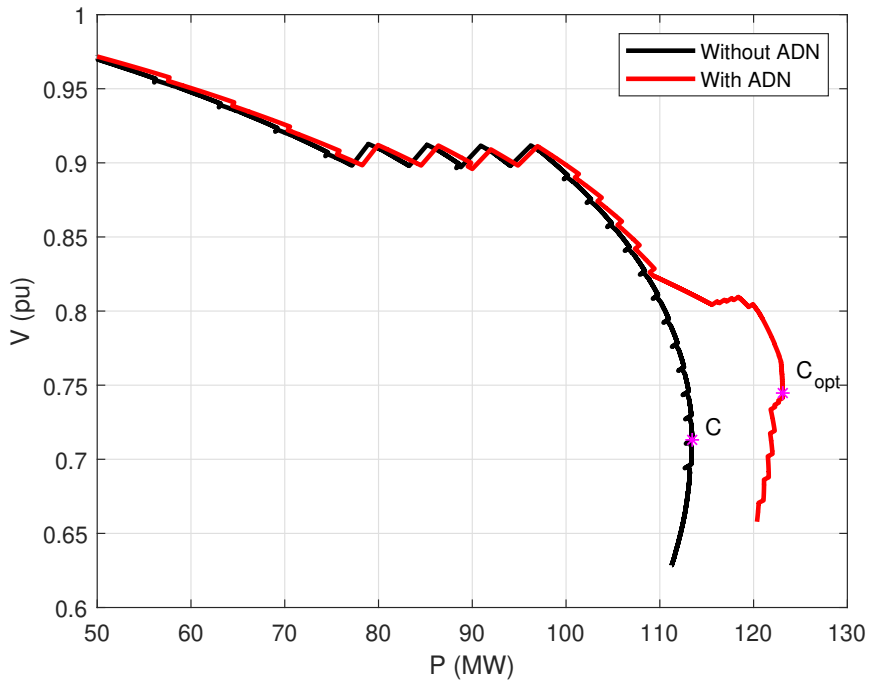

Figure 5.20: PV curve for remote load bus with and without ADN support

Chapter 6

A fast method to approximate the Flexibility Region

6.1 Need for fast FR radial scan

In the previous section we introduced a preventive approach to maximize the VSM using ADNs (Section 5.4). The outline of this approach is also repeated here in Fig. 6.1. The ADN operator is responsible to calculate its FR and send it to the central controller in regular time intervals (depending on the TSO required services). To facilitate the optimization process of the central controller, the FR is provided in the form of a polygon (linear constraints) around the current operating point.

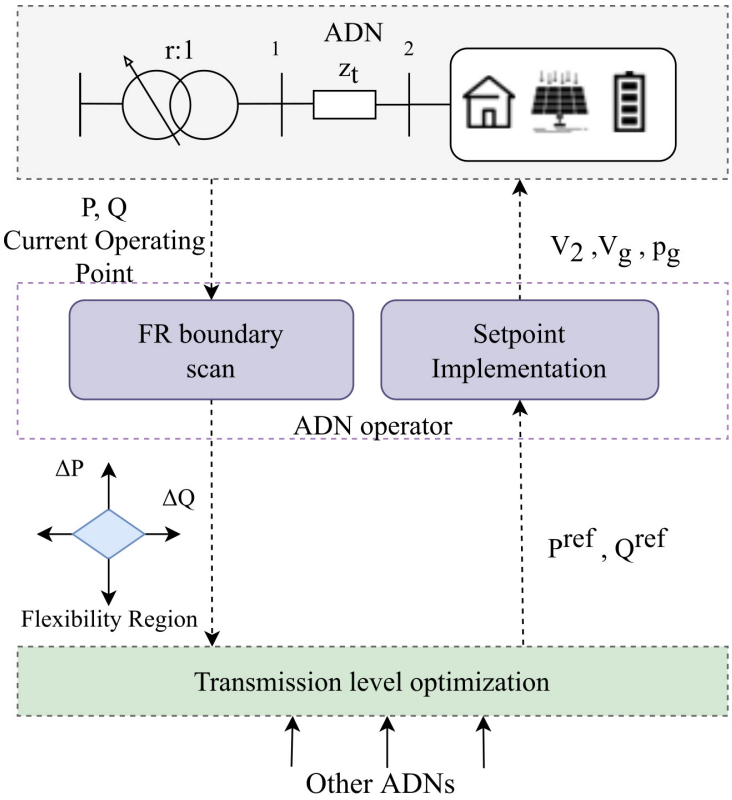

Figure 6.1: Complete conceptual framework

The central controller gathers the FR from each ADN, solves an optimization problem at the transmission level, and sends back P^{ref}, Q^{ref} reference values to each ADN, aiming in the secure operation of the whole system. The ADN operator will control the setpoints of its controllable devices accordingly to regulate the P and Q consumption to achieve the requested setpoints within its FR. The objectives of the transmission level optimization may vary depending on the application (active/reactive power support in normal or emergency emergency conditions).

A key element is that the FR of each ADN needs to be calculated using an OPF as explained in Chapter 4, section 4.3.5. This has to be performed periodically, as the operating point changes during the day. The computed FR should also be relatively recent when used by the central controller to optimize the VSM. More specifically, the optimization problem (4.44)-(4.50) is non-linear and non-convex, while the radial boundary scan requires it to be solved multiple times. Non-convex solvers are typically slow and do not scale well when the number of decision variables increase, i.e., longer and more complex feeders may hinder this approach. In that regard, for a reasonable period of around 5 minutes, the complete scan with e.g. 120 points to be calculated, will require significant computation time, making periodic cycling problematic.

This introduces the need for a fast FR calculation, even if approximate. The usefulness of the flexibility region is not limited to the above application of VSM maximization, as it can be used also in different applications, such as frequency or voltage regulation and support in non-voltage stability constrained systems.

As a solution, in this chapter, a convex relaxation of the power flow constraints based on SOCP formulation first used in [71] is utilized as basis for the FR determination. This decreases significantly the computation time while offering accurate solutions.

6.2 Second Order Cone OPF Relaxation

6.2.1 Introduction to SOC programming

Different relaxation methods have been proposed in the literature. One of them is the use of second order cone programming (SOCP) in order to relax the power balance equations of the power flow. The SOCP relaxation turns the OPF problem into convex, also guarantying a global optimum for the solution, under some conditions. Most importantly, it requires much less time than the non-linear solvers, so it is possible to use it to determine the FR periodically, in limited time. Last but not least, it has very good scalability, as it can solve for complex feeders with multiple decision variables with no exponential increase in the computation time.

The SOCP relaxation of the OPF problem involves using Second Order Cone Programming techniques to reformulate the original non-convex OPF problem into a convex optimization problem. In this formulation, various non-convex constraints (like the power flow equations, voltage limits, and reactive power limits) are approximated using second-order cones, which are convex sets. This allows for efficient solution methods to be applied. The advantage of using SOCP relaxation in OPF is that it provides a computationally tractable approach to solve power system optimization problems. It ensures that a globally optimal solution can be found, though it might not be exactly the same as the solution of the original non-convex problem. Keep in mind that the effectiveness of the SOCP re-

laxation for OPF depends on the specific characteristics of the system being studied, and different variants and extensions of SOCP formulations may be used in practice to address specific nuances of the problem.

6.2.2 Non-Linear OPF formulation

First, the non-linear OPF is rewritten similarly to (4.44)-(4.50), introduced in Chapter 4. Then, based on this formulation the SOCP problem will be formulated. In Chapter 4, an objective function ζ was used, where:

$$\zeta = a\Delta P + b\Delta Q \tag{6.1}$$

for $a = \pm 1$ and $b = 0$.

In this chapter, for more convenience in the SOCP formulation that will be presented later, we assume vector $\boldsymbol{C}$, where $C_i, i \in \mathcal{N}$ corresponds to the cost of generation p_{gi}. It should be noted that P, Q consumptions at the PCC are considered as generation at bus 1 (which belongs in $\mathcal{N}$), as shown in Fig. 6.1. Thus:

$$p_{g1} = P \tag{6.2}$$
$$q_{g1} = Q \tag{6.3}$$
$$p_{d1} = 0 \tag{6.4}$$
$$q_{d1} = 0 \tag{6.5}$$

Let $\mathcal{N}$ be set of buses and L the set of lines. As a result, for $C_1 = \pm 1$ the OPF formulation below for a FR boundary point along a fixed search direction θ is equivalent to (4.44)-(4.50):

$$\min_{\boldsymbol{e},\boldsymbol{f},\boldsymbol{p_g},\boldsymbol{q_g}} \quad C_1 P \tag{6.6}$$

subject to:

$$\Delta Q = tan\theta \Delta P \tag{6.7}$$

$$\begin{aligned} p_{ij} = (e_i^2 + f_i^2)g_{ij} - (e_i e_j + f_i f_j)g_{ij} + \\ (e_i f_j - e_j f_i)b_{ij}, \quad \forall (i,j) \in L \end{aligned} \tag{6.8}$$

$$\begin{aligned} q_{ij} = -(e_i^2 + f_i^2)(b_{ij} + b_{sij}) + (e_i e_j + f_i f_j)b_{ij} + \\ (e_i f_j - e_j f_i)g_{ij}, \quad \forall (i,j) \in L \end{aligned} \tag{6.9}$$

$$p_{gi} - p_{di} = g_{si}(e_i^2 + f_i^2) + \sum_{j \in \delta(i)} p_{ij}, \quad \forall i \in \mathcal{N} \tag{6.10}$$

$$q_{gi} - q_{di} = -b_{si}(e_i^2 + f_i^2) + \sum_{j \in \delta(i)} q_{ij}, \quad \forall i \in \mathcal{N} \tag{6.11}$$

$$V_i^2 = e_i^2 + f_i^2, \quad \forall i \in \mathcal{N} \tag{6.12}$$

$$V_i^{min} \leq V_i \leq V_i^{max}, \quad \forall i \in \mathcal{N} \tag{6.13}$$

$$p_{gi}^{min} \leq p_{gi} \leq p_{gi}^{max}, \quad \forall i \in \mathcal{G} \tag{6.14}$$

$$p_{gi}^2 + q_{gi}^2 \leq (V_i i_i^{lim})^2, \quad \forall i \in \mathcal{G} \tag{6.15}$$

$$p_{ij}^2 + q_{ij}^2 \leq (S_{ij}^{lim})^2, \quad \forall (i,j) \in L \tag{6.16}$$

where (6.8), (6.9) represent the flow equations in every line of the system, g_{ij},b_{ij} are the line series admittance and susceptance respectively and b_{sij} is one half of the line charging susceptance. This should not be confused with the previous representations of the use of the columns of the admittance matrix, in previous chapters. As a result, (6.10), (6.11) represent the power balance equations at each bus i where $\delta(i)$ denotes the set of buses j connected to bus i and g_{si}, b_{si} represent the shunts connected to bus i. Accordingly, p_{gi} and q_{gi} are the active and reactive power generations at each bus while p_{di} and q_{di} correspond to the loads. The loads are modeled using the following voltage depended models:

$$p_{di} = p_{di}^0(\frac{V_i}{V_i^0})^a, \quad q_{di} = q_{di}^0(\frac{V_i}{V_i^0})^b \quad \forall i \in \mathcal{N} \tag{6.17}$$

In the examples of this chapter active load is considered as constant current with $a = 1$ and reactive load as constant admittance with $b = 2$.

Equation (6.7) defines the search direction for the boundary points. Voltage limits are presented in (6.13) for each bus i. Finally, the inequality constraints (6.14) and (6.15) correspond to the limits of the IBRs, referring to the active power generation limitations and the current constraints respectively. It should be noted that (6.14) is only relevant if the IBRs can regulate their active power e.g. by employing BESS. Branch flow constraints are also checked by (6.16), which guarantees that limits S_{ij}^{lim} are respected.

The LTC in Fig. 6.1 is not explicitly represented and the effect of its deadband is neglected in the OPF formulation. The regulated voltage V_2 of the secondary side of the HV/MV transformer, as seen in Fig. 6.1, is one of the variables. Consumptions P, Q are calculated at bus 1 downstream of the ideal transformer (Fig.6.1) to include reactive losses on the leakage impedance of the transformer z_t. For the decision variable V_2, equation (6.13) defines its limits together with those of other ADN buses. This assumption is plausible as long as the LTC tap range is not exhausted, so that it can regulate the distribution side voltage close to its setpoint, as is assumed in this Chapter.

6.2.3 SOCP OPF formulation

As in the previous formulation, for the first node of the ADN, $P = p_{g1}$ and $Q = q_{g1}$. The non-convexity and non-linearity of the problem is attributed to (6.10) and (6.11), and more specifically terms:

$$e_i^2 + f_i^2 = V_i^2 \tag{6.18}$$

$$e_i e_j + f_i f_j = |V_i||V_j|cos(\theta_i - \theta_j) \tag{6.19}$$

$$e_i f_j - e_j f_i = -|V_i||V_j|sin(\theta_i - \theta_j) \tag{6.20}$$

To deal with the non-convexity and non-linearity, the decision variables c_{ii}, c_{ij} and s_{ij} are introduced as follows:

$$c_{ii} = e_i^2 + f_i^2, \quad i \in \mathcal{N} \tag{6.21}$$

$$c_{ij} = e_i e_j + f_i f_j, \quad i \in \mathcal{N} \tag{6.22}$$

$$s_{ij} = e_i f_j - e_j f_i, \quad i \in \mathcal{N} \tag{6.23}$$

$$\tag{6.24}$$

These new variables satisfy the relation:

$$c_{ij}^2 + s_{ij}^2 = c_{ii}c_{jj} \tag{6.25}$$

The general SOCP formulation that minimizes the active power generation cost is defined as folows:

$$\min_{\boldsymbol{c},\boldsymbol{s},\boldsymbol{p_g},\boldsymbol{q_g}} \quad \sum_{i\in G} C_i p_{gi} \tag{6.26}$$

subject to

$$p_{ij} = c_{ii}g_{ij} - c_{ij}g_{ij} + s_{ij}b_{ij}, \quad (i,j) \in L \tag{6.27}$$

$$q_{ij} = -c_{ii}(b_{sij} + b_{ij}) + c_{ij}b_{ij} + s_{ij}g_{ij}, \quad (i,j) \in L \tag{6.28}$$

$$p_{gi} - p_{di} = g_{si}c_{ii} + \sum_{j\in\delta(i)} p_{ij} \quad i \in \mathcal{N} \tag{6.29}$$

$$q_{gi} - q_{di} = -b_{si}c_{ii} + \sum_{j\in\delta(i)} q_{ij} \quad i \in \mathcal{N} \tag{6.30}$$

$$c_{ii}^{min} \leq c_{ii} \leq c_{ii}^{max} \quad i \in \mathcal{N} \tag{6.31}$$

$$p_{gi}^{min} \leq p_{gi} \leq p_{gi}^{max} \quad i \in \mathcal{N} \tag{6.32}$$

$$p_{gi}^2 + q_{gi}^2 \leq c_{ii}(i_i^{lim})^2 \quad i \in \mathcal{N} \tag{6.33}$$

$$c_{ij} = c_{ji}, \quad s_{ij} = -s_{ji} \quad (i,j) \in L \tag{6.34}$$

$$c_{ij}^2 + s_{ij}^2 \leq c_{ii}c_{jj} \quad (i,j) \in L \tag{6.35}$$

$$p_{ij}^2 + q_{ij}^2 \leq (S_{ij}^{lim})^2 \quad (i,j) \in L \tag{6.36}$$

where (6.27), (6.28) refer to the branch flow equations, (6.29) and (6.30) refer to the active and reactive power balance at each bus. The voltage and power generation limits are represented by (6.31) and (6.32), respectively. The current limit of the IBRs is forced by (6.33) and the line thermal limits are ensured by (6.36), where S_{ij}^{lim} is the flow limit of the line.

Turning (6.25) from equality to inequality constraint (6.35) is what essentially turns the problem into the SOC programming formulation and the relaxed version of the formulation of subsection 6.2.2. As a result, the problems are equivalent only if all the second-order cone constraints (6.35) hold as equalities. Only then the solution of the SOCP formulation will correspond to a real solution of the AC power flow problem.

In accordance with (6.17) reactive power load is modelled as constant impedance. For active power load, half is modelled as constant power and half as constant impedance in order to maintain convexity of the SOCP and approximate (6.17) adequately. Formulation is as follows:

$$p_{di} = \frac{1}{2}p_{di}^0\frac{c_{ii}}{c_{ii}^0} + \frac{1}{2}p_{di}^0 \tag{6.37}$$

$$q_{di} = q_{di}^0\frac{c_{ii}}{c_{ii}^0} \tag{6.38}$$

It is noted that (6.37) and (6.38) results in problems of subsection 6.2.2 and subsection 6.2.3, not being completely identical, but very close.

6.3 Modified formulation and radial boundary scan

In this section, the FR boundary is calculated with the SOCP OPF formulation. Similarly to the formulation (6.6)-(6.15), to calculate the FR boundary at the space of negative consumption, the optimization problem (6.6)-(6.7), (6.29)-(6.35) is solved for $C_1 = 1$ and at the space of positive consumption, by changing the objective function (6.6) parameter to $C_1 = -1$ and different values of θ.

However, the calculation of the FR boundary for some angles, belonging either in the space of negative or positive consumption, is not accurate as the SOCP formulation is not providing exact solutions. This can be observed in Figures 6.2 and 6.3, for the test distribution feeder of 30 buses and 99 buses respectively the flexibility region of which was also presented in Fig. 4.17 and 4.19.

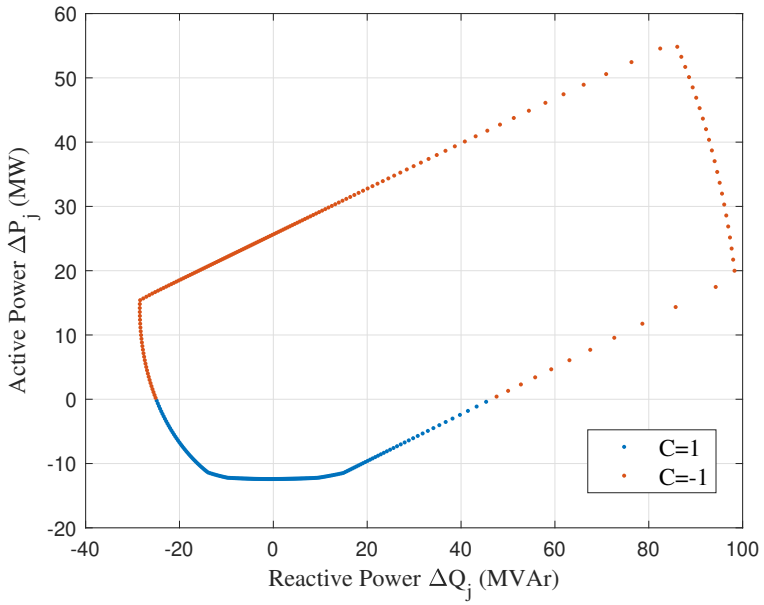

Figure 6.2: Flexibility Region of 30-bus ADN using original formulation and SOCP

When compared to the original NLP formulation, it is observed that the SOCP formulation provides a wider region but the points that form this region are not providing exact solutions, meaning that they do not represent feasible solution of the AC power flow problem. It is interesting that this only occurs for specific angles. To better showcase the problem, in Figures 6.4 and 6.5, FRs are presented using both SOCP and NLP formulation.

Therefore, to obtain the best approximation of the FR boundary points and tackle the exactness problem for the angle steps, as presented in the previous figures, an alternative approach is devised. The proposed problem is solved for two types of objective functions for each fixed angle θ:

$$\min_{\boldsymbol{c,s,p_g,q_g}} \quad C_1 P + \sum_{i \in G, i \neq 1} C_i p_{gi} \tag{6.39}$$

$$\min_{\boldsymbol{c,s,p_g,q_g}} \quad C_1 Q + \sum_{i \in G, i \neq 1} C_i q_{gi} \tag{6.40}$$

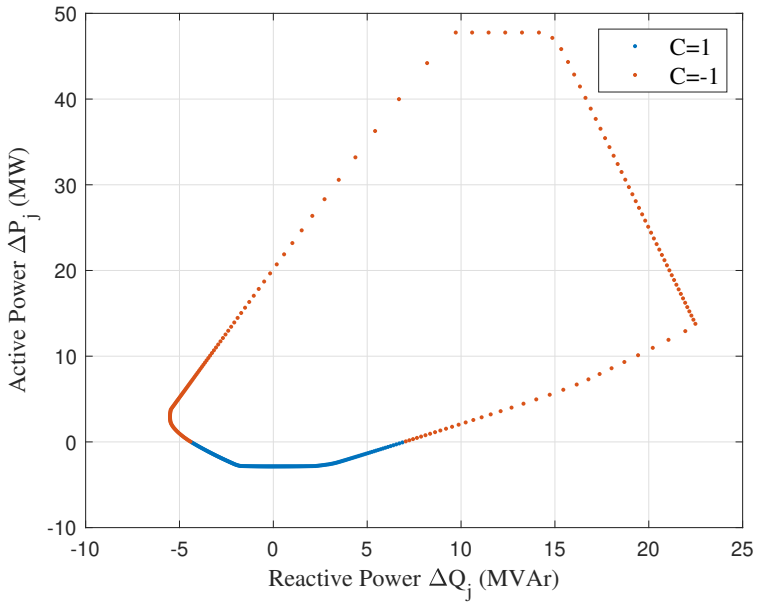

Figure 6.3: Flexibility Region of 99-bus ADN using original formulation and SOCP

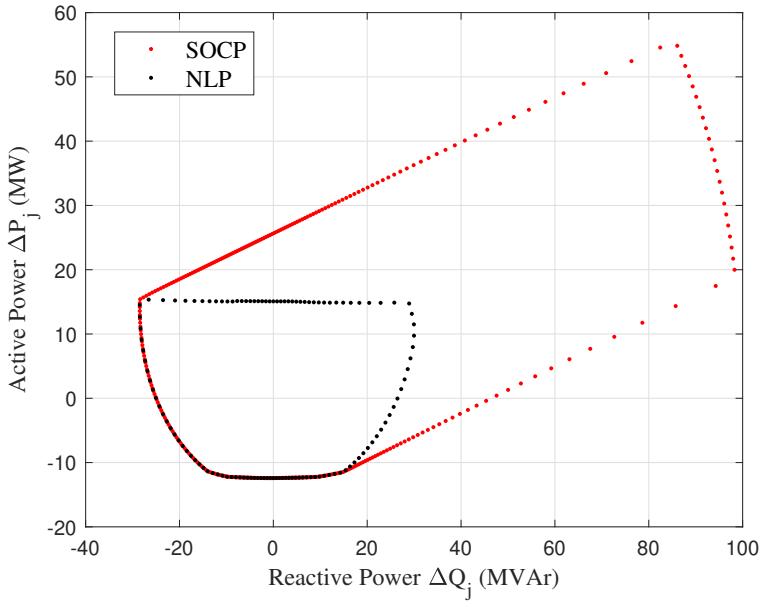

Figure 6.4: Flexibility Region of 30-bus ADN, SOCP vs NLP

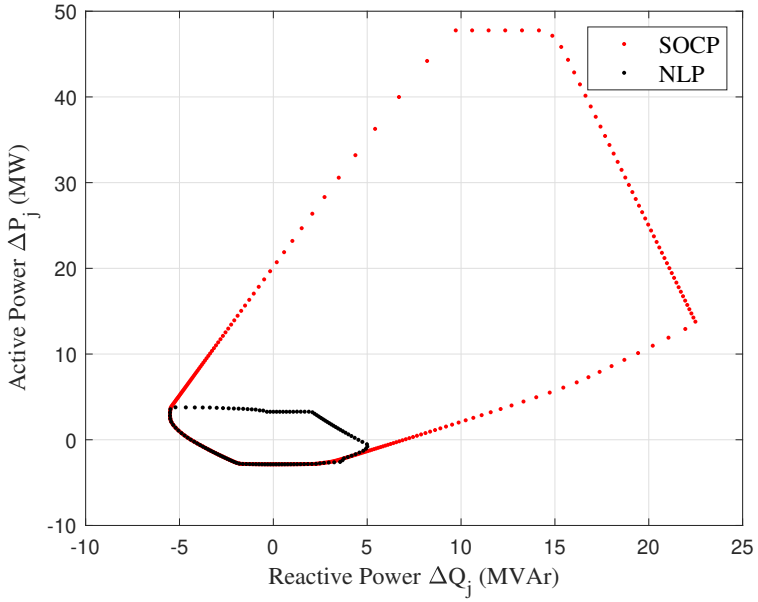

Figure 6.5: Flexibility Region of 99-bus ADN, SOCP vs NLP

subject to constraints (6.7), (6.29)-(6.35). The problem with objective function (6.39) is solved two times; once with cost parameters that $C_1 \ll C_i$ towards maximization of P, and once with cost parameters $C_1 \gg C_i$ towards minimization of P, for each $\theta \in [0°, 180°]$, ensuring the search towards a maximum and minimum P given the power balance. The problem with objective function (6.40) is solved two times; once with cost parameters that $C_1 \ll C_i$ towards maximization of Q, and once with cost parameters $C_1 \gg C_i$ towards minimization of Q for $\theta \in [0°, 180°]$.

As a result, for every fixed θ, four separate problems corresponding to the objective functions (6.39) and (6.40) are solved providing four solutions for P and Q. For each test feeder the solution points of each objective function solved for each $\theta \in [0°, 180°]$ are shown in Figures 6.6 and 6.7. It can be observed that each objective function provides a sub-region of the whole flexibility region. As a result, solution points from each sub-region need to be combined to form the total FR of the ADN.

It is obvious that depending on the relationship between C_1 and C_i, the sub regions may vary. Of course, using a high analogy between them will result in greater sub-regions, but there is the possibility of resulting in non-exact results, as explained and shown in the previous figures. For that reason, different combinations of C_1 and C_i are used to define a good approximation of the FR.

Since for each angle step, multiple points may occur, due to the multiple objectives, between the solution points, the ones further away from the current operating point are kept, meaning a total of 2 points for every search direction.

Finally, it is noted that all solutions of the SOCP problem are checked for feasibility. The points that are non-exact are discarded and not used in the final FR.

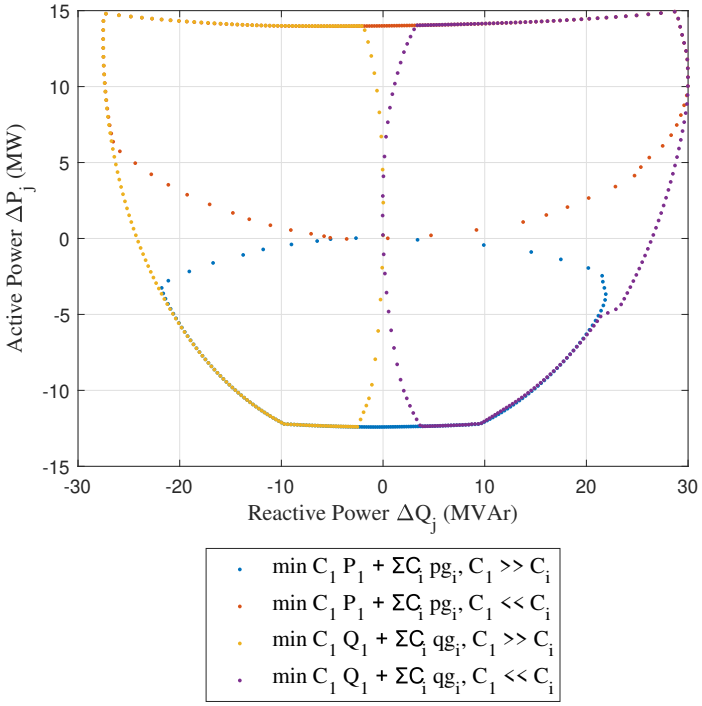

Figure 6.6: Solution points of 4 objective functions for 30 bus ADN

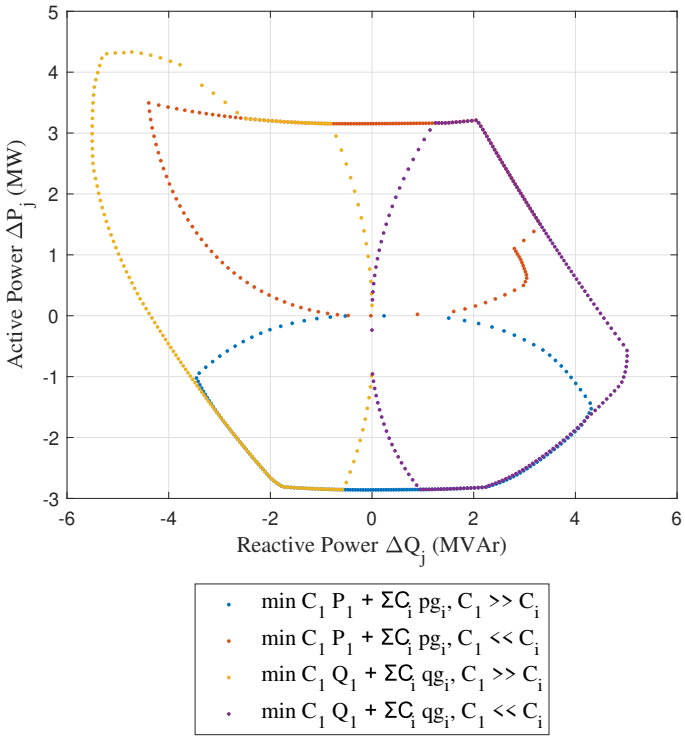

Figure 6.7: Solution points of 4 objective functions for 99 bus ADN

6.3.1 FR calculation

In all cases the angle step considered is $\Delta\theta = 3^o$ resulting in 120 FR boundary points. Both NLP and SOCP problems are solved using MATLAB [53], where for the non-convex problem, the *fmincon* function is used with a sequential quadratic solver (sqp). The SOCP problem is formulated with the Yalmip interface for MATLAB [72], using the Gurobi solver [73]. All problems are solved with a PC with the following specifications: a GPU Core i9, 3.8 GHz and 16 GB RAM.

The resulting FRs are presented in Fig. 6.8 for the 30-bus, and in Fig. 6.9 for the 99-bus feeder, for the SOCP and the NLP radial boundary scan. It is observed that for both test feeders the SOCP formulation with the radial boundary scan is very close to the one calculated using the NLP, with only slight differences, mostly close to maximum ΔP. This is expected, since the objective function is not identical in the two methods for the positive consuption space. It is noted that the branch flow constraints (6.16) or (6.36) were not violated in the test systems in any of the cases. The most significant difference lies in the objective function. This can be observed mainly in the upper part of the graphs, which corresponds to the maximization of the active power consumption at the PCC.

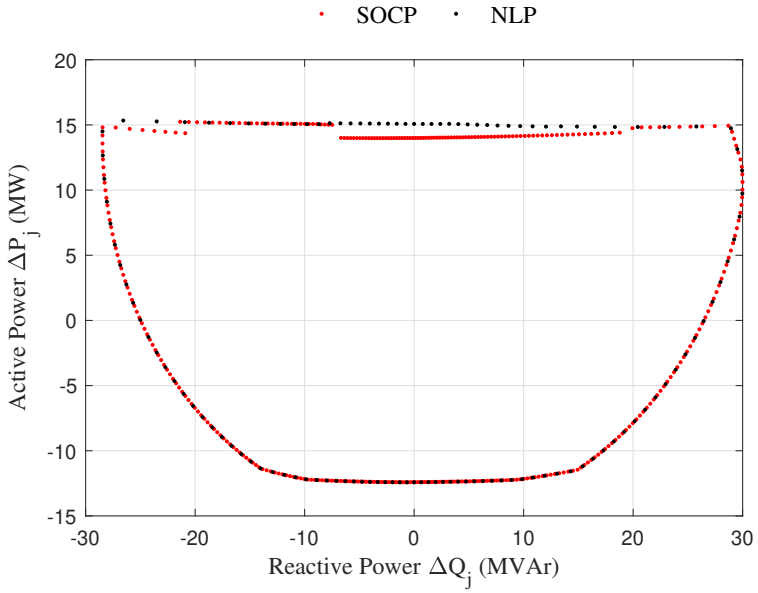

Figure 6.8: Flexibility Region of 30-bus ADN

In Table 6.1 the execution time is presented for the calculation of the FR, using the NLP and the SOCP problem formulation. It is obvious that the SOCP can decrease the computation time significantly, by 27 to 74 times. Moreover, it can be observed that the non-linear solver does not scale well in terms of computation time, with longer and more complex networks, which is not the case with the convex relaxation. Yalmip time for the formulation of the constraints, is included in the execution time.

In Figures 6.11 and 6.12, the polygon FR approximations of subsection 4.4 with a number of 6 vertices are shown for each network. As expected SOCP formulation gives in both cases very similar results to those obtained with the NLP, even though they are not exactly identical. As a result, the 6 inequality constraints for the system optimization problem are close to the NLP solutions.

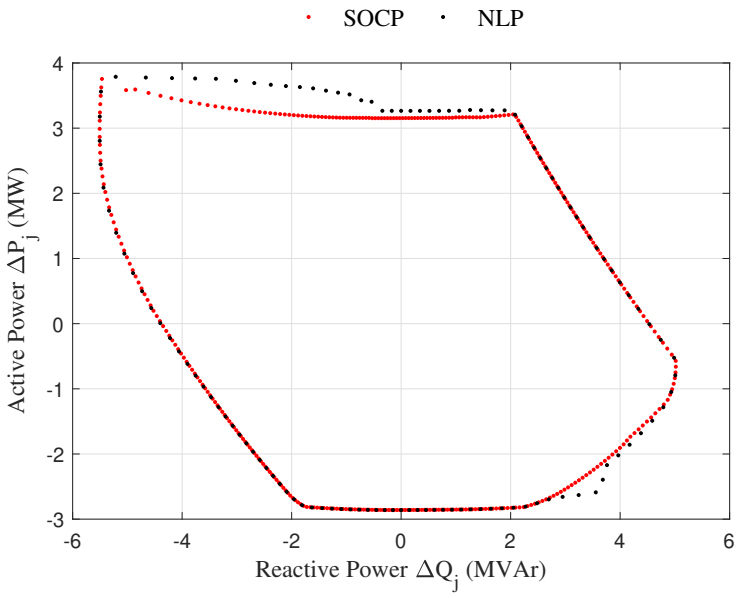

Figure 6.9: Flexibility Region of 99-bus ADN

Table 6.1: Execution time of each formulation for the test feeders

ADN	**Execution Time (s)**		acceleration factor
	NLP	SOCP	
30-bus	175.12	6.49	27
99-bus	914.18	12.24	74.7

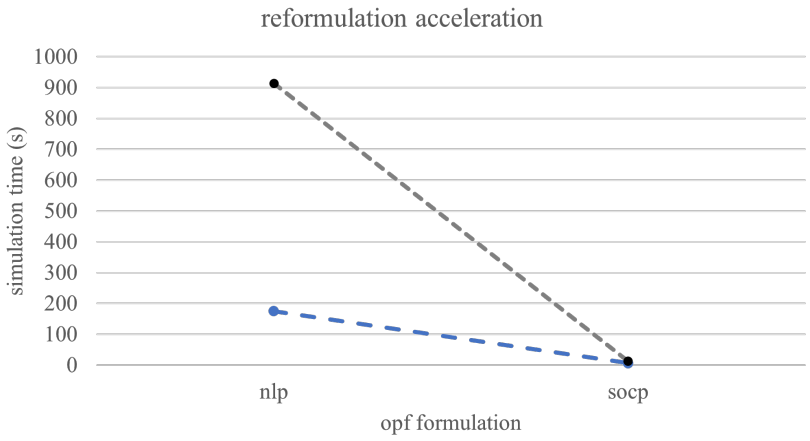

Figure 6.10: Execution time for each formulation and feeder

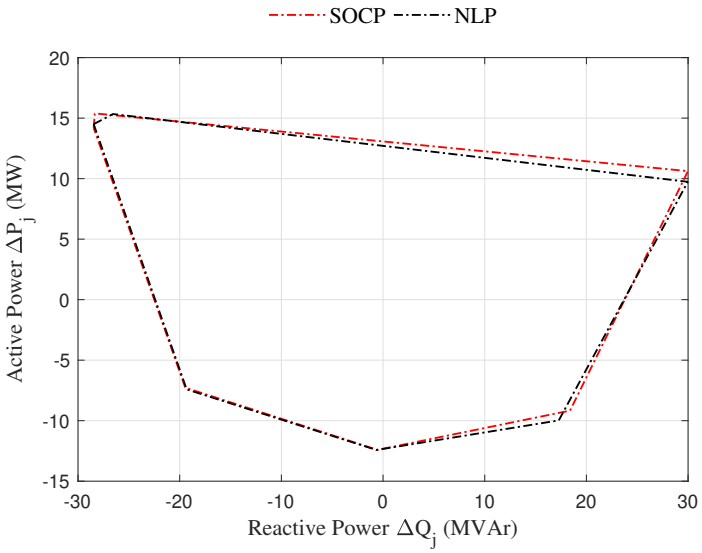

Figure 6.11: FR Polygon approximation of 30-bus, SOCP vs NLP

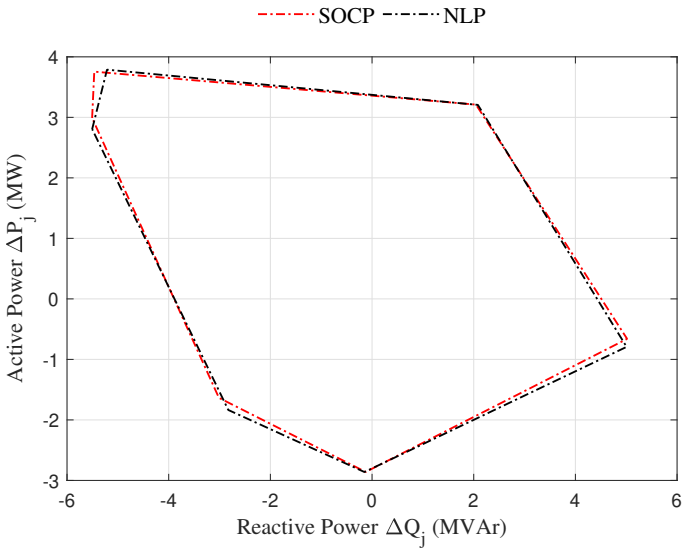

Figure 6.12: FR Polygon approximation of 99-bus, SOCP vs NLP

As presented also in Figures 6.13 and 6.14, the FR using the SOCP formulation can be approximated for different operation constraints for the decision variables. In these figures for example, the different FRs for normal and emergency needs (Section 4.3.8 from the transmission system are presented.

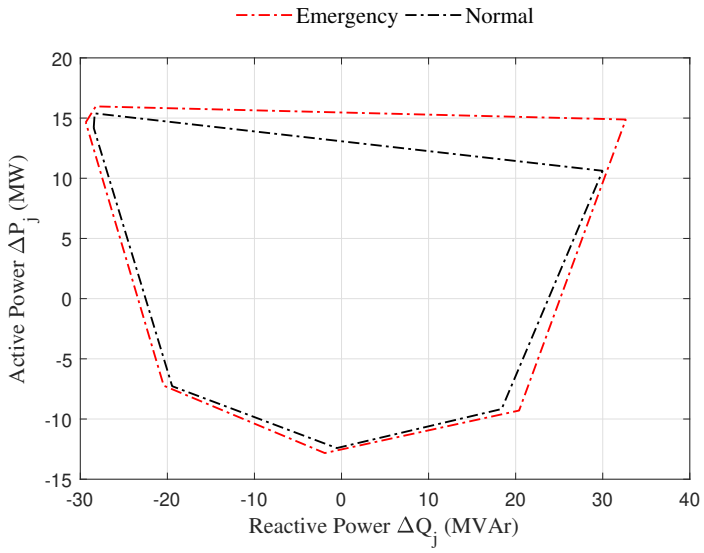

Figure 6.13: FR Polygon approximation of 30-bus for different operational constraints

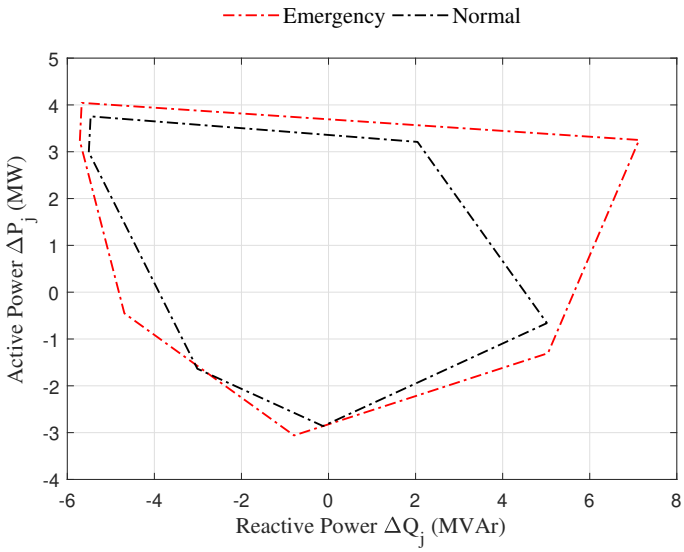

Figure 6.14: FR Polygon approximation of 30-bus for different operational constraints

In conclusion, a fast method to approximate the flexibility region of an Active Distribution Network in the PQ space at its point of common coupling with the transmission grid is proposed. The method is solving a set of optimization problems using multiple search directions of fixed P/Q (defined as radial boundary scan), to find boundary points of the flexibility region. In chapter, the second-order cone constraint relaxation of the corresponding power flow constraints is utilized, dealing with the limitations of the non-convex formulation, such as large computation time and can provide global optimallity guarantees when exact.

Results, on two different test feeders, containing multiple decision variables, show that the proposed SOCP-based formulation achieves a very good approximation of the FR significantly faster that the NLP formulation, as presented in Table 6.1 and Fig. 6.10. The polygon approximation of the FR deducted from the boundary points is also very similar when computed by either method.

Finally, to calculate the ADN setpoints that would enable the PCC power to follow the reference P, Q values sent by the transmission level, and also address the uncertainty due to the time delay between the determination of the FR and the reception of reference values, a final optimization step to minimize the distance between reference and actual consumption is included in the overall framework as already presented and implemented in Section 5.6.3.

Implementation of faster methods, such as the SOCP relaxation, can make it possible to consider uncertainty and in general, scenario-based approaches that introduce great computational limitations.

Chapter 7

Hellenic Interconnected System Implementation

7.1 Overview of the Greek Power System

7.1.1 System Description

The Hellenic Interconnected System (HIS) is a transmission system consisting of mainland Greece and interconnected islands, including 150kV and 400kV transmission lines and cables. It is interconnected to the synchronous European Area with six AC 400kV overhead lines, located in the Northern area of the system, one AC 150kV overhead line and a 400kV HVDC cable to Italy. Moreover, it is split in two different bidding zones, the island of Crete and mainland Greece grid, which are connected with two AC 150kV cable and act as different load-frequency control (LFC) areas. Sole responsible for the operation and maintenance of the Hellenic Interconnected Power system is the Independent Transmission System Operator (IPTO) or ADMIE.

The one-line geographical diagram of the Greek Power System is presented in Figure 7.1, taken from the Ten-Year Network Development Plan (TYNDP), published in IPTO's website [74].

The Hellenic Interconnected Power System has several attributes that make it interesting. All the interconnections are located in the northern area of the System, while majority of load consumption is in the southern part of the country. Moreover, due to the decommissioning of lignite Power Plants, the greatest share of generation is located in Central and Southern Greece. Moreover, Renewable Energy Sources are continuously increasing, as is observed in Figure 7.2, for some days even covering the 100% of the load demand in the HIS.

The HIS consists of approximately 641 150kV buses, 181 400kV buses and 644 branches, consisting of 150 and 400kV overhead lines and underground or submarine cables. Moreover, there are about 63 400/150kV auto-transformers. The generation share is distributed among coal power plants, gas stations, hydroelectric power plants and a high share of RES.

As also mentioned in Chapter 3, the increase in power provided by RES and the subsequent retirement of traditional thermal generating units leads to a lack of ancillary services provided in the system. For that reason it is of interest to study in a real-power system the

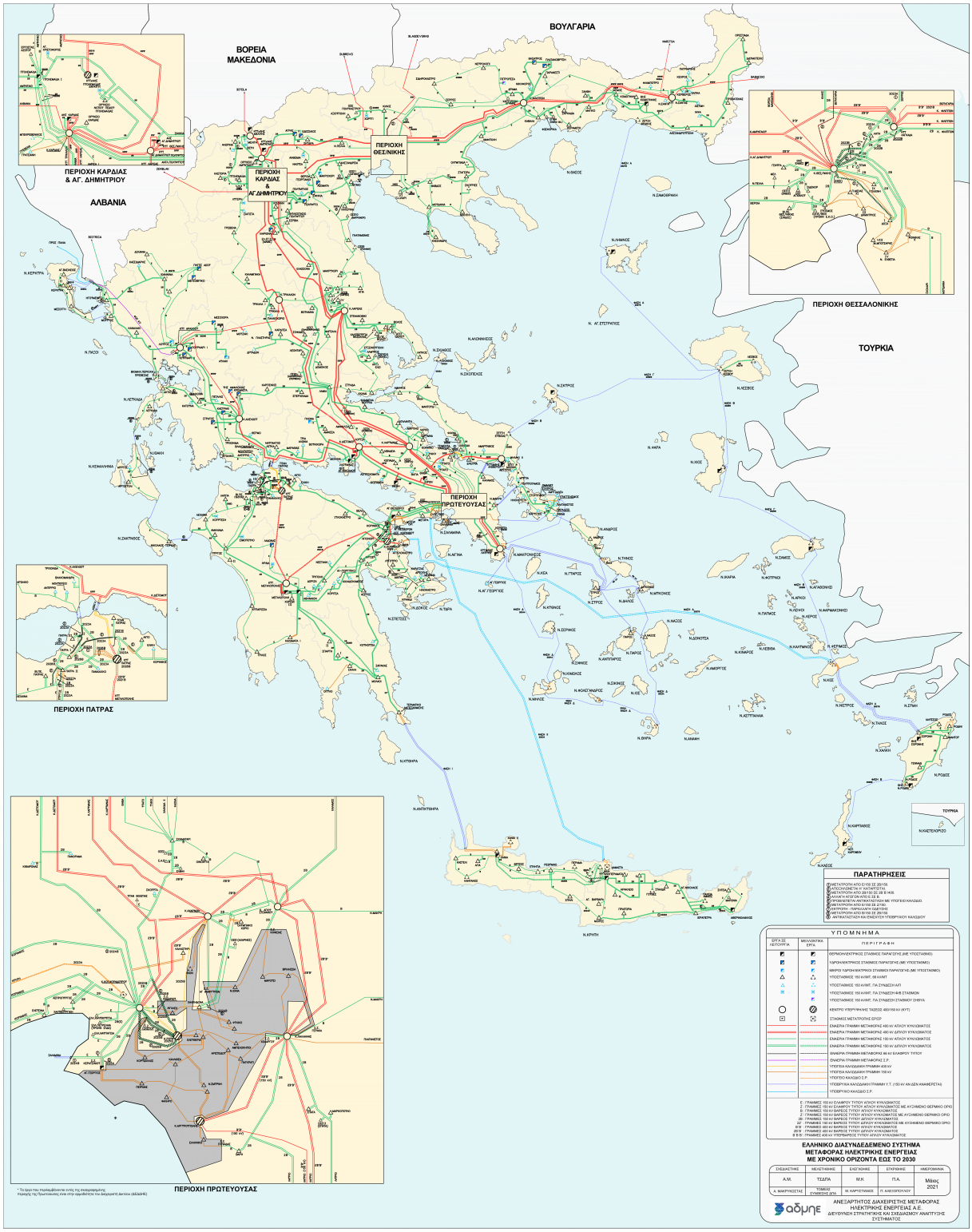

Figure 7.1: One line Diagram of Hellenic Interconnected Power System

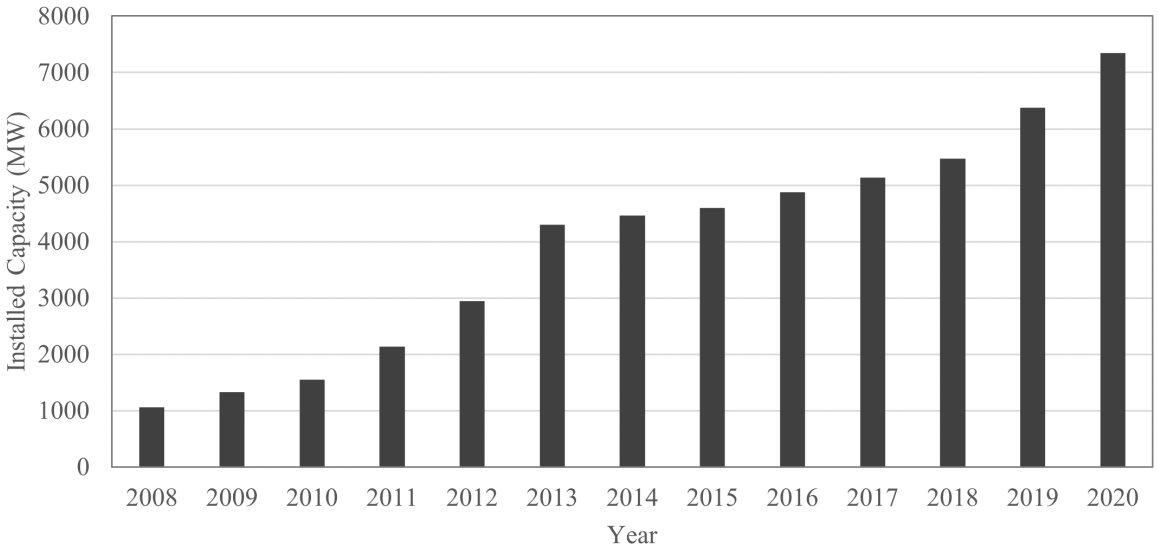

Figure 7.2: RES Installed Capacity in the HIS

voltage stability margins. Another current problem, tied with the increase of generation in the distribution network, is the rising of over-voltages especially during low loading conditions.

Several specific snapshots of the Greek Power system will be studied in this chapter, in terms of voltage security margins, for actual and contingency scenarios.

7.1.2 System Representation

The snapshots of the Greek Power System are taken from the Energy Management System (EMS) after the solution of the state estimation. State estimation is performed every five minutes and snapshots are taken every hour. The snapshots contain all the Greek 150kV and 400kV buses and branches and the observability area of the neighboring TSOs, meaning that several buses and plants from neighboring countries are also included. For each snapshot, two files are exported, a *full* and a *reduced* file.

The *full* snapshot contains the 150/20kV step-down transformers and the aggregate load is located on the 20kV bus, for all distribution transformers. Also, for synchronous generators, the step-up transformers are included and the generation is placed on the medium voltage side along with the auxiliary loads. Finally, 3-winding auto-transformers are represented as follows: a fictitious 400kV bus is created and three 2-winding transformers are placed, one 400/400kV, one 400/150kV, and a 400/30kV where usually a shunt reactor is placed.

The *reduced* snapshot consists only of 150kV and 400kV buses. Loads are moved to the high voltage buses and generation is considered also in the high voltage as net generation (minus the auxiliary loads). Similarly, in reduced files, the 3-winding auto-transformers are represented as two 2-winding transformers, and the shunt reactor is considered in the 400kV fictitious bus. In this chapter, *full* snapshots are used in the qss simulations, while *reduced* snapshot are used for the optimization problem formulation.

System-connected RES are considered as PV buses, with constant reactive power genera-

tion, $q_g = q_{min} = q_{max}$, so essentially when reactive power limits are enforced in the load flow, they are turned to PQ buses.

Full and *reduced* snapshots must provide the same (or very similar) power flow solution. Measurements and state estimation solutions might sometimes differ slightly, thus there is always the need for data quality checks and data cleaning. In this respect, several corrections are made in the Greek snapshot to ensure the feasibility of the initialization. The following checks are mandatory:

- Active power generation is checked against the maximum value, so that $p_g^{meas} \leq p_g^{max}$. In case this is violated in the snapshot, then the constraint limit is relaxed to $p_g^{max} = p_g^{meas}$.
- Stator current limits are checked at the initial point of the snapshot. Again, if they are violated, then the limits are relaxed.
- Branch flow limits are also checked at the initial point. Similarly, limits are relaxed if there is a violation.

The formulation presented in Chapter 2 for the VSM optimization, (2.41)-(2.47) is used also in the Greek Power System. In this case, the objective function refers to the maximization of the stress λ in the direction defined by the vector d_{pk}:

$$\zeta = -\Delta P = -\lambda \sum_{k \in \mathcal{N}} d_{pk} \tag{7.1}$$

Specifically, for this case the stress direction d_{pk} is only non-zero in the buses k of the Ionian corridor, meaning that the load shift only refers to the area load. As a result, the VSM corresponds to the margin of the specific area load. Even though a specific corridor is considered in this Chapter, the OPF software developed represents the whole HIS and can be used for studying various other potentially stressed areas, such as Attica or Crete.

The distributed slack approach (2.43) is used, for the active power generation shift, to follow the shift of the load (and losses). In the participation vector $\boldsymbol{K}$, only gas power stations and hydroelectric power plants are included. Also, the slack bus which is the interconnection with Turkey is also included in the distributed slack approach. Different factors are used for hydroelectric and gas power plants, which are then normalized so that $\sum_{k \in G} K_k = 1$. Of course, constraints (2.44) are used for all generating units. Generating units like lignite (coal) power plants do not participate in the load shift. Moreover, RES as mentioned earlier are considered as constant active and reactive power generation.

Regarding the current limits of Synchronous Generators, only the stator current limits (2.45) are taken into consideration, while field current limits are neglected. Since the cases that are studied in this chapter focus on a very specific area of the HIS, current limits of the synchronous generators are expected to not have big impact on the voltage security margins that are calculated. Branch flow (2.34),(2.35) constraints can be also optionally included as in (2.36).

As mentioned in the previous subsection, the Greek power system consists of many high voltage buses, thus making the optimization problem quite demanding. For that reason, it should be noted that unlike Chapter 3, the problem is solved using the IPOPT [75] solver

and the Yalmip [72] optimization interface in MATLAB [53]. The IPOPT solver is an open source software package for large-scale nonlinear optimization. IPOPT implements an interior point line search filter method that aims to find a local solution of non-linear programming problem. The problem formulation remains practically the same, as no equation or inequality is reworked, only the solver is changed

7.2 Ionian Islands Transmission Corridor

7.2.1 Case Study Description

The transmission corridor under investigation in this section is shown in Fig. 7.3. The area of interest includes three Ionian islands which are connected to the Mainland grid through submarine cables. More specifically, island of Lefkada is connected to the Substation of Aktio in the north part of the area, while Zakinthos is connected to Killini in the south part of the figure. Tripping of this cable leads to a quite long 150kV transmission corridor, which especially during summer months, can be heavily loaded. A total of 6 reactors are placed in the three Substations as presented in Table 7.1.

Table 7.1: Reactor shunt data in the three S/S

Substation	Bus	Reactors (MVar)	
		A	B
Zakinthos	21032	-14.51	-12.5
	21033	-8.16	
Argostoli	21232	-14.51	
	21233	-14.51	-12.5

7.2.2 Incident of July 10, 2023

On 10/07/2023, 8:46am, a submarine cable tripped, connecting Substations, Zakinthos and Killini, as shown in a map of the area in Figure 7.3.

The tripping resulted in very low voltages in Zakinthos and the neighboring islands of Lefkada and Kefalonia as shown in Figure 7.4, where the voltage of the 150kV buses of the three substations (Zakinthos, Argostoli and Lefakada) are displayed. The voltages measurements from the SCADA system have a resolution of 1 minute data. It was deemed necessary to examine the exact voltage drop, as well as the voltage security margin after the contingency. The 1-minute resolution voltage data are presented in Fig. 7.4, along with the events that transpired.

It can be observed that, one of the reactors was disconnected immediately due to protection tripping, while the rest (4 reactors) were disconnected manually by the dispatchers on duty in the next few minutes. Two minutes after the disturbance the cable was reconnected. The re-closure of the cable lead to a short over-voltage (due to the disconnections of the reactors). The sequence of events is presented in Table 7.2.

In order to examine the incident, the two following snapshots taken form the System State Estimator (SE) are examined in this thesis:

- July 10, 2023, 08:31 - This is the snapshot taken few minutes before the incident, so system conditions are very similar.

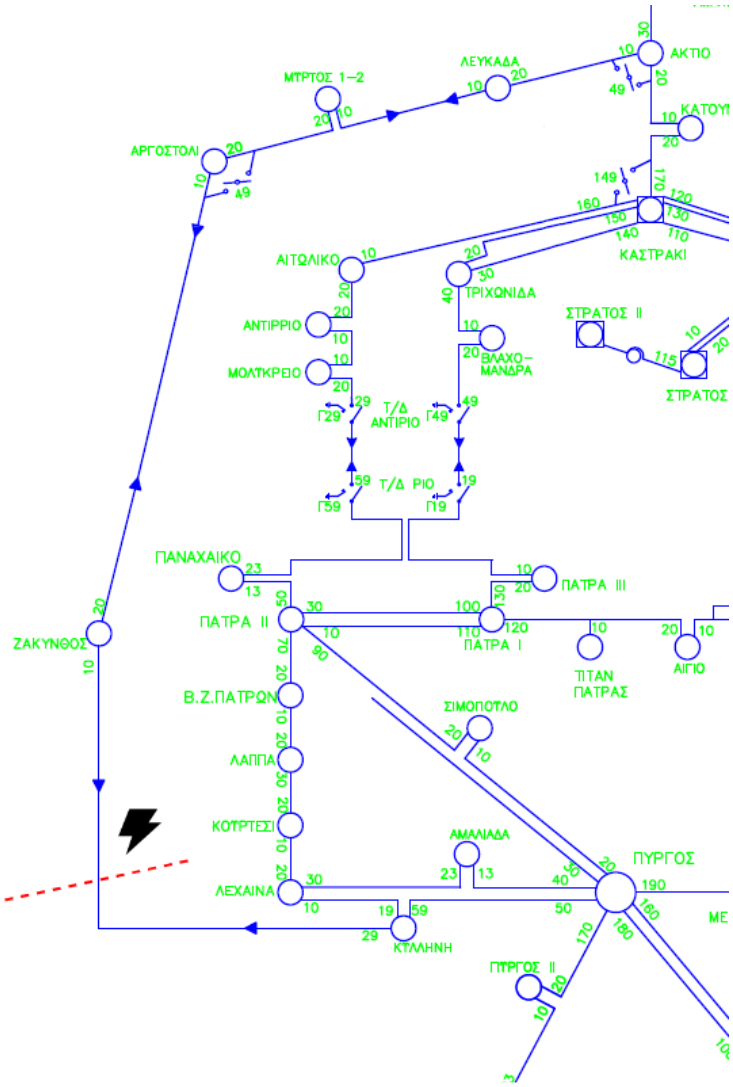

Figure 7.3: Ionian Islands Transmission Corridor

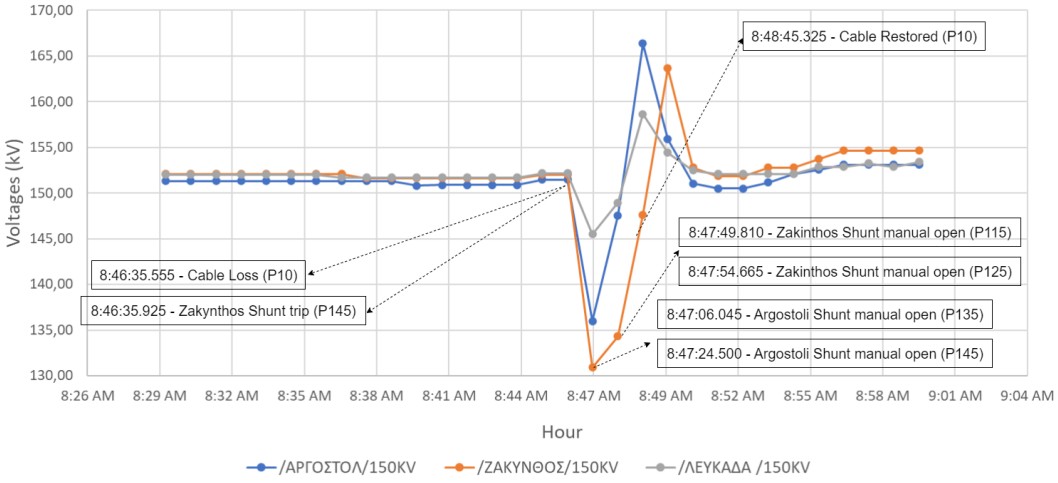

Figure 7.4: Events and voltages in Ionian islands

Table 7.2: Sequence of Events (SoE)

Date	Time	Substation	Base kV	Switch	Status
10.07	08:46:35,645	Pyrgos	150KV	P50	open
10.07	08:46:35,575	Zakinthos	150KV	P10	open
10.07	08:46:35,925	Zakinthos	150KV	P145	open
10.07	08:47:06,045	Argostoli	150KV	P135	open
10.07	08:47:24,500	Argostoli	150KV	P145	open
10.07	08:47:49,810	Zakinthos	150KV	P115	open
10.07	08:47:54,665	Zakinthos	150KV	P125	open
10.07	08:47:51,800	Mourtos	150KV	P115	open
10.07	08:48:45,325	Zakinthos	150KV	P10	close
10.07	08:49:04,330	Zakinthos	150KV	P115	close
10.07	08:49:05,085	Argostoli	150KV	P135	close
10.07	08:49:13,890	Argostoli	150KV	P125	close
10.07	08:49:32,165	Zakinthos	150KV	P145	close
10.07	08:50:06,595	Zakinthos	150KV	P155	close

- July 25, 2023, 20:31 - This snapshot corresponds to the peak summer load.

The first snapshot is the one closest to the contingency. As a result, it is considered that system conditions are very similar and the contingency is applied on it.

The second snapshot is selected because it is the day and hour of the peak load for this Ionian islands corridor. It is picked as a hypothetical scenario to examine the same contingency in an already more stressed system.

7.3 Analysis of July 10 Snapshot

7.3.1 Optimal Power Flow Results

At the specific snapshot, the area load data are presented in Table 7.3. In the Table, active and reactive power load is shown for each 20kV bus at the three substations.

Table 7.3: Load Data in the three Ionian Islands

Substation	Bus	Active Power Load (MW)	Reactive Power Load (MVar)
Zakinthos	21081	17.461	3.285
	21082	18.574	4.042
	21083	6.78	5.47
Argostoli	21281	16.481	4.295
	21282	11.421	4.036
Lefkada	26881	8.17	2.73
	26882	9.642	3.523
Total		88.529	27.381

Also, it is noted that reactors are connected to the Substations in this snapshot as shown in Table 7.1. One trips immediately due to the contingency, while the rest are manually

disconnected by the dispatchers on duty. The data for the shunt reactors are presented in Table 7.1.

In Myrtos substation, there are 4 WF connected through two 50MVA transformers with LTC at MV buses 28481 and 28482. The generation in each transformer for this specific snapshot is shown in Fig. 7.4. The injection from RES, as also mentioned before, is considered constant, meaning that buses are treated as PQ buses.

Table 7.4: Myrtos Wind Farms

Substation	Bus	Pg (MW)	Qg (Mvar)
Myrtos	28481	4.028	0.118
	28482	4.029	2.387

In Table 7.5, the stress and the total area load are presented in Table 7.5 for the following different cases:

- Initial Snapshot - The system condition as exported from the EMS State Estimator (SE).
- Post Contingency LF - The load flow calculation immediately after the contingency, where both the line and the reactor A in bus 21033 are disconnected.
- Case A - Maximum Area Load with reactor A in bus 21033 disconnected and a hard voltage constraint of 0.8 pu imposed.
- Case B - Maximum Area Load with reactor A in bus 21033 disconnected and no voltage constraint imposed (VSM).
- Case C - Optimal Solution with all reactors disconnected and a hard voltage constraint of 0.8 pu imposed.
- Case D - Optimal Solution with all reactors disconnected and all branch flow constraints imposed.
- Case E - Optimal Solution with all reactors disconnected and no voltage constraint imposed (VSM).

From the results on Table 7.5 it can be observed that for Cases A and B, if reactors are not disconnected, the VSM is limited and the voltages drop very fast. Voltage value V_{maxP} refers to the voltage value of 150kV bus 21031 of Zakinthos at the solution point of the VSM OPF. For Cases C,D and E, where shunt reactors are disconnected, margins are significantly larger. Still, cases C and D reveal the margins where the TSO would start considering load shedding, since both voltage and flow limitations are reached. Case E corresponds to the maximum load, assuming full load restoration (if possible) by the LTCs. Case E solution point corresponds to a bifurcation point.

It is noted at this point that the total load of Table 7.3, slightly differs from the initial area load of Table 7.5. This happens because for the optimization problem, the loads are placed in the 150kV buses, so the difference is due to the active power losses on the transformer.

Table 7.5: VSM Results for Snapshot of July 10, 2023, 08:31

Case	Area Load (MW)	VSM (MW)	Stress	V_{maxP} (pu)
Initial Snapshot Point	88.78	-	0	1.0098
Post Contingency LF	88.78	-	0	0.8021
A	89.25	0.47	0.0053	0.8000
B	118.56	29.78	0.3354	0.5307
C	133.32	44.54	0.5017	0.8000
D	136.99	48.21	0.5430	0.7559
E	140.92	52.14	0.5873	0.6422

In all cases where voltage constraints are imposed, bus 21031 of Zakinthos is the one where the limit is violated. More specifically, in case A, the margin is very small. This is due to the strict 0.8 pu voltage constraint and the presence of the reactors which are not disconnected. This case essentially proves the post-contingency measurements, before the manual disconnection of the reactors and proves that any further stress in the load would drop the voltage below the limit that is considered safe for the operation of the system.

Nonetheless, in Case B it is shown that there is a security margin of about 30MW, before the system becomes unstable, even without manually disconnecting the reactors.

Moreover, for Case D, the branch flow limit violated is the one for the cable between the bus of Aktio and Lefkada. No other branch flow limits are violated in the cases examined, as problem is focused on the specific area. The VSM if the branch flow violations are taken into account, is almost 50MW.

Case E actually represents a saddle-node bifurcation (SNB), as it is the unconstrained maximum of the load area, meaning that it represents a point in the maximum loadability surface. The voltage security margin in this case is 52.14 MW, which corresponds to about a 58% increase in the area load. As a results it can be deducted that since the reactors were disconnected, there was quite a significant margin before the stability limit.

7.3.2 QSS Time Domain Simulation

Similarly to Chapter 5, results of the optimization are validated and compared to the quasi steady state (qss), time-domain simulation performed with the software WPSTAB.

In the qss simulation generators are fully modelled, inluding the over-excitation limitations (OELs) and magnetic saturation [7]. Also, the *full* snapshot is used, where the LTC is explicitly modelled and the loads are placed at the 20kV buses. The data of the LTC in the three substations are presented in Table 7.6.

The simulation is performed as follows:

- No disturbance until t=10s, to ensure that the initialization is correct and steady state was achieved.
- Cable between substations Zakinthos and Killini trips at t=10s.
- One shunt reactor trips at t=10s at bus 21033 of Zakinthos.
- A load ramp is initiated at t=10s with a constant rate of 0.5 %/s.

Table 7.6: Transformer Data

Substation	150kV	20kV	r_{max}	r_{min}	V_{max}	V_{min}	step
Zakinthos	21031	21081	1.075	0.875	1.016	0.996	0.0125
	21031	21082	1.075	0.875	1.01	0.99	0.0125
	21031	21083	1.075	0.875	1.011	0.991	0.0125
Argostoli	21231	21281	1.075	0.875	1.003	0.983	0.0125
	21231	21282	1.075	0.875	1.011	0.991	0.0125
Lefkada	26831	26881	1.075	0.875	1.006	0.986	0.0125
	26831	26882	1.075	0.875	1.014	0.994	0.0125

- One reactor shunt at bus 21232 of Argostoli is manually opened at t=20s.
- Two reactor shunts at bus 21233 of Argostoli are manually opened at t=30s.
- Two reactor shunts at bus 21032 of Zakinthos are manually opened at t=40s.
- Simulation ends at t=800s.

The voltages of a single bus in each substation of the three islands of Zakinthos, Argostoli and Lefkada are presented in Fig. 7.5.

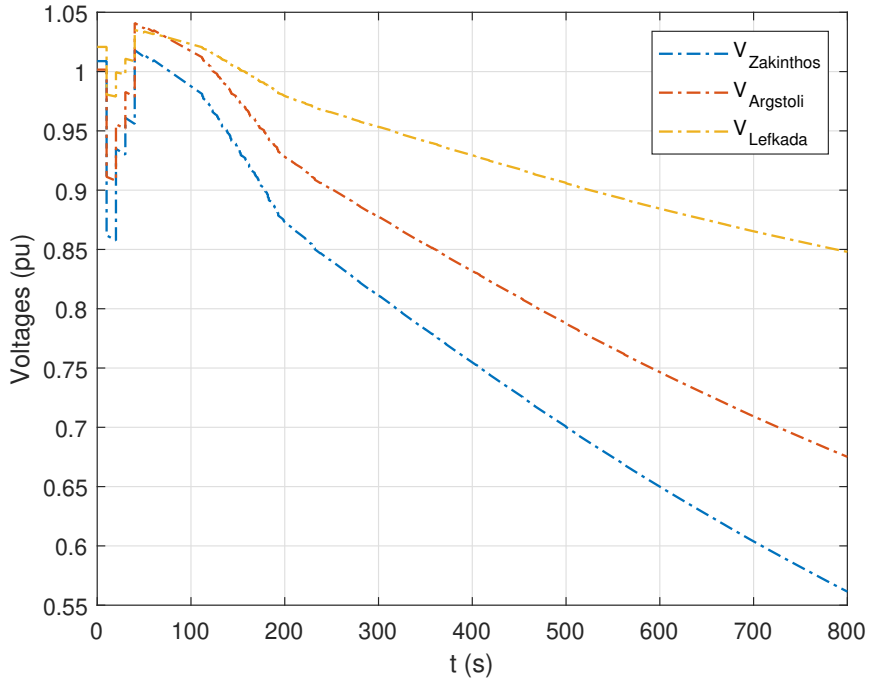

Figure 7.5: Voltages in 150kV buses of three S/S

It can be observed in Fig. 7.5 that the initial drop, after the submarine cable disconnection, is quite large, but the successive disconnection of the reactors brings back the voltages to accepted values. Nonetheless, the load increase due to the ramp imposed will eventually bring down the voltages significantly.

The voltage of the medium voltage (MV) buses in the three substations are presented in Fig. 7.6. As shown, after the cable disconnection, the LTCs are keeping the voltages

inside the permissible deadband. When the LTC tap range is exhausted, the voltage for the medium voltage buses also fall significantly. For bus 26831 of Lefkada, which is the one closer to the mainland grid, it is shown that the voltage is kept for quite a long time inside the deadband, and the LTC tap range is exhausted after 560 seconds of simulation. The ratio along with the voltage of HV bus 21031 and the MV controlled bus 21081 are shown in Figure 7.7. The LTC tap range in buses 21081,21082 and 21083 of Zakinthos are exhausted around t=200s, while for 21281,21282 around t=240s.

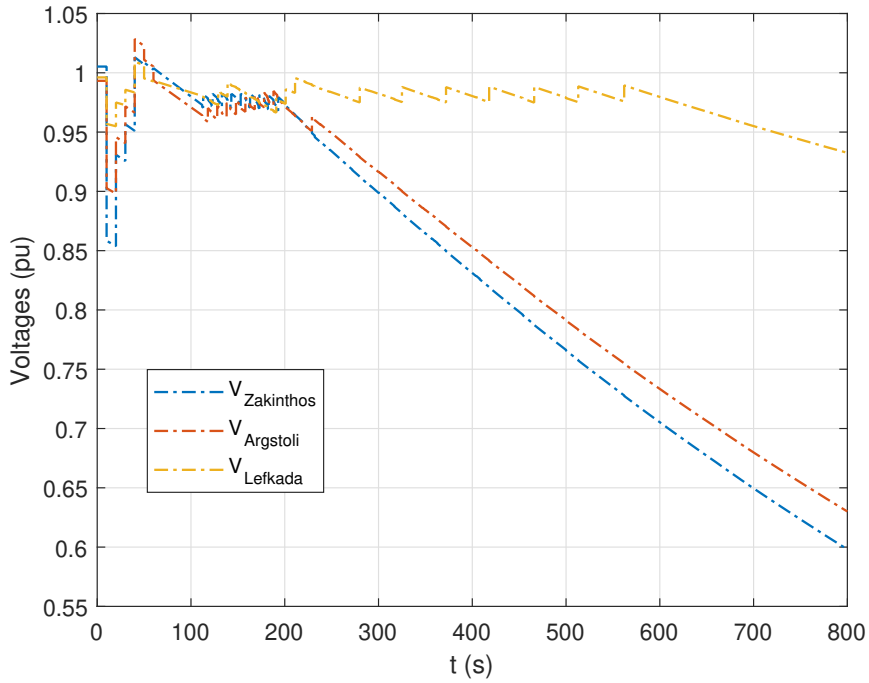

Figure 7.6: Voltages in 20kV buses of three S/S

As also described in Chapter 1 subsection 1.4.3, voltage stability limit can be assessed through sensitivity analysis. In Fig. 7.8, the sensitivity of the reactive power generation with respect to bus reactive power load S_{QgQ} is plotted against time. It can be obsrved in the plot that at t=654s the sensitivity changes sign. These sensitivities change sign through infinity at the maximum loadability point [4], where also the long-term eigenvalue changes sign through zero and the long-term Jacobian is singular.

Also, it is noted that before the change of sign in sensitivity S_{QgQ}, only one synchronous machine reaches its over-excitation limit. More specifically, the hydro power plant of Louros in bus 21481, reaches it's OEL at time t=435s.

The total area load of the Ionian corridor is presented in Fig. 7.9, against the voltage of the 150kV HV bus 21031. The PV curve shows that there is a maximum value for the area load close to 142 MW. In the same plot, the point found from the optimization of subsection 7.3.1 for Case E is presented.

In Fig. 7.10, the total load of the area is plotted in time, together with the sum of the loads in the two substations of Zakinthos and Argostoli. It can be seen in this figure, that the maximum loading of the two islands is achieved earlier than the maximum of the total area loading and before the change of sign in the sensitivity. This behaviour is thoroughly explained in [14] where it is stated that at least one line must reach its static

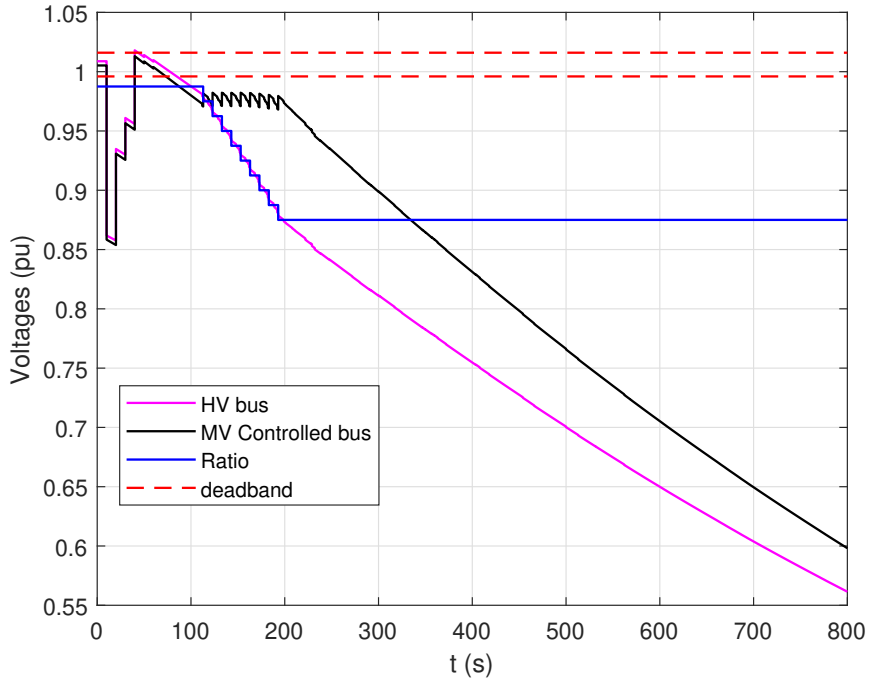

Figure 7.7: LTC transformer with controlled bus 21081

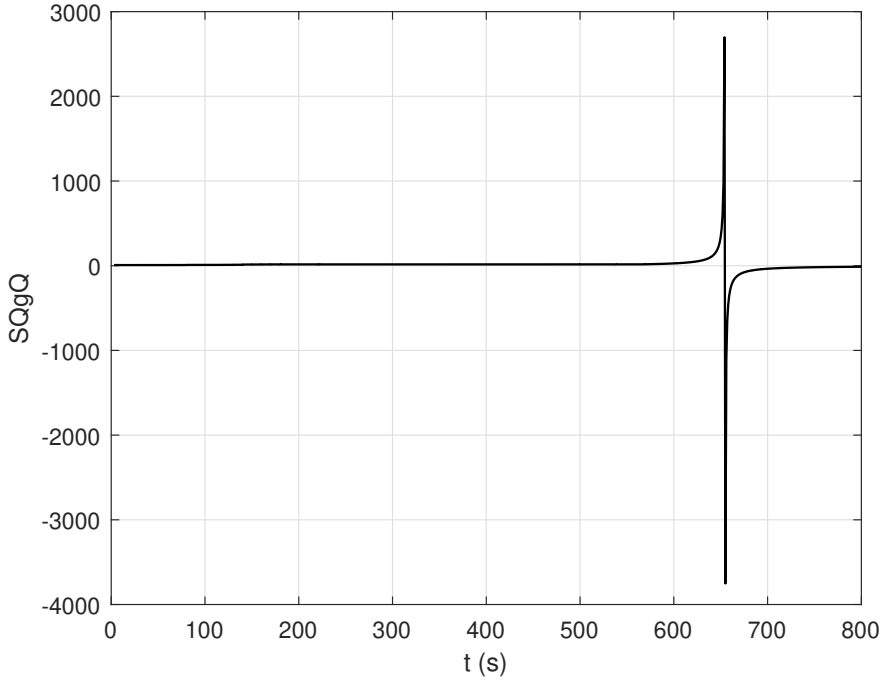

Figure 7.8: Sensitivity of reactive power generation to reactive power load

transfer stability limit (STSL) at or before the point of voltage collapse.

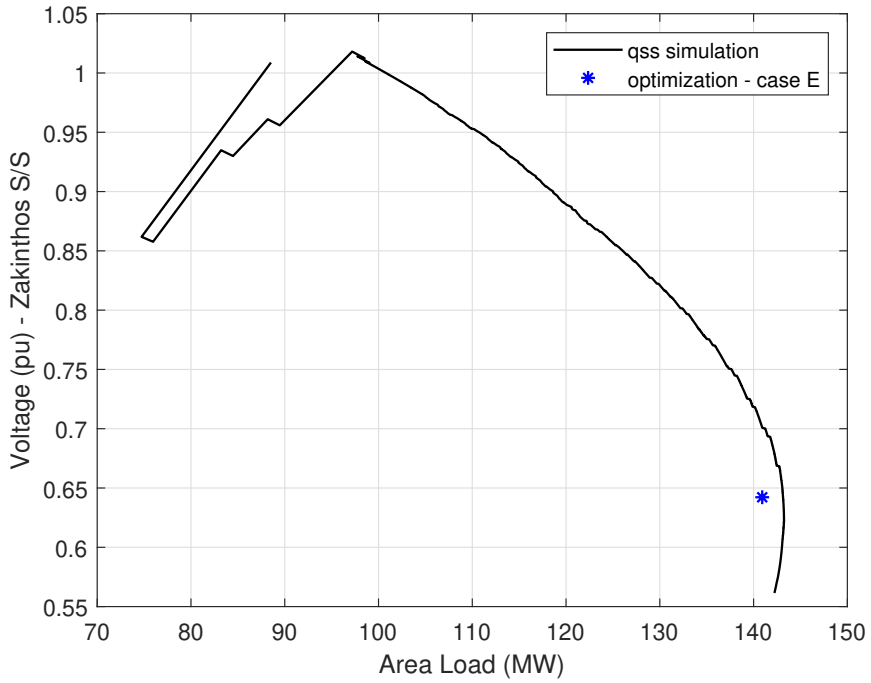

Figure 7.9: PV curve and Optimization results

It can be observed from Fig. 7.10 that the point found from the optimization problem, corresponding to case E is close to the maximum obtained by simulation, but not exactly the same. While both points correspond to maximum loading conditions, they do not represent the same points on the maximum loadability surface. This is due to the difference in the load consumption in each case, caused by the sensitivity of the loads to the voltage. This is shown in Fig. 7.11, where for 20kV load buses 21081, 21281 and 26881 the value of p_{dk}/p_{dk0} is plotted in time. It can be observed that for the load in Lefkada, where medium voltage is retained closer to the nominal value, the load increase is linear, closer to the one of the optimization. This is not the case for the other substations where the LTC tap range are exhausted quite early in the simulation and the 20kV load bus voltages drop significantly (Fig. 7.7).

Note that in the OPF formulation it is assumed that active loads as seen from the transmission buses increase linearly, which is not the case in the simulation, mainly due to the LTC tap range limits.

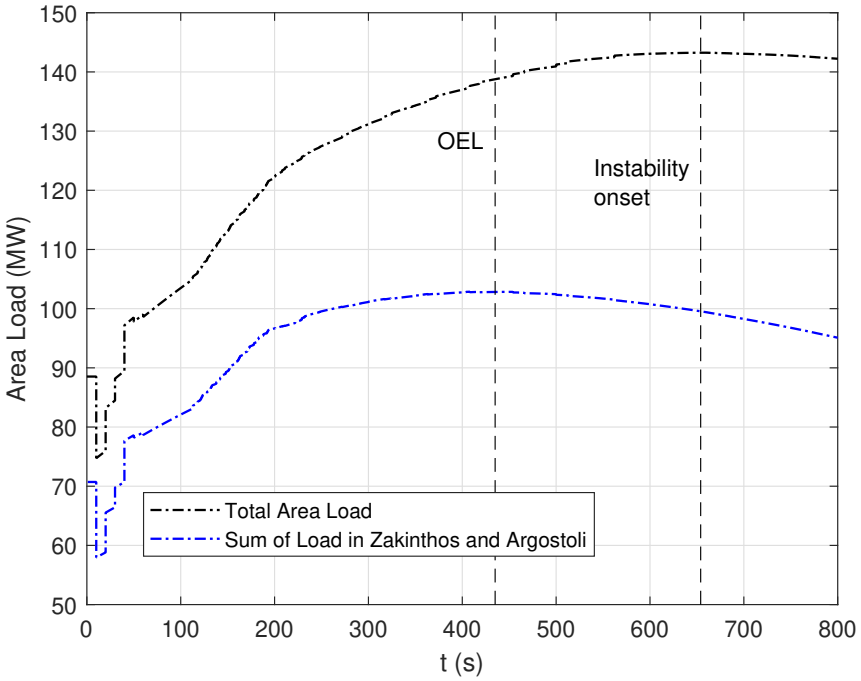

Figure 7.10: Total area load vs Zakinthos and Argostoli load

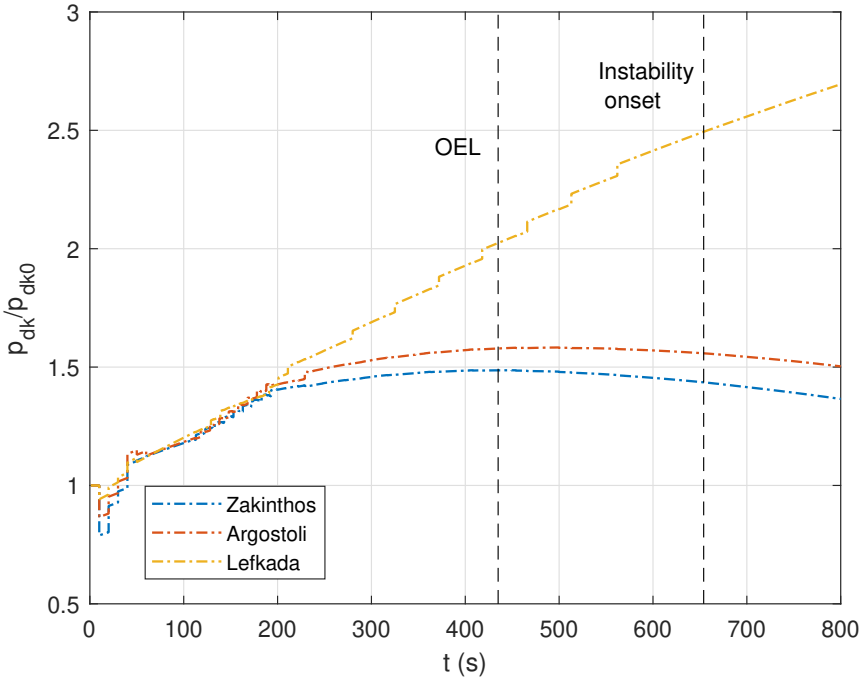

Figure 7.11: Active power load consumption in three S/S

7.4 Analysis for summer peak load

7.4.1 Optimal Power Flow Results

This snapshot corresponds to the peak load for the area load of interest, where in Table 7.7, active and reactive power load is shown for each 20kV bus at the three substations.

Table 7.7: Load Data in the three S/S

Substation	Bus	Active Power Load (MW)	Reactive Power Load (MVar)
Zakinthos	21081	31.115	-4.564
	21082	32.93	6.384
	21083	12.28	10.106
Argostoli	21281	30.636	7.787
	21282	24.053	7.601
Lefkada	26881	14.453	3.744
	26882	19.099	4.958
Total		164.566	36.016

In this snapshot, due to the high loading (peak load), there is only one reactor connected at the initial point. As a result, only cases C-E are examined, as the reactor connected is the one that trips when the contingency happens.

The generation from the WFs connected to Myrtos substation is presented in Table 7.8. In this case, a shunt capacitor is also connected to a 20kV bus of the substation.

Table 7.8: Myrtos Wind Farm

Substation	Bus	Pg (MW)	Qg (Mvar)	Capacitor (Mvar)
Myrtos	28481	6.05	0.49	4.3
	28482	6.282	3.007	-

The results for the VSM and the safe operating loading are presented in the table.

Table 7.9: VSM Results for Snapshot of July 25, 2023, 20:31

Case	Area Load (MW)	VSM (MW)	Stress	$V_{maxP}^{zakinthos}$ (pu)
Initial Snapshot Point	165.44	-	0	1.0169
Post Contingency LF	-	-	0	No Convergence
C	145.40	-20.04	-0.1211	0.8000
D	140.62	-24.82	-0.1500	0.8499
E	151.51	-13.93	-0.0842	0.6592

In this snapshot, it can be observed in Table 7.9 that after the contingency the margins are negative, meaning that the system would not be able to withstand this contingency. This is also indicated by the non-convergence of the post-contingency load flow calculation.

In essence, full load restoration by the LTCs would lead to voltage collapse of the area. For this reason, a QSS simulation is run for this snapshot, to show more accurately the behaviour of the system and determine the final outcome.

7.4.2 QSS Time Domain Simulation

Simulation without load ramp

In this case, qss simulation is performed first without a load ramp imposed, since according to the results of the optimization of Table 7.9, the voltage security margin after the contingency is negative.

In this case, the contingency (cable loss) occurs at t=10s and the simulation ends at t=500s. In Fig. 7.12, it can be observed that the voltages of HV buses 21031,21231 and 26831 drop up to some point, and reach a new low-voltage operating point. The MV voltage buses 21081, 21281 and 26881 are shown in Fig. 7.13. From this figure, it can be observed that for bus 26881 in Lefkada, voltage is restored inside the deadband, while the other two buses achieve a lower value, which is outside the deadband due to LTC tap range limitation.

Similarly, the total load area, presented in Fig. 7.16 is restored up to 146.9 MW, which is less than the initial loading and close but less than the OPF maximum loading (151.51 MW) from Table 7.9.

This system behaviour that has been called pseudo-stable steady state is attributed to the exhaustion of the tap range of the LTC. As shown in Fig. 7.14 and Fig. 7.15, for controlled MV bus 21081 and 21281, the tap range is exhausted at t=160s and t=90s respectively, so there is no other mechanism to restore the load to its pre-disturbance levels. Similar behaviour is also observed in the other buses of Zakinthos as well as Argostoli. This also explains the behaviour of the voltages of buses in Fig. 7.13, where for bus 21281, after the tap ratio is exhausted, voltage continues to drop due to the LTC in bus 21081 which is still active.

Figures 7.12-7.14, below, present the system conditions when no ramp is imposed:

Simulation with load ramp

In order to deal with the exhaustion of the tap range of the LTC, and the pseudo-stable steady state condition, in this simulation a load demand ramp is imposed, to further stress the system to its maximum. In this way, the actual maximum loading point can be reached. Simulation steps are performed as follows:

- No disturbance until t=10s.
- Cable between buses 21032 and 18831 trips at t=10s.
- One shunt reactor trips at t=10s at bus 21032.
- A load ramp is initiated at t=10s with a constant rate of 0.2 %/s.
- Simulation ends at t=800s.

As shown in Fig. 7.17, where voltages of 150kV buses 21031, 21231 and 26831 are presented, due to the heavy loading of the Ionian corridor, voltages drop fast. The voltage drop is increased, further away from the mainland grid.

In Fig. 7.18, the 20kV buses for the three substations are shown. Similarly to the previous snapshot, voltages in buses 21081, 21082, 21083 in Zakinthos and 21281, 21282

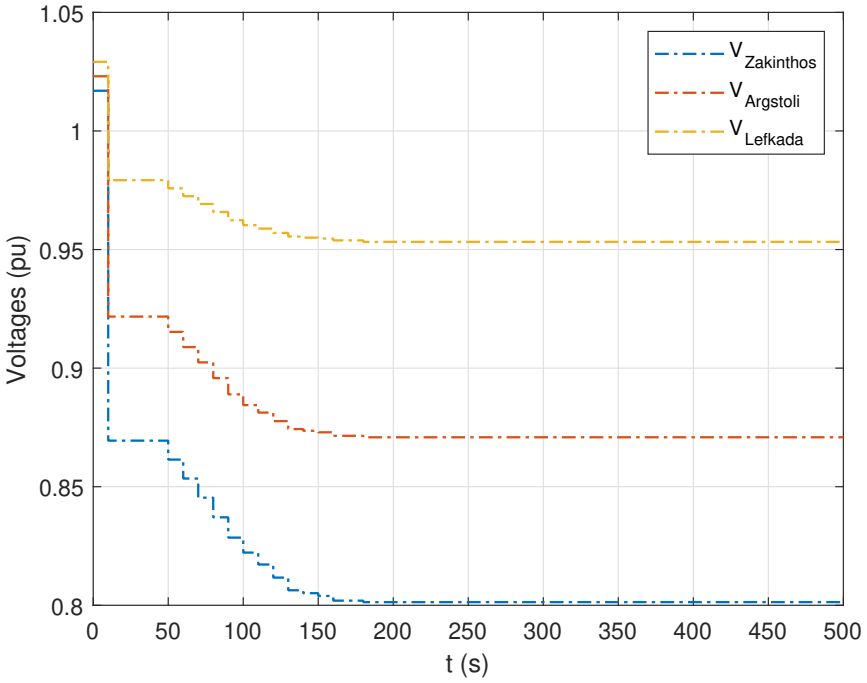

Figure 7.12: Voltages in 150kV buses 21031,21231 and 26831

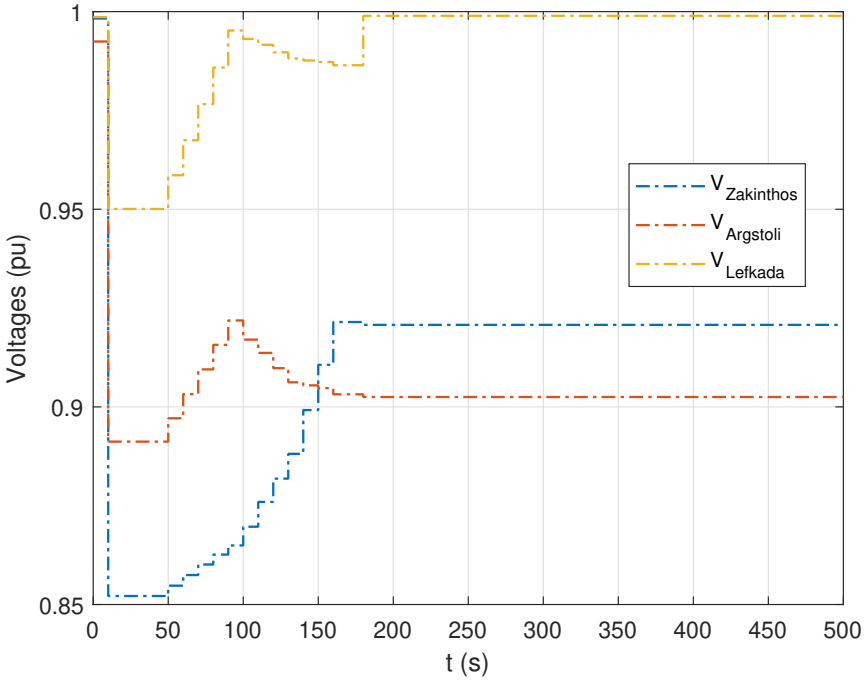

Figure 7.13: Voltages in 20kV buses 21081, 21281 and 26881

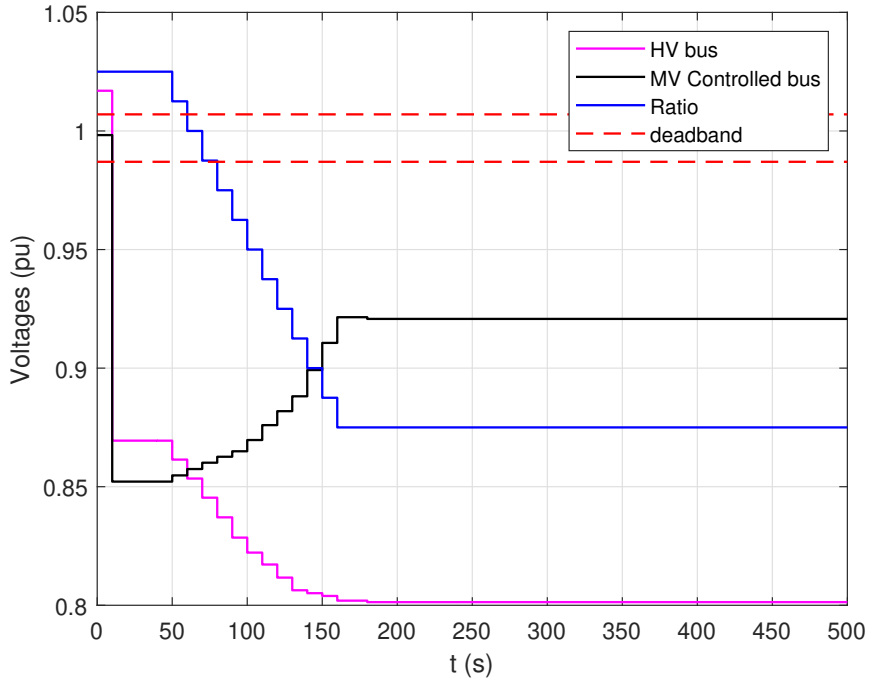

Figure 7.14: LTC transformer with controlled bus 21081

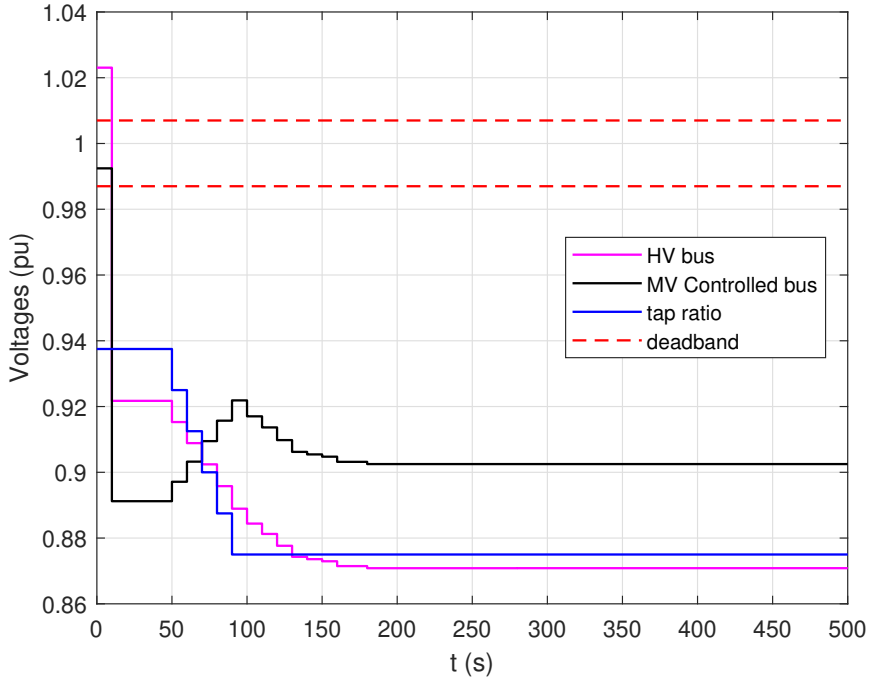

Figure 7.15: LTC transformer with controlled bus 21281

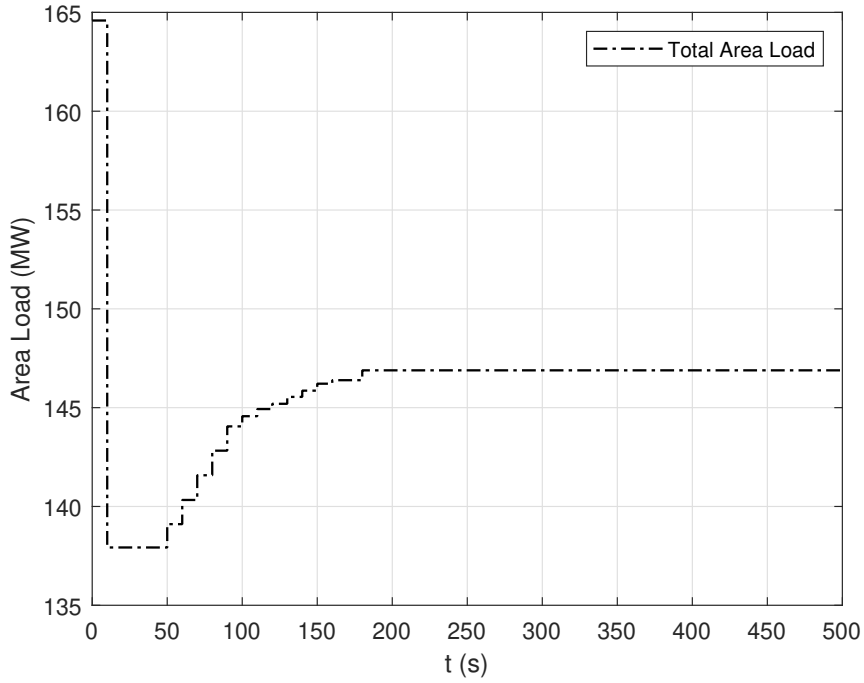

Figure 7.16: Total area load

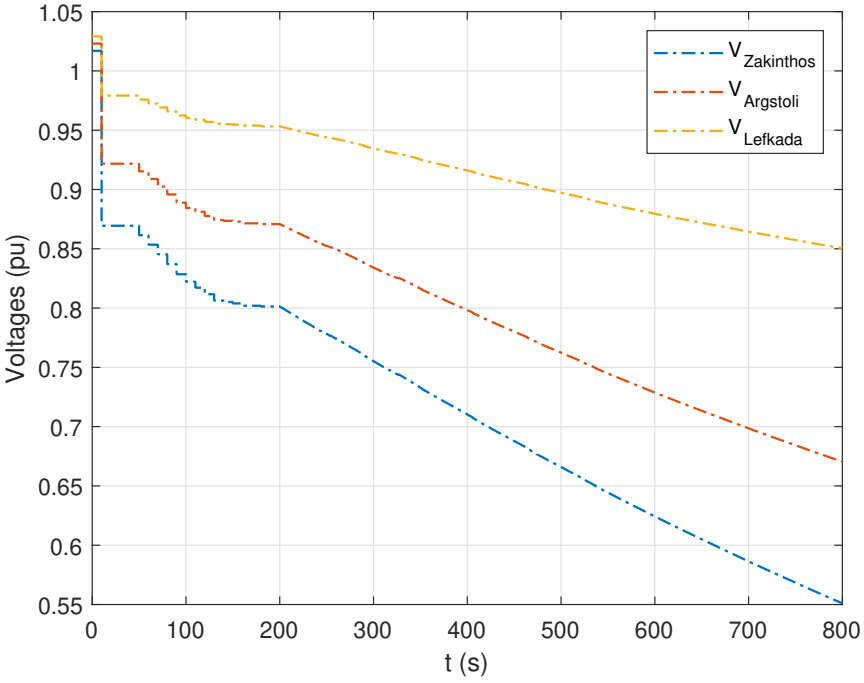

Figure 7.17: Voltages in 150kV buses of three S/S

in Argostoli cannot be kept inside the deadband, as the LTC tap range is exhausted. In Lefkada, the LTC is able to keep the voltages in the desired deadband, until almost the end of the simulation. The ratio along with the voltage of HV bus 21031 and the MV controlled bus 21081 are shown in Figure 7.19 and Fig. 7.20.

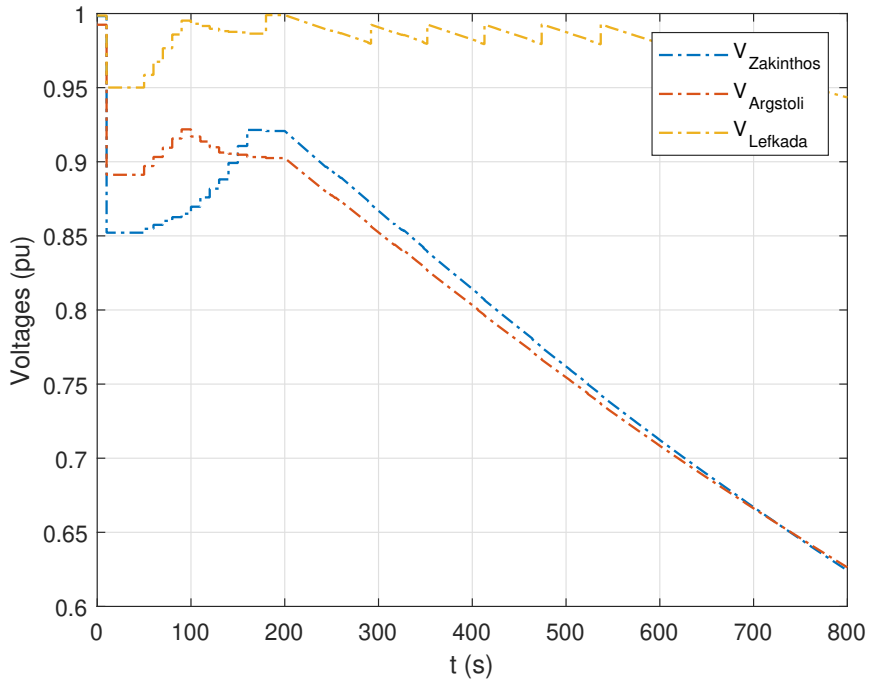

Figure 7.18: Voltages in 20kV buses of three S/S

In Fig. 7.21, the sensitivity S_{QgQ} is plotted in time. It can be seen that at t=545s the sensitivity changes sign, indicating a maximum power transfer.

The total area load of the Ionian corridor is presented in Fig. 7.23, against the voltage of the 150kV HV bus of Zakinthos S/S. The PV curve shows that there is a maximum value for the area load. Together, in the same plot, the point found from Table 7.9 for Case E is presented. In Fig. 7.22, the total load of the area and the load of the two furthest islands is plotted against time. In this figure, it is observed that maximum of the two islands of Zakinthos and Argostoli are met before the point of instability.

In this case, no over-excitation limit of generator is met, proving that for this specific stress and area, neglecting OELs is not significant for the VSM.

Once again, in Fig. 7.24, for a single load in each S/S the value of p_{dk}/p_{dk0} is plotted in time. It can be observed that for the load in Lefkada, where medium voltage is retained closer to the nominal value.

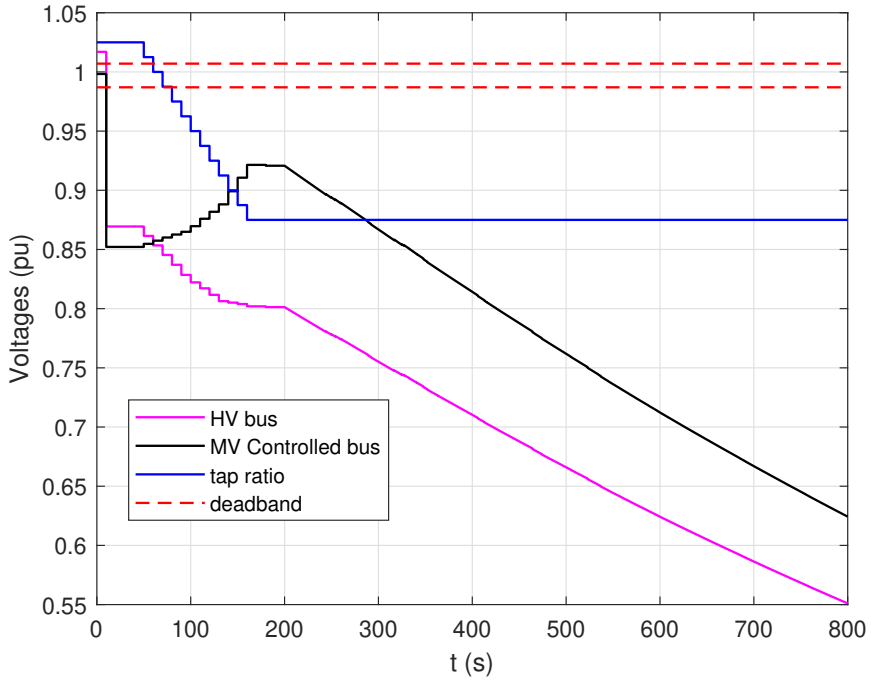

Figure 7.19: LTC transformer with controlled bus 21081

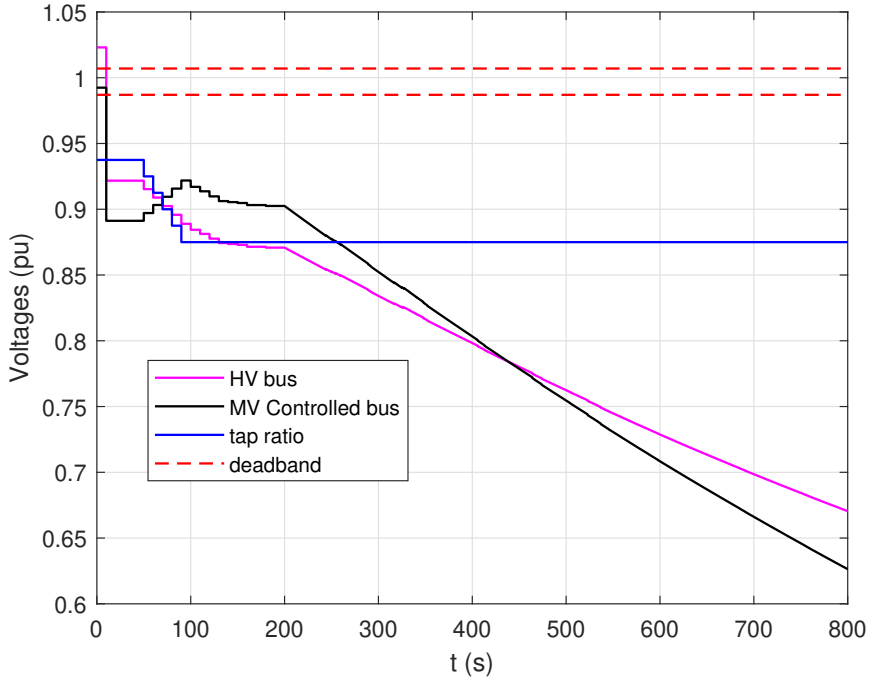

Figure 7.20: LTC transformer with controlled bus 21281

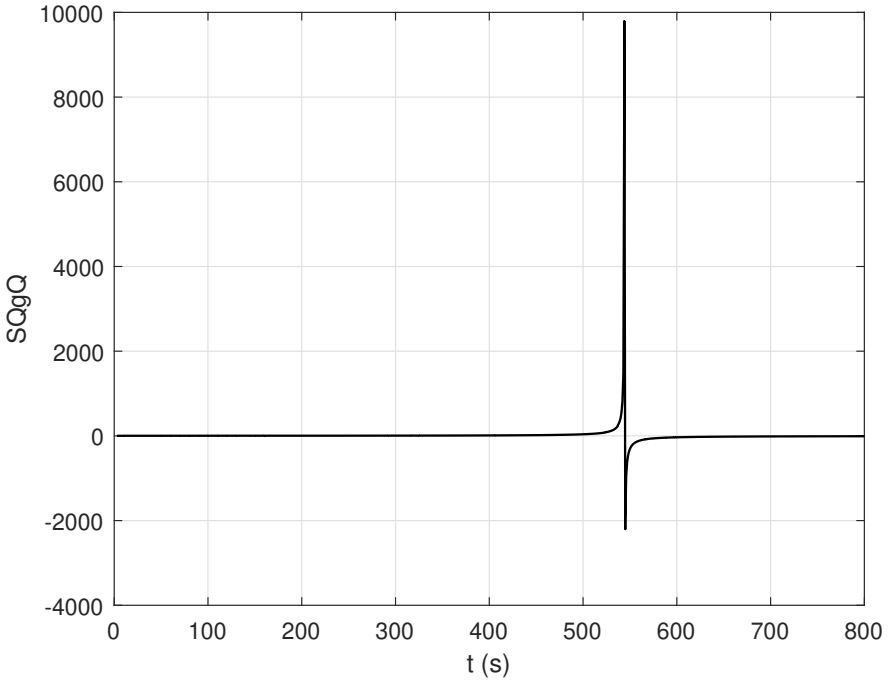

Figure 7.21: Sensitivity of reactive power generation to reactive power load

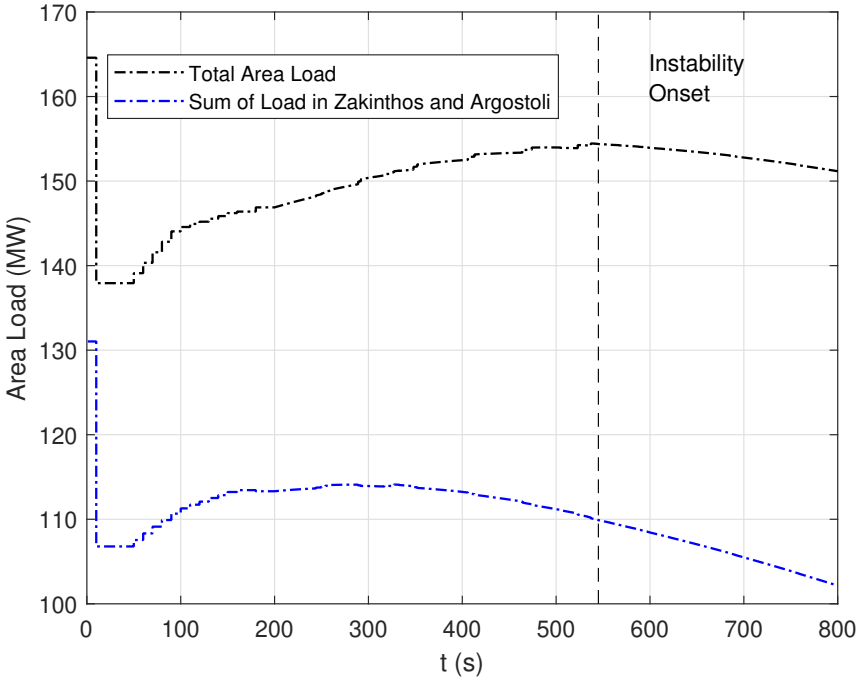

Figure 7.22: Total area load vs Zakinthos and Argostoli load

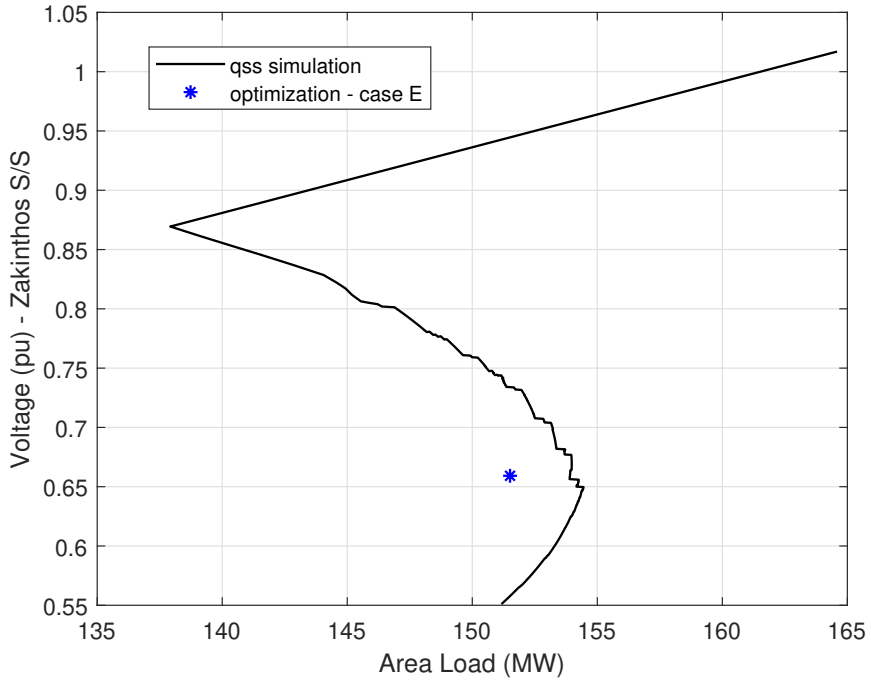

Figure 7.23: PV curve and Optimization results

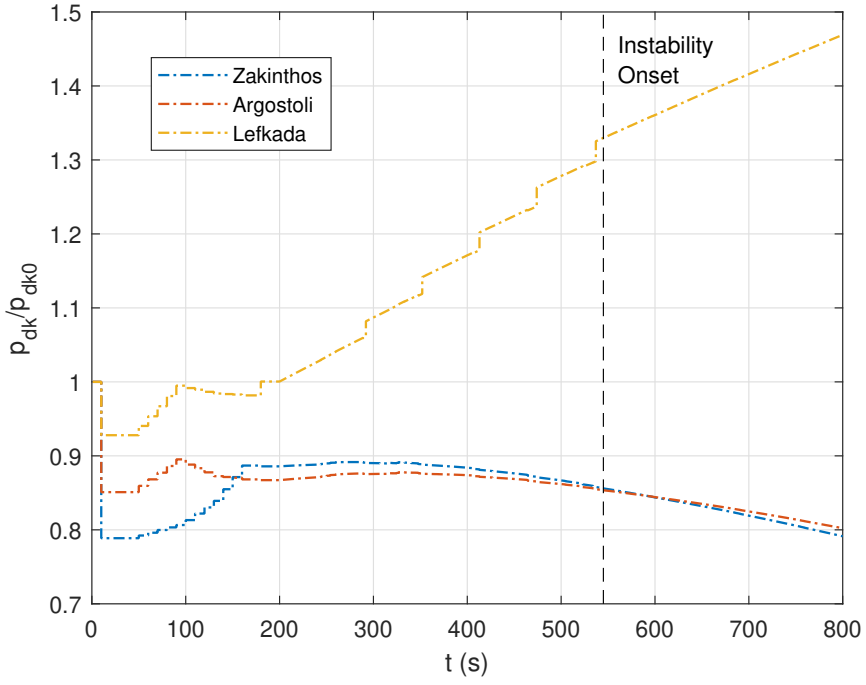

Figure 7.24: Active power load consumption in three S/S

7.5 Effect of RES current injections on the VSM of the Ionian Corridor

As explained in Chapter 3, RES current injections and the respective requirements for fast current injections can also greatly affect the voltage security margin. For that reason, in this Section, the effect of the current injections from the RES located in the substation of Myrtos will be examined.

In previous sections, the power generation from the WF of bus 28431 of Myrtos substation were treated as constant power injections (effectively as PQ buses). In this section, the modelling is more detailed, including the 150/20kV transformer as well as the 20kV dedicated feeder for each wind farm connected to 20kV buses 28481 and 28482.

As shown in the one line diagram of Myrtos substation in Fig. 7.25, the wind generation is divided between two 50MVA transformers, two 20kV buses and seven dedicated 20kV feeders. The feeders may consist of both overhead lines and underground cables. Each feeder corresponds to a specific switch gear as shown in the figure. On switch P315, there is a series of capacitors with three stages of 4MVar.

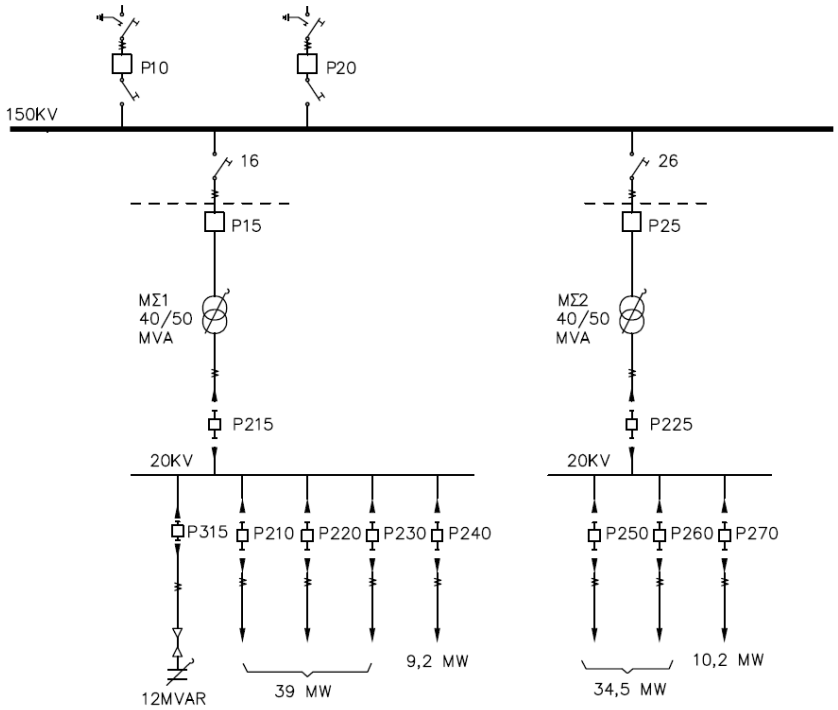

Figure 7.25: Myrtos Substation

On Table 7.10, the data of each feeder and the respective installed capacity are presented. The data are in per unit, in the 100MVA system base.

Table 7.10: Feeder Data

Breaker	R (pu)	X (pu)	B (pu)	P_{inst} (MW)
P210	0.126385	0.08635	0.00122	9
P220	0.026988	0.03872	0.00098	15
P230	0.04318	0.061952	0.00157	15
P240	0.467194	0.670838	0.00072	9.2
P250	0.137181	0.13666	0.00132	17.25
P260	0.137181	0.13666	0.00132	17.25
P270	0.255509	0.209357	0.00187	10.2

7.5.1 Optimization Results

In order to show the effects of the RES on the voltage security margin of the Ionian corridor, the second, insecure snapshot of section 7.4 will be used. In that snapshot, available wind generation from Myrtos was around $P_w = 12MW$, which is considerably low, compared to the installed capacity of all the wind parks which is around 90 MW. For that reason, a second case is examined with high wind generation for the same snapshot.

The following scenarios will be examined, to assess the RES current injection support. Similarly, to Chapter 3, available control includes injection of reactive current even at the cost of active power curtailment. In this case, voltage limits are set for the medium voltage 20kV buses of ±0.05pu.

$$0.95 \leq V_g \leq 1.05 \tag{7.2}$$

For all the wind farm connected to Myrtos substation, depending on the case examined the following constraints are included:

In the case where no control over the active power generation is assumed,

$$P_{min} = P_g = P_{max} \tag{7.3}$$

while when there is the possibility of active power curtailment:

$$P_{min} \leq P_g \leq P_{max} \tag{7.4}$$

where, P_{max} corresponds to the available wind generation.

Regarding reactive power injections, when no control over reactive power is assumed,

$$Q_{min} = Q_g = Q_{max} \tag{7.5}$$

For all cases, including the case where there is control over the reactive power, the current injections constraints are imposed:

$$q_g = \sqrt{(I_n V_g)^2 - p_g^2} \tag{7.6}$$

where, I_n is the nominal current for nominal voltage.

On Table 7.11, the results are presented for the different scenarios examined. More specifically, other than the original snapshot of low wind and no control, another four

Table 7.11: Effect of RES injection control on VSM

Wind	p-control	q-control	Area Load (MW)	VSM (MW)	E_{Sn} (%)
low wind	no	no	151.51	-13.93	-
high wind	no	no	162.43	-3.01	12%
high wind	no	yes	185.31	19.87	37%
low wind	no	yes	186.55	21.11	38%
high wind	yes	yes	198.43	32.99	51%

cases are calculated, based on the constraints (7.2)-(7.6). The last column of the table, as also used in Chapter 3, represents the increase in the VSM with respect to the nominal value of the apparent power of all the WF connected to the substation of Myrtos. Also, it can be observed that for high wind penetration, if there is no curtailment possibility, the VSM can prove to be lower than in low wind conditions. This is due to the fact that reactive current injections are limited. It can be observed that the results are in line with the observations made in Chapter 3. More specifically, due to the proximity of the WF substation to the mainland, and not the load area, the active power injections prove less significant for the VSM than the reactive power injections.

Table 7.12: WF active and reactive power generation for low wind conditions

	Initial		q control	
WF bus	Pg	Qg	Pg	Qg
70001	1.0	0.8	1.0	9.2
70002	2.0	-1.4	2.0	15.2
70003	2.0	1.9	2.0	15.3
70011	1.0	-0.1	1.0	4.2
70021	2.0	1.2	2.0	17.7
70022	2.0	1.2	2.0	17.7
70031	2.1	-0.4	2.1	10.3

Table 7.13: WF active and reactive power generation for high wind conditions

	Initial		q control		p and q control	
WF bus	Pg	Qg	Pg	Qg	Pg	Qg
70001	8.6	-5.7	8.6	4.0	6.2	7.0
70002	14.3	-0.4	14.3	6.4	10.2	11.7
70003	14.3	-0.6	14.3	6.6	10.2	11.7
70011	8.7	-4.5	8.7	-3.6	8.7	-1.8
70021	16.4	-1.2	16.4	7.0	12.0	13.2
70022	16.4	-1.2	16.4	7.0	12.0	13.2
70031	9.7	-1.9	9.7	4.0	7.1	7.7

In Table 7.12 and 7.13 the active and reactive power generation of each WF is presented for the initial condition and at the VSM solution point for the considered available control. In low wind conditions it can be seen that the reactive power is increased until the current limit of the inverter is reached. In high wind conditions, due to already increased active power generation there is little margin for reactive current. As a result, reactive power will

increase only unitl the inverter current limits are met. When active power curtailment is available (p and q control), then the optimal solution in most WFs is to increase reactive power even at the expense of active power which is curtailed.

7.5.2 QSS Time Domain Simulation

The cases of Table 7.11, are also validated through the qss time domain simulation performed on WPSTAB.

For the qss simulation, similarly to previous subsections, LTCs are explicitly modelled. In this case, the IBRs are also modelled. More specifically, in the cases where q control is assumed, IBRs operate with constant voltage control (CVC). After the contingency occurs, the voltage setpoint is changed with a ramp, to the values that occurred from the optimization problem in subsection 7.5.1. Similarly, for the last case, where the active power generation can be curtailed, after the new voltage setpoints are implemented, active power is also reduced.

The simulation is similar to the previous cases, where the contingency happens at t=10s, and then a load ramp is imposed. The PV curves for the different cases are presented in Fig. 7.26.

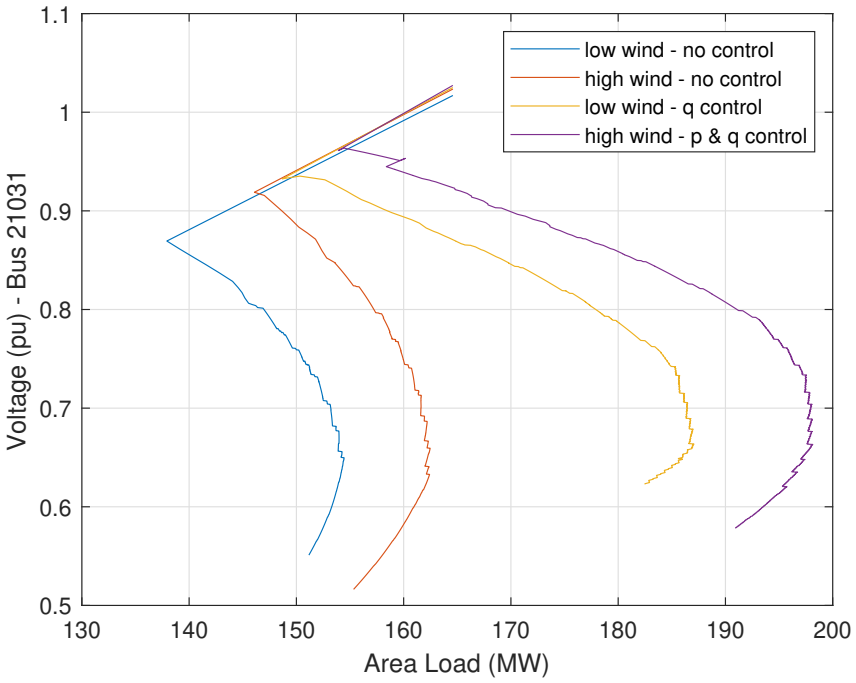

Figure 7.26: PV curve for different types of IBR control

As also presented in the optimization results in Table 7.11, VSM can be significantly increased when controlling the IBRs. Specifically, in cases with high wind and the possibility of active power curtailment, optimal current injections can be achieved to ensure maximization of the VSM, without violating medium voltage limits and inverter current constraints.

Chapter 8

Conclusions

This doctoral thesis focused on the support that a transmission system can receive from active distribution networks in terms of increasing the voltage security margins (VSM) for specific contingencies. In the following Sections, the contributions of the thesis, its conclusions and prospects for future work are presented.

8.1 Contribution

A first contribution of this thesis was the formulation of a centralized OPF problem, in order to quantify the VSM i.e. to define the voltage instability limit of the transmission system for a list of credible contingencies. The OPF is solved as a non-linear, non-convex optimization problem with the use of a sequentially quadratic programming solver and an interior-point programming solver.

Two novel frameworks were proposed in the thesis for achieving ADN support for Voltage Stability, namely:

- A novel corrective control scheme with Distributed Optimization by ADNs based on sensitivity information of the VSM sent by the control centre.
- A novel preventive central VSM optimization based on the received flexibility region information sent by the contributing ADNs.

The distributed optimization approach relies on a two-stage optimization scheme, consisting of the VSM OPF problems which is the first (or upper) stage and the OPF that is performed at each ADN which is the second (or lower) stage. More specifically, the central OPF for the VSM is solved, and the VSM is calculated for each critical contingency along with the Lagrange multipliers which correspond to sensitivities of P,Q consumption by each ADN. Then, a local controller solves for each ADN a local OPF problem using these sensitivities in order to maximize the VSM by changing its P,Q consumption. In practice, the transmission system control centre will first identify critical contingencies, and only after one of them occurs, will distribute sensitivities as control signals to achieve maximum support, thus acting correctively on a pre-identified critical contingency. These control signals will ensure that the controls on each ADN will increase the voltage security margins, due to the fact that the Lagrange multipliers are sensitivities of the VSM with respect to the active and reactive power consumptions of each ADN. In this term, this is

a corrective measure that is implemented after an emergency, such as a contingency that would lead to instability.

The centralized approach relies on the determination of the flexibility region of each ADN, which defines how much the active and reactive power consumptions at the PCC can vary from the initial operating point. In this approach the flexibility region of each ADN is calculated at small time intervals (e.g. minutes) and are sent to the control centre. Then the flexibility regions are used in the centralized OPF to maximize the security margins. The central optimization includes also the FR of each ADN as constraint and will compute an increased VSM, as well as the reference values for the active and reactive power of each ADN at the PCC. As a result, for a contingency with low VSM, the reference values are sent to each ADN to achieve VSM maximization. In that sense, this method can be applied preventively to achieve an acceptable security level for the most critical contingency. In order to achieve the P,Q reference values at the PCC, a third OPF is solved at the ADN level, to provide the required setpoints to ADN controllers.

The second important contribution was the proposed radial scan method to calculate the flexibility region of an ADN and the inclusion of the calculated flexibility region in the aforementioned centralized optimization problem for Voltage Stability. The proposed method consists of a detailed way to find points on the boundary, approximate the flexibility region with a convex polygon and turn the polygon into linear constraints. Moreover, the use of the SOCP convex relaxation for the formulation of the flexibility region problem calculation is a novel contribution of this thesis.

To implement and test the aforementioned contributions, several programming scripts were developed by the author, mainly in MATLAB programming interface. More specifically, the most imporatnt pieces of programming code developed for this thesis are the following:

- Formulation of the Centralized OPF for VSM using MATLAB. The code includes reading of the network data, quality check, formulation of all the system equations, including equality and inequality constraints. For the solution of the optimization problem, an sqp solver (fmincon-sqp) is used for small-scale problems and an interior-point method (IPOPT) for large-scale systems.

- For the above centralized OPF, a distributed slack technique is used to cover the load-shift, and a new approach to include to over-excitation limits in the optimization problem.

- Additional equations for the requirements for fast RES current injections were included in the OPF VSM formulation.

- For the flexibility region calculation, programming code was developed in MATLAB for reading the network data and formulation of all the network equations. Then for the solution of the optimization problems for the boundary points calculation, again the sqp solver was used.

- The previous problem was then reworked into a second-order cone programming problem, using MATLAB and was solved again with a Gurobi SOCP solver. The reformulation of the Flexibity region calculation problem with the SOCP OPF relaxation is a novel contribution of the thesis, to the author's knowledge.

8.2 Conclusion

Three systems were used in the thesis:

1. IEEE Nordic test system
2. a two-bus radial transmission test system
3. a real power system, the Hellenic Interconnected Power System

The VSM results of the Nordic Test System for the considered operating point showed that the OPF identifies several critical Contingencies, which have negative margins, meaning that they would result in voltage instability. Contingencies with small positive margin were also identified, which can be also considered as critical. The results for VSM optimization are also validated with time-domain simulation. All time-domain simulations were performed using NTUA simulation software WPSTAB, which performs a quasi-steady-state simulation analysis for long-term voltage stability.

Before assessing the support offered by ADNs, the effect of system connected RES and their requirements for fast current injections on the VSM were examined in Chapter 3. The VSM was calculated using the OPF formulation developed in the thesis for a radial transmission test system. The results showed that while current injection requirements can offer support and increase the VSM following a contingency, the optimal tuning of the parameters for active/reactive current injection heavily relies on the topology of the system and the proximity of the RES to the stressed load area. Curtailment of active power to maximize reactive current is not always optimal, as proved in the thesis. The optimization proposed can calculate the optimal RES active/reactive current injections to ensure maximization of the voltage security margins and optimal tuning of the parameters (K-factor) considered in the current injection requirements.

Regarding the corrective (distributed optimization to maximize VSM) and the preventive (centralized control based on flexibility regions provided by the ADNs) developed in this thesis the following advantages and disadvantages have been demonstrated:

The distributed optimization has the following advantages (+) and disadvantages (-):

(+) Ensures that ADN control will definitely be in the right direction, in terms of voltage stability and the VSM (either negative or positive) will be maximized.

(+) Each ADN will only solve one local optimization problem, so the computational cost is distributed among ADN operators.

(+) Exchange of data between the operator of the transmission system and the local controller of each ADN is limited and will be activated only when the contingency occurs.

(-) It is possible that more control than needed will be activated, leading to a waste of resources that could be reserved for another contingency, thus making the approach inefficient. Nonetheless, identification of a critical contingency means proximity to voltage instability, and possible collapse, so it is justified to ask for maximum support even if more than absolutely necessary. It is noted that all actions taken do not cause any disruption to system service and comfort level of the consumers is maintained, as explained in the relevant Chapter of the thesis.

(-) There is no prioritization of the most efficient resources, even if this can be indirectly decided by off-line pre-selections.

The centralized approach has the following advantages and disadvantages:

(+) The utilization of available resources is efficient, since the contribution of each ADN control by varying its consumption setpoint is optimal. Thus most effective ADNs are prioritized.

(+) Update of the flexibility regions at regular intervals means that it can be used preventively whenever the VSM for some credible contingency is below a specified desired threshold.

(+) This approach can be generalized for different transmission system problems other than voltage stability, e.g. static overloads, overvoltages, small signal stability etc.

(-) Requires more data exchange between the ADNs and the operator of the transmission system and in particular, FR constraints in the form of a polygon.

(-) Identification of the FR can be a time-consuming process and this can be problematic if it needs to be updated regularly. This disadvantage is addressed in the relevant thesis Chapter by developing the convex cone relaxation.

Both approaches present advantages and disadvantages, mainly in terms of efficiency and ease of implementation. Also, both approaches were validated using time-domain simulation. Results showed that the support of the ADNs can be very important in dealing with an imminent voltage instability.

It should be noted that the optimization approaches rely on a static modelling of the system, thus excluding the time needed for each separate piece of equipment to achieve the reference setpoint. In particular, IBRs are way faster than the LTC control. For this reason, it is important to establish an appropriate scheme to apply the optimal setpoints that were calculated. Two different ways were used for the activation of the controller setpoints:

- LTC setpoint is sent without delay while IBR setpoints are activated only after the LTC has achieved the new reference voltage i.e. has reached its deadband.

- The LTC control again starts without delay, and the IBR setpoint is achieved through a ramp. The slope of the ramp is determined by the time needed for the LTC to bring the regulated voltage within the new deadband.

Both ways ensure that the fast reaction of the IBRs will not cause transient overvoltages in the feeders and consequently will not increase the load consumption, worsening the situation and accelerating collapse.

Regarding the computation of ADN flexibility region, three different methods are examined and compared:

- Monte Carlo simulations

- Points of multiple binding constraints
- Radial boundary scan (with nonlinear programming, or second-order cone relaxation)

Monte Carlo simulations calculate the flexibility region by creating random sets of setpoints for the decision variables and then checking if the solution is acceptable, according to the operational constraints. While MC simulations are easy to implement, it was shown that they do not scale well for longer ADNs with multiple decision variables and may underestimate the FR. Also, they are very time-consuming, as many random generated scenarios are needed to appropriately form the FR.

Point of multiple binding constraints depend on finding points where multiple of the constraints of the decision variables are active. These points also known as corner points are usually at the boundary of the feasible solution set. This approach was easily implemented on 2-bus ADN configurations, but it was found that it is not easy to identify these points in more complex feeders. Also, there is high chance of underestimation of the FR as points of multiple binding constraints are not necessarily maxima or minima.

The method of the radial boundary scan maximizes the distance from the initial operating point in the PQ plane along multiple search directions ensuring that the points found are on the boundary of the feasible region. It proves efficient and precise in determining the flexibility region of different ADN configurations, especially for more complex ADNs. On the other hand, depending on the desired granularity and the complexity of ADN, this method may prove time-consuming. As a consequence, update of the flexibility regions at short time intervals may not be possible. This limitation is addressed in the thesis by using second-order cone relaxation of the nonlinear OPF problem.

The same non-linear solver was used for the solution of all optimization problems in both transmission and distribution systems in this thesis. Non-linear solvers do not offer good scalability, so for long complex feeders solution time increased exponentially.

Finally, a case based on a real incident on the Hellenic Interconnected System was examined in the thesis using the OPF formulation developed in Chapter 2 of the thesis to calculate the voltage security margins following an actual contingency and the actions taken. For the solution of the OPF, for a large power system, an interior-point programming solver was chosen, that is designed for large scale optimization problems (IPOPT). Results showed that for one of the two snapshots examined, the VSM for the specific contingency was negative, meaning that the pre-contingency load could not be restored. This was confirmed with a qss simulation that was performed. The effect of a system-connected Wind Farm in the stressed area was also examined and it was shown that a substantial VSM increase is possible by using the controls that are available in the Wind Generators and their associated converters.

8.3 Future Research

One of the most critical research directions is the one towards the improvement of the communication protocol and data exchange between the TSO and the DSO. While the frameworks proposed are mathematically sound and simulations prove them efficient, it is mandatory for real system operators to be able to adopt them. Moreover, in that direction economic incentives may be useful.

- *Enhanced Communication Protocols:* Explore and design improved communication protocols and frameworks between TSOs and DSOs to facilitate seamless data exchange and coordination for optimal voltage stability support (or other transmission system support services).
- *Economic Incentives:* Develop market-based frameworks with economic incentives for the entities that operate the Distribution networks and provide support services.
- *Intelligent Decision Support Systems:* Develop intelligent decision support systems that enable efficient information sharing and decision-making between TSOs and DSOs, ensuring coordinated actions for voltage stability enhancement across transmission and distribution networks.

Regarding the computation of the flexibility region, other optimization approaches may prove to be efficient, especially with the inclusion of uncertainty introduced by the increasing renewables in the system. Moreover, other techniques such as machine learning can be taken into consideration.

- *Probabilistic Methods:* Develop and evaluate probabilistic models or stochastic approaches for estimating flexibility regions, considering uncertainties in renewable energy generation and load variations.
- *Optimization Algorithms:* Further investigate and refine existing optimization-based approaches for estimating flexibility regions in active distribution networks, especially when dealing with complex feeders with numerous decision variables.
- *Advanced Computational Techniques:* Explore alternative computational methods, such as machine learning algorithms, to improve the speed and accuracy of flexibility region estimation, particularly in scenarios involving intricate network configurations.

Also, regarding the centralized OPF for the VSM calculation, there are various research directions that can have significant value.

- *Multi-Criteria Optimization:* Explore multi-objective or multi-criteria optimization techniques to balance conflicting objectives, such as maximizing voltage stability while minimizing system losses including market cost information or optimizing resource utilization.
- *Security Assessment:* Investigate the robustness and resilience of proposed frameworks against various contingencies, including extreme weather events, cyber-attacks, or equipment failures, to ensure their effectiveness under adverse conditions.
- *Case Studies in Diverse Grids:* Extend research to encompass diverse grid structures and geographical locations, considering regional differences in renewable energy penetration, grid topology, and regulatory frameworks.

Publications

Journal Publications

- Giorgos Prionistis, Theodoros Souxes, Costas Vournas, Voltage stability support offered by active distribution networks, Electric Power Systems Research, Volume 190, 2021, 106728, ISSN 0378-7796, https://doi.org/10.1016/j.epsr.2020.106728.
- Giorgos Prionistis, Costas Vournas, An optimization framework for voltage stability support from active distribution networks, Electric Power Systems Research, Volume 211, 2022, 108569, ISSN 0378-7796, https://doi.org/10.1016/j.epsr.2022.108569.

Conference Publications

- Giorgos Prionistis, Costas Vournas, Using Active Distribution Network Flexibility to Increase Transmission System Voltage Stability Margins, In proceedings of the 11th Bulk Power Systems Dynamics and Control Symposium (IREP 2022), July 25-30, 2022, Banff, Canada
- G. Prionistis, C. Vournas and M. Vrakopoulou, "A Fast Method to Approximate the Flexibility Region of an Active Distribution Network in PQ Space," 2023 IEEE Belgrade PowerTech, Belgrade, Serbia, 2023, pp. 1-6.
- Giorgos Prionistis, Panos Mandoulidis, Costas Vournas,Effect of RES current injection requirements on Voltage Stability Margin, 2023 IEEE Power & Energy Society Innovative Smart Grid Technologies Conference (ISGT), Grenoble, France, 2023

Other Publications

- Y. Kampouris, P. Mandoulidis and G. Prionistis, "Adaptive Day-Ahead and Intra-Day Frequency Restoration Reserves Calculation Methodology for Electricity Balancing Markets," 2023 IEEE Belgrade PowerTech, Belgrade, Serbia, 2023, pp. 1-6, doi: 10.1109/PowerTech55446.2023.10202721.

Appendix I

Test Feeder Data

Detailed data for the test feeder firstly presented in Chapter 4 and used in the simulations, are presented here.

A Two-bus feeder

The two-bus configuration is used for five different ADNs, representing feeders with a WF connected and an aggregate load. For each of the five feeders connected in the Nordic Test System, the R, X and the data of each WF are presented in Table A1. It should be noted that in X, the reactance of the step-up transformer of the WF is also assumed.

Table A1: WF data connected to the system

WF	HV bus	P_{WF} (MW)	S_N (MVA)	P_{max} (MW)	R (pu)	X (pu)
1	1041	97.2	113.68	108	0.004413	0.0608
2	1042	99.3	110.05	104.55	0.04505	0.09165
3	1043	64.6	71.58	68	0.077986	0.147573
4	1044	90	100	90	0.0308	0.1396
5	1045	81	94.74	90	0.005296	0.07296

The initial active and reactive power load of each of the five ADNs is presented in Table A2.

Table A2: Active and reactive power load data

ADN	P (MW)	Q (Mvar)
1	696.78	142.47
2	425.22	62.65
3	321.60	78.12
4	927.60	241.11
5	800.65	185.60

B 30-bus feeder

Branch Data of the 30 bus ADN are shown in Fig. A3. The generation data, consisting of the IBRs are shown in Table A4.

Table A3: Branch data

From	To	R (pu)	X(pu)	From	To	R (pu)	X(pu)
100	1	0.0366	0.1029	15	16	0.0336	0.0943
1	2	0.0305	0.0858	16	17	0.0305	0.0858
2	3	0.0336	0.0943	16	18	0.0397	0.1115
2	4	0.0427	0.1201	18	19	0.0336	0.0943
4	5	0.0305	0.0858	19	20	0.0305	0.0858
4	6	0.0305	0.0858	15	21	0.0366	0.1029
6	7	0.0336	0.0943	21	22	0.0366	0.1029
7	8	0.0366	0.1029	22	23	0.0336	0.0943
1	9	0.0366	0.1029	22	24	0.0305	0.0858
9	10	0.0366	0.1029	21	25	0.0397	0.1115
10	11	0.0305	0.0858	25	26	0.0366	0.1029
10	12	0.0305	0.0858	25	27	0.0366	0.1029
12	13	0.0305	0.0858	27	28	0.0397	0.1115
13	14	0.0305	0.0858	27	29	0.0336	0.0943
9	15	0.0336	0.0943				

Table A4: IBR data

Bus	Pg (MW)	Sn (MVA)	Pmax (MW)
4	4	8.8	8
10	3.3	6.6	6
16	2	5.5	5
22	2	2.75	1.5
25	3	5.5	5

C Rural distribution feeder

For the rural distribution feeder of Xanthi, Northern Greece, the branch data are presented in Table A6, and generation data, consisting of the IBRs are shown in Table A5.

From	To	R (pu)	X(pu)	From	To	R (pu)	X(pu)
1000	1	0.95783	0.31991	46	47	0.74605	0.24814
1	2	0.34765	0.11563	48	49	3.04131	1.01153
1	3	0.14384	0.22345	48	51	0.12513	0.19439
3	6	1.28312	1.99331	49	50	6.61045	2.19862
3	4	0.97571	0.32452	51	52	0.39333	0.13082
4	5	0.21062	0.07005	51	54	0.26725	0.41516
6	7	3.73915	1.24363	52	53	1.48576	0.49416
6	9	0.2823	0.43854	54	55	0.62171	0.20678
7	8	1.58092	0.52581	54	57	0.18404	0.2859
9	10	2.59596	0.86341	55	56	0.41363	0.13757
9	12	0.09138	0.14195	57	58	0.21443	0.07132
10	11	1.59869	0.53172	57	60	0.08364	0.12993
12	13	2.74441	0.91279	58	59	3.32806	1.10691
12	15	0.16878	0.26219	60	61	1.12796	0.37516
13	14	0.90592	0.30131	60	63	0.44075	0.6847
15	16	0.51923	0.80661	61	62	0.50625	0.16838
15	66	0.11137	0.17301	63	64	0.5329	0.17724
16	19	0.92988	1.44455	64	65	1.72176	0.57265
16	17	0.87293	0.29034	66	67	0.93891	0.31228
17	18	0.5367	0.17851	66	69	0.5274	0.8193
19	20	15.21037	5.05894	67	68	6.70434	2.22985
19	21	0.26854	0.41717	69	70	0.37303	0.12407
21	22	0.96683	0.32156	69	72	0.24037	0.37341
21	24	0.45322	0.70407	70	71	0.42378	0.14095
22	23	0.36034	0.11985	72	74	2.37519	0.78998
24	25	5.78827	1.92516	72	75	0.18318	0.28457
24	27	1.4018	2.17768	75	76	0.88943	0.29582
25	26	8.04165	2.67464	75	78	0.15416	0.23948
27	30	1.0734	0.35701	76	77	1.38045	0.45914
27	28	0.81964	0.27261	78	79	9.59847	3.19243
28	29	13.58885	4.51962	78	81	0.80905	1.25684
30	31	2.04023	0.67858	79	80	4.92802	1.63905
30	33	0.2107	0.32732	81	84	0.41667	0.64729
31	32	3.23798	1.07694	81	82	0.16748	0.0557
33	36	0.41775	0.64896	82	83	0.65851	0.21902
33	34	0.12054	0.04009	84	85	4.91533	1.63483

Table A5: IBR data of rural feeder

Bus	Pg (MW)	Sn (MVA)	Pmax (MW)
2	0	1.1	1
28	0	2.2	2
31	3	3	3

Table A6: Branch data

33	34	0.12054	0.04009	84	85	4.91533	1.63483
34	35	0.4352	0.14475	84	87	0.09546	0.1483
36	37	1.1711	0.38951	85	86	5.1729	1.72049
36	39	0.26983	0.41917	87	88	2.56932	0.85455
37	38	1.34239	0.44648	87	90	0.33218	0.51603
39	40	0.45931	0.15276	88	89	5.59287	1.86018
39	42	0.2924	0.45424	90	91	2.89667	0.96343
40	41	2.5173	0.83725	90	92	0.47107	0.73179
42	43	6.4417	2.14249	92	93	6.12196	2.03615
42	45	0.21049	0.32699	92	96	0.34422	0.53473
43	73	18.61837	6.19243	93	95	21.36152	7.10479
43	44	5.20335	1.73062	93	94	16.31423	5.42608
45	46	0.74732	0.24856	96	97	1.3665	0.45449
45	48	0.16018	0.24883	97	98	13.91874	4.62934
46	47	0.74605	0.24814				

Glossary

Voltage Security Margin (VSM)	Περιθώριο Ασφάλειας Τάσεως
Loadability Margin (LM)	Περιθώριο Φόρτισης
Flexibility Region (FR)	Περιοχή Ευελιξίας
Active Distribution Network (ADN)	Ενεργό Δίκτυο Διανομής
Optimal Power Flow (OPF)	Βέλτιση Ροή Ισχύος
Transmission System Operator (TSO)	Διαχειριστής Συστήματος Μεταφοράς
Distribution Network Operator (DNO)	Διαχειριστής Δικτύου Διανομής
Distributed Generation (DG)	Διεσπαρμένη Παραγωγή
Renewable Energy Sources (RES)	Ανανεώσιμες Πηγές Ενέργειας
Battery Energy Storage System (BESS)	Σύστημα Αποθήκευσης Ενέργειας με Μπαταρίες
Point of Common Coupling (PCC)	Σημείο Κοινής Σύνδεσης
Quasi Steady State (QSS)	Οιωνεί στατική προσέγγιση
Inverter Based Generation (IBR)	Γεννήτριες με αντιστροφείς
(On) Load Tap Changer (LTC)	Σύστημα Αλλαγής Τάσης Υπό Φορτίο
Emergency Reactive Support (EMRS)	Έκτακτη Άεργη Υποστήριξη
Non-Linear Programming (NLP)	Μη-Γραμμικός Προγραμματισμός
Second Order Cone Programming (SOCP)	Κωνικός Προγραμματισμός Δευτέρας Τάξης
Over Excitation Limit (OEL)	Όριο Υπερδιέγερσης

References

[1] P. Kundur et al. «Definition and classification of power system stability IEEE/CIGRE joint task force on stability terms and definitions». In: *IEEE Transactions on Power Systems* 19.3 (2004), pp. 1387–1401. DOI: 10.1109/TPWRS.2004.825981.

[2] Prabha S Kundur and Om P Malik. *Power system stability and control*. McGraw-Hill Education, 2022.

[3] Nikos Hatziargyriou et al. «Definition and Classification of Power System Stability – Revisited & Extended». In: *IEEE Transactions on Power Systems* 36.4 (2021), pp. 3271–3281. DOI: 10.1109/TPWRS.2020.3041774.

[4] Thierry Van Cutsem and Costas Vournas. *Voltage stability of electric power systems*. Springer Science & Business Media, 2007.

[5] Jack K Hale and Hüseyin Koçak. *Dynamics and bifurcations*. Vol. 3. Springer Science & Business Media, 2012.

[6] Petar Kokotović, Hassan K. Khalil, and John O'Reilly. *Singular Perturbation Methods in Control: Analysis and Design*. Society for Industrial and Applied Mathematics, 1999. DOI: 10.1137/1.9781611971118. eprint: https://epubs.siam.org/doi/pdf/10.1137/1.9781611971118. URL: https://epubs.siam.org/doi/abs/10.1137/1.9781611971118.

[7] Thierry Van Cutsem et al. «Application of Real-Time Voltage Security Assessment to the Hellenic Interconnected System». In: *Generation, Transmission and Distribution, IEE Proceedings-* 152 (Feb. 2005), pp. 123–131. DOI: 10.1049/ip-gtd:20041206.

[8] Theodoros Souxes, Ioannis-Marios Granitsas, and Costas Vournas. «Effect of stochasticity on voltage stability support provided by wind farms: Application to the Hellenic interconnected system». In: *Electric Power Systems Research* 170 (2019), pp. 48–56. ISSN: 0378-7796. DOI: https://doi.org/10.1016/j.epsr.2019.01.007. URL: https://www.sciencedirect.com/science/article/pii/S0378779619300136.

[9] Panagiotis Mandoulidis, Theodoros Souxes, and Costas Vournas. «Impact of converter interfaced generators on power system long-term voltage stability monitoring and control». In: *Electric Power Systems Research* 199 (2021), p. 107438. ISSN: 0378-7796. DOI: https://doi.org/10.1016/j.epsr.2021.107438. URL: https://www.sciencedirect.com/science/article/pii/S0378779621004193.

[10] Vladimir I Arnol'd. *Catastrophe theory*. Springer Science & Business Media, 2003.

[11] I. Dobson and L. Lu. «Voltage collapse precipitated by the immediate change in stability when generator reactive power limits are encountered». In: *IEEE Transactions on Circuits and Systems I: Fundamental Theory and Applications* 39.9 (1992), pp. 762–766. DOI: 10.1109/81.250167.

[12] Nicholas G. Maratos and Costas D. Vournas. «Relationships between static bifurcations and constrained optima». In: *2000 IEEE International Symposium on Circuits and Systems. Emerging Technologies for the 21st Century. Proceedings (IEEE Cat No.00CH36353)* 2 (2000), 477–480 vol.2.

[13] Costas Vournas and Thierry Van Cutsem. «Online Voltage Security Assessment». In: *Real-Time Stability in Power Systems: Techniques for Early Detection of the Risk of Blackout*. Ed. by Savu C. Savulescu. Cham: Springer International Publishing, 2014, pp. 305–333. ISBN: 978-3-319-06680-6. DOI: 10.1007/978-3-319-06680-6_10. URL: https://doi.org/10.1007/978-3-319-06680-6_10.

[14] Santiago Grijalva. «Individual Branch and Path Necessary Conditions for Saddle-Node Bifurcation Voltage Collapse». In: *IEEE Transactions on Power Systems* 27.1 (2012), pp. 12–19. DOI: 10.1109/TPWRS.2011.2161346.

[15] Jacques Carpentier. «Contribution a l'etude du dispatching economique». In: *Bulletin de la Societe Francaise des Electriciens* 3.1 (1962), pp. 431–447.

[16] Hermann W. Dommel and William F. Tinney. «Optimal Power Flow Solutions». In: *IEEE Transactions on Power Apparatus and Systems* 10 (1968), pp. 1866–1876.

[17] Mary B Cain, Richard P O'neill, Anya Castillo, et al. «History of optimal power flow and formulations». In: *Federal Energy Regulatory Commission* 1 (2012), pp. 1–36.

[18] F. Capitanescu et al. «State-of-the-art, challenges, and future trends in security constrained optimal power flow». In: *Electric Power Systems Research* 81.8 (2011), pp. 1731–1741. ISSN: 0378-7796. DOI: https://doi.org/10.1016/j.epsr.2011.04.003. URL: https://www.sciencedirect.com/science/article/pii/S0378779611000885.

[19] Fabrizio Pilo et al. «Planning and optimisation of active distribution systems — An overview of CIGRE Working Group C6.19 activities». In: *CIRED 2012 Workshop: Integration of Renewables into the Distribution Grid*. 2012, pp. 1–4. DOI: 10.1049/cp.2012.0767.

[20] Maria Zerva and Martin Geidl. «Contribution of active distribution grids to the coordinated voltage control of the swiss transmission system». In: *2014 Power Systems Computation Conference*. 2014, pp. 1–8. DOI: 10.1109/PSCC.2014.7038467.

[21] VDE. *Technical rules for operation and planning by network operators - Part 1: Interface between transmission and distribution systems*. FNN, September 2017.

[22] Luis F. Ochoa, Chris J. Dent, and Gareth P. Harrison. «Distribution Network Capacity Assessment: Variable DG and Active Networks». In: *IEEE Transactions on Power Systems* 25.1 (2010), pp. 87–95. DOI: 10.1109/TPWRS.2009.2031223.

[23] Caisheng Wang and M.H. Nehrir. «Analytical approaches for optimal placement of distributed generation sources in power systems». In: *IEEE Transactions on Power Systems* 19.4 (2004), pp. 2068–2076. DOI: 10.1109/TPWRS.2004.836189.

[24] Weilin Zhong, Georgios Tzounas, and Federico Milano. «Improving the Power System Dynamic Response Through a Combined Voltage-Frequency Control of Distributed Energy Resources». In: *IEEE Transactions on Power Systems* 37 (Nov. 2022), pp. 1–1. DOI: 10.1109/TPWRS.2022.3148243.

[25] C.W. Taylor, N.J. Balu, and D. Maratukulam. *Power System Voltage Stability*. EPRI power system engineering series. McGraw-Hill, 1994. ISBN: 9780070631847. URL: https://books.google.gr/books?id=CPtSAAAAMAAJ.

[26] C.A. Canizares. «Calculating optimal system parameters to maximize the distance to saddle-node bifurcations». In: *IEEE Transactions on Circuits and Systems I: Fundamental Theory and Applications* 45.3 (1998), pp. 225–237. DOI: 10.1109/81.662696.

[27] G.D. Irisarri et al. «Maximum loadability of power systems using interior point nonlinear optimization method». In: *IEEE Transactions on Power Systems* 12.1 (1997), pp. 162–172. DOI: 10.1109/59.574936.

[28] W.D. Rosehart, C.A. Canizares, and V.H. Quintana. «Multiobjective optimal power flows to evaluate voltage security costs in power networks». In: *IEEE Transactions on Power Systems* 18.2 (2003), pp. 578–587. DOI: 10.1109/TPWRS.2003.810895.

[29] W. Rosehart, C. Canizares, and V. Quintana. «Optimal power flow incorporating voltage collapse constraints». In: *1999 IEEE Power Engineering Society Summer Meeting. Conference Proceedings (Cat. No.99CH36364)*. Vol. 2. 1999, 820–825 vol.2. DOI: 10.1109/PESS.1999.787422.

[30] Rafael J. Avalos et al. «Equivalency of Continuation and Optimization Methods to Determine Saddle-Node and Limit-Induced Bifurcations in Power Systems». In: *IEEE Transactions on Circuits and Systems I: Regular Papers* 56.1 (2009), pp. 210–223. DOI: 10.1109/TCSI.2008.925941.

[31] Abbas Rabiee et al. «Optimal Cost of Voltage Security Control Using Voltage Dependent Load Models in Presence of Demand Response». In: *IEEE Transactions on Smart Grid* 10.3 (2019), pp. 2383–2395. DOI: 10.1109/TSG.2018.2797103.

[32] J.A. Peças Lopes et al. «Integrating distributed generation into electric power systems: A review of drivers, challenges and opportunities». In: *Electric Power Systems Research* 77.9 (2007). Distributed Generation, pp. 1189–1203. ISSN: 0378-7796. DOI: https://doi.org/10.1016/j.epsr.2006.08.016. URL: https://www.sciencedirect.com/science/article/pii/S0378779606001908.

[33] Nikos D. Hatziargyriou et al. «Contribution to Bulk System Control and Stability by Distributed Energy Resources connected at Distribution Network». In: 2017.

[34] Costas Vournas, Ioannis Anagnostopoulos, and Theodoros Souxes. «Transmission support using Wind Farm controls during voltage stability emergencies». In: *Control Engineering Practice* 59 (2017), pp. 100–110. ISSN: 0967-0661. DOI: https://doi.org/10.1016/j.conengprac.2016.11.007. URL: https://www.sciencedirect.com/science/article/pii/S0967066116302568.

[35] Souxes Theodoros. «Utilization of wind farm converters for Voltage Stability Enhancement». PhD dissertation. National Technical University of Athens, 2019.

[36] Nikos Hatziargyriou et al. «Microgrids». In: *IEEE Power and Energy Magazine* 5.4 (2007), pp. 78–94. DOI: 10.1109/MPAE.2007.376583.

[37] Vito Calderaro et al. «Optimal Decentralized Voltage Control for Distribution Systems With Inverter-Based Distributed Generators». In: *IEEE Transactions on Power Systems* 29.1 (2014), pp. 230–241. DOI: 10.1109/TPWRS.2013.2280276.

[38] Luis David Pabón Ospina and Thierry Van Cutsem. «Emergency Support of Transmission Voltages by Active Distribution Networks: A Non-Intrusive Scheme». In: *IEEE Transactions on Power Systems* 36.5 (2021), pp. 3887–3896. DOI: 10.1109/TPWRS.2020.3027949.

[39] Petros Aristidou, Gustavo Valverde, and Thierry Van Cutsem. «Contribution of Distribution Network Control to Voltage Stability: A Case Study». In: *IEEE Transactions on Smart Grid* 8.1 (2017), pp. 106–116. DOI: 10.1109/TSG.2015.2474815.

[40] Agnes M. Nakiganda, Thierry Van Cutsem, and Petros Aristidou. «Microgrid Operational Optimization with Dynamic Voltage Security Constraints». In: *2021 IEEE Madrid PowerTech*. 2021, pp. 1–6. DOI: 10.1109/PowerTech46648.2021.9494823.

[41] Seyed Masoud Mohseni-Bonab et al. «Voltage Security Constrained Stochastic Programming Model for Day-Ahead BESS Schedule in Co-Optimization of TD Systems». In: *IEEE Transactions on Sustainable Energy* 11.1 (2020), pp. 391–404. DOI: 10.1109/TSTE.2019.2892024.

[42] Arthur Gonçalves Givisiez, Kyriacos Petrou, and Luis F. Ochoa. «A Review on TSO-DSO Coordination Models and Solution Techniques». In: *Electric Power Systems Research* 189 (2020), p. 106659. ISSN: 0378-7796. DOI: https://doi.org/10.1016/j.epsr.2020.106659. URL: https://www.sciencedirect.com/science/article/pii/S0378779620304624.

[43] Daniel Mayorga Gonzalez et al. «Distribution network control scheme for power flow regulation at the interconnection point between transmission and distribution system». In: *2016 IEEE Innovative Smart Grid Technologies - Asia (ISGT-Asia)*. 2016, pp. 23–28. DOI: 10.1109/ISGT-Asia.2016.7796355.

[44] Mohsen Kalantar-Neyestanaki et al. «Characterizing the Reserve Provision Capability Area of Active Distribution Networks: A Linear Robust Optimization Method». In: *IEEE Transactions on Smart Grid* 11.3 (2020), pp. 2464–2475. DOI: 10.1109/TSG.2019.2956152.

[45] Florin Capitanescu. «TSO–DSO interaction: Active distribution network power chart for TSO ancillary services provision». In: *Electric Power Systems Research* 163 (2018), pp. 226–230. ISSN: 0378-7796. DOI: https://doi.org/10.1016/j.epsr.2018.06.009. URL: https://www.sciencedirect.com/science/article/pii/S0378779618301822.

[46] Shariq Riaz and Pierluigi Mancarella. «On Feasibility and Flexibility Operating Regions of Virtual Power Plants and TSO/DSO Interfaces». In: *2019 IEEE Milan PowerTech*. 2019, pp. 1–6. DOI: 10.1109/PTC.2019.8810638.

[47] Shariq Riaz and Pierluigi Mancarella. «Modelling and Characterisation of Flexibility From Distributed Energy Resources». In: *IEEE Transactions on Power Systems* 37.1 (2022), pp. 38–50. DOI: 10.1109/TPWRS.2021.3096971.

[48] Peng Li et al. «Operational flexibility of active distribution networks: Definition, quantified calculation and application». In: *International Journal of Electrical Power & Energy Systems* 119 (2020), p. 105872. ISSN: 0142-0615. DOI: https://doi.org/10.1016/j.ijepes.2020.105872. URL: https://www.sciencedirect.com/science/article/pii/S0142061519331862.

[49] D. Mayorga Gonzalez et al. «Determination of the Time-Dependent Flexibility of Active Distribution Networks to Control Their TSO-DSO Interconnection Power Flow». In: *2018 Power Systems Computation Conference (PSCC)*. 2018, pp. 1–8. DOI: 10.23919/PSCC.2018.8442865.

[50] João Silva et al. «Estimating the Active and Reactive Power Flexibility Area at the TSO-DSO Interface». In: *IEEE Transactions on Power Systems* 33.5 (2018), pp. 4741–4750. DOI: 10.1109/TPWRS.2018.2805765.

[51] Holm Hinners and Johanna Myrzik. «Validation and Flexibility Region of the Model Order Reduction of an Active Distribution Grid». In: *2021 IEEE Madrid PowerTech*. 2021, pp. 1–6. DOI: 10.1109/PowerTech46648.2021.9495085.

[52] W. Rosehart, C. Roman, and A. Schellenberg. «Optimal power flow with complementarity constraints». In: *IEEE Transactions on Power Systems* 20.2 (2005), pp. 813–822. DOI: 10.1109/TPWRS.2005.846171.

[53] MATLAB. *Release R2018a*. Natick, Massachusetts: The MathWorks Inc., 2018.

[54] Ray Daniel Zimmerman, Carlos Edmundo Murillo-Sánchez, and Robert John Thomas. «MATPOWER: Steady-State Operations, Planning, and Analysis Tools for Power Systems Research and Education». In: *IEEE Transactions on Power Systems* 26.1 (2011), pp. 12–19. DOI: 10.1109/TPWRS.2010.2051168.

[55] Paul T Boggs and Jon W Tolle. «Sequential quadratic programming for large-scale nonlinear optimization». In: *Journal of computational and applied mathematics* 124.1-2 (2000), pp. 123–137.

[56] Philip E Gill and Elizabeth Wong. «Sequential quadratic programming methods». In: *Mixed integer nonlinear programming*. Springer, 2011, pp. 147–224.

[57] Tor Arne Johansen, Thor I Fossen, and Stig P Berge. «Constrained nonlinear control allocation with singularity avoidance using sequential quadratic programming». In: *IEEE transactions on control systems technology* 12.1 (2004), pp. 211–216.

[58] Thierry Van Cutsem et al. «Test Systems for Voltage Stability Studies». In: *IEEE Transactions on Power Systems* 35.5 (2020), pp. 4078–4087. DOI: 10.1109/TPWRS.2020.2976834.

[59] Council of European Union. «Commission Regulation (EU) 2016/631 of 14 April 2016 establishing a network code on requirements for grid connection of generators». In: *OJ* L 112 (2016), p.1–68.

[60] Bernd Weise. «Impact of K-factor and active current reduction during fault-ride-through of generating units connected via voltage-sourced converters on power system stability». In: *IET Renewable Power Generation* 9.1 (2015), pp. 25–36. DOI: https://doi.org/10.1049/iet-rpg.2014.0116. eprint: https://ietresearch.onlinelibrary.wiley.com/doi/pdf/10.1049/iet-rpg.2014.0116. URL: https://ietresearch.onlinelibrary.wiley.com/doi/abs/10.1049/iet-rpg.2014.0116.

[61] Stefan Stanković, Thierry Van Cutsem, and Lennart Söder. «Fault-Current Injection Strategies of Inverter-Based Generation for Fast Voltage Recovery». In: *IEEE Transactions on Power Systems* 37.2 (2022), pp. 1543–1553. DOI: 10.1109/TPWRS.2021.3108064.

[62] VDE/FNN. «Technical Connection Rules for High-Voltage (VDE-AR-N 4120 and 4130)». In: (2018).

[63] P. Mandoulidis et al. «Overview, comparison, and extension of emergency controls against voltage instability using Inverter-Based Generators». In: *Sustainable Energy, Grids and Networks* 31 (2022), p. 100710. ISSN: 2352-4677. DOI: https://doi.org/10.1016/j.segan.2022.100710. URL: https://www.sciencedirect.com/science/article/pii/S235246772200056X.

[64] Luis David Pabón Ospina and Thierry Van Cutsem. «Power factor improvement by active distribution networks during voltage emergency situations». In: *Electric Power Systems Research* 189 (2020), p. 106771. ISSN: 0378-7796. DOI: https://doi.org/10.1016/j.epsr.2020.106771. URL: https://www.sciencedirect.com/science/article/pii/S0378779620305745.

[65] Giorgos Prionistis and Costas Vournas. «An optimization framework for voltage stability support from active distribution networks». In: *Electric Power Systems Research* 211 (2022), p. 108569. ISSN: 0378-7796. DOI: https://doi.org/10.1016/j.epsr.2022.108569. URL: https://www.sciencedirect.com/science/article/pii/S0378779622006642.

[66] ENTSO-E. *Requirements for Generators (RfG)*. Commission Regulation (EU) 2016/631. April, 2016.

[67] Working Group. «Common Format For Exchange of Solved Load Flow Data». In: *IEEE Transactions on Power Apparatus and Systems* PAS-92.6 (1973), pp. 1916–1925. DOI: 10.1109/TPAS.1973.293571.

[68] Aristotelis M. Tsimtsios, Anastasia S. Safigianni, and Vassilis C. Nikolaidis. «Generalized distance-based protection design for DG integrated MV radial distribution networks — Part I: Guidelines». In: *Electric Power Systems Research* 176 (2019), p. 105949. ISSN: 0378-7796. DOI: https://doi.org/10.1016/j.epsr.2019.105949. URL: https://www.sciencedirect.com/science/article/pii/S0378779619302688.

[69] Michael E. Karystianos, Nicholas G. Maratos, and Costas D. Vournas. «Maximizing Power-System Loadability in the Presence of Multiple Binding Complementarity Constraints». In: *IEEE Transactions on Circuits and Systems I: Regular Papers* 54.8 (2007), pp. 1775–1787. DOI: 10.1109/TCSI.2007.902529.

[70] Siemens. *PSS®E*. Version v33. 2013. URL: https://new.siemens.com/global/en/products/energy/energy-automation-and-smart-grid/pss-software.

[71] R.A. Jabr. «Radial distribution load flow using conic programming». In: *IEEE Transactions on Power Systems* 21.3 (2006), pp. 1458–1459. DOI: 10.1109/TPWRS.2006.879234.

[72] J. Löfberg. «YALMIP : A Toolbox for Modeling and Optimization in MATLAB». In: *In Proceedings of the CACSD Conference*. Taipei, Taiwan, 2004.

[73] Gurobi Optimization, LLC. *Gurobi Optimizer Reference Manual*. 2022. URL: https://www.gurobi.com.

[74] IPTO. *Ten-Year Network Developmet Plan*. 2023. URL: https://www.admie.gr/systima/anaptyxi/dekaetes-programma-anaptyxis.

[75] Andreas Wächter and Lorenz T Biegler. ≪On the implementation of an interior-point filter line-search algorithm for large-scale nonlinear programming≫. In: *Mathematical programming* 106 (2006), pp. 25–57.